BRITISH ANTARCTIC SURVEY

SCIENTIFIC REPORTS

No. 112

THE GEOLOGY OF PARTS OF THE WEST COAST OF PALMER LAND

By

C. G. SMITH, B.Sc., Ph.D.

Earth Sciences Division, British Antarctic Survey
and
Department of Geological Sciences, University of Birmingham

CAMBRIDGE: PUBLISHED BY THE BRITISH ANTARCTIC SURVEY: 1987
NATURAL ENVIRONMENT RESEARCH COUNCIL

BRITISH ANTARCTIC SURVEY SCIENTIFIC REPORTS: No. 112

THE GEOLOGY OF PARTS OF THE WEST COAST OF PALMER LAND

By

C. G. SMITH, B.Sc., Ph.D.

ABSTRACT

The geology of parts of the west coast of Palmer Land is described and 107 new chemical analyses are presented. The oldest exposed rocks are considered to be wedges of granitic and granulitic pre-Mesozoic continental crust which, together with (?) Carboniferous sedimentary and volcanic rocks, were regionally metamorphosed during the early Mesozoic Gondwanian orogeny.

Most of the metamorphic rocks are banded gneisses which were derived from mineralogically and chemically similar syn-kinematic tonalites by metamorphic differentiation. Diorite-gneisses, metagabbros and two generations of amphibolites (meta-basic dykes) are also present. The textures and mineralogical assemblages of these rocks are typical products of high-temperature–low-pressure metamorphism, suggesting the area lay above an easterly dipping subduction zone. Three metamorphic events, ranging from upper amphibolite to greenschist facies, and two associated episodes of potash metasomatism are recognized. Granites of limited areal extent, which are chemically and mineralogically different from later plutonic rocks, were emplaced late in the second metamorphism.

In the extreme north of this area, Late Jurassic marine argillaceous and arenaceous sedimentary rocks were probably deposited in an unstable shelf environment. They are interbedded with and overlain by basalt, basaltic andesite and andesite lavas and tuffs. Similar andesites occur on the Palmer Land plateau where, in association with dacitic and rhyodacitic lavas, tuffs and agglomerates, they form the relic of a composite volcanic cone. Amongst the volcanic rocks, two chemical series can be distinguished principally on the basis of their potassium content. These are thought to reflect differing depths of formation and a change with time from an island-arc to a continental margin environment.

Widespread plutonic rocks appear to belong to a single mid-Cretaceous intrusive suite, with an ultrabasic to acid trend, emplaced during the Andean orogeny. The peridotites and some of the gabbros are cumulate rocks and it is shown that the quartz-diorites and granites also formed by continued fractionation of the primary gabbroic magma. The granodiorites, on the other hand, are most probably products of crustal melting. Outcrops of granodiorite are cupolas of the same mesozonal batholith whose orientation was controlled by structures in the metamorphic rocks. The granites are high-level bodies showing some degree of spatial association with the volcanic rocks.

Some of the post-metamorphic minor intrusions are associated with volcanic and plutonic rocks but most of them are later. Acid porphyries of a limited local extent are post-dated by basic and intermediate dykes which were emplaced over much of the area in the early Tertiary. The higher K/Na ratios of these dykes point to them having formed farther from the trench and consequently imply a westerly displacement of the Benioff Zone.

The later history of the area comprises planation, uplift and glaciation.

This report is based on a Ph.D. thesis submitted in 1977 (Smith, 1977).

CONTENTS

I. INTRODUCTION

The southern half of the Antarctic Peninsula, between lat. 68°30′ and 75°00′S, is called Palmer Land. The area described here (Fig. 1) covers approximately 2 400 km^2 of the west coast between lat. 70° and 71°S. Only the narrow coastal strip was mapped, between Carse Point and Wade Point, but at Gurney Point the survey was extended into the hinterland and includes most of the nunataks in upper Bertram and Millett glaciers.

This part of the Palmer Land coast was first surveyed in 1936 by members of the British Graham Land Expedition (Stephenson, 1940; Stephenson and Fleming, 1940), although it had been seen in the previous year by Lincoln Ellsworth during a flight from Dundee Island to 'Little America' near the Bay of Whales, Ross Ice Shelf. They recorded the occurrence of igneous rocks in the coastal areas and realized the structural significance of George VI Sound. However, the first detailed petrological study was done on rocks collected from the Palmer Land plateau by the United States Antarctic Services Expedition, 1940–41, when Knowles (1945) described quartz-felsites, quartz-diorites and granodiorites from the Batterbee Mountains, and hornfelses from the southern side of upper Meiklejohn Glacier. Much of northern Palmer Land and parts of Alexander Island were photographed from the air by the Ronne Antarctic Research Expedition in 1946–48, and the trimetrogon photographs of flight lines M3 and M7 were of considerable assistance in mapping and route finding during the present study. Further ground surveys, including detailed mapping of the coast between Carse Point and Moore Point, were carried out between 1948 and 1950 by members of the Falkland Islands Dependencies Survey working from a base station on Stonington Island. Geological interest in northern Palmer Land was revived in 1958 when N. A. A. Procter investigated the Mount Edgell area. The rock types described by Procter (1959) included schists and gneisses overlain by volcanic rocks. In 1960 an advance field station was established at Fossil Bluff to enable detailed surveys to be made in Alexander Island and Palmer Land, and 3 years later a reconnaissance journey on to the Palmer Land plateau was undertaken. The rock specimens collected were later described by Ayling (1966), who in 1964 carried out a more detailed survey with J. F. Pagella. Although this was prematurely curtailed by the loss of an aircraft, Ayling was able to map the Batterbee Mountains and a part of the plateau immediately south of the area described here. A further air photographic survey of the west coast of Palmer Land was completed by the United States Navy in 1966–67.

The field work described in this report was carried out during the southern summers of 1967–68 and 1968–69 from the British Antarctic Survey scientific station on Stonington Island (lat. 68°11′S, long. 67°00′W). In 1967 the author commenced mapping from the main field depot at lat. 70°50′S, long. 66°20′W, thus establishing a link with Ayling's survey. The survey was extended first to the west, to within 8 km of George VI Sound, and then northward to include all exposures in upper Bertram and Millett glaciers. Logistics limited the 1968–69 summer programme to a reconnaissance survey of the coast between Gurney Point and Carse Point.

All areas except Carse Point were mapped by plane table at a scale of 1:100 000 and distances were measured with a sledge wheel. All altitude data are based on an assumed height of 30 m a.s.l. for the surface of the ice shelf in George VI Sound and on a barometrically determined spot height at lat. 70°50′S, long 66°20′W. The graticule was derived from the existing triangulation network.

II. STRATIGRAPHY

The rocks of western Palmer Land belong to six main groups, which are listed chronologically in Table I. Although their relative ages can be established with some certainty in the field, the paucity of palaeontological and radiometric ages has meant that the age estimates are heavily dependent on data from adjacent areas.

The metamorphic complex is composed almost exclusively of *ortho*gneisses, the overwhelming bulk of which are synkinematic acid to intermediate intrusions, emplaced during the first metamorphic episode. By analogy with the metamorphic rocks of Graham Land and north-eastern Palmer Land, this event is likely to have occurred during the Triassic. Two lithological units apparently pre-date this metamorphism; first, essentially granulitic rocks of granitic composition are interpreted as fragments of Palaeozoic (or possibly older) continental crust and secondly, a probable metavolcanic horizon is correlated with the somewhat lower-grade Carboniferous volcaniclastic sediments of central Alexander Island. The second metamorphism (of uncertain age) was bracketed by two episodes of basic dyke intrusion, and the radiometric age of 152 ± 7 Ma (Rex, 1971) obtained from one of the younger suite is assumed to represent the effects of the third metamorphism.

Mesozoic stratified rocks were observed at three widely separated localities and, though lacking correlatable horizons, they are assumed to be contemporaneous. The dominance of volcanic rocks amongst these reflects a trait of the Upper Jurassic rocks of Graham Land, and the underlying sediments at Carse Point contain a Late Jurassic ammonite fauna (personal communication from L. E. Willey). Since these rocks

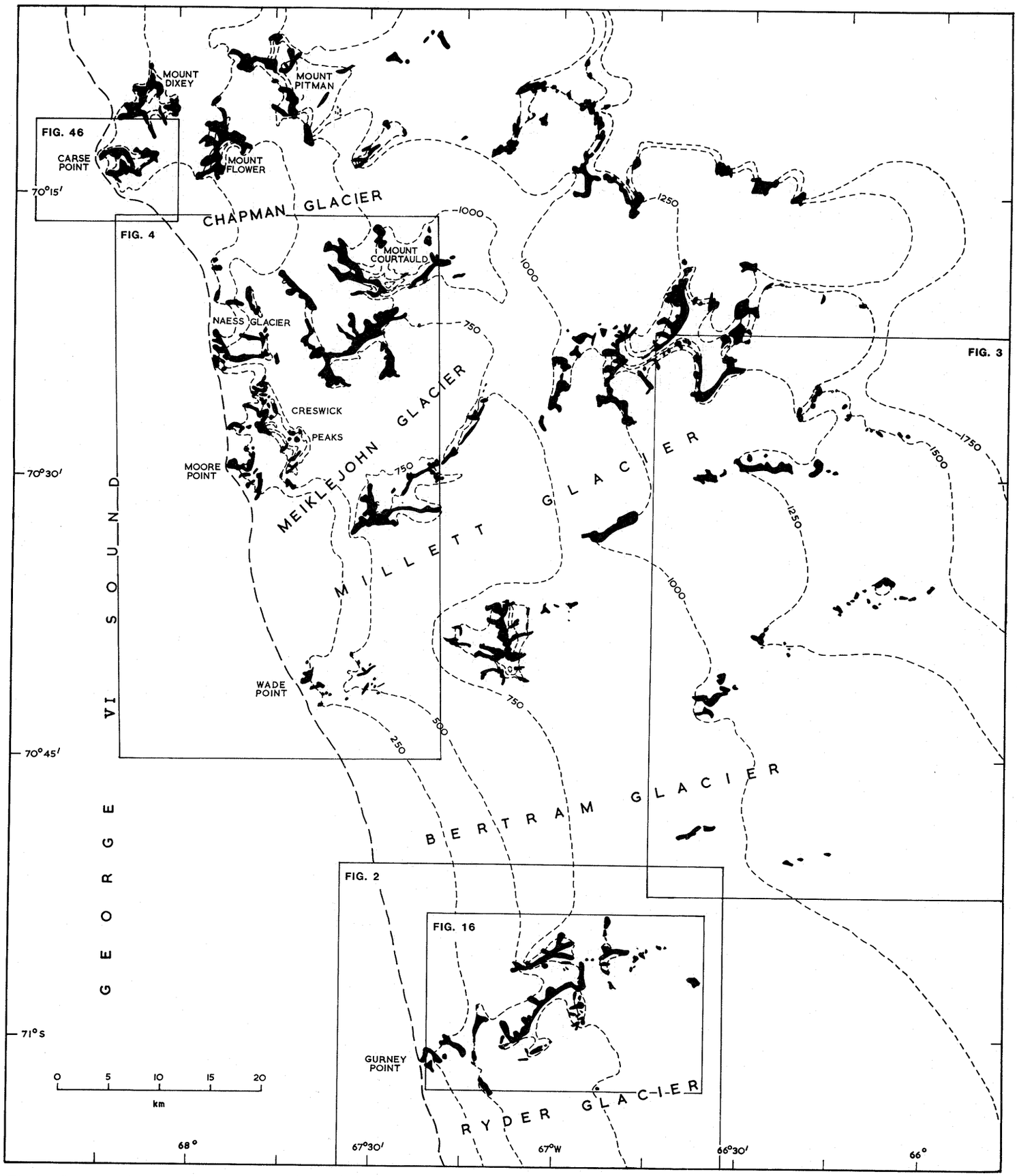

Fig. 1. Topographical sketch map of the west coast of Palmer Land between Carse Point and Ryder Glacier and part of Alexander Island, with insets showing the locations of the geological sketch maps (Figs 2, 3, 4, 16 and 46).

Table I. General stratigraphy.

Recent		Moraines		
Eocene–Oligocene		Basic and intermediate dykes Acid porphyry dykes	Andean orogeny	
Middle Cretaceous	Andean Intrusive Suite	Granite Granodiorite Diorite Gabbro		
Lower Cretaceous to Upper Jurassic	Carse Point, Millett Glacier and Gurney Point successions	Basic, intermediate and acid lavas, agglomerates, tuffs, mudstones, sandstones and conglomerates		
		Amphibolites		Metamorphism
Middle Jurassic	Pre-Upper Jurassic plutonic rocks	Diorites and granodiorites		
		Amphibolites	Gondwanian orogeny	Metamorphism
Middle Jurassic to Triassic	Metamorphic complex	Basic, intermediate and acid orthogneisses, including possible Palaeozoic amphibolites and granulites		Metamorphism

were probably deposited in the same basin as those of eastern Alexander Island (where there is evidence of volcanicity up to the Aptian), it is highly likely that activity in Palmer Land persisted beyond the Jurassic–Cretaceous boundary.

Amongst the plutonic rocks is a suite of limited areal occurrence comprising, in chronological order, diorite and granodiorite; the presence of similar fragments in the Mesozoic sediments suggests that these plutons were emplaced in pre-Late Jurassic times. Indeed there are many features in the more acid rocks which point to their being late kinematic (Marmo, 1971) relative to the third metamorphism.

The bulk of the major intrusions are similar in character to those of many localities in the Antarctic Peninsula which are known to have been emplaced in the Cretaceous and early Tertiary, and to which the term 'Andean' has been applied (Adie, 1955). A basic to acid trend is apparent and the granodiorites are distinguished from the earlier rocks by the presence of orthoclase (as opposed to microcline).

Hypabyssal rocks found in western Palmer Land range in age from (?) Triassic (now metamorphosed) to Tertiary. After the metabasic dykes (amphibolites), the oldest are quartz-plagioclase-porphyries which by analogy with adjacent areas probably belong to the volcanic group. The older granodiorites of Moore Point contain basic dykes which pre-date 'Andean'-type microgranites and hence are regarded as possible offshoots of the nearby gabbro. Since a chemically similar dyke (intruding volcanic rocks) was dated at 85 Ma, it would seem that the gabbros, if not the entire 'Andean' suite, belong to Rex's (1972) Middle Cretaceous episode. Although acid porphyries are locally common, most of the minor intrusions belong to an extensive suite of basic and intermediate dykes which were emplaced along joints in the metamorphic and plutonic rocks during the Eocene and Oligocene (cf. Rex, 1972).

III. METAMORPHIC COMPLEX

Regionally metamorphosed rocks, which form much of the mountainous area east (Fig. 2) and north-east (Fig. 3) of Gurney Point and the coastal cliffs south of Chapman Glacier (Fig. 4), have been grouped together as the metamorphic complex. Within the metamorphic complex eight main rock groups have been recognized and they are shown in approximate stratigraphical order in Table II. Since these rocks are exclusively igneous in origin and in parts show evidence of later mobilization, any succession must be regarded as tentative. The predominantly vertical foliation of the gneisses strikes north-north-west to south-south-east, thus paralleling the main structural axis of the Antarctic Peninsula; the only variations recorded were on the two easternmost outcrops, where the strike is east–west and the dips range from 30° to the north to vertical. Also, on the western margin, both at Gurney Point and south of Chapman Glacier, the dip ranges from 25° to 45° to the east, and in the highly sheared zone, 15 km east-north-east of Gurney Point, the dip of the schistosity varies from 50° to vertical. The deflection of the foliation in the metagabbros at station KG.525 (p. 26) is the only recorded occurrence of a second foliation.

A. White Granites

The white granites probably comprise the oldest rock unit of the metamorphic complex. Since the present composition of the white granites is in part due to potash metasomatism, their origin is even more enigmatic than that of the quartz-plagioclase-amphibolites.

The white granites definitely pre-date the older of the two amphibolite groups but, although they are in contact with the banded gneisses, their age relationship was not positively established. On their degree of deformation, however, the white granites appear to be older than the banded gneisses.

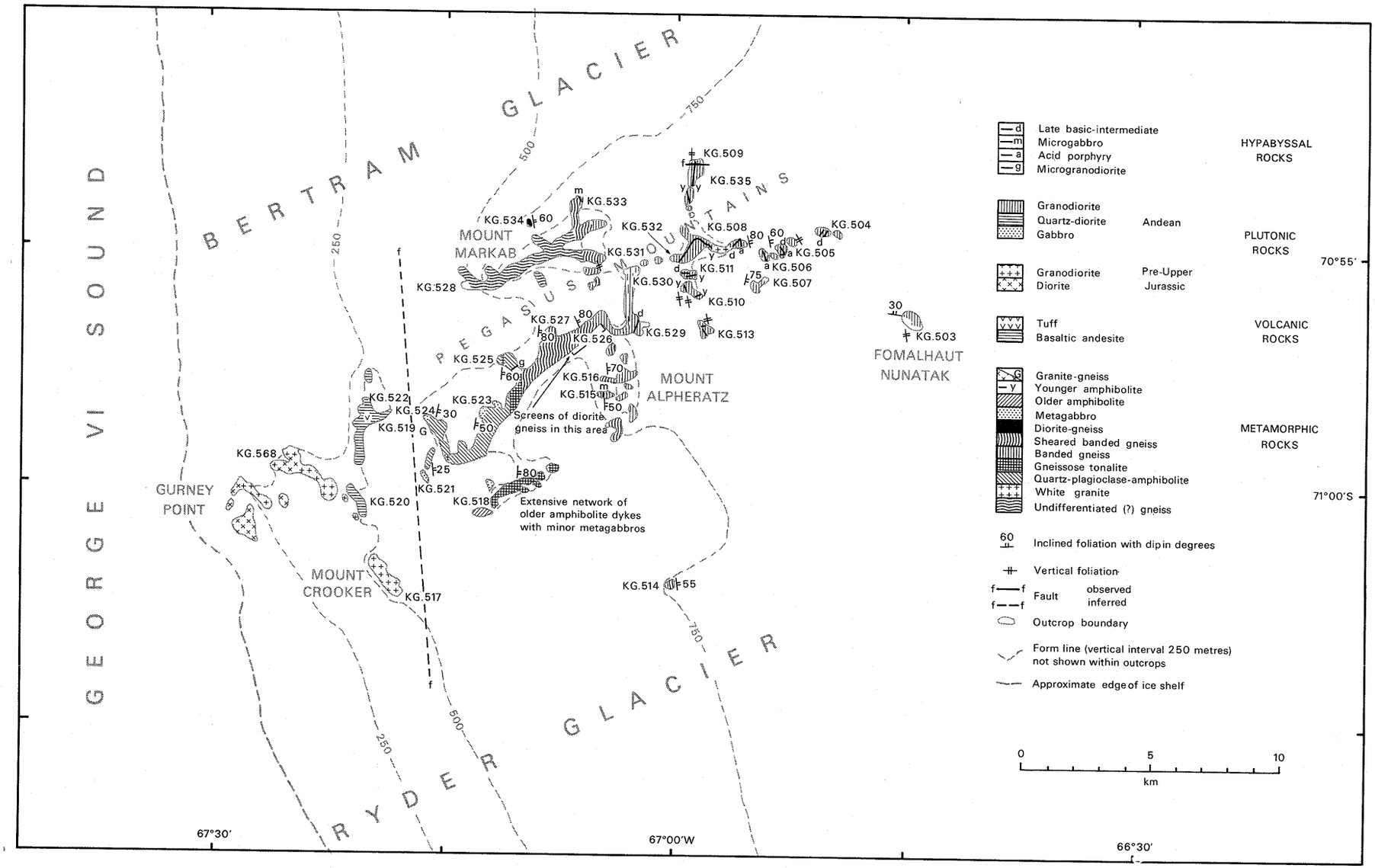

Fig. 2. Geological sketch map of the area east of Gurney Point, showing geological stations.

Table II. Stratigraphy and evolution of the metamorphic complex.

Parent rock	*Metamorphic rock*	*Metamorphic event*	*Metasomatism*
	Sheared banded gneisses		
	Younger amphibolites	Third metamorphism	Minor potash
Basic dykes →			
Basic dykes →	Older amphibolites	Second metamorphism	
Gabbros →	Metagabbros		
Diorites →	Diorite-gneisses		
			Potash
Tonalites →	Banded gneisses	First metamorphism	
	Quartz-plagioclase-amphibolites		
	White 'granites'		
(?) Basic tuffs with quartz →			
(?) Granites →			

1. Field description

These rocks form much of Auriga Nunataks (KG.536–539) and, although they extend continuously over 4 km, there appears to be little change in the bulk composition despite conspicuous local heterogeneity. In the field, the main variants are the colour index and the quartzitic lenses, although staining with sodium cobaltinitrite and potassium rhodizonate shows that the distribution of the potash feldspar is also random. At the northern tip (KG.538) are bands of a greyish white foliated rock which resemble the flow-banded Andean granodiorite (p. 67), whereas on the two nunataks near the south-eastern corner there is a marked absence of ferromagnesian minerals, their place being taken by pale pink garnets. On the more southerly of these two nunataks the white granites pass into banded biotite-gneisses with predominantly concordant but occasionally cross-cutting veins of purplish quartzite.

White granites occur beneath the banded gneisses at Fomalhaut Nunatak (station KG.503), and near the base of the outcrop the rocks are banded (the result of alternating garnet and quartz-rock layers), whereas massive blue potash feldspars are patchily developed.

Possibly the only occurrences of white granites within the banded gneisses are at station KG.507 and on the summit of station KG.508, eastern Pegasus Mountains, where the coarse white rock is studded with magnetite crystals up to 5 mm in size, although it is noticeably deficient in ferromagnesian minerals.

2. Petrography

The white granites are massive rocks (commonly iron stained on weathered surfaces) composed mainly of bluish white feldspar with lenses of brown quartz, and pale pink garnet (up to 5 mm in diameter) which occur sporadically or in bands 5–9 mm thick. In specimen KG.503.1 (Table III, analysis 1) the texture is granoblastic lobate or amoeboid, most of the rock comprising a mosaic of xenoblastic strained quartz with common inclusions of feldspar, chlorite and rutile. Most of the remainder is microperthitic orthoclase with common lobate and rounded inclusions of quartz, whereas plagioclase is restricted to small myrymekitic intergrowths with quartz around the edges of the potash feldspar. Reddish brown biotite is frequently replaced by chlorite and calcite, and is common at station KG.503 but exceedingly rare at Auriga Nunataks. Sub-idioblastic almandine with rare inclusions of quartz (Fig. 5a) has been partly granulated and replaced by chlorite around the margins and along the numerous transverse cracks.

At the north-eastern corner of station KG.538 plagioclase (An_{31}) is locally dominant, although overall the two feldspars appear to be present in equal proportions. The plagioclase is often interstitial and may occur as inclusions in the potash feldspar, suggesting potash feldspar has grown at the expense of plagioclase. Isolated clots (up to 5 mm in diameter) of pale green to colourless diopside (Fig. 5b) are a unique feature of specimen KG.538.2. Marginal replacement of the diopside by hornblende (α = yellow, β = green, γ = pale blue-green and $\gamma : c = 22°$), epidote and calcite is ubiquitous.

B. Quartz-plagioclase-amphibolites

1. Field description

Although quartz-plagioclase-amphibolites probably form most of the western half of the Pegasus Mountains, the exposures are generally inaccessible and they remain the least known of the metamorphic rocks. They are, however, amongst the oldest of the metamorphic rocks and enough is known about them to suggest they are metamorphosed volcanic rocks, probably tuffs.

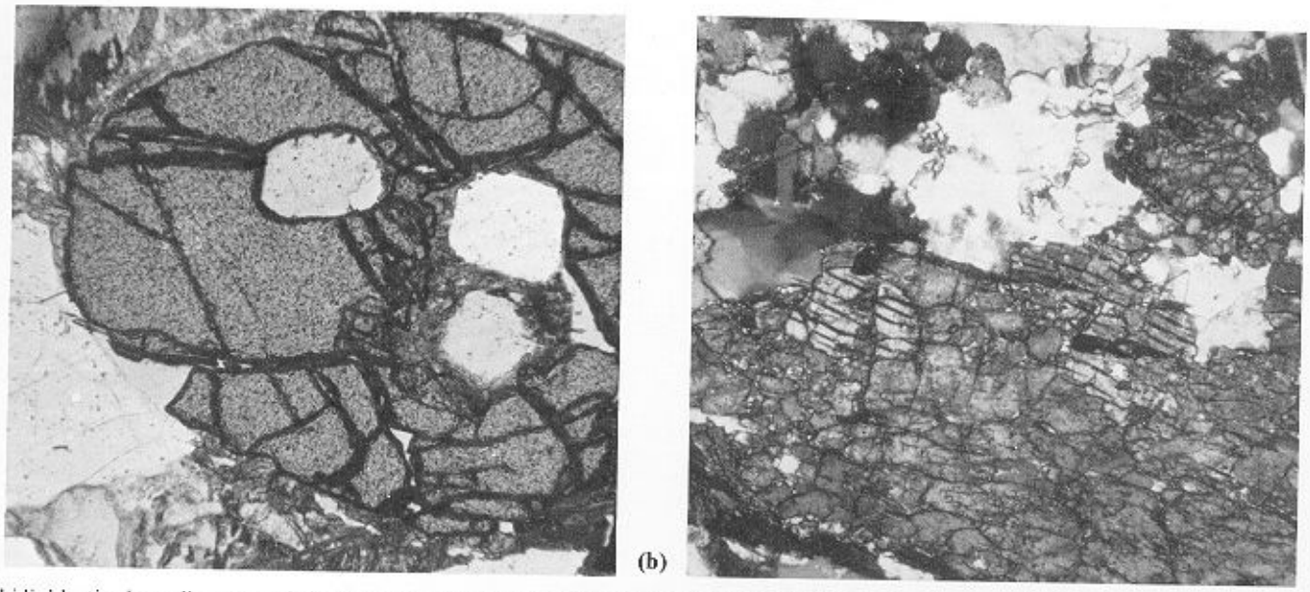

Fig. 5. a. Subidioblastic almandine garnet in white granite, showing rounded quartz inclusions and partial replacement by chlorite and biotite (KG.503.1; ordinary light; × 50). b. Diopside porphyroblast with marginal hornblende (dark) in white granite. The remainder is quartz, plagioclase and orthoclase (KG.538.2; X-nicols; × 50).

Fig. 6. Granite-gneisses ranging in thickness from 20 m (centre) to over 100 m (left) in quartz-plagioclase-amphibolites at station KG.524, Pegasus Mountains. A small metagabbroic boss forms the lower part of the spur on the right.

At the southern end of station KG.521 dark fine-grained amphibolites, showing little foliation, predominate but, traced to the north, they pass within a short distance into laminated quartz-plagioclase-amphibolites containing amphibolitic pods and lenses with characteristic fish-tail terminations. The lamination is the result of alternating hornblende and quartzo-feldspathic layers, which are frequently discontinuous and affected by tight isoclinal folding. Ranging in thickness from 1 to 3 mm, the laminae are thought to represent the original bedding. A well-developed foliation, defined by parallel orientation of the ferromagnesian minerals, generally parallels the lamination. At the western end of the main ridge (KG.524) these rocks are cut by a small metagabbro boss but, since the two rocks are mineralogically similar and the country rock is not laminated, it is difficult to delineate the boundary of the intrusion. On the cliffs behind this station (Fig. 6) two pink granitic dykes (approximately 20 m thick) have been intruded parallel to the foliation of the amphibolites and, to the east, most of the accessible lower slopes are composed of granite and metagabbro. At their easternmost occurrence (KG.525), the amphibolites are bounded on the northern side by metagabbro and tonalite, but they are separated from the sheared banded gneisses to the south by a 2 m wide microgranodiorite dyke. A typical specimen from this station is considerably more leucocratic than elsewhere, its darker fraction ranging from thin films to bands up to 7 mm thick which contain discontinuous white quartzo-feldspathic laminae. There is a strong foliation parallel to the bedding and a weak lineation.

2. Petrography

The quartz-plagioclase-amphibolites are medium-grained light green or grey rocks composed essentially of quartz, plagioclase, hornblende and biotite. Two of the three specimens examined in thin section (KG.524.2 and 525.10; Table III, analysis 4) possess plagioclase porphyroblasts (An_{26}) 1.0–1.5 mm long, or two to three times the average grain-size. These crystals are most probably products of the first metamorphism; despite the presence of Carlsbad-albite twinning and vague patchy zoning, survival of relict igneous textures through three periods of metamorphism (p. 43) is considered highly unlikely. Many of these feldspar crystals have recrystallized to aggregates of small grains with sutured margins; a few show polysynthetic twinning. Others have been partly replaced by granular quartz, or have irregular inclusions of potash feldspar, which may also be a replacement feature. The remainder of the rock comprises a hemigranoblastic amoeboid aggregate of plagioclase (An_{26}), quartz, hornblende and biotite with minor amounts of apatite and magnetite. The quartz shows strain shadows and sutured grain boundaries, evidence of post-crystalline deformation, whereas the hornblende is partly replaced by biotite, chlorite, epidote and sphene with magnetite cores. The third specimen (KG.521.9) is a more equigranular

Table III. Modal analyses of white 'granites' and quartz-plagioclase-amphibolites.

	KG.503.1	*KG.508.11*	*KG.521.9*	*KG.524.2*
Quartz	49.00	32.08	22.44	22.80
K-feldspar	24.56	50.48	–	tr.
Plagioclase	6.04	16.29	50.64	55.00
Hornblende	–	–	12.00	12.40
Biotite	2.04	–	10.28	2.40
Muscovite	–	0.06	–	–
Chlorite	4.48	0.03	0.32	–
Garnet	12.20	–	–	–
Magnetite	1.68	1.06	3.56	2.10
Sphene	–	–	0.40	0.80
Apatite	–	–	0.16	0.30
Epidote	–	tr.	0.20	4.20

tr. Trace.

KG.503.1 Garnetiferous white 'granite'.
KG.508.11 White 'granite'.
KG.521.9 Quartz-plagioclase-amphibolite.
KG.524.2 Quartz-plagioclase-amphibolite.

rock showing a variation in grain-size from 0.1 to 0.6 mm in the melanocratic laminae but constant at 0.3 mm in the leucocratic ones. The composition of the felsic element remains constant through the entire rock but hornblende is absent and biotite is somewhat restricted in the leucocratic bands.

A noteworthy feature of specimen KG.525.10 is a layer of hornblende (α = straw-yellow, β = green, γ = olive-green and $\gamma : c = 25°$) one crystal thick, in which individual grains may be up to 1 mm across. This is almost certainly a feature of the original composition, and of particular relevance to the origin of these rocks (p. 43).

C. Banded gneisses

1. *Nomenclature*

In the Pegasus Mountains, the country is dominated by a group of banded rocks composed of alternating layers of biotite-gneiss and granitic material, referred to collectively as banded gneisses. These rocks are believed to have originated from tonalites by metamorphic differentiation and subsequent potash metasomatism, and hence display a wide diversity of mineral proportions. To facilitate their description, the leucosomes which consist of quartz, potash feldspar and plagioclase, are referred to as 'granites', irrespective of the potash feldspar:total feldspar ratio. Biotite, plagioclase and quartz are the main constituents of the melanosomes, referred to as biotite-gneisses.

2. *Field description*

It is perhaps logical to describe first the two outcrops of tonalite; although separated from the banded gneisses by a microgranodiorite dyke and not part of the metamorphic complex. Strictly speaking, they probably represent the nearest approximation to the primary rock.

The largest exposure (3 km long and 200 m high) of undifferentiated tonalite occurs in the Pegasus Mountains and is medium- to coarse-grained with large pink feldspars and local wavy biotite partings. The second exposure lies 5 km to the north (KG.525) at the tip of a small spur projecting northward from the main ridge. This is one of the most critical exposures of the metamorphic complex (Fig. 7) upon which much of the stratigraphy is based. This rock differs from that of station KG.518 in having a higher proportion of potash feldspar, biotite and hornblende, and a more distinct foliation. The contact with the metagabbro may be sharp or gradational, and schistose amphibolitic pods are ubiquitous.

The process of differentiation is well-illustrated at station KG.503 where there is a vertical section of over 130 m and four distinct units can be determined. The lowest unit, which overlies 30 m of white granite, is a biotite-gneiss with discontinuous granitic bands, up to 2 cm in thickness, that are generally parallel to the foliation of the gneiss. Towards the top of the unit the amount of acidic material increases (Fig. 8), contacts become diffuse, and the bands broaden and rapidly

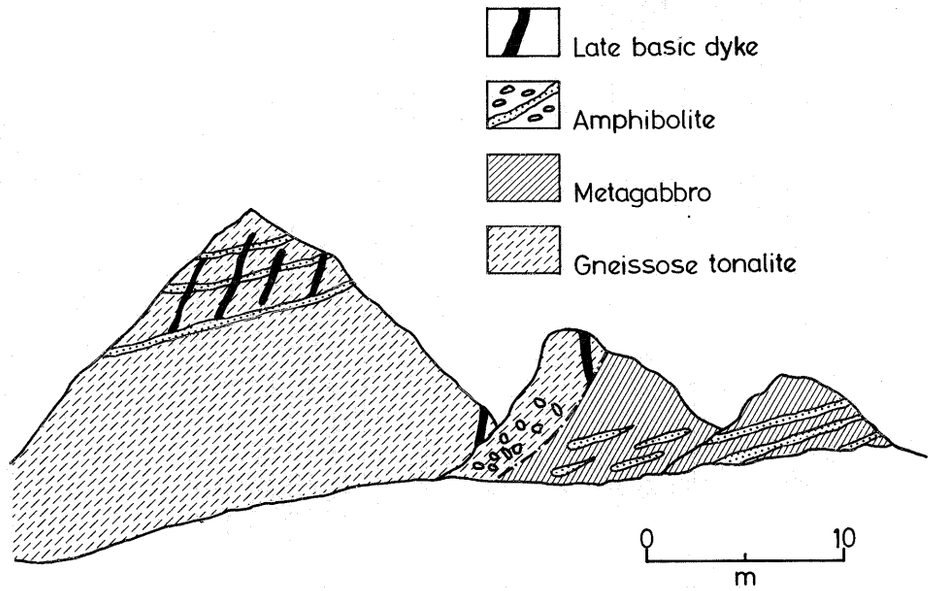

Fig. 7. Drawing from a field sketch of the north face of station KG.525, Pegasus Mountains, showing the contact between gneissose tonalites and metagabbros, and the variable deformation of amphibolite dykes.

Fig. 8. Biotite-gneisses at station KG.503, Fomalhaut Nunataks, with discontinuous granite bands and amphibolite rafts. The hammer shaft is 55 cm long.

Fig. 9. Top section of the lowest banded gneiss unit at station KG.503, Fomalhaut Nunataks, showing the transition from banded gneisses to granites with nebulitic biotite-gneiss. The hammer head is 20 cm long.

coalesce to form irregular acidic patches with ghost-like remnants of country rock (Fig. 9). These banded gneisses pass into the second unit, predominantly a medium-grained granite with porphyroblastic microcline and thin micaceous partings, that impart a wavy foliation to the rock. The sequence is repeated in the third and fourth units.

A similar granite forms the two nunataks of station KG.504, where the potash-feldspar porphyroblasts (after plagioclase) range up to 3 cm in length and have a common orientation (Fig. 10) that is probably a feature of the original rock. Likewise, in the banded gneisses at station KG.505 the leucosome reaches almost pegmatitic proportions (Fig. 11) and the melanosome is studded with microcline porphyroblasts (Fig. 12). Relatively unaltered blastoporphyritic gneissose tonalites occur at the western end of station KG.508. They pass westward through banded gneisses into pink granites and give way in turn to white granites at the summit.

The banded gneisses and tonalites contain amphibolitic dykes which are frequently reduced to lines of isolated rafts and pods. The amphibolites are in turn invaded by acid veins, 1–1.5 cm thick, locally traversing the gneisses but mostly stemming from the leucosomes. The course taken by these veins within the amphibolites is variable: some appear to penetrate only a few millimetres, although the colour index of the surrounding amphibolites suggests a certain amount of diffusion might have occurred (Fig. 13); others cross the dyke with little variation in thickness or direction, whereas many are ptygmatically folded (Fig. 14) with characteristic attenuation of limbs and thickening of cores. These folded veins always occur in those amphibolites possessing distinct foliations, to which the axial planes of the folds are always parallel. This suggests they were relatively straight when intruded, but were deformed some time afterwards and synchronously with the recrystallization of the amphibolites. Veins of white pegmatite, ranging in width from 1 to 8 mm, which cut the mobilizates and have diffuse borders against the leucosomes (Fig. 13), are evidence of a second episode of mobilization.

Fig. 10. Orientated potash feldspar porphyroblasts and diffuse leucogranite bands in granite at station KG.504, eastern Pegasus Mountains. The hammer head is 20 cm long.

Fig. 11. Gently folded banded gneisses at station KG.505, eastern Pegasus Mountains. The photograph shows attenuated bands of biotite-gneiss and thin micaceous partings in coarse granite. The clinometer case is 10.5 cm square.

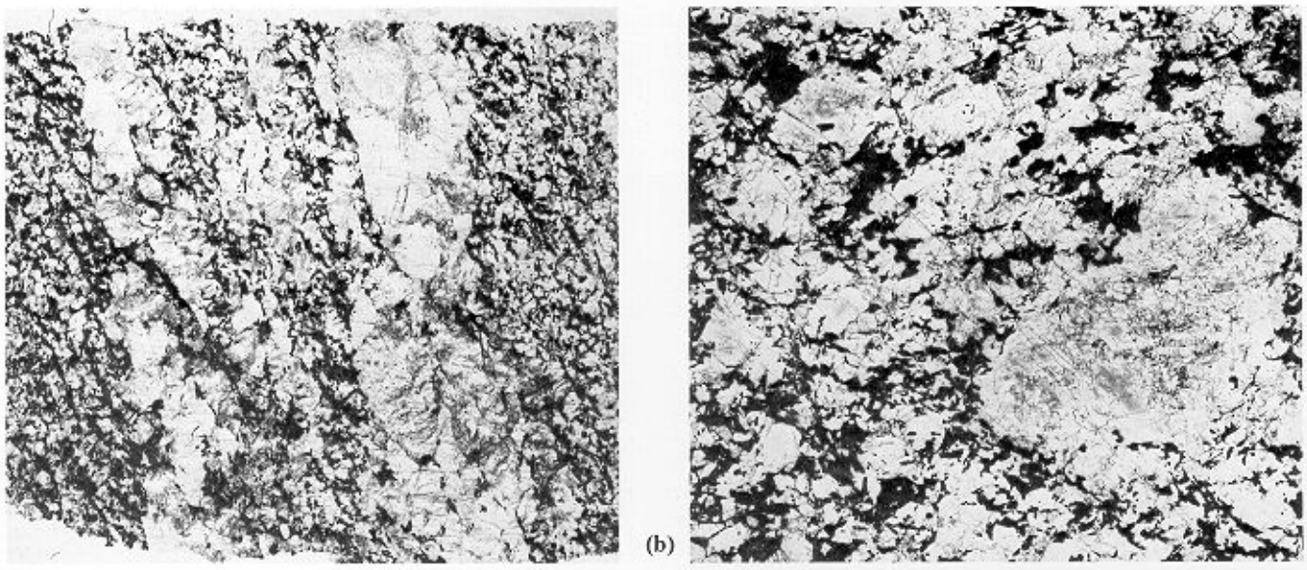

Fig. 12. a. Microcline porphyroblasts in biotite gneiss (KG.505.4; ordinary light; × 3). b. Blastoporphyritic plagioclase in a quartz-plagioclase-biotite aggregate (KG.508.2; ordinary light; × 3).

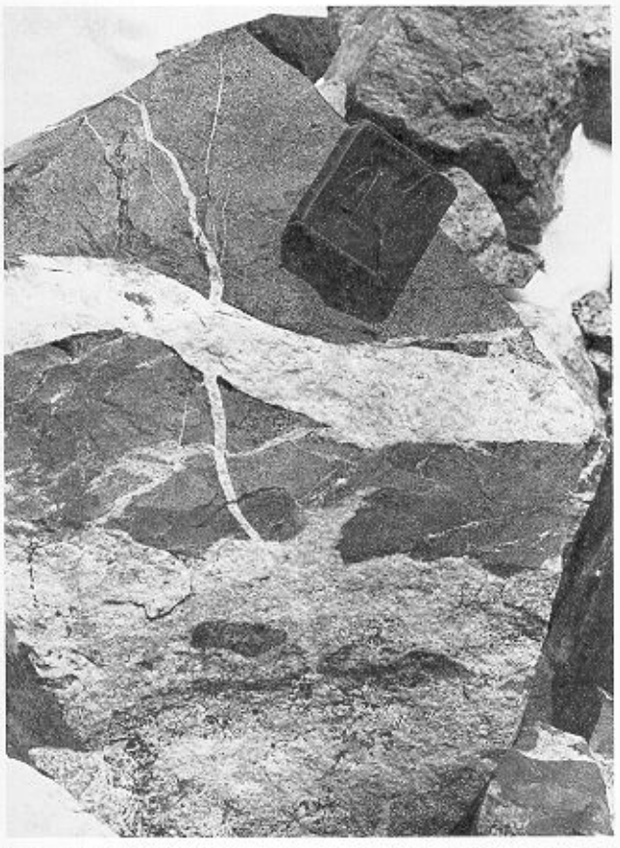

Fig. 13. Amphibolite raft penetrated by re-mobilized granite. The larger veins appear to represent a second episode of re-mobilization. The clinometer case is 10.5 cm square.

Fig. 14. Amphibolite raft and biotite-gneiss cut by a ptygmatically folded vein of re-mobilized granite. The clinometer case is 10.5 cm square.

3. Petrography

Although there are complete gradations between the tonalites and banded gneisses, it is convenient to consider each of the major rock types (tonalite, biotite-gneiss and granite) separately.

a. *Tonalite.* As a result of partial recrystallization, these rocks have a blastoporphyritic texture (Fig. 12b) defined by lath-like plagioclase (An_{28}) phenocrysts set in a hemigranoblastic aggregate of quartz, plagioclase and biotite. Despite the absence of obvious magmatic zoning, the idiomorphism of the phenocrysts, the predominance of Carslbad and Carlsbad-albite twinning and the presence of synneusis twins (Vance, 1961) leaves little doubt as to their igneous origin. The effect of the subsequent metamorphism on these crystals is somewhat varied. Some have simply been deformed plastically. Where the resultant grains are still in contact the intergranular boundaries are sutured, and where they are separated the cracks are filled with quartz. Others have undergone marginal recrystallization to aggregates of untwinned or polysynthetically twinned grains, but the majority have been replaced by quartz or more rarely by potash feldspar. Many of the larger quartz crystals are strained and have sutured margins, whereas recrystallized quartz has straight grain boundaries and 120° triple junctions, evidence of equilibrium having been reached (Spry, 1969). In specimens KG.506.1 and 525.5 sub-idioblastic hornblende (α = pale straw, β = green, γ = olive-green and $\gamma:c = 25°$) is mostly pseudomorphed by decussate aggregates of biotite similar to those which feature in all other specimens. By their intimate association with the pseudomorphs, it is concluded that magnetite and sphene have also developed from the hornblende during a period of retrograde metamorphism. Apatite is ubiquitous, whilst idioblastic allanite, mantled by pistacite, was found only in specimen KG.525.5. Because the potash was introduced into these rocks along well-defined narrow channels, the potash feldspar content is proportional to the distance of the rock from such channels, and in all cases the mineral grew at the expense of plagioclase. In specimen KG.508.2 indeterminate potash feldspar occurs within plagioclase as irregular blebs, resembling patch antiperthite, whereas in a thin section of specimen KG.518.6 one of the plagioclase phenocrysts is almost completely replaced and myrmekite has developed at the margins of many others. The progressive replacement of plagioclase and the origin of myrmekite are described on p. 17–21.

b. *Biotite-gneiss.* The biotite-gneisses are strongly foliated rocks with a great range of grain-size (medium- to fine-grained, granoblastic to porphyroblastic) depending on the degree of deformation and recrystallization. The finer-grained rocks (e.g. KG.509.1; Table IV, analysis 3) are a granoblastic amoeboid aggregate of quartz, plagioclase and minor potash feldspar with an average grain-size of less than 2 mm. Quartz is frequently aligned parallel to the foliation and the larger grains have irregular cracks and strain shadows. Small plates of interstitial biotite (α = pale straw and $\beta = \gamma$ = dark brown) are invariably aligned parallel to the foliation. Inclusions of ilmenite are common, particularly along the cleavage, and round the edges the biotite is replaced by pale green penninite. The inclusions of biotite within plagioclase orientated parallel to individual grains in the matrix suggest that some of the recrystallized plagioclase (An_{29}) has grown *in situ*. Myrmekitic intergrowths of quartz and plagioclase occur at the potash feldspar/plagioclase grain boundaries. These rocks which have only partly recrystallized possess blastophenocrysts of plagioclase (An_{27}) up to 2 mm long showing vague Carslbad-albite twinning. Minor amounts of zircon, apatite and magnetite are common in most rocks.

c. *Granite.* A coarse aggregate of microperthitic potash feldspar, plagioclase (An_{26-31}) and quartz with subsidiary mica (Table IV, analyses 6–8) characterizes the majority of the metamorphic complex granites. These rocks are dominated by sub-idioblastic potash feldspars up to 3 mm long (compared with less than 2 mm in the biotite-gneiss) with subsidiary plagioclase ranging from 0.1 to 1.5 mm. Minute needles of sericite are ubiquitous within the plagioclase, but in the microcline the development of this mineral is restricted to occasional flakes up to 0.5 mm wide. Quartz, strained and partly recrystallized, forms pools up to 3 mm in diameter, and biotite, including zircon crystals with

Table IV. Modal analyses of banded gneisses.

	1	*2*	*3*	*4*	*5*	*6*	*7*	*8*	*9*	*10*
Quartz	13.15	31.35	25.90	17.90	31.32	26.76	37.95	23.00	37.80	60.50
Potash feldspar	0.60	1.00	9.80	8.85	24.72	25.92	29.00	39.90	16.60	13.50
Plagioclase	61.80	54.50	32.74	48.85	29.80	39.16	29.95	31.95	36.10	4.50
Hornblende	–	–	–	–	–	–	–	–	1.20	–
Biotite	22.05	10.55	30.10	23.90	11.92	7.36	–	1.25	7.20	11.50
Muscovite	–	–	–	–	1.44	–	0.35	1.75	–	8.5
Chlorite	0.15	0.95	–	–	tr.	0.40	1.65	1.70	0.20	–
Magnetite	1.00	0.70	0.47	0.10	0.44	0.28	0.40	0.40	0.30	0.50
Sphene	0.95	0.40	0.05	–	–	0.04	–	–	0.40	–
Apatite	0.30	0.25	0.94	0.40	0.36	0.08	–	0.05	0.10	0.30
Epidote	–	0.30	–	–	–	–	0.55	–	0.10	0.20
Calcite	–	–	–	–	–	–	0.15	–	–	0.50

tr. Trace.

1. KG.508.2 Tonalite.
2. KG.518.6 Tonalite.
3. KG.509.1 Biotite-gneiss.
4. KG.505.4 Banded gneiss.
5. KG.505.1 Banded gneiss.
6. KG.506.7 Granite
7. KG.503.4 Granite.
8. KG.505.2 Granite.
9. KG.525.5 Granodiorite.
10. KG.515.1 Quartz-mica-schist (sheared banded gneiss).

pleochroic haloes, is only sparingly developed. Allanite is uncommon but may form crystals up to 1.5 mm long. It is difficult to generalize about the types of potash feldspar present in the banded gneisses; some rocks possess only orthoclase but others have both orthoclase and microcline, whilst a few have microcline and no recognizable orthoclase.

Verification of these essentially optical determinations was obtained by X-ray diffraction (Fig. 15). Thus, in those rocks in which no microcline twinning was observed (e.g. KG.510.4 and 529.3), the single sharp peak at $2\theta = 29.8°$ denotes the exclusive presence of a monoclinic potash feldspar (orthoclase). The somewhat less sharply defined peak of specimen KG.503.4 reflects small amounts of microcline which, in thin section, shows poorly defined cross-hatch twinning. For those rocks in which such twinning is common and sharply defined, the traces obtained signify potash feldspars of variable obliquity, with orthoclase still much in evidence (cf. Parsons and Boyd, 1971). The third category noted in this section, that of (apparently) microcline alone, is typified by specimen KG.529.1. However, even here, X-ray diffraction revealed traces of orthoclase, with the apparent implications that most of the microcline is inverted orthoclase. The two remaining diffractometer traces (KG.503.1 and 508.11) were obtained from potash feldspars of white 'granites' and, since their structural states conform to the overall geographical distribution in the banded gneisses, it must be assumed that growth in the two rock types was synchronous.

Within any specific outcrop, however, the same polymorph is common to both leucosome and melanosome (Fig. 16). No distinction between orthoclase and microcline can be made on the grounds of shape and size, for both show complete gradations from sub-rounded interstitial grains to sub-idioblastic porphyroblasts. In those rocks containing orthoclase and microcline the relationship is far from clear, especially since they are seldom in contact with each other. However, in several specimens (e.g. KG.510.3) large orthoclase plates were seen to enclose sub-rounded microcline with well-developed cross-hatch twinning. The shape of the microcline grains is reminiscent of the plagioclase which occurs within many of the potash feldspars, suggesting that the microcline is merely 'mopping up' the plagioclase which remained after the initial (orthoclase) potash metasomatism. The presence in many of the microcline crystals of patchy, ill-formed cross-hatch twinning (Fig. 17a) is also indicative of an origin by replacement of plagioclase (Smith, 1962, p. 249). In many gneisses the potash feldspar has untwinned cores and strongly twinned margins (Fig. 17b) which, like the accompanying undulose extinction (Heier, 1961), is thought to indicate a metamorphic transition from orthoclase to microcline. In conclusion, two periods of potash metasomatism occurred, producing first orthoclase and then microcline, but both at the expense of plagioclase. It will be shown later (p. 44) that the second episode was of relatively limited extent and is more likely to have resulted from the re-distribution of potash than from further introduction of potash into the metamorphic complex. Since orthoclase was unstable under the prevailing pressure-temperature conditions, widespread inversion to microcline took place during the second episode.

Many of the plagioclase blastophenocrysts contain patchy antiperthite, whose orientation appears to be controlled by the cleavage directions (Fig. 17c and d). The potash feldspar may form over half of an individual crystal (Fig. 17e and f). This is considerably more than the plagioclase could conceivably dissolve (Sen, 1959), and it must therefore be the product of replacement rather than exsolution. The potash feldspar porphyroblasts are frequently rimmed by narrow zones of granular sericitized plagioclase (occasionally myrmekitic) (Fig. 17a and b), apparently identical in composition to the primary plagioclase. They are particularly common between adjacent potash feldspar crystals but rarely develop against quartz. It is evident, from their absence at other crystal boundaries, that the origin of this granular plagioclase is related to the presence of potash feldspar and is intimately connected with the development of myrmekite. In addition to the localities listed above, myrmekite also forms epitaxially on primary plagioclase, but only (Fig. 18a and b) where the plagioclase–potash feldspar boundary is a high-angle boundary, i.e. above 10–15° (Voll, 1960).

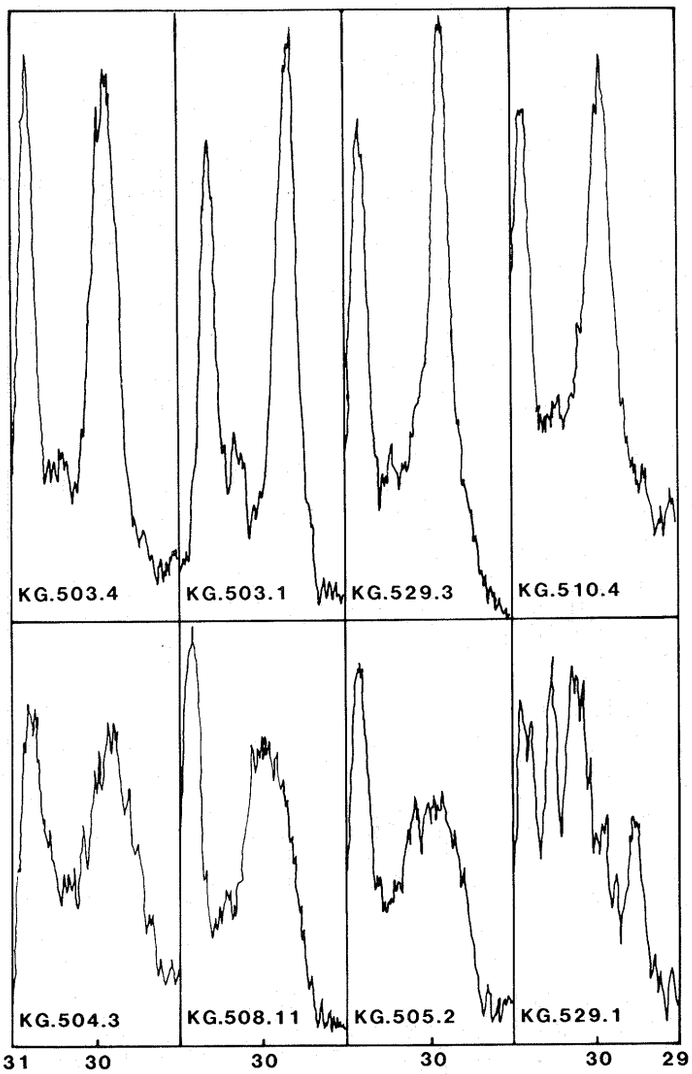

Fig. 15. Examples of X-ray diffraction traces between 29° and 31° 2θ for potash feldspar from white granites and banded gneisses. The instrument settings used were: ratemeter 2×10^2; time constant 2; slits 2°–0.2°–2°; scanning speed 1° 2θ/min; chart speed 160 mm/h; Cu Kα radiation.

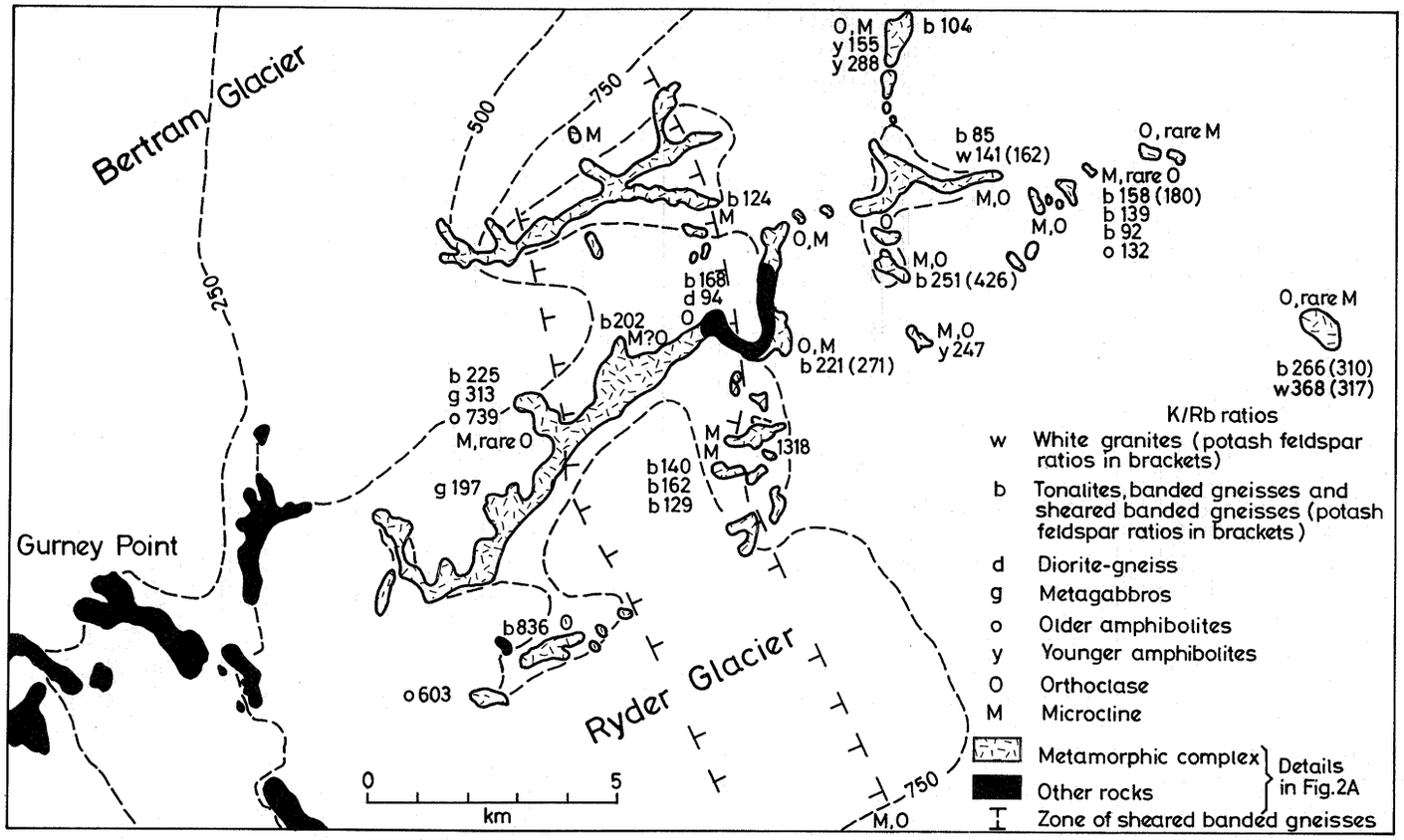

Fig. 16. Sketch map of the western Pegasus Mountains illustrating the geographical distribution of potash feldspar polymorphs in the banded gneisses and the zone of sheared banded gneisses, and the variations in whole-rock and potash feldspar K/Rb ratios.

Myrmekite (Becke, 1908) consists of wart-like intergrowths of quartz and plagioclase, seldom exceeding 1 mm in diameter, which are predominantly convex towards the potash feldspar. The quartz worms are normally elongated quasi-parallel to the direction of growth (Fig. 18c), and terminate inwards in blunt lobes from which apparently detached drops extend. In the immediate vicinity of the myrmekite–potash feldspar contact there are occasionally narrow rims of fresh, more albitic plagioclase in which the quartz rods are finer and more tightly packed (Fig. 18d).

Discussion on the origin of myrmekite was initiated by Becke (1908), who postulated that such intergrowths resulted from sodium and calcium metasomatism of potash feldspar:

$$2KAlSi_3O_8 + Ca^{2+} \rightarrow CaAl_2Si_2O_8 + 4SiO_2 + 2K^+$$
$$KAlSi_3O_8 + Na^+ \rightarrow NaAlSi_3O_8 + K^+.$$

Harker (1909, p. 261) and Schwantke (1909) suggested that myrmekite forms by exsolution from an originally homogeneous feldspar phase richer in SiO_2 than the stochiometric feldspar composition, a theory which has found increasing support in recent years, e.g. Carman and Tuttle (1963), Hubbard (1966, 1967), Carstens (1967), Mehnert (1968), Phillips and Ransom (1968), Widenfalk (1969), Barth (1969) and Sturt (1970). Shelley (1964, 1966, 1967, 1969, 1970), on the other hand, believed that myrmekite formed by the incorporation of recrystallized quartz into albite exsolved from potash feldspar. However, a review of the literature, e.g. Barker (1970), does suggest that myrmekite can form either by exsolution or by metasomatism, and it only remains to decide which process was operative in the present rocks.

Some exsolution (unmixing) has occurred in most of the potash feldspars but nowhere are these perthites associated with myrmekite, and it is difficult to explain the similarity in composition of myrmekite and primary feldspar with such an origin. On the other hand, it has been shown that these rocks have undergone extensive potash metasomatism, a process which should produce sodium and calcium in the ratio of the primary plagioclase.

Potash feldspar appears to nucleate simultaneously at several points within a particular plagioclase crystal (Fig. 19a), and subsequent enlargement will cause the ousted sodium and calcium to migrate out towards the crystal boundaries (Fig. 19b). When the potash 'front' approaches a high-angle intergranular boundary, diffusion of Ca and Na is inhibited and small plagioclase crystals will become isolated (Fig. 19c). The more active paths of diffusion, viz. the tongues of potash feldspar between the plagioclase grains, will continue to function and replacement of plagioclase will continue. The displaced Ca and Na again diffuse away but it is unable to leave the plagioclase with the result that the crystals begin to grow at the expense of potash feldspar, and myrmekite forms according to Becke's equation (Fig. 19d).

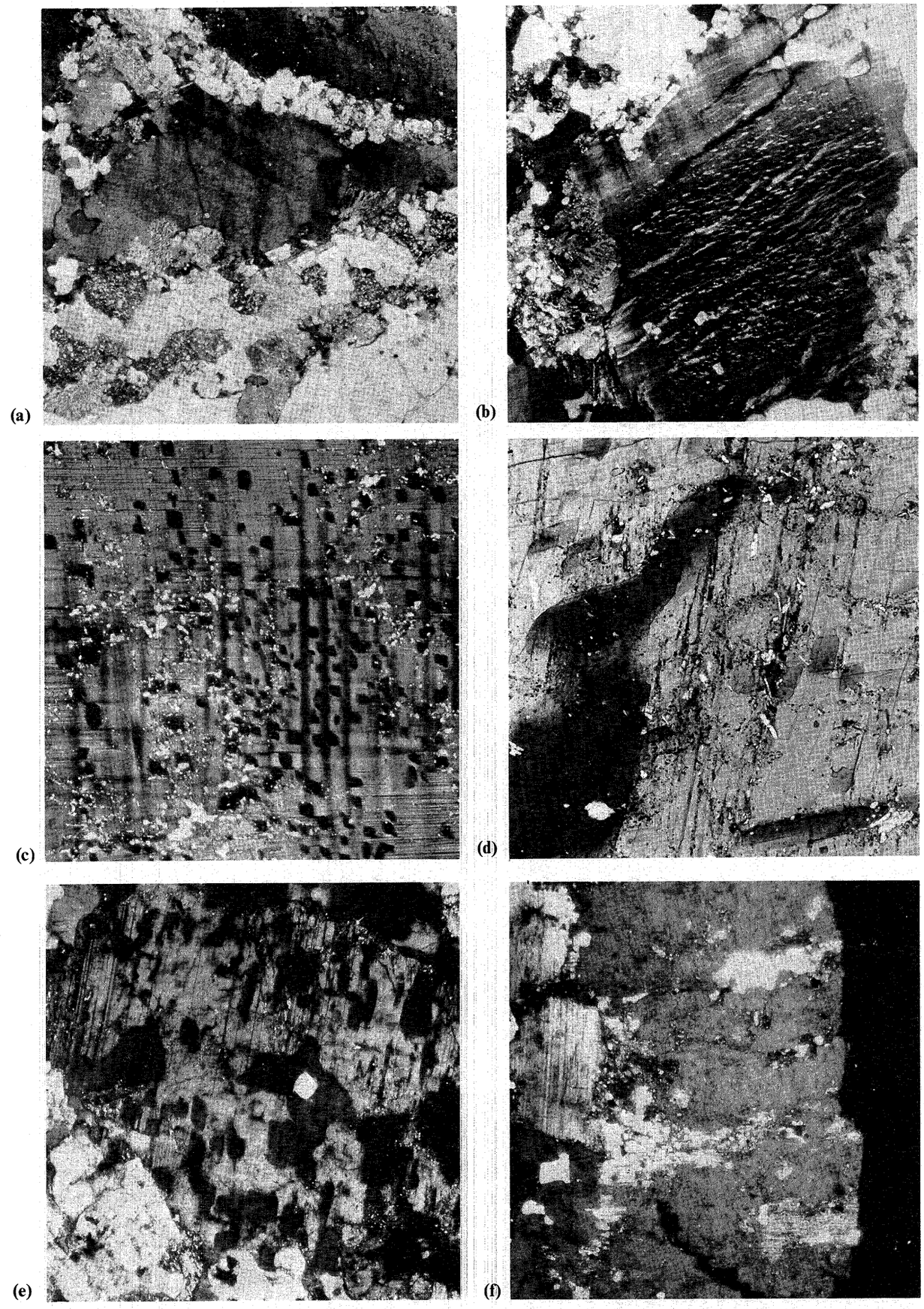

Fig. 17. a. Potash feldspar with poorly developed cross-hatch twinning and marginal granular myrmekitic plagioclase (KG.506.7; X-nicols; × 60). b. Potash feldspar porphyroblast showing marginal cross-hatch twinning and undulose extinction, indicating a metamorphic transition from orthoclase to microcline (KG.506.7; X-nicols; × 60). c–f. Progressive replacement of plagioclase by potash feldspar. c. Nucleation: regularity of outline appears related to cleavage directions in host plagioclase (KG.504.3; X-nicols; × 60). d. Prolonged growth: regular outline disappears (KG.504.3; X-nicols; × 200). e. Prolonged growth: potash feldspar patches begin to coalesce (KG.503.4; X-nicols; × 45). f. Prolonged growth; almost total replacement of plagioclase (KG.518.6; X-nicols; × 25).

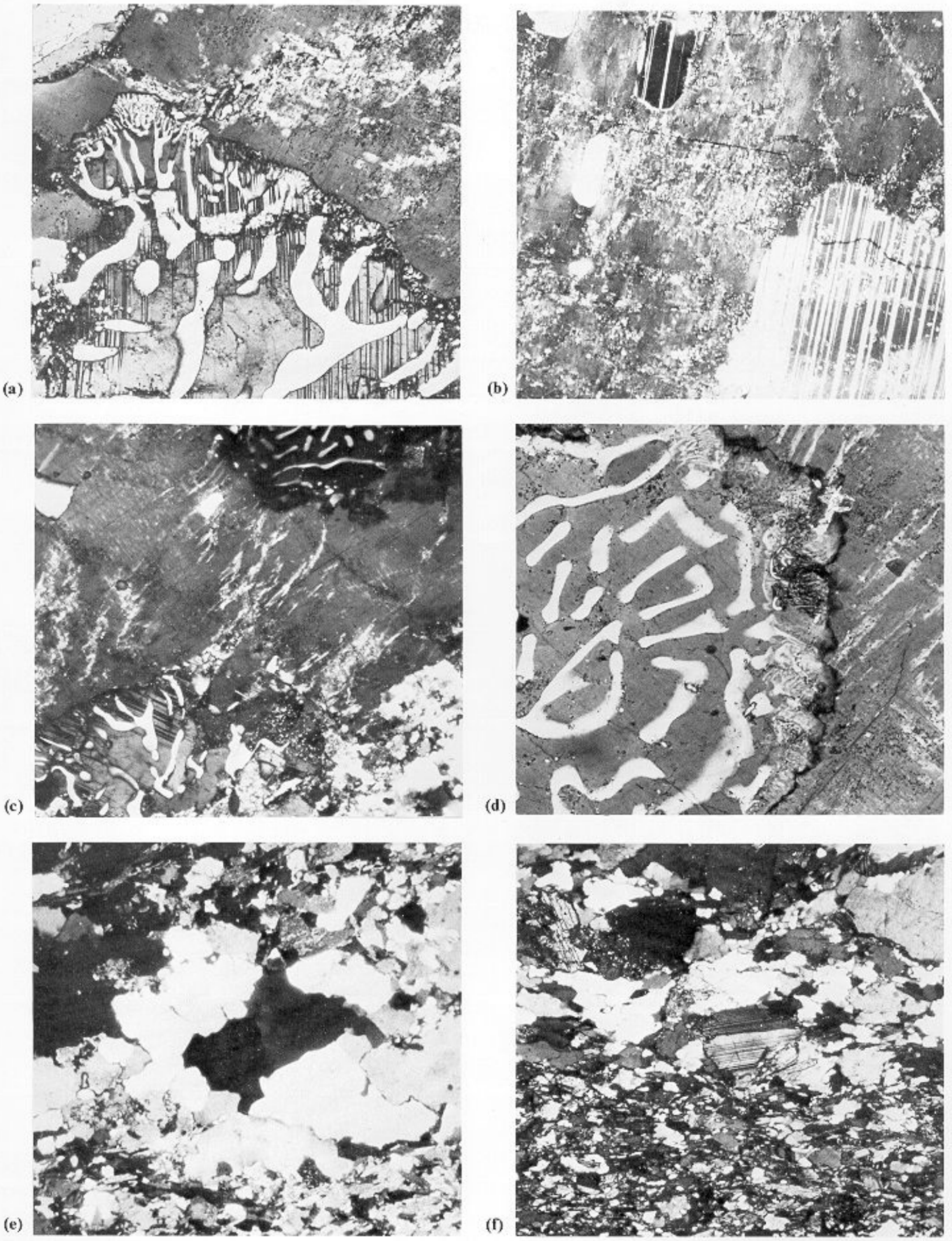

Fig. 18. a–d. Growth of myrmekite in banded gneisses. a. Development of myrmekite at high-angle boundary between plagioclase and orthoclase (KG.504.3; X-nicols; ×235). b. Plagioclase within the same orthoclase plate rimmed by more albitic plagioclase. Because it is structurally concordant with the host, no myrmekite has developed (KG.504.3; X-nicols; ×60). c. Myrmekitic plagioclase marginal to and within microperthitic orthoclase (KG.504.3; X-nicols; ×105). d. Myrmekite rimmed by more albitic plagioclase in which the quartz rods are smaller and more tightly packed (KG.504.3; X-nicols; ×240). e. Quartz–microcline vein in biotite-gneiss (KG.509.1; X-nicols; ×30). f. Quartz–plagioclase–epidote vein cutting amphibolite dyke (KG.518.5; X-nicols; ×55).

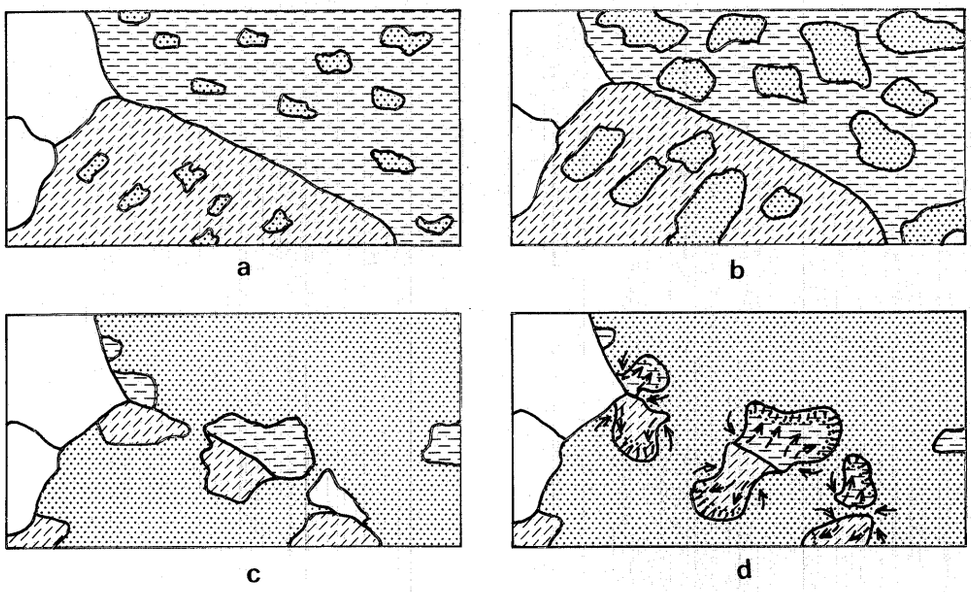

Fig. 19. a–d. Hypothetical model demonstrating the probable method of myrmekite growth in banded gneisses. Quartz, white; plagioclase, dashed lines; potash feldspar, stippled; myrmekitic quartz, shaded. Diffusion tracks of K and Ca + Na are shown by continuous and broken arrows, respectively.

This still leaves the question of why some of the myrmekitic quartz extends into the potash feldspar and why some of the myrmekite has a rim of more albitic plagioclase. These features are most simply explained by postulating a similar but more limited period of potash metasomatism which occurred during a subsequent lower-grade metamorphism. Under such conditions, any plagioclase formed would be rather more sodic than the primary plagioclase.

d. *Re-mobilized granites.* The textures and compositions of these mobilizates are essentially similar to those of the adjacent acidic rocks, although the proportion of mafic minerals is rather less. Consequently, in specimen KG.509.1 (the only recorded instance of a ptygmatically folded vein in biotite-gneisses), microcline and quartz predominate (Fig. 18e), whereas in specimen KG.518.5 the veins consist of magmatically zoned and twinned plagioclase (An_{33}) with smaller amounts of quartz and only rare potash feldspar (Fig. 18f). It is probable that such veins were emplaced in tension gashes in a semi-crystalline state and under strong hydrostatic pressure.

D. Sheared Banded Gneisses

1. Field description

Banded gneisses which have been subjected to strong dynamic metamorphism occur within a belt 3 km wide extending across the breadth of the Pegasus Mountains. At station KG.514, a remote nunatak in Ryder Glacier, granites with a marked greenish hue pass eastward into greenish quartz-mica-schists possessing large augen of white feldspar similar to those in the granites. The quartz-mica-schists attain their maximum thickness (300 m) 8 km to the north on the western flank of Mount Alpheratz. On the southern summit ridge (KG.515) thin quartzitic partings, which are frequently folded and boundinaged, give rise to a distinctly banded rock within which are two horizons (the lower 9 m and the upper 27–36 m) of orange-yellow siliceous schists with thin often discontinuous micaceous partings (Fig. 20). On the higher slopes the schists appear to pass into granitic rocks. The eastern margin of the shear zone occurs at a much lower level on the ridge immediately to the north (KG.516), where over a distance of approximately 30 m, granites typical of those to the east, pass through granitic augen-gneisses into quartz-mica-schists. Separated from this exposure by a pluton of Andean granodiorite, the rocks of station KG.531 comprise highly sheared granites and well-cleaved bluish grey siliceous schists with biotite-rich bands. West of the quartz-mica-schist band, at least six 3–6 m wide bands of granitic augen-gneiss occur within the diorite-gneiss at station KG.526, the contacts being concordant with the foliation; still farther west, station KG.527 is composed of banded gneisses with plagioclase augen.

2. Petrography

a. *Granitic augen-gneisses.* These rocks (e.g. KG.514.1 and 526.2), which represent partly recrystallized granites, are characterized by a flaser structure in which a fine intergrowth of quartz and biotite is wrapped around large feldspar porphyroblasts (Fig. 21). In common with the undeformed banded gneisses, the relative proportions of two feldspars is variable. In specimen KG.514.1, characteristically twinned microperthitic microcline is up to 3 mm in length, whereas strongly deformed and heavily sericitized plagioclase (An_{28}) rarely exceeds 0.75 mm. However, at station KG.516, plagioclase (An_{36-45}) with oscillatory zoning and Carlsbad-albite twinning occurs in lath-like or equidimensional blastophenocrysts (1–2 mm long), whose longer axes are either parallel or sub-parallel to the foliation, and microcline is absent or only sparingly developed. The slightly smaller quartz augen

Fig. 20. Sheared banded gneisses at station KG.515. The outcrop consists principally of quartz-mica-schists but two bands of siliceous schist (arrowed) are also visible, the upper being 27–36 m thick.

Fig. 21. Mylonitic biotite-gneiss (KG.514.1; ordinary light; × 3).

have recrystallized; locally they show straight grain boundaries and 120° triple junctions but strain shadows and sutured margins are the norm, and in the more highly deformed rocks a second marginal recrystallization is present. Minute grains of green hornblende are present within some of the plagioclase in specimen KG.516.4, but in all other rocks chloritized biotite forms a felted aggregate intergrown (in specimen KG.514.1) with flakes of muscovite, sphene and allanite. Transverse cracks, 0.5 mm wide (Fig. 22), are filled with epidote, calcite, granular magnetite and occasional quartz; adjacent plagioclase is partly masked by a fine red-brown dust.

b. *Quartz-mica-schists.* The quartz-mica-schists, which are considered to be recrystallized granites and biotite-gneisses, are extremely fissile (Fig. 23), medium- to fine-grained banded rocks in which small open folds are commonly developed. A thin section (KG.515.1; Table IV, analysis 10) revealed a granoblastic aggregate of quartz, muscovite, biotite and some plagioclase, with an average grain-size of <0.1 mm. Quartz, which is commonly flattened, has undulose extinction and frequent inclusions of muscovite. Microcline is restricted to the axial planes of micro-folds; it is heavily sericitized and the needles, like the host, parallel the fold axial planes. Muscovite is interstitial to quartz and commonly altered to pale green chlorite; biotite forms slightly smaller plates and is frequently associated with sphene. Rounded grains of magnetite, unlike idioblastic pyrite, form trains parallel to the foliation. The quartzitic bands (average grain-size 1 mm) are practically monomineralic and are probably the products of metamorphic differentiation.

In contrast, the siliceous schists are characterized (Fig. 24a) by large relict grains of quartz, microcline and rare plagioclase (An_{37}) set in a granular aggregate of the same minerals. Composite augen, up to 3 mm long contain microperthitic microcline and granular quartz (Fig. 24b), the latter forming mainly in the corners of the eyes, but also surrounding the potash feldspar. Quartz locally forms up to half the volume of the augen and is regarded as a product of the replacement of plagioclase by potash feldspar. The only mica is muscovite, present in fibrous aggregates wrapped around the porphyroblasts.

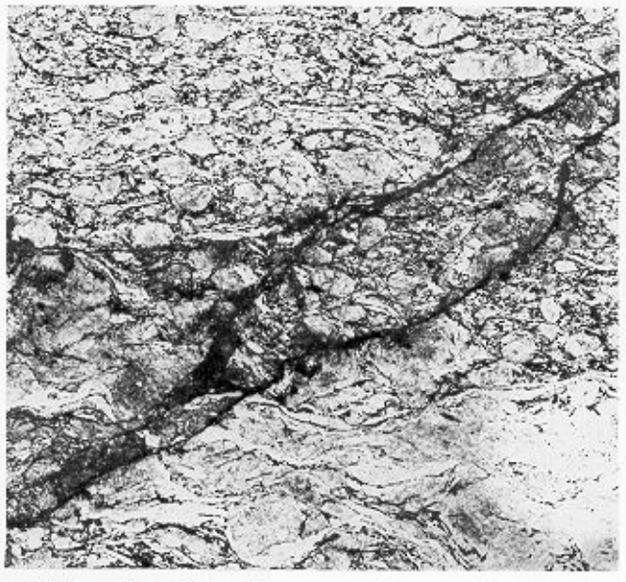

Fig. 22. Oblique shear in granitic augen-gneiss containing epidote, calcite, magnetite and quartz. The dark coloration in the adjacent feldspar is due to fine red-brown dust (KG.516.3; × 3).

Fig. 23. Quartz-mica-schists at station KG.515 showing extreme fissility and thin quartzitic partings. The darker rock is microgabbro. The hammer head is 20 cm long.

E. Diorite-gneisses

1. Field description

Diorite-gneisses, intruded by amphibolite dykes and *lit-par-lit* granite-gneisses (Figs 25 and 26) form most of the coastal cliffs between Chapman Glacier and Creswick Peaks. Before the emplacement of the acid gneisses, the diorite-gneisses were partially mobilized and the basic dykes were reduced to lensoid bodies 1.8–15 m by 0.6–0.9 m intruded by ptygmatically folded veins of coarse diorite. At station KG.526, central Pegasus Mountains, several 50–200 m wide dykes of diorite-gneiss occur within granitic augen-gneisses, and at the eastern end of the ridge one such intrusion is in contact with Andean granodiorite.

2. Petrography

At station KG.526 a medium- to coarse-grained foliated aggregate of white feldspar and greenish amphibole is the dominant rock (e.g. KG.526.2; Table V, analysis 1). It has a distinctly mylonitic texture and contains plagioclase blastophenocrysts, ranging from 0.5 to 2 mm, which frequently have their longest axes aligned parallel to the foliation. Although there is no obvious zoning, some of the larger crystals are calcic andesine (An_{46}), whilst the majority are sodic andesine (An_{32}). Within the phenocrysts are small areas of granular feldspar with sericite and finely divided iron ore, whilst marginal replacement by potash feldspar and quartz is a feature of many of the larger crystals. There are many characters of the plagioclase (e.g. shape, size, oscillatory zoning and the destruction of primary twinning by secondary glide twinning (Vance, 1961)) which indicate they are of an igneous origin and have only undergone slight modification in the subsequent metamorphisms. The orientation of the plagioclase phenocrysts is attributed to shearing stresses which were operative during the intrusion.

The hornblende (α = straw-yellow, β = green, γ = olive-green and γ: $c = 26°$) is poikilitic (Fig. 27a), being crammed

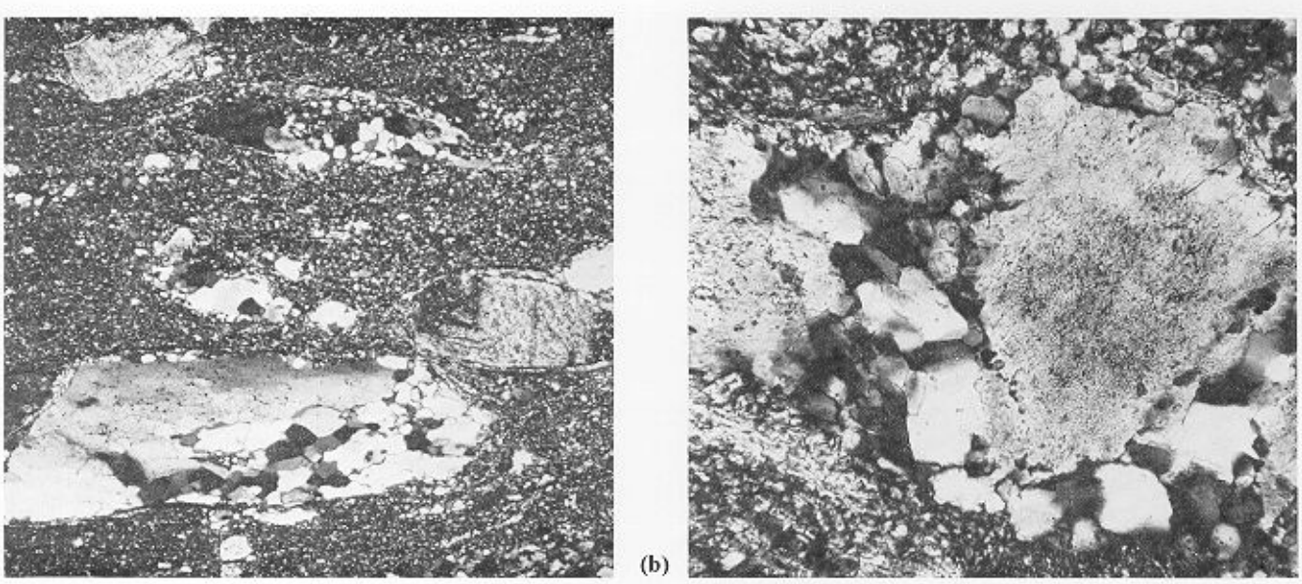

(a) (b)

Fig. 24. a. Siliceous schist from the zone of sheared banded gneisses. Quartz, strained and partly recrystallized, plagioclase and microcline in a fine aggregate of quartz, plagioclase and muscovite (KG.515.6; X-nicols; × 60). b. Composite porphyroblast comprising microcline and granular quartz in siliceous schist (KG.515.6; X-nicols; × 150).

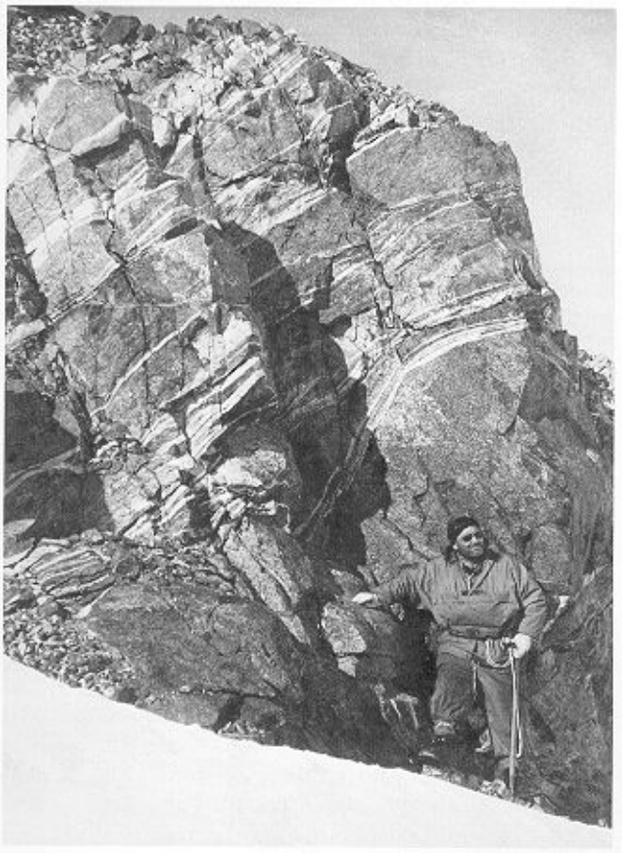

Fig. 25. *Lit-par-lit* injected granite-gneiss at station KG.573, 6 km north of Moore Point. The granitic bands parallel the foliation in the host rock.

Fig. 26. Diorite-gneisses at station KG.573 with amphibolite pods and thin veins of granite-gneiss. The hammer head is 20 cm long.

with rounded or lobate quartz, magnetite, and partly replaced by biotite. Such a texture is seen as a thermal overprint and probably developed during the intrusion of the adjacent Andean granodiorite. Exsolution of ilmenite along the cleavage traces of the biotite accompanied the development of pale green chlorite probably during a period of retrograde metamorphism. The remainder is a mosaic of granular quartz with occasional needles of apatite.

Mylonitic textures are more strongly developed in the coastal rocks, particularly those with low colour indices. For example, in specimen KG.576.1 (Table V, analysis 3) most of the rock has recrystallized to a granular mosaic (Fig. 27b), although rare hornblende blastophenocrysts are idioblastic. However, in specimen KG.573.3 (Table V, analysis 2) the plagioclase occurs in predominantly lensoid crystals (Fig. 27c) 2–3 mm long

Table V. Modal analyses of diorite-gneisses, metagabbros and amphibolites.

	1	*2*	*3*	*4*	*5*	*6*	*7*	*8*	*9*	*10*	*11*	*12*	*13*	*14*
Quartz	19.04	2.80	26.63	–	0.80	–	0.70	0.60	–	0.45	3.90	–	–	tr.
Potash feldspar	1.72	–	1.33	0.75	–	–	–	–	–	–	0.50	–	–	–
Plagioclase	56.04	59.00	58.20	75.00	71.15	28.90	41.95	29.30	31.10	58.60	57.40	33.06	25.20	41.85
Hornblende	7.52	33.80	3.66	18.00	21.23†	68.55	45.55	66.20	65.30	35.35	26.90	60.99	52.80	37.55
Biotite	13.46	–	5.32	–	3.83	0.65	6.60	0.50	–	0.45	4.80	–	16.60	11.00
Chlorite	0.44	2.60	2.46	4.10	0.03	–	1.55	1.40	–	0.10	4.80	–	–	0.25
Magnetite	1.60*	0.70	1.40	0.45	2.73	0.70	3.50	1.90	0.50	4.55	0.20	4.90*	4.10*	5.55*
Pyrite	–	–	–	–	–	–	–	–	–	–	–	0.48	–	–
Sphene	–	0.60	0.60	0.40	0.10	1.15	–	–	1.50	0.25	0.50	0.41	–	3.05
Epidote	–	0.30	0.40	1.00	–	0.05	–	–	1.60	–	0.90	–	1.30	tr.
Apatite	0.28	0.10	–	0.05	0.13	–	0.15	0.10	tr.	0.25	–	0.16	–	–
Allanite	–	0.10	–	–	–	–	–	–	–	–	–	–	–	–
Calcite	–	–	–	0.05	–	–	–	–	–	–	0.10	–	–	0.75

tr. Trace.
* Ilmenite.
† Includes 2.18% cummingtonite.

1. KG.526.2 Diorite-gneiss.
2. KG.573.3 Diorite-gneiss.
3. KG.576.1 Diorite-gneiss.
4. KG.523.5 Metagabbro.
5. KG.525.2 Metagabbro.
6. KG.516.2 Older amphibolite.
7. KG.505.3 Older amphibolite.
8. KG.536.1 Older amphibolite.
9. KG.525.1 Older amphibolite.
10. KG.518.1 Older amphibolite.
11. KG.541.1 (?) Older amphibolite (xenolith in Andean granodiorite).
12. KG.509.2 Younger amphibolite.
13. KG.513.4 Younger amphibolite.
14. KG.535.2 Younger amphibolite.

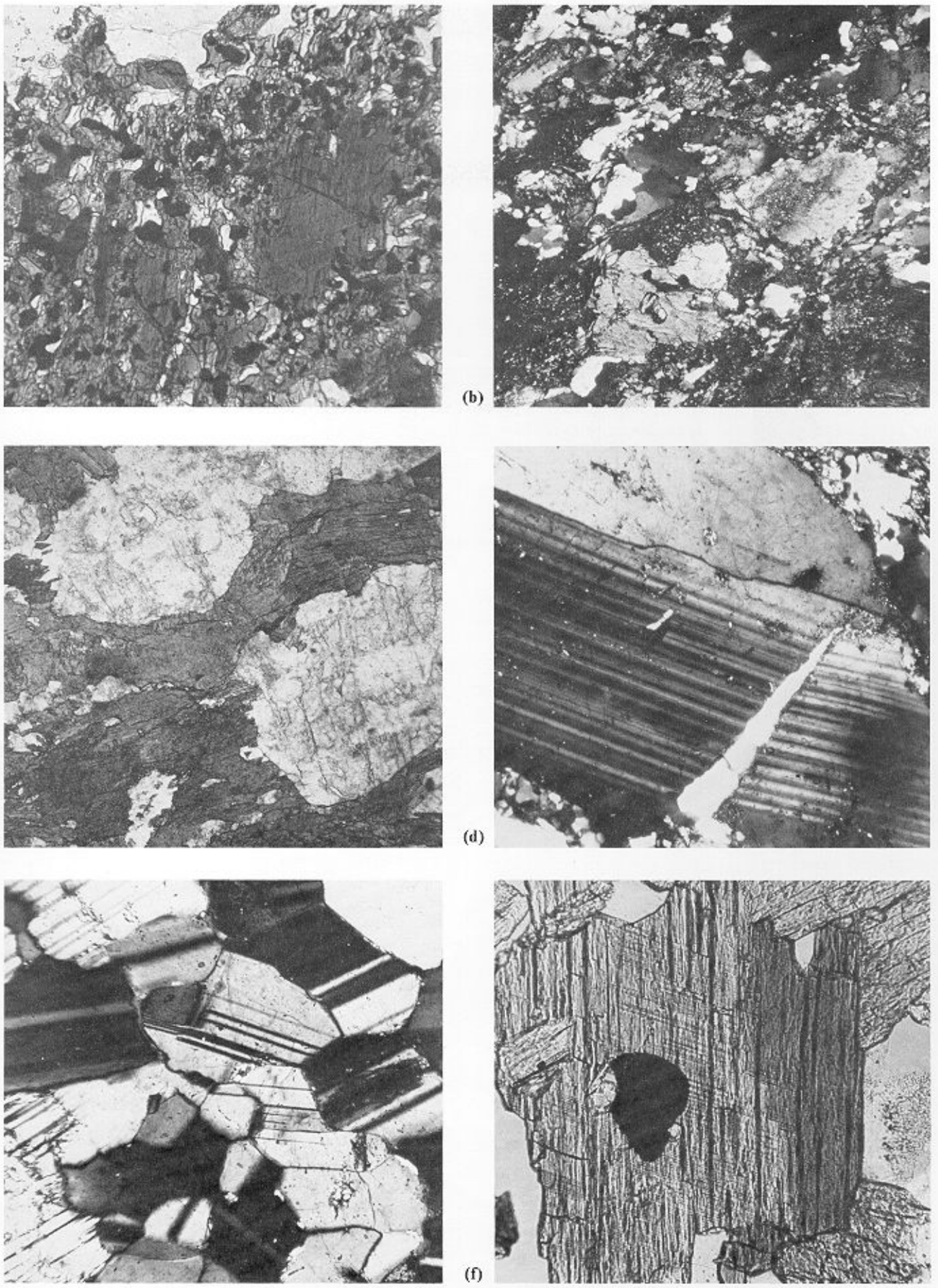

Fig. 27. a. Sieved hornblende in diorite-gneiss containing granular quartz and ilmenite (KG.526.2; ordinary light; × 160). b. Leucocratic diorite-gneiss showing a single hornblende crystal and extensive recrystallization (KG.576.1; X-nicols; × 55). c. Relatively undeformed plagioclase in hornblende-rich diorite-gneiss (KG.573.3; ordinary light; × 210). d. Relict plagioclase phenocryst in diorite-gneiss, showing a wedge-shaped fracture infilled with recrystallized feldspar (KG.573.1; X-nicols; × 45). e. Granular aggregate of recrystallized plagioclase with straight grain boundaries and 120° triple junctions in metagabbro (KG.518.10; X-nicols; × 150). f. Cummingtonite in metagabbro showing exsolution lamellae, a rounded ilmenite inclusion and marginal replacement by secondary hornblende (KG.525.2; ordinary light; × 150).

which, despite strong cataclastic features (bent twin lamellae, secondary glide twinning and fractures (Fig. 27d)), show little recrystallization. It seems that this is mainly because the interjacent zone of actinolitic hornblende provided a place of relief for the shearing stresses. In effect the incompetency of the mafic minerals increased the competency of the feldspars. In the rocks invaded by the *lit-par-lit* granite-gneisses, the plagioclase is heavily sericitized, and mantled by fresh albitic plagioclase, and the fractures infilled with quartz and potash feldspar.

F. Metagabbros

1. Field description

Only one outcrop of metagabbro was positively identified within the tonalites of station KG.518 but, as the shape of the intrusion and its colour index resemble those of the amphibolites (which are exceedingly common in this outcrop), they may possibly be more widespread. The intrusion is approximately 60 m wide at the base and tapers towards the top. The contact with the tonalites is generally sharp with marginal chilling and there are indications on the eastern side of subsequent mobilization of the acid rock. There is further evidence of mobilization 15 m above the base where a narrow aplitic dyke cuts across the entire intrusion.

The metagabbros, which form the bulk of the southern nunatak at station KG.521, are devoid of structure but contain amphibolite rafts (ranging in thickness from 5 to 60 cm) which are commonly orientated with their longer axes parallel to each other. These bodies probably represent the remnants of synorogenic basic intrusions whose orientation was controlled by the prevailing stresses. Because crystallization was not quite complete, the dykes were readily lensed, while the metagabbros retained a degree of rigidity which inhibited the development of structures. Some variations in rock type occur over the outcrop with a leucocratic metagabbro (probably a quartz-metagabbro) at the top passing downward into the typical plagioclase-hornblende assemblage. Frequent pegmatitic patches have tabular hornblende crystals nearly 40 mm long, and near the base of the outcrop the metagabbros are intruded by two gneissose acid dykes.

The easternmost of the three spurs which comprise station KG.523 was inaccessible, but the rock on the lower slopes appears similar to the medium- to coarse-grained metagabbros cropping out on the central spur. The roof of the intrusion is just above the level of these spurs and the remainder of the ridge is composed of a dark banded rock, probably the quartz-plagioclase-amphibolite. The country rock crops out on the western spur where it is intruded by narrow veins of metagabbro. There, too, the metagabbros have been invaded by massive granitic and granodioritic veins which frequently reduce the extent of the basic rock to dyke-like bodies seldom more than 2 m wide. The commonest rock is composed of a coarse, almost pegmatitic, aggregate of white feldspar and pale green fibrous amphibole.

The field relations of the metagabbro at the northern end of station KG.525 are shown in Fig. 2. At the north-western tip, the rock has a sharp junction with the amphibolite and is cut by a small tonalitic dyke similar in composition to those occurring just to the east. This dyke is intruded along the line of the foliation in the metagabbro defined by the parallel arrangement of mica and amphibole. When traced towards the tonalite, the rock becomes paler, and adjacent to the gneiss the basic rock resembles the flow-banded Andean granodiorite. At the top of the cliff the contact is parallel to the vertical foliation which is concordant in the two rocks, but when traced towards the base it swings eastward cutting the foliation obliquely.

Within the numerous amphibolite rafts (Fig. 28) are lenses of metagabbro which are probably relict enclaves but, since the outcrop only provides a two-dimensional section, the possibility that they represent metagabbro mobilized and injected during the subsequent metamorphism cannot be eliminated. The foliation within a lens is concordant with that of the enclosing amphibolite, making an angle of 45° with that in the host rock but, on the underside of the amphibolites the foliation in the host swings round to parallel to rafts. It is probable that during the metamorphism which followed their emplacement the amphibolites acted as planes of weakness in which shearing occurred and this resulted in deflection of the foliation in the adjacent metagabbros.

2. Petrography

At station KG.518 the metagabbro in the centre of the intrusion outcrop (e.g. KG.518.10) is a coarse equigranular or porphyritic aggregate of white feldspar and dark green amphibole, but when traced towards the margins (e.g. KG.518.13) the grain-size, particularly that of the mafic mineral, decreases. Tabular plagioclase phenocrysts are normally zoned from An_{54} to An_{47} and twinned principally on the albite law, although Carslbad and pericline twins do occur. Much of the twinning is secondary, frequently cutting ghosts of the primary twins. Sericite is common in the cores and often accompanies granulation; unaltered oligoclase (An_{24}) forms a narrow rim on several of the larger grains. A second generation of plagioclase, with an average grain-size not exceeding 0.5 mm and a composition similar to the more sodic parts of the phenocrysts, occurs in granular aggregates (Fig. 27e), often with straight boundaries and 120° triple junctions, indicative of primary textural equilibrium.

Fig. 28. Metagabbros cut by amphibolite dykes at station KG.525, western Pegasus Mountains. The foliations of the dyke and the metagabbro (?) xenoliths are sub-horizontal whereas the structures in the metagabbros are sub-vertical. The hammer head is 20 cm long.

Broad laths of hornblende up to 3 mm wide and with α = yellow, β = light brown, γ = brownish green and γ: $c = 24°$ have been partly replaced by pale green actinolitic hornblende (α = pale straw, β = light green, γ = pale blue-green and γ: c = 15–20°). This replacement varies from simple epitaxial growth on the edges to large decussate aggregates enclosing granular ilmenite, pyrite, quartz and plagioclase. Anhedral magnetite and smaller partly limonitized pyrite crystals are the main accessory minerals and there are small pools of interstitial quartz.

Specimen KG.518.13 was collected from the marginal zone of the same intrusion and it has an essentially similar mineralogy. Apart from the reduced grain-size, this rock differs from the previous one in that the degree of alteration of the feldspar is greater and the hornblende has small colourless patches in the cores associated with granular quartz. The colourless amphibole is probably cummingtonite, the quartz being exsolved during a subsequent reaction with the anorthositic component of the plagioclase (Deer and others, 1963, p. 245). Granular pistacite with rims of fine leucoxene and rare flakes of partly chloritized biotite are other notable additions.

Certain mineralogical differences in specimen KG.521.3, in particular a more calcic plagioclase (normally zoned from An_{63} to An_{46}) and green hornblende (α = straw, β = green, γ = dark green) in place of the usual greenish brown variety, are attributed to primary chemical differences. Along with the pale green actinolitic hornblende, chlorite and occasional white mica have grown on the hornblende; apatite is a common accessory. In the extremely coarse-grained rock from station KG.523, hornblende and cummingtonite are almost completely replaced by sheaves of fibrous actinolite and pale green chlorite.

Specimen KG.525.2 is undoubtedly the most atypical of all the metagabbros, resembling (apart from the absence of quartz) in the hand specimen the flow-banded Andean granodiorite (p. 67). In this section, however, the rocks were found to differ from the others only in the relatively small amount of ferromagnesian minerals, although three different amphiboles are present. The texture is still igneous, although the larger plagioclase crystals and two of the amphiboles are orientated. Plagioclase (An_{55}) forms broad laths averaging 1.5 mm in width which are frequently replaced by aggregates of granular or stumpy crystals 0.5–0.7 mm long. Details of the amphiboles are as follows:

i. Greenish brown hornblende (α = pale yellow, $\beta = \gamma$ = greenish brown and γ: $c = 29°$). Occurs in sub-idioblastic laths averaging 2 mm and up to 4 mm in length, and is marginally replaced by (iii).
ii. Cummingtonite. Colourless and optically positive, the mineral has exsolution lamellae which make an angle of 68° with the cleavage (Fig. 27f). Occurs in idioblastic laths invariably associated with and frequently within (i). Commonly has a thin peripheral rim of (iii).
iii. Actinolitic hornblende (α = yellow, β = green, γ = pale blue-green and γ: c = 15–20°). A secondary amphibole occurring solely on the margins of (i) and (ii), and along the exsolution lamellae of (ii).

The amphiboles of the metagabbros and amphibolites possess various features in common and their paragenesis is discussed on p. 30–31.

G. Amphibolites

The amphibolite group embraces all those medium- to coarse-grained dark rocks which are considered to be metamorphosed basic dykes. Two distinct generations have been identified, mainly on the basis of field relations and the degree of metamorphism.

1. Older amphibolites

a. *Field description.* Medium- to coarse-grained amphibolites ranging from 15 cm lensoid xenoliths to massive dykes over 0.5 km wide occur within all other rock types in the metamorphic complex. Because of their widespread occurrence and relatively uniform mineralogy, only the major outcrops will be described in detail.

Almost the entire western half of station KG.518 (southern Pegasus Mountains) is composed of a large body of amphibolite 0.8 km long and 180 m high, of which only the extreme western end was accessible. However, even at such a limited exposure the rock varied considerably with numerous lens-shaped patches of coarse amphibolite whose mineralogical similarity with the finer-grained rocks suggests that they are late-stage pegmatite veins disrupted during the subsequent metamorphism. The basic rocks are intruded by light grey acid veins and dykes ranging from 2 to 5 cm and which are thought to have originated from the nearby granodiorite.

The tonalites of the eastern part of this station are invaded by a network of interconnected amphibolite dykes (Fig. 29) ranging in thickness from 1 m to over 30 m, and showing pinch-and-swell structures. Though having no constant direction, the contact with the tonalites is always sharp with many veins of the country rocks cutting the dykes. Together with the numerous lensoid or angular 'xenoliths' of amphibolite and the segregation of the larger dykes into smaller parallel bands, these veins are further evidence of the subsequent mobilization of the tonalites.

Granitic veins, which cut both the dyke and country rocks, show a complete disregard for the structure and are regarded as a post-metamorphic event.

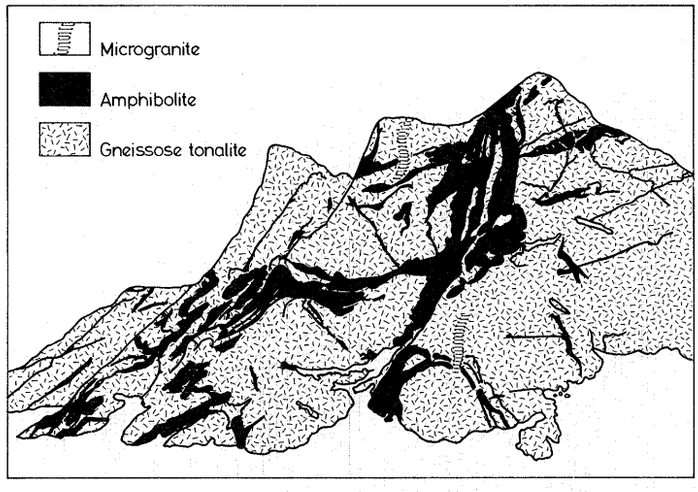

Fig. 29. Sketch from a photograph of part of the northern face of station KG.518, south-west Pegasus Mountains showing the network of older amphibolite dykes and minor microgranites in gneissose tonalites. The ridge is approximately 200 m high.

The only other large body of amphibolite crops out on the north-west tip of station KG.525, where the intrusion is 100 m long and 10 m high. A fine-grained aggregate of plagioclase and hornblende with occasional biotite, it is traversed by numerous narrow epidote-filled shears. Although there is no apparent relationship, apart from a mineralogical one, this body is thought to be of the same generation as the rafts and pods in the adjacent metagabbro, referred to previously. Because the same dyke can be traced through the metagabbro, its leucocratic margin and the tonalites, it was possible to study the relative behaviour of acid and basic rocks under the same metamorphic conditions. Thus, in the typical metagabbro the dykes show little evidence of deformation, whilst in the leucocratic variety discrete rafts 1 m long have developed with their longer axes following the strike of the original dyke. Narrow tongues of amphibolite branch into the metagabbro, generally along fissures parallel to the foliation of the country rock. In the tonalites immediately adjacent to the contact no large bodies of amphibolite are present; only lensoid or fish-tailed 'xenoliths' (Fig. 30) of similar thickness to the original dykes. However, the presence of three unbroken dykes in the tonalites less than 200 m to the east suggests that the mobility varied considerably, even within the acid rocks.

Within the banded gneisses the amphibolites are reduced to lens-shaped pods or rafts seldom exceeding 3 m in length and invariably concordant with the foliation. A faint foliation is generally detectable (perhaps where there is an abundance of biotite) and intrusions of acid mobilizates, occasionally of pegmatitic proportions, are common. Amphibolites occur within the white granites over most of the Auriga Nunataks but they are especially evident on the north face (Fig. 31), where individual dykes can be followed for 1 km or more despite having been rafted (Fig. 32). Unlike station KG.518, the predominant attitude of the dykes on the north face is horizontal, although sub-vertical examples occur in other parts of the nunatak. This probably reflects variations in the foliation, for where such a structure is present in the gneiss, the bodies are generally aligned to it. Within the other outcrop of white granite at Fomalhaut Nunataks, the dykes have a greatly reduced extent and are always aligned parallel to the foliation of the country rock.

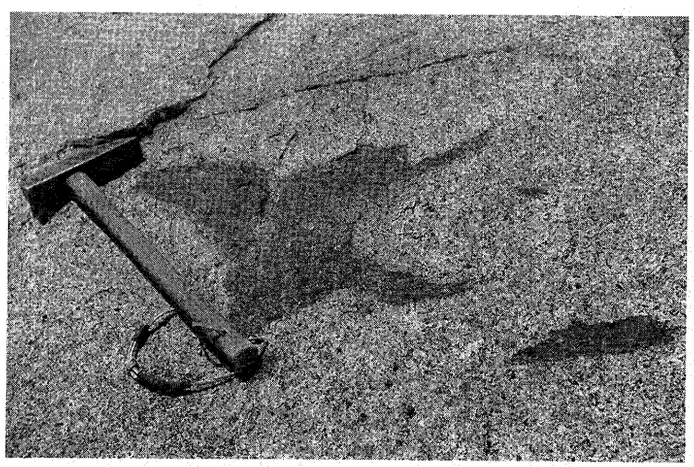

Fig. 30. Amphibolite pod in tonalite at station KG.525. The hammer shaft is 55 cm long.

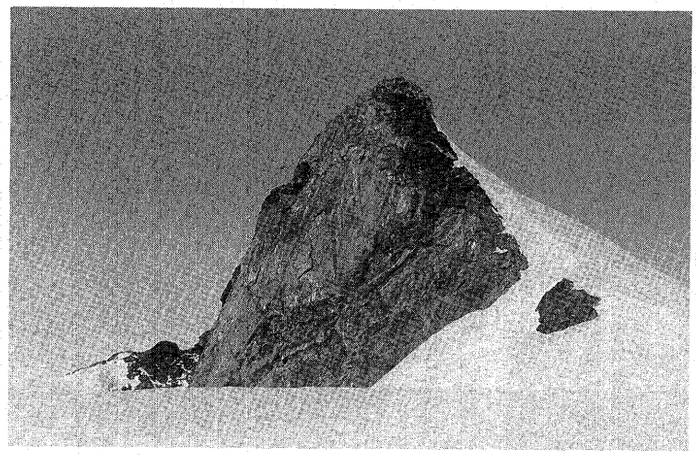

Fig. 31. Deformed amphibolite dyke in white granite at station KG.536, Auriga Nunataks. The face is approximately 30 m high.

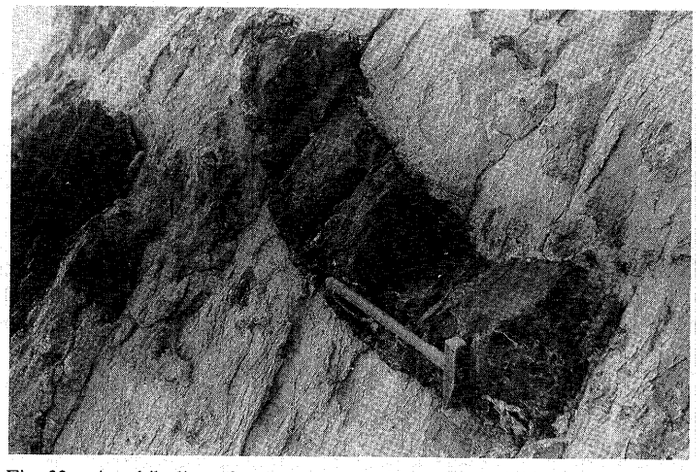

Fig. 32. Amphibolite rafts, remnants of a former basic dyke, in white granite at station KG.539, Auriga Nunataks. The hammer shaft is 55 cm long.

b. *Petrography.* Despite their widespread occurrence, the amphibolites show little mineralogical variation (Table V, analyses 6–11). In the hand specimen, the rock is greenish grey with a distinct foliation and local relict white feldspar phenocrysts. In this section a granoblastic to hemi-granoblastic aggregate of plagioclase and hornblende constitutes the bulk of the rock, commonly with subsidiary biotite. Relicts of an original brownish green hornblende (α = yellow, β = light brown, γ = olive-green and $\gamma : c = 20°$) survive locally (e.g. in specimens KG.518.1 and 2) and in the coarser parts of specimen KG.518.2 where this original hornblende forms broad columnar crystals between 1 and 1.5 mm in length. A green actinolitic hornblende (α = pale yellow, β = green and γ = pale blue-green) frequently mantles the brown variety and develops on small areas of colourless, optically positive amphibole riddled with vermicular quartz. Comparison with specimen KG.518.13 (p. 27) suggests the colourless amphibole is cummingtonite. Cummingtonite is also present in specimen KG.531.2, a rock in which the predominantly igneous habit of the plagioclase suggests that metamorphic equilibrium has not

been attained. It appears that this mineral has a preferred orientation, for only basal sections (commonly twinned) are present in the available thin section. The cummingtonite is also porphyritic and a pale green fibrous actinolitic hornblende is wrapped round its edges.

In most specimens, particularly those from the smaller dykes, a green hornblende similar to that in specimen KG.521.3 (p. 27) is the only one present, but its frequent association with sphene suggests that it has developed from a more titaniferous amphibole. Both Binns (1965) and Deer (1938) have drawn attention to the connection between titanium content and the brown colour of hornblendes and, since brown hornblende is known to have a higher temperature of formation than green hornblende, it is probable that, during retrograde metamorphism, exsolved titanium combined with calcium liberated from anorthitic plagioclase to form sphene. Fibrous actinolitic hornblende and brown biotite commonly grew at the expense of hornblende, but in specimens KG.503.3 and 8 the amphibole has been completely pseudomorphed by fibrous chlorite (penninite in specimen KG.503.3), carbonate and iron ore, although the biotite has survived.

Relicts of igneous plagioclase (Fig. 33a) are common particularly in the larger bodies. In specimen KG.516.3 (Fig. 33b) an original porphyritic texture is preserved with 2–3 mm grains of plagioclase set in a groundmass with an average grain-size of 0.5 mm. The phenocrysts with an average composition of An_{60} are heavily sericitized and slight recrystallization has occurred at their edges. The groundmass feldspar (An_{51}) is also sericitized but it has partly recrystallized to small rounded alteration-free grains, which show faint twinning and undulating extinction.

2. Younger amphibolites

A suite of amphibolite dykes of limited extent intrudes the banded gneisses in the eastern part of the Pegasus Mountains. The following criteria distinguish them from the older group:

i. They are continuous over several kilometres and are never rafted.
ii. They are generally intruded along fissures parallel to the joints in the banded gneisses, and always at right-angles to the foliation in the country rocks.
iii. They have mineralogical assemblages typical of the upper greenschist facies and are never intruded by veins of re-mobilized granite.

a. *Field description.* A 9–15 m horizontal dyke cuts vertical banded gneisses at station KG.509, and can be traced for several kilometres to the south along the west face of the ridge. A second dyke, apparently at a slightly higher level and with a gentle dip to the south-west crops out on the north-west face of station KG.532, the west end of station KG.508 (Fig. 34) and at station KG.510. At station KG.532 there are at least three parallel subsidiary dykes joined by a vertical feeder of the same dimensions as the large body. One such horizontal dyke extends over 60 m along the summit of station KG.510 parallel to one of the joints in the banded gneisses, and a similar feature, dipping at 25° to the south-west was noted on the small rock ridge 790 m to the north (KG.511). Eight other vertical dykes vary from 30 cm to 6 m in width; they are sometimes parallel to the joint planes but more often are cross-cutting.

The contact with the banded gneisses is always sharp and narrow amphibolitic veins fill cracks in the country rock. Small rounded quartzo-feldspathic xenoliths are common and at station KG.532 rectangular blocks of granite 15 cm by 60 cm accompany 3–5 cm rounded xenoliths of metagabbro. At stations KG.510 and 511 the sub-horizontal dykes have been affected by small displacements of unknown magnitude, whilst on the west face of station KG.535 the large horizontal dyke has suffered a vertical displacement of approximately 30 m, the downthrow being to the south.

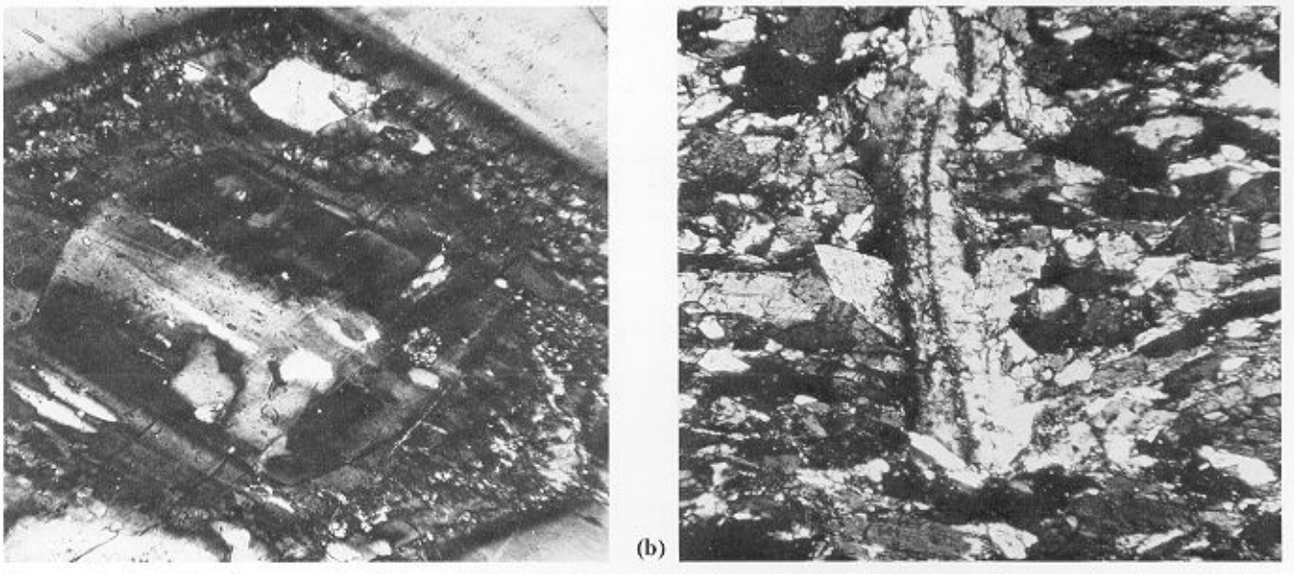

Fig. 33. a. Relict zoned plagioclase phenocryst in older amphbiolite (KG.539.1; X-nicols; × 150). b. Relict porphyritic texture in older amphibolite (KG.516.3; X-nicols; × 65).

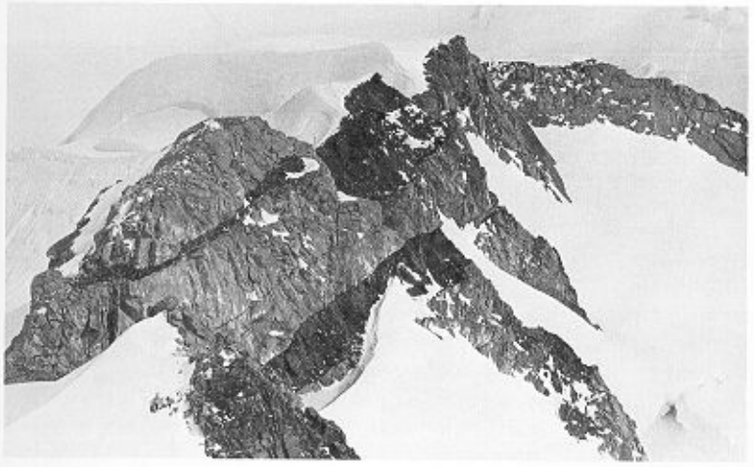

Fig. 34. Gently dipping younger amphibolite dykes in banded gneisses at station KG.508 eastern Pegasus Mountains. The larger intrusion is approximately 15 m thick.

b. *Petrography*. A specimen (KG.509.2; Table V, analysis 12) from the large horizontal dyke at station KG.509 is a coarse-grained black rock with subsidiary purplish feldspars. In thin section, a relict ophitic texture is preserved (Fig. 35a), although the pyroxene has been pseudomorphed by aggregates of fibrous actinolitic hornblende and ilmenite. Anhedral laths of cloudy labradorite (An_{50} with slight zoning), averaging 1 mm in length and showing slight marginal recrystallization, are twinned on the Carlsbad, albite and pericline laws. The actinolitic hornblende (α = pale straw, β = green, γ = pale blue-green and $\gamma:c = 17°$), commonly grows into the plagioclase (Fig. 35b) and has partly destroyed the ophitic texture, whereas the skeletal ilmenite within the amphibole aggregates often delineates the original pyroxene. Granular iron pyrites and euhedral apatite are common accessories.

In some of the smaller dykes (e.g. specimens KG.510.1 and 6) relict porphyritic textures are preserved, with 0.5–1 mm long euhedral plagioclase phenocrysts and local amphibole pseudomorphs after pyroxene in a felt of green actinolitic hornblende and irregular grains of plagioclase. The plagioclase (An_{48-62}), possesses well-developed Carlsbad and albite twinning, whose lamellae are frequently bent in the phenocrysts. The actinolitic hornblende, commonly developed within the plagioclase, resembles the amphibole in the larger dyke, although its grain-size is much reduced. Small irregular flakes of brown biotite have grown at the expense of the hornblende and, within two narrow belts (probably shear zones), biotite is dominant. Granular ilmenite is particularly abundant in association with the hornblende, whilst in specimen KG.510.6 finely developed sphene is the only titanium-bearing mineral. Complete recrystallization has occurred in some dykes (e.g. specimen KG.509.3; Fig. 36), the basic plagioclase being replaced by albite and epidote, whilst the actinolitic hornblende crystals occur singly.

3. Amphiboles of the metagabbros and amphibolites

The aim of this discussion is to elucidate the paragenesis of the three amphiboles common to the metagabbros and amphibolites (Table VI) and its relationship to the three metamorphic events. The first point requiring clarification is whether the cummingtonite is magmatic or metamorphic.

Cummingtonite, resulting from the uralitization of orthopyroxene in gabbros and norites, has been noted by Asklund (1925) and Stewart (1947) but, in the majority of the Palmer Land rocks, any late-stage crystallization must have been syn-orogenic. Hence the cummingtonite and its associated green-brown hornblende are almost certainly metamorphic minerals. The particular significance of this statement is that the metamorphic environment favoured the growth of cummingtonite, a fact which will have important bearing on the discussion on the metamorphic history.

Cummingtonite is well-known as a constituent of

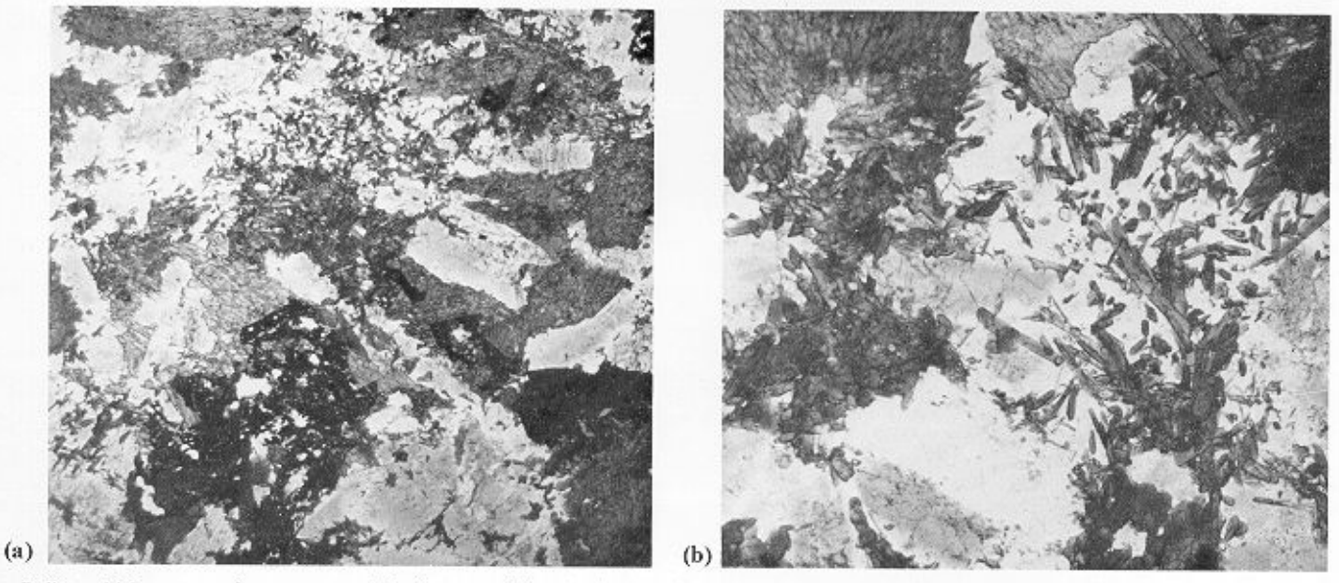

Fig. 35. a. Relict ophitic texture of younger amphibolite comprising plagioclase, fibrous actinolitic hornblende and skeletal ilmenite (KG.509.2; ordinary light; × 25).
b. Fibrous actinolitic hornblende growing in plagioclase (KG.509.2; ordinary light; × 60).

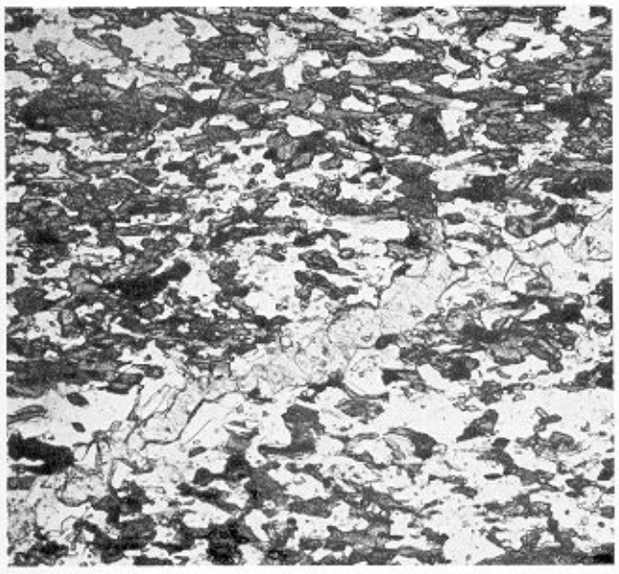

Fig. 36. Metamorphic texture typical of the smaller younger amphibolite dykes. The rock is traversed by an epidote-filled shear (KG.509.3; ordinary light; × 220).

metamorphosed basic rocks and its association with hornblende has attracted considerable discussion (e.g. Eskola, 1950; Watters, 1959; Seitsaari, 1952). The following account, which broadly follows that of Asklund (1925), is considered the most likely interpretation of the cummingtonite-hornblende association in these rocks. The original basic rock contained clinopyroxene and orthopyroxene (with exsolved clinopyroxene lamellae), and during the second metamorphism the former was replaced by greenish brown hornblende and the latter by cummingtonite.

There can be no doubt that, where the cummingtonite includes vermicular quartz, the mineral has been partly replaced by hornblende. However, the rectilinearity of the boundary between the two amphiboles and the preferential replacement of the exsolution lamellae in many instances suggest that the orthopyroxene may have possessed a narrow rim, identical in composition to the clinopyroxene forming the exsolution lamellae. In common with the other clinopyroxene crystals, they were probably replaced by greenish brown hornblende during the second metamorphism, although no evidence of this remains.

The actinolitic hornblendes of the younger amphibolites, the metagabbros and older amphiboltes are sufficiently alike to suggest they are products of the third metamorphism. The difference in crystal form (i.e. the lack of a fibrous structure in the metagabbros and older amphibolites) appears to be more dependent on whether the replacement is epitaxial than on the identity of the mineral being replaced.

The conclusions can be summarized:

i. The cummingtonite and greenish brown hornblende of the metagabbros may have formed (at the expense of orthopyroxene and clinopyroxene respectively) during the first metamorphism, but they are considered more likely to have grown concomitantly with similar amphiboles in the older amphibolites during the second metamorphism.

ii. The pale green actinolitic hornblende of the metagabbros and older amphibolites, which grew at the expense of greenish brown hornblende and possibly cummingtonite, is equated with the fibrous amphibole replacing pyroxene in the younger amphibolites, and hence it is a product of the third metamorphism.

H. Geochemistry

Chemical analyses of 35 metamorphic rocks were obtained by X-ray fluorescence spectrometry, as described by Leake and others (1969), except for H_2O, CO_2 and FeO which were determined by conventional methods. The results are shown in Tables VII and VIII. The purpose of the analyses was to determine whether the chemistry of these rocks supported the conclusions established from field and microscopic evidence, particularly regarding genesis. However, in keeping with the general reconnaissance nature of the field work, the analyses are of a wide variety of rock types, and any conclusions drawn must be regarded as tentative.

1. Banded gneisses and white granites

a. *Major elements.* The main chemical variations in the banded gneisses, based on the average of ten rocks, are shown in Fig. 37 together with the two undifferentiated tonalites, plotted to illustrate their similarity to the banded gneisses. The compositional differences, which are mirrored in the small-scale banding, show an enrichment in the leucosome of SiO_2 and the alkalis and a corresponding deficiency in Al_2O_3, TiO_2, Fe_2O_3, MgO, MnO and CaO. It has been shown previously (p. 17) that much (if not all) of the potassium was introduced metasomatically, almost certainly after the development of the banding. Furthermore, since Na and K are more readily interchangeable than Ca and K, it follows that the leucosomes were preferentially enriched in K. A smaller amount of K entered the melanosomes, presumably at the expense of Ca, and

Table VI. Details of amphiboles common to the metagabbros, older and younger amphibolites.

Amphibole	*Pleochroism*			*γ:c*	*Rock type*
	α	*β*	*γ*		
Cummingtonite		Colourless			Metagabbro; older amphibolite
Hornblende	Pale yellow	Greenish brown	Greenish brown	29°	
	Pale straw	Green	Dark green		Metagabbro; older amphibolite
	Yellow	Light brown	Olive-green	20°	
Actinolitic hornblende	Yellow	Green	Pale blue-green	15–20°	Metagabbro; older and younger amphibolites

Table VII. Chemical analyses of white 'granites' and banded gneisses.

	White 'granites'					*Banded gneisses*				
	1	*2*	*3*	*4*	*5*	*6*	*7*	*8*	*9*	*10*
SiO_2	75.13	76.91	69.58	64.83	68.88	66.16	65.88	63.15	64.84	57.50
TiO_2	0.84	0.08	0.05	0.54	0.37	0.77	0.47	0.69	0.78	1.01
Al_2O_3	11.41	13.76	18.04	16.70	15.96	14.21	17.00	17.14	14.25	17.98
Fe_2O_3	1.25	0.67	0.12	2.52	1.79	2.39	1.01	1.64	2.12	3.24
FeO	4.61	0.34	0.25	1.69	1.28	3.11	1.86	2.30	2.90	2.86
MnO	0.12	0.01	0.01	0.13	0.10	0.09	0.02	0.03	0.08	0.10
MgO	0.99	–	0.06	1.29	0.79	0.89	1.21	1.74	2.34	1.94
CaO	0.53	0.23	2.27	4.02	2.86	3.04	2.08	3.64	1.75	5.02
Na_2O	1.25	1.89	3.58	4.53	4.13	2.25	3.83	4.17	2.81	4.49
K_2O	3.96	6.32	6.60	1.54	3.04	4.34	4.61	2.39	4.86	2.01
P_2O_5	0.02	–	0.02	0.15	0.10	0.21	0.23	0.21	0.15	0.34
H_2O^+										
H_2O^-	0.51	0.52	0.31	1.03	0.77	0.65	0.55	0.42	1.28	1.14
CO_2	0.53	0.39	0.60	0.84	0.61	1.10	0.69	0.79	1.00	1.22
Total	101.15	101.12	100.95	99.81	100.68	99.21	99.44	98.31	99.16	98.85
ANALYSES LESS TOTAL WATER (RECALCULATED TO 100)										
SiO_2	74.66	76.45	69.14	65.62	68.94	67.13	66.62	64.51	66.24	58.63
TiO_2	0.84	0.08	0.05	0.54	0.37	0.78	0.48	0.70	0.79	1.04
Al_2O_3	11.33	13.68	17.93	16.91	15.97	14.42	17.18	17.51	14.56	18.49
Fe_2O_3	1.24	0.67	0.12	2.55	1.79	2.42	1.02	1.67	2.17	3.33
FeO	4.58	0.34	0.25	1.71	1.29	3.15	1.88	2.35	2.96	2.94
MnO	0.12	0.01	–	0.13	0.10	0.09	0.02	0.03	0.09	0.10
MgO	0.99	–	0.06	1.31	0.79	0.91	1.22	1.77	2.39	2.00
CaO	0.53	0.23	2.25	4.07	2.86	3.09	2.10	3.72	1.79	5.17
Na_2O	1.24	1.88	3.56	4.59	4.13	2.29	3.87	4.26	2.87	4.62
K_2O	3.93	6.28	6.02	1.56	3.05	4.40	4.66	2.44	4.96	2.07
P_2O_5	0.02	–	0.02	0.15	0.10	0.21	0.23	0.22	0.15	0.35
CO_2	0.52	0.51	0.59	0.85	0.61	1.11	0.70	0.81	1.02	1.25
ELEMENT WEIGHT PERCENTAGES (ANHYDROUS)										
Si^{4+}	34.90	35.74	32.32	30.68	32.23	31.38	31.14	30.16	30.96	27.41
Ti^{4+}	0.50	0.05	0.03	0.33	0.22	0.47	0.29	0.42	0.48	0.62
Al^{3+}	6.00	7.24	9.49	8.95	8.45	7.63	9.09	9.26	7.70	9.79
Fe^{3+}	0.87	0.47	0.08	1.79	1.25	1.69	0.71	1.17	1.51	2.33
Fe^{2+}	3.56	0.26	0.19	1.33	1.00	2.45	1.46	1.82	2.30	2.29
Mn^{2+}	0.09	0.01	–	0.10	0.07	0.07	0.02	0.02	0.07	0.08
Mg^{2+}	0.59	–	0.03	0.79	0.48	0.55	0.74	1.07	1.44	1.21
Ca^{2+}	0.38	0.17	1.61	2.91	2.04	2.21	1.50	2.66	1.28	3.69
Na^{+}	0.92	1.39	2.64	3.40	3.06	1.70	2.87	3.16	2.13	3.42
K^{+}	3.26	5.21	5.00	1.29	2.53	3.65	3.87	2.02	4.12	1.72
P^{5+}	0.01	–	0.01	0.07	0.04	0.09	0.10	0.09	0.07	0.15
C^{4+}	0.14	0.11	0.16	0.23	0.17	0.30	0.19	0.22	0.28	0.34
O^{2-}	48.77	49.36	48.42	48.13	48.44	47.80	48.00	47.90	47.64	46.94
BARTH MESONORMS										
Mt	1.37	0.71	0.12	2.70	1.89	2.63	1.07	1.76	2.31	3.53
Ti	1.65	0.18	0.09	1.17	0.78	1.68	0.99	1.47	1.71	2.19
Ap	0.02	–	0.06	0.36	0.24	0.54	0.54	0.51	0.36	0.84
Or	16.60	43.50	32.25	5.37	15.57	21.90	22.68	7.93	21.60	5.67
Ab	11.70	17.10	32.00	41.65	37.55	21.25	34.95	38.50	26.35	42.00
An	–	0.85	10.90	17.15	12.25	11.25	7.05	14.40	5.00	23.50
C	5.75	2.65	1.73	1.62	1.60	2.18	3.51	2.87	2.98	1.77
Bi	12.61	0.08	0.64	6.39	4.13	8.08	7.93	10.51	13.36	10.69
Q	50.27	34.93	17.21	23.65	25.99	30.49	21.28	22.05	26.33	13.82
Il	0.12	–	–	–	–	–	–	–	–	–
A	45.4	90.0	96.1	54.6	67.2	53.3	69.8	56.0	54.3	46.9
F	48.1	10.0	3.5	36.3	27.1	41.3	22.5	32.4	33.2	42.1
M	6.5	–	0.4	9.1	5.7	5.4	7.6	11.6	12.5	11.0
K	71.5	77.0	54.0	17.0	33.1	48.3	47.0	25.8	54.7	19.4
Na	20.2	20.6	28.5	44.7	40.1	22.5	34.8	40.3	28.3	38.8
Ca	8.3	2.4	17.5	38.3	26.8	29.2	18.2	33.9	17.0	41.8
Q	64.0	36.6	23.0	33.5	31.8	41.4	27.0	32.2	35.5	22.5
Or	21.1	45.5	38.6	7.6	22.2	29.7	28.7	56.2	291.	68.3
Ab	14.9	17.9	38.4	58.9	46.0	28.9	44.3	11.6	35.4	9.2
Or	58.6	70.8	42.9	8.4	23.8	40.3	35.1	13.0	40.8	8.0
Ab	41.4	27.8	42.6	64.9	57.4	39.0	54.0	63.3	49.8	59.0
An	–	1.4	14.5	26.7	18.8	20.7	10.9	23.7	9.4	33.0

Table VII. Chemical analyses of white 'granites' and banded gneisses (continued).

	Banded gneisses								
	11	*12*	*13*	*14*	*15*	*16*	*17*	*18*	*19*
SiO_2	58.04	68.21	65.68	78.92	73.80	74.28	75.60	71.60	72.93
TiO_2	0.81	0.37	0.88	0.61	0.11	0.10	0.06	0.12	0.17
Al_2O_3	192.1	15.61	14.82	10.26	15.17	14.79	14.90	16.80	14.85
Fe_2O_3	2.73	2.10	2.17	0.86	0.54	0.74	0.15	0.37	0.99
FeO	2.24.	1.82	3.04	1.25	0.27	0.22	0.11	0.41	0.59
MnO	0.09	0.09	0.09	0.05	0.04	0.02	–	0.01	0.03
MgO	1.32	0.84	2.46	1.19	0.19	0.09	0.02	0.22	0.22
CaO	4.30	2.94	1.94	1.20	0.40	0.53	1.01	1.49	1.04
Na_2O	4.31	3.78	1.81	2.43	3.40	3.51	2.91	4.11	2.62
K_2O	3.63	2.26	3.11	1.53	5.15	4.89	5.17	4.62	6.11
P_2O_5	0.22	0.10	0.18	0.14	0.01	–	0.02	0.08	0.05
H_2O^+									
H_2O^-	1.43	1.03	1.89	1.11	0.92	0.42	0.48	0.38	0.24
CO_2	0.75	0.58	1.11	0.74	0.54	0.50	0.37	0.44	0.46
Total	99.08	99.73	99.18	100.29	100.54	99.61	100.80	100.65	100.30
ANALYSES LESS TOTAL WATER (RECALCULATED TO 100)									
SiO_2	59.23	69.09	67.50	79.56	74.08	74.53	75.37	71.41	72.89
TiO_2	0.83	0.38	0.90	0.61	0.11	0.10	0.06	0.12	0.17
Al_2O_3	19.77	15.81	15.23	10.35	15.23	14.84	14.85	16.75	14.84
Fe_2O_3	2.18	2.13	2.23	0.87	0.55	0.74	0.15	0.37	0.98
FeO	2.30	1.85	3.13	1.26	0.27	0.22	0.11	0.41	0.59
MnO	0.09	0.09	0.09	0.05	0.04	0.02	–	0.01	0.03
MgO	1.36	0.85	2.53	1.20	0.19	0.09	0.02	0.22	0.22
CaO	4.42	2.98	1.99	1.21	0.40	0.53	1.01	1.48	1.04
Na_2O	4.44	3.83	1.86	2.45	3.41	3.52	2.90	4.10	2.62
K_2O	3.74	2.29	3.20	1.54	5.17	4.90	5.15	4.60	6.11
P_2O_5	0.23	0.10	0.19	0.14	0.01	–	0.02	0.08	0.05
CO_2	0.77	0.58	1.14	0.75	0.54	0.51	0.37	0.44	0.46
ELEMENT WEIGHT PERCENTAGES (ANHYDROUS)									
Si^{4+}	27.69	32.30	31.56	37.19	34.63	34.84	35.23	33.38	34.08
Ti^{4+}	0.50	0.23	0.54	0.37	0.07	0.06	0.04	0.07	0.10
Al^{3+}	10.46	8.37	8.06	5.47	8.06	7.85	7.86	8.87	7.85
Fe^{3+}	1.96	1.49	1.56	0.61	0.38	0.52	0.10	0.26	0.69
Fe^{2+}	1.79	1.44	2.43	0.98	0.21	0.17	0.08	0.32	0.46
Mn^{2+}	0.07	0.07	0.07	0.04	0.03	0.01	–	0.01	0.02
Mg^{2+}	0.82	0.51	1.52	0.73	0.11	0.05	0.01	0.13	0.13
Ca^{2+}	3.16	2.13	1.42	0.87	0.28	0.38	0.72	1.06	0.74
Na^{2+}	3.29	2.84	1.38	1.82	2.53	2.61	2.15	3.04	1.94
K^+	3.10	1.90	2.66	1.28	4.29	4.07	4.27	3.82	5.07
P^{5+}	0.10	0.04	0.08	0.06	–	–	0.01	0.03	0.02
C^{4+}	0.21	0.16	0.31	0.20	0.15	0.14	0.10	0.12	0.12
O^{2-}	46.83	48.51	48.39	50.37	49.24	49.29	49.41	48.88	48.76
BARTH MESONORMS									
Mt	2.98	2.27	2.42	0.95	0.57	0.71	0.17	0.39	1.05
Ti	1.77	0.78	1.95	1.32	0.24	0.21	1.26	0.24	0.36
Ap	0.54	0.24	0.27	0.36	0.03	0.09	0.06	0.18	0.12
Or	20.20	9.35	10.55	5.42	30.37	29.12	30.72	26.46	35.97
Ab	40.55	34.75	17.30	22.85	31.00	32.00	26.30	37.45	23.90
An	17.60	12.85	6.10	2.85	1.50	2.05	2.75	6.40	4.25
C	2.32	2.62	7.42	4.13	3.84	3.30	3.80	2.83	2.67
Bi	3.67	6.69	14.40	6.53	0.85	0.37	0.13	1.34	1.17
Q	10.38	30.21	39.59	55.59	31.60	32.15	34.75	24.83	30.51
Il	–	–	–	–	–	–	–	–	–
A	58.3	58.0	42.3	57.3	90.7	90.1	97.0	90.6	84.6
F	34.2	35.7	41.8	29.3	7.8	9.2	2.8	7.7	13.8
M	7.5	6.3	16.0	13.4	1.5	0.7	0.2	1.7	1.6
K	32.5	27.7	48.7	32.3	60.4	57.7	59.8	48.2	65.4
Na	34.5	41.3	25.3	45.8	35.6	37.0	30.1	38.4	25.1
Ca	33.0	31.0	26.0	21.9	4.0	5.3	10.1	13.4	9.5
Q	14.6	40.7	58.7	66.3	34.0	34.5	37.9	28.0	33.8
Or	28.4	12.6	15.6	6.5	32.7	31.2	33.5	29.8	39.8
Ab	57.0	46.7	25.7	27.2	33.3	34.3	28.6	42.2	26.4
Or	25.8	16.4	31.1	17.4	48.3	46.1	51.4	37.6	56.1
Ab	51.8	61.0	51.0	73.5	49.3	50.7	44.0	53.3	37.3
An	22.4	22.6	17.9	9.1	2.4	3.2	4.6	9.1	6.6

Table VII. Chemical analyses of white 'granites' and banded gneisses (continued).

	White 'granites'					*Banded gneisses*				
	1	*2*	*3*	*4*	*5*	*6*	*7*	*8*	*9*	*10*
TRACE ELEMENTS (ppm)										
S	38	7	50	39	18	97	248	180	140	179
Cr	98	10	9	8	7	12	36	41	60	7
Ni	33	–	1	2	2	7	22	15	33	6
Rb	89	372	216	54	112	163	275	215	389	196
Sr	168	219	536	300	237	178	374	483	216	507
Y	91	6	7	20	23	37	265	12	27	92
Zr	449	29	99	220	197	307	429	245	269	440
Ba	1601	1982	2344	620	943	1478	1164	1198	927	569
La	19	–	8	15	18	37	38	36	40	24
Ce	9	6	16	30	40	63	77	72	69	69
Pb	54	44	50	16	21	40	64	40	45	22
K/Rb	369	141	233	236	226	221	139	92	104	85
K/Ba	20.5	26.5	21.5	20.6	26.8	24.4	32.9	16.5	43.5	29.3
Ca/Sr	22.6	7.6	30.3	95.8	86.2	122.2	39.7	53.9	57.9	70.9
Ba/Sr	9.5	9.1	4.4	2.1	4.0	8.3	3.1	2.5	4.3	1.1
Rb/Sr	0.53	1.70	0.40	0.18	0.47	0.92	0.74	0.45	1.80	0.39

1. KG.503.1 Garnetiferous white 'granite'.
2. KG.508.11 White 'granite'.
3. KG.538.2 Diopside-bearing foliated white 'granite'.
4. KG.518.6 Gneissose tonalite.
5. KG.525.5 Gneissose granodiorite.
6. KG.529.3 Granodiorite.
7. KG.505.1 Banded gneiss.
8. KG.505.4 Banded gneiss.
9. KG.509.1 Biotite-gneiss.
10. KG.508.2 Biotite-gneiss.

most of the hornblende was altered to biotite. The net result of the increase in K in the melanosome was to reduce the difference in total alkalis between leucosome and melanosome.

On a triangular diagram with the coordinates (Fe″ + Fe‴)–Mg–Alk (Fig. 38), the banded gneisses and white granites exhibit a distinct trend, not unlike that of the Andean calc-alkaline suite. However, if the coordinates K–Ca–Na are substituted, the analyses plot on the sodium-rich side of the curve for the Andean rocks. They also show a wide scatter and are displaced, relative to the Andean trend, towards the K apex, suggesting selective enrichment in potash. Plots of Fe/(Fe + Mg) against Si revealed further similarities between the metamorphic and igneous rocks, although the former show a greater scatter of points.

Plots of (meso)normative Q, Or, Ab and An proportions of the granitic rocks with Q + Or + Ab greater than 75% (Fig. 39a and b) were compared with the experimental work of Tuttle and Bowen (1958) and Luth and others (1964) in the system $KAlSi_3O_8$–$NaAlSi_3O_8$–SiO_2–H_2O, and of Kleeman (1965) in the system $KAlSi_3O_8$–$NaAlSi_3O_8$–$CaAl_2Si_2O_8$–SiO_2. By comparing their results with the normative Q, Or and Ab proportions of all analysed rocks in Washington's (1917) tables with normative Q + Or + Ab greater than 80%, Tuttle and Bowen showed that there is a close relationship between the minimum melting point for low water-vapour pressures and the normative compositions of the granites. Kleeman went further and established an even closer link between the (normative) average 'granite' and the low-temperature trough in the $KAlSi_3O_8$–$NaAlSi_3O_8$–$CaAl_2Si_2O_8$–SiO_2 system especially at P_{H_2O} greater than 2 000 bar.

It is immediately apparent from Fig. 39a and b that the three white granites are unrelated to the minimum melting curve (P_{H_2O} 500–2 000 bar) in the Q–Or–Ab systems and the low-temperature trough in the Or–Ab–An system. The three granites, which plot within the contoured area and a fourth one which plots just outside (on the Or side), fall in the thermal trough of the Or–Ab–An system. The obvious inference is that the granitic components of the banded gneisses have crystallized from minimum melting-point liquids and the white granites have not. However, these conclusions do not take into consideration the subsequent potash metasomatism and, if an arbitrary 2% of K (less than half of the K content of most of these rocks) is removed and credited to Na, it becomes evident that none of the leucosomes could have crystallized from a minimum melting-point liquid. Conversely, the plot of specimen KG.508.11 will be deflected into the granite field and the plot of specimen KG.538.2 will approach the minimum melting point at P_{H_2O} 10 000 bar. Specimens KG.503.1 and 505.1 plot well away from the others and they are thought to be the products of extreme metamorphic differentiation.

b. *Trace elements.* Cr and Ni show a closer correlation with Mg than with Ca and Fe, suggesting that the micas are likely to be the main sites for these elements, which is in accordance with the findings of Carr and Turekian (1962). In direct contrast to the trend of the Andean rocks, Zr has a strong negative correlation with SiO_2 (Fig. 40). A similar but less pronounced relationship exists between La, Ce and SiO_2. The rare earths, and to a lesser extent Y, have strong positive correlations with P_2O_5, suggesting that in the absence of other recognizable phosphates they are mainly combined in apatite, even in those rocks containing allanite. Pb shows an overall positive correlation with SiO_2, although there is considerable scattering of the points. However, a far stronger positive correlation exists between Pb and K, particularly in rocks containing microcline (e.g. specimens KG.505.2 and 526.3). Rb concentrations range

Table VII. Chemical analyses of white 'granites' and banded gneisses (continued).

	Banded gneisses								
	11	*12*	*13*	*14*	*15*	*16*	*17*	*18*	*19*
TRACE ELEMENTS (ppm)									
S	72	180	269	267	95	64	19	35	320
Cr	7	7	61	32	7	8	6	7	7
Ni	3	3	30	17	–	1	–	4	2
Rb	120	93	160	91	371	327	161	242	302
Sr	520	198	208	153	155	149	530	338	86
Y	28	17	40	35	23	23	1	12	34
Zr	604	164	429	542	105	129	122	167	136
Ba	2594	510	1013	499	442	824	2662	909	288
La	59	14	52	76	27	28	10	21	19
Ce	114	36	98	76	51	51	48	46	50
Pb	28	23	42	26	67	50	3	75	71
K/Rb	251	202	162	140	129	124	266	158	168
K/Ba	11.6	36.9	25.5	25.4	96.8	49.2	16.1	42.2	176.1
Ca/Sr	59.1	106.2	66.6	56.2	18.3	25.2	13.6	31.5	86.3
Ba/Sr	5.0	2.6	4.9	3.3	2.9	5.5	5.0	2.7	3.3
Rb/Sr	0.23	0.47	0.77	0.60	2.14	2.20	0.30	0.72	3.51

11. KG.510.4 Biotite-gneiss.
12. KG.527.1 Sheared banded gneiss.
13. KG.515.2 Quartz-mica-schist.
14. KG.515.1 Quartz-mica-schist.
15. KG.515.6 Siliceous schist.
16. KG.531.1 Siliceous schist.
17. KG.503.4 Granite.
18. KG.505.2 Granite.
19. KG.526.3 Granitic augen-gneiss.

from 54 to 389 ppm but, in view of the close relationship with potassium (Ahrens and others, 1952), little emphasis is placed on specific values. However, K/Rb ratios are significant, the average over the area being 189, which is somewhat lower than the accepted value of 230 for continental rocks. Variation in K/Rb ratios appears to be spatially rather than lithologically controlled, the lower values occurring in two distinct north–south zones (Fig. 16) which coincide with the zones of maximum microcline development and, in the cae of the more westerly zone, with the belt of sheared banded gneisses. Locally, K/Rb ratios in the leucosomes are higher by 50–60 than in the melanosomes, evidently as a result of partitioning of K and Rb between feldspar in the leucosome and biotite in the melanosome. The similarity between whole-rock K/Rb ratios and those of the potash feldspars (Tables VII and IX) is further evidence of crystal growth after the formation of the banded gneisses.

Ca/Sr ratios range from 122 to 8 with a mean of 55, and they show a general decrease in the more acid rocks, whilst Ba/Sr and Rb/Sr have a less pronounced correlation with SiO_2. The variation of the last two ratios (1.1–9.5 and 0.2–2.2, respectively) is almost certainly a reflection of the variable content of Rb and Ba but, whereas the Rb has obviously been affected by the potash metasomatism, K/Ba plots suggest that the Ba contents are those of the pre-metasomatism banded gneisses.

2. Metagabbros

When plotted on a triangular diagram with the coordinates Fe″ + F‴–Mg–Alk (Fig. 41), the two analysed metagabbros plot on or close to the 'Andean' trend but rather nearer the granodiorite field than those of the gabbros; in effect they are alkali-enriched and Mg deficient gabbros. Using the coordinates Na–Ca–K, specimen KG.523.5 again plots on the Andean curve, albeit at the Na-rich end of the gabbro field, whereas the plot of specimen KG.525.2 is significantly displaced toward the Na apex. Like their Andean counterparts, the metagabbros have high Al_2O_3 which favoured the early crystallization of the plagioclase, and the resultant deficiency of CaO in the magma meant that orthopyroxene formed before clinopyroxene. The higher TiO_2 and Na_2O contents of specimen KG.525.2 are reflected in the deeper brown of the hornblende and the more albitic plagioclase. This specimen also has considerably higher Y, Zr, La and Ce, which probably reflects its close proximity to tonalites in which these elements are common.

3. Diorite-gneisses

The name diorite-gneiss has been applied to rocks of somewhat differing appearance but with an essentially similar mineralogy (Table V). However, their chemistry does show certain differences (Table VIII), particularly in such oxides as MgO and CaO, which probably explains the relatively high percentage of hornblende in specimen KG.573.1. In overall chemistry (Table VIII), apart from higher K_2O and MgO, this rock is quite similar to the metagabbros; when plotted on the Fe″ + Fe‴–Mg–Alk triangular diagram, it is quite remote from other meta-igneous rocks, but when plotted in the Na–Ca–K field it lies close to the amphibolites. Within the same outcrop are bands of more quartz-rich diorite-gneiss (e.g. KG.573.3) which suggest that the higher MgO may be the result of metamorphic differentiation. The field relations and major-element chemistry of specimen KG.526.2 suggest a possible analogy with some of the basic members of the banded gneisses. However, comparison of the respective Fe″ + Fe‴–Mg–Alk and K–Ca–Na triangular diagrams reveals an enrichment of

Table VIII. Chemical analyses of diorite-gneisses, metagabbros and amphibolites.

	Diorite-gneisses			*Metagabbros*		*Older amphibolites*		
	1	*2*	*3*	*4*	*5*	*6*	*7*	*8*
SiO_2	57.56	64.37	51.40	53.62	51.84	48.92	49.85	47.90
TiO_2	0.78	0.49	0.54	0.47	1.10	1.31	1.19	1.09
Al_2O_3	16.24	16.57	19.04	21.10	20.33	16.14	15.52	12.30
Fe_2O_3	3.43	2.36	2.24	2.66	3.45	3.70	4.96	4.29
FeO	3.83	1.36	3.12	3.05	4.23	6.60	6.44	7.72
MnO	0.19	0.07	0.10	0.11	0.21	0.13	0.18	0.21
MgO	3.02	1.73	6.84	3.39	2.91	6.81	5.85	8.23
CaO	6.33	4.77	9.23	9.82	8.23	9.53	10.39	12.78
Na_2O	3.60	4.54	2.61	3.20	5.06	2.52	3.04	1.86
K_2O	1.78	1.24	1.87	0.62	0.38	0.94	0.36	0.36
P_2O_5	0.26	0.11	0.04	0.03	0.30	0.22	0.16	0.11
H_2O^+	1.03	1.88	1.85	0.41	0.95	1.11	1.16	1.72
H_2O^-								
CO_2	0.89	0.68	0.69	0.85	0.62	1.02	0.55	0.49
Total	98.94	100.17	99.57	99.33	99.61	98.95	99.66	99.06
ANALYSES LESS TOTAL WATER (RECALCULATED TO 100)								
SiO_2	58.79	65.48	52.59	54.20	52.54	49.98	50.58	49.21
TiO_2	0.80	0.50	0.55	0.47	1.11	1.33	1.21	1.12
Al_2O_3	16.59	16.86	19.48	21.33	20.61	16.49	15.75	12.64
Fe_2O_3	3.50	2.40	2.29	2.69	3.50	3.78	5.03	4.41
FeO	3.92	1.38	3.20	3.08	4.29	6.74	6.53	7.93
MnO	0.19	0.07	0.11	0.11	0.21	0.13	0.18	0.22
MgO	3.08	1.76	6.99	3.43	2.95	6.96	5.93	8.45
CaO	6.46	4.85	9.44	9.93	8.34	9.74	10.54	13.13
Na_2O	3.68	4.62	2.67	3.24	5.13	2.57	3.08	1.91
K_2O	1.82	1.26	1.91	0.62	0.38	0.96	0.37	0.37
P_2O_5	0.26	0.12	0.04	0.03	0.30	0.22	0.16	0.11
CO_2	0.91	0.70	0.71	0.86	0.63	1.04	0.56	0.50
ELEMENT WEIGHT PERCENTAGES (ANHYDROUS)								
Si^{4+}	27.49	30.61	24.59	25.34	24.56	23.36	23.65	22.98
Ti^{4+}	0.48	0.30	0.33	0.28	0.67	0.80	0.72	0.67
Al^{3+}	8.78	8.92	10.31	11.29	10.91	8.73	8.33	6.69
Fe^{3+}	2.45	1.68	1.60	1.88	2.45	2.64	3.52	3.08
Fe^{2+}	3.04	1.08	2.48	2.39	3.33	5.24	5.08	6.16
Mn^{2+}	0.15	0.06	0.08	0.09	0.16	0.10	0.14	0.17
Mg^{2+}	1.86	1.06	4.22	2.07	1.78	4.19	3.58	5.10
Ca^{2+}	4.62	3.47	6.75	7.09	5.96	6.96	7.53	9.39
Na^{+}	2.73	3.43	1.98	2.40	3.80	1.91	2.28	1.42
K^{+}	1.51	1.04	1.59	0.52	0.32	0.80	0.31	0.31
P^{5+}	0.11	0.05	0.02	0.01	0.13	0.10	0.07	0.05
C^{4+}	0.25	0.19	0.19	0.24	0.17	0.28	0.15	0.14
O^{2-}	46.54	48.11	45.85	46.39	45.74	44.82	44.55	43.84
BARTH MESONORMS								
Mt	1.71	2.52	2.37	2.84	3.65	4.02	5.33	4.74
Ti	0.56	1.05	1.14	0.99	2.34	2.85	4.11	2.40
Ap	3.72	0.24	0.08	0.05	0.65	0.48	0.35	0.24
Ab	33.55	41.76	23.79	29.25	45.99	23.50	28.00	17.59
Or	3.85	2.95	–	–	–	–	–	–
An	23.80	21.70	35.29	42.16	32.02	31.10	28.40	25.43
Act	6.30	0.08	13.65	8.48	5.10	17.63	24.83	29.57
Di	–	–	–	–	–	–	–	–
Bi	11.28	7.27	17.99	5.92	3.68	9.28	3.44	3.60
Hy	–	–	0.10	2.50	6.52	8.94	4.40	16.24
Ed	–	–	–	–	–	–	–	0.20
Q	15.23	22.45	5.59	7.81	0.05	2.21	1.14	–
COORDINATES OF TRIANGULAR DIAGRAMS								
A	36.6	53.9	30.1	31.5	35.3	18.3	17.5	10.7
F	47.4	33.3	34.4	46.2	49.5	53.3	58.2	57.6
M	16.0	12.8	35.5	22.3	15.2	28.4	24.3	31.7
K	17.0	13.1	15.4	5.2	3.1	8.3	3.0	2.7
Na	30.8	43.2	19.2	24.0	37.7	19.7	22.6	12.8
Ca	52.2	43.7	65.4	70.8	59.2	72.0	74.4	84.5

Table VIII. Chemical analyses of diorite-gneisses, metagabbros and amphibolites (continued).

	Older amphibolites			*Younger amphibolites*			*Quartz-plagioclase-amphibolites*	
	9	*10*	*11*	*12*	*13*	*14*	*15*	*16*
SiO_2	53.83	48.70	49.70	48.84	51.30	48.01	60.86	67.90
TiO_2	1.27	1.66	0.77	2.18	2.51	2.20	0.89	0.61
Al_2O_3	13.89	10.57	18.42	11.95	14.24	14.42	15.83	15.15
Fe_2O_3	3.43	4.90	4.19	4.55	4.74	2.58	3.67	1.50
FeO	5.94	9.93	5.07	9.33	6.49	9.77	3.15	1.55
MnO	0.12	0.21	0.15	0.18	0.15	0.15	0.18	0.14
MgO	5.80	7.12	5.55	4.20	5.86	6.84	2.24	1.13
CaO	8.19	10.42	9.37	8.99	7.81	8.93	5.73	4.70
Na_2O	2.80	1.85	2.67	2.61	3.31	2.76	4.22	5.21
K_2O	1.47	0.71	1.87	1.04	1.74	0.90	0.84	0.56
P_2O_5	0.19	0.12	0.12	0.52	0.46	0.34	0.16	0.14
H_2O^+ / H_2O^-	1.47	1.43	1.86	1.55	1.67	1.71	1.30	1.05
CO_2	0.89	0.70	0.83	0.95	1.14	1.06	0.74	0.56
Total	99.29	99.32	99.71	99.35	99.26	99.67	99.81	100.20
ANALYSES LESS TOTAL WATER (RECALCULATED TO 100)								
SiO_2	55.02	50.77	49.92	52.46	50.35	48.99	61.78	68.48
TiO_2	1.30	1.70	0.79	2.23	2.57	2.24	0.90	0.62
Al_2O_3	14.20	10.80	18.82	12.23	14.59	14.71	16.07	15.28
Fe_2O_3	3.51	5.01	4.28	4.65	4.85	2.63	3.72	1.51
FeO	6.70	10.14	5.18	9.54	6.64	9.97	3.19	1.56
MnO	0.13	0.21	0.15	0.18	0.16	0.15	0.18	0.15
MgO	5.93	7.27	5.67	4.29	6.00	6.98	2.27	1.14
CaO	8.38	10.64	9.58	9.19	8.00	9.11	5.81	4.74
Na_2O	2.86	1.89	2.73	2.67	3.39	2.82	4.29	5.26
K_2O	1.50	0.73	1.91	1.06	1.78	0.92	0.85	0.56
P_2O_5	0.20	0.12	0.12	0.50	0.48	0.35	0.17	0.14
CO_2	0.91	0.72	0.85	0.97	1.17	1.08	0.75	0.56
ELEMENT WEIGHT PERCENTAGES (ANHYDROUS)								
Si^{4+}	25.72	23.70	23.31	24.50	23.54	22.90	28.88	32.01
Ti^{4+}	0.78	1.02	0.47	1.34	1.54	1.35	0.54	0.37
Al^{3+}	7.51	5.71	9.96	6.47	7.72	7.79	8.50	8.08
Fe^{3+}	2.45	3.50	2.99	3.25	3.40	1.84	2.60	1.06
Fe^{2+}	4.72	7.80	4.02	7.41	5.16	7.75	2.48	1.22
Mn^{2+}	0.10	0.16	0.12	0.14	0.12	0.12	0.14	0.11
Mg^{2+}	3.57	4.38	3.42	2.59	3.62	4.21	1.37	0.69
Ca^{2+}	5.99	7.61	6.85	6.57	5.72	6.51	4.15	3.39
Na^{+}	2.12	1.40	2.03	1.98	2.52	2.09	3.18	3.90
K^{+}	1.24	0.61	1.59	0.88	1.48	0.76	0.71	0.47
P^{5+}	0.09	0.05	0.05	0.23	0.21	0.15	0.07	0.06
C^{4+}	0.25	0.20	0.23	0.26	0.32	0.30	0.20	0.15
O^{2-}	45.44	43.78	44.96	44.38	44.65	44.20	47.18	48.49
BARTH MESONORMS								
Mt	3.74	5.48	4.56	5.10	5.19	2.82	3.96	1.59
Ti	2.76	3.72	1.68	4.89	5.49	4.80	1.92	1.29
Ap	0.42	0.27	0.27	1.17	1.21	0.74	0.35	0.29
Ab	26.19	17.75	25.00	25.15	31.15	24.65	39.15	47.46
Or	1.22	–	2.63	–	–	–	–	2.77
An	21.85	19.72	34.12	19.17	19.75	25.34	22.47	16.55
Act	21.83	42.74	16.05	25.05	11.33	12.19	3.90	6.08
Di	–	–	–	–	–	–	–	–
Bi	12.53	7.20	14.19	10.56	17.20	8.88	8.16	0.93
Hy	–	0.28	–	0.24	3.80	16.62	0.30	–
Ed	–	–	–	–	–	3.96	–	–
Q	9.46	2.84	15.00	8.67	4.88	–	19.79	23.04
COORDINATES OF TRIANGULAR DIAGRAMS								
A	23.8	11.3	25.6	17.8	24.7	17.1	37.6	59.6
F	50.8	64.0	50.0	66.2	52.9	57.6	49.2	31.0
M	25.4	24.7	24.4	16.0	22.4	25.3	13.2	9.4
K	13.3	6.3	15.2	9.4	15.2	8.2	8.8	6.0
Na	22.7	14.6	19.3	21.0	25.9	22.3	39.5	50.3
Ca	64.0	79.1	65.5	69.6	58.9	69.5	51.7	43.7

Table VIII. Chemical analyses of diorite-gneisses, metagabbros and amphibolites (continued).

	Diorite-gneisses			*Metagabbros*		*Older amphibolites*		
	1	*2*	*3*	*4*	*5*	*6*	*7*	*8*
TRACE ELEMENTS (ppm)								
S	66	19	49	140	392	799	1136	1046
Cr	10	20	172	27	12	44	33	165
Ni	1	9	47	12	4	12	13	18
Rb	158	37	76	26	10	59	5	4
Sr	322	688	675	484	575	553	340	251
Y	28	7	11	10	35	27	13	17
Zr	176	168	106	91	666	116	83	75
Ba	389	1060	643	258	197	621	166	97
La	11	13	4	–	8	22	6	2
Ce	23	27	19	6	31	5	14	10
Pb	17	14	13	6	7	18	15	3
K/Rb	94	277	204	197	313	133	603	739
K/Ba	38.0	9.7	24.1	19.8	15.9	12.6	18.2	30.5
Ca/Sr	140.5	49.6	97.8	145.1	102.3	123.2	218.4	364.1
Ba/Sr	1.2	1.5	1.0	0.5	0.3	1.1	0.5	0.4
Rb/Sr	0.49	0.05	0.11	0.05	0.02	0.11	0.02	0.02
Ca/Y	1615	4870	6000	7021	1681	2523	5712	5376
Ca/Ce	1967	1263	3474	11702	1898	13920	5304	9139
Ce/Y	0.82	3.85	1.73	0.60	0.89	0.19	1.08	0.59
Ca/TRE	1330	852	2870	11702	1508	2577	3713	7616

1. KG.526.2 Diorite-gneiss.
2. KG.576.1 Diorite-gneiss.
3. KG.573.1 Diorite-gneiss.
4. KG.523.5 Metagabbro.
5. KG.525.2 Metagabbro.
6. KG.505.3 Older amphibolite.
7. KG.518.1 Older amphibolite.
8. KG.525.1 Older amphibolite.

iron relative to the banded gneisses, and a deficiency of potassium although the rock is known to have undergone potash metasomatism. When the case of specimen KG.576.1 is considered in the same fashion (and here the field relations are of no assistance), the triangular plots confirm a possible comparison which is also apparent in the norms. However, in the trace elements certain differences are evident; in particular, the diorite-gneiss has lower Y and Zr, lower Ba/Sr and Ca/Sr ratios, and higher Ca/Y, Ca/Ce, Ce/Y and Ca/total rare earth ratios. Thus, despite a quite considerable compositional range, the diorite-gneisses are chemically distinguishable from the banded gneisses. The K and Rb contents and the K/Rb ratios conform to the zonal distribution noted in the banded gneisses.

4. Amphibolites

The overall chemistry (Table VIII) of the younger and older amphibolites compares quite favourably with that of the post-Andean basic dykes but, when plotted on Fe″ + Fe‴–Mg–Alk and K–Ca–Na triangular diagrams (Fig. 42), the amphibolites are somewhat richer in Fe and Ca. Amongst the trace elements those which are least likely to be affected by weathering and metamorphism (e.g. Y and Zr) show favourable comparison with the later dykes. With the exception of specimen KG.541.1, about which more will be said later, the TiO_2 values of the older amphibolites are noticeably higher than those of the later dykes but seldom are they more than half the values of the three younger amphibolites. It is also possible to distinguish between younger and older amphibolites on the basis of the P_2O_5 content. There is a strong similarity in K and Rb, and K/Rb ratios between the diorite-gneisses, metagabbros, quartz-plagioclase-amphibolites and amphibolites together with a spatial distribution identical to that of the banded gneisses. This would seem to indicate that the second (microcline-forming) potash metasomatism occurred late in the metamorphic history.

Within the Andean granodiorite at station KG.541 (one of the closest to the metamorphic complex) are numerous rounded to sub-angular xenoliths of foliated and non-foliated amphibolite, some (if not all) of which were derived from the metamorphic complex. One of the unfoliated examples, specimen KG.541.1, has a chemistry similar to that of the older amphibolites but with slightly lower TiO_2 and higher K_2O.

Apart from slightly higher SiO_2 and lower K_2O, the two quartz-plagioclase-amphibolites show affinities to two of the diorite-gneisses, although the field relations and texture, combined with considerable differences in Y and Zr, preclude any correlation between the two groups.

If the analyses are plotted on triangular diagrams with the coordinates Fe–Mg–Alk and K–Ca–Na (Fig. 43), a more positive link with the Mesozoic volcanic rocks is apparent. A closer investigation reveals that in the volcanic rocks the relative positions of the analyses are more or less common to both curves, whereas the plots of the two quartz-plagioclase-amphibolites are anomalous. Thus, on the K–Ca–Na plot, specimen KG.524.2 lies alongside specimen KG.581.9 (basaltic andesite) but on the other plot its immediate neighbour is specimen KG.554.2 (andesite), and the rocks have apparently exchanged curves. The latter situation could be rectified by assuming a loss of potash. Certainly, when compared with the Upper Jurassic volcanic rocks and other metamorphic rocks, the quartz-plagioclase-amphibolites are deficient in potash, and it is possible they provided some of the material for the subsequent potash metasomatism. However, both analysed rocks have unusually high (Fe + Mg + Mn + Ca)/Si ratios and a more likely explanation of their unusual chemistry is that they are basic tuffs admixed with detrital quartz.

Table VIII. Chemical analyses of diorite-gneisses, metagabbros and amphibolites (continued).

	Older amphibolites			*Younger amphibolites*			*Quartz-plagioclase-amphibolites*	
	9	*10*	*11*	*12*	*13*	*14*	*15*	*16*
TRACE ELEMENTS (ppm)								
S	206	330	51	69	38	453	81	14
Cr	71	56	33	28	17	32	31	8
Ni	21	39	19	12	17	23	8	–
Rb	103	7	76	35	93	26	24	12
Sr	406	119	595	279	493	479	226	186
Y	25	34	14	18	22	22	40	53
Zr	234	88	120	179	301	228	249	364
Ba	472	2339	430	412	388	313	311	303
La	25	12	5	25	29	23	10	16
Ce	55	29	21	50	53	33	33	32
Pb	43	40	30	18	11	7	7	12
K/Rb	118	844	204	247	155	288	291	387
K/Ba	25.8	2.53	36.0	21.0	37.2	24.0	22.5	15.3
Ca/Sr	144.3	376.2	112.7	230.4	113.3	133.3	181.2	180.7
Ba/Sr	1.2	11.8	0.7	1.5	0.8	0.7	1.4	1.6
Rb/Sr	0.25	0.04	0.13	0.13	0.19	0.05	0.11	0.07
Ca/Y	2343	2191	4787	3571	2539	2903	1024	634
Ca/Ce	1065	2569	3192	1286	1054	1935	1241	1050
Ce/Y	2.20	0.85	1.50	2.78	2.41	1.50	0.83	0.60
Ca/TRE	732	1671	2578	857	681	1140	952	700

9. KG.529.2 Older amphibolite.
10. KG.536.1 Older amphibolite.
11. KG.541.1 Older amphibolite.
12. KG.513.4 Younger amphibolite.
13. KG.535.2 Younger amphibolite.
14. KG.535.3 Younger amphibolite.
15. KG.521.9 Quartz-plagioclase-amphibolite.
16. KG.524.2 Quartz-plagioclase-amphibolite.

I. Origin of the Metamorphic Rocks

1. White granites

Consideration of the available information, particularly the chemistry, points towards the white granites being initially homogeneous igneous rocks upon which metamorphic differentiation imposed a distinct heterogeneity.

2. Banded gneisses

It is fairly evident from the chemistry and mineralogy of the banded gneises that the parent rock was an igneous rock of tonalitic composition, probably a syn-orogenic intrusion. The formation of their conspicuous banding is rather more problematical, since any one, or a combination of two or more, of the following mechanisms might have been responsible:

a. Preservation of primary structures.
b. Magmatic intrusion.
c. Metasomatism.
d. Anatexis.
e. Metamorphic differentiation.

a and b. The banded gneisses are occasionally reminiscent of the flow-banded Andean granodiorites, particularly where the latter possess 'schlieren' and have been invaded by veins of granite-aplite. Despite the recognition of possible flow-aligned crystals in the banded gneisses, there are many features which deny such comparison; in particular, the vast chemical differences between aplite, granodiorite and amphibolite xenoliths (contrasting sharply with the similarity between leucosome and melanosome), and the frequent cross-cutting nature and fine grain-size of the aplites. In addition to these characteristics, the presence of both sharp and gradational contacts serves to distinguish them from the more obviously injected *lit-par-lit* granite-gneisses which are described on p. 45. Also, if the leucosomes had originated by injection of liquid magma, they would be expected to approximate to eutectic composition.

c. Permeation of these rocks by magmatically derived pore solutions (metasomatism) is known to have occurred, but some time after formation of the banding. Comparison of chemical analyses (Table VII), with due allowance for subsequent potash metasomatism, indicates the tonalite–banded gneiss conversion is an isochemical process.

d. Hughes (1970), in a discussion on the significance of biotite selvages in migmatites, concluded that the marked metamorphic differentiation displayed by contact migmatites with veinite structure and biotite selvages can be explained by the combination of such diffusion processes (long-continued diffusion through intergranular pore fluids), accentuated by incipient anatexis and the ensuing interaction between two contrasting intergranular liquid phases.

The application of these conclusions to the rocks being discussed here is valid for, although the banded gneisses are not contact migmatites *sensu stricto*, they were formed in a similar high-temperature–low-pressure environment. The absence of biotite selvages in the banded gneisses implies that one or both of the pore fluids was absent and, as a corollary, it follows that partial melting most probably did not occur. Further evidence against formation by anatexis is the occurrence of relict igneous textures both in the leucosome and melanosome, and the lack of any recognizable restites.

The discrepancy between leucosome and eutectic composition does not necessarily preclude anatexis (White, 1966; Hughes, 1970) and, in general, the major elements provide little direct evidence on genesis. However, the trace-

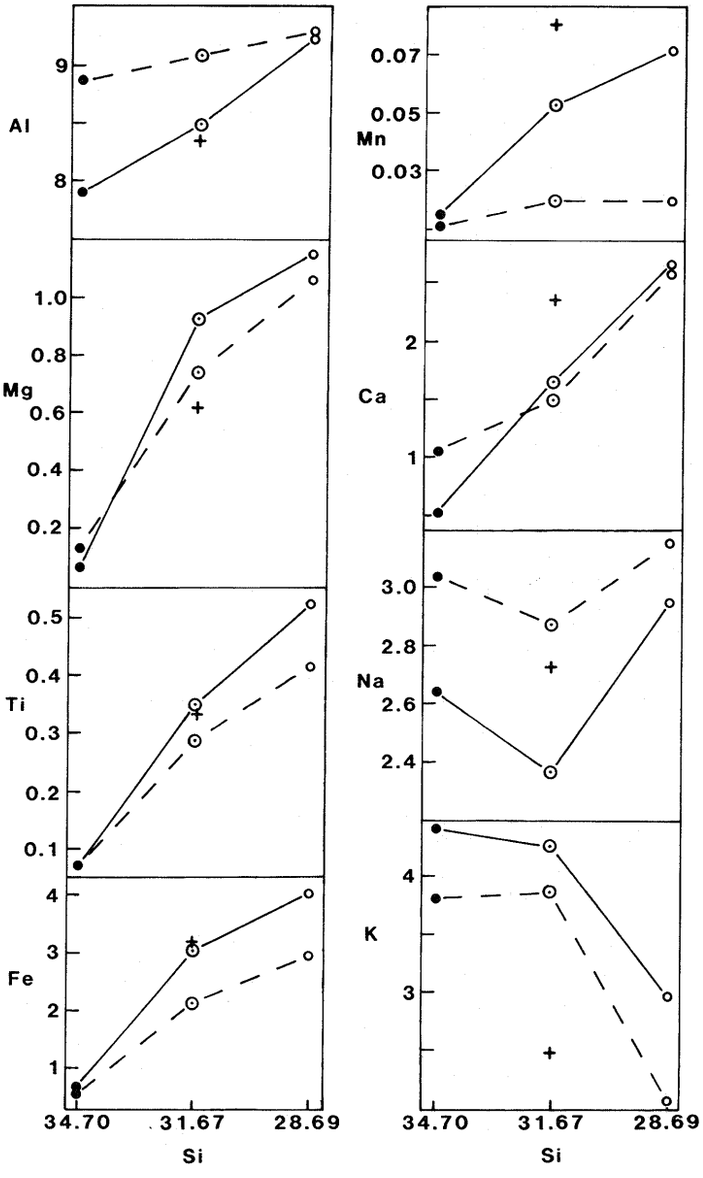

Fig. 37. Major element variation in the banded gneisses based on 13 analyses. The average of three undifferentiated tonalites (+) is plotted for comparison. Large-scale banding (> 10 cm), continuous line; small-scale banding (< 10 cm), broken line; granite (●); banded gneiss (⊙); biotite-gneiss (○).

element proportions of an anatectic melt should approximate to those produced by prolonged magmatic fractionation, and by analogy with the acid end members of the Andean Intrusive Suite (p. 76) the Sr content of such melts should, with increasing acidity, rise relative to Ca and decline against Ba. In the banded gneisses Sr/Ba ratios show no distinct trend, whilst Sr/Ca ratios have a positive correlation with SiO_2. However, in view of probable later adjustments during two episodes of potash metasomatism, the meaningfulness of this trend is open to doubt. For similar reasons, Heier and Taylor's (1959) conclusions on the trace-element distribution in potash feldspars must also be discounted.

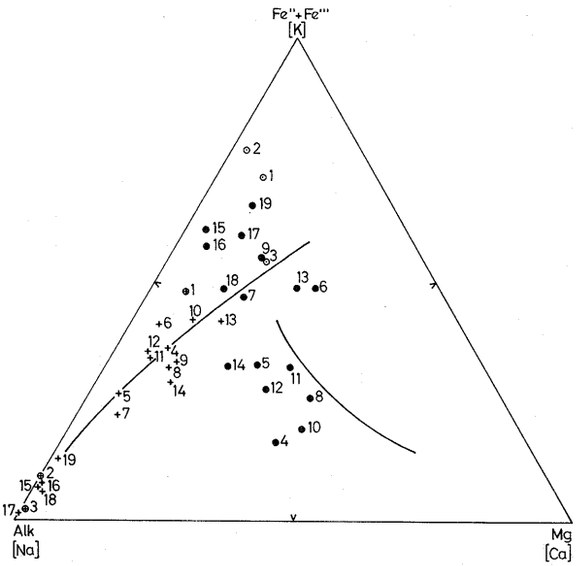

Fig. 38. Alk–(Fe″ + Fe‴)–Mg and Ca–Na–K triangular variation diagrams for the banded gneisses (+ and ●) and white granites (⊕ and ⊙). Variation trends for the Graham Land Andean Intrusive Suite (after Adie, 1964*b*) are superimposed.

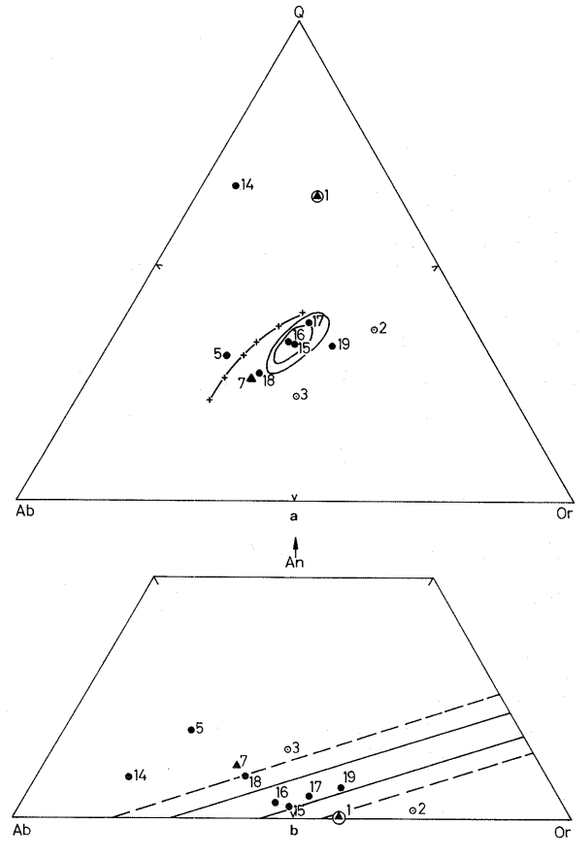

Fig. 39. Triangular plots of normative (a) Q–Or–Ab and (b) Or–Ab–An proportions for banded gneisses and white granites, numbered as in Table VII, with Q + Or + Ab > 80% (● and ⊙) or <80% but >75% (▲ and ⊙). (a) shows the minimum melting-point curve P_{H_2O} 500–100 000 bar (after Tuttle and Bowen (1958) and Luth and others (1964)) and the maximum distribution of granitic rocks (after Tuttle and Bowen, 1958). (b) shows the region of the thermal trough (after Kleeman, 1965).

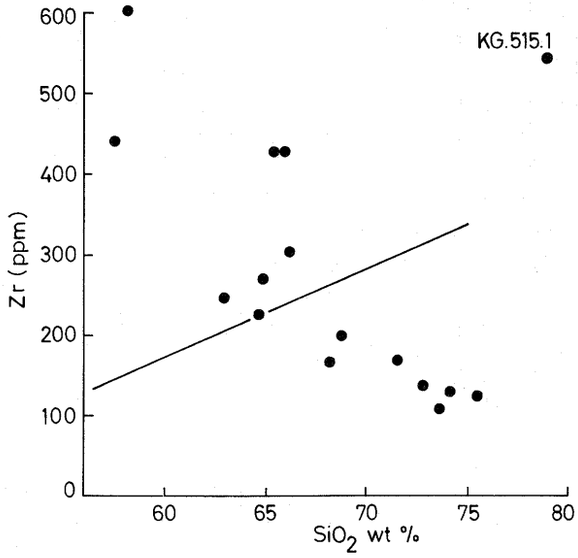

Fig. 40. Plot of Zr against SiO_2 for banded gneisses. The plot emphasizes the negative correlation of Zr with SiO_2, opposite to the superimposed trend of the Andean granites and granodiorites (Table XXII).

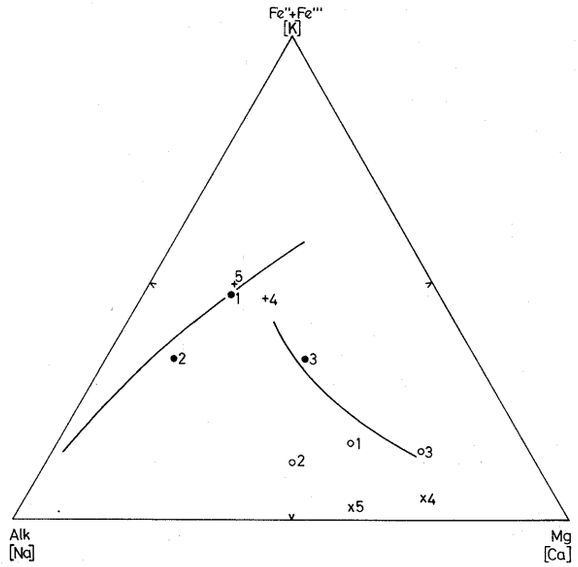

Fig. 41. Alk–(Fe″ + Fe‴)–Mg and Ca–Na–K triangular variation diagrams for diorite-gneisses (● and ○) and metagabbros (+ and ×), numbered in Table VIII. Variation trends for the Graham Land Andean Intrusive Suite (after Adie, 1964*b*) are superimposed.

Table IX. Partial chemical analyses of potash feldspars from white 'granites' and banded gneisses.

	1	*2*	*3*	*4*	*5*	*6*	*7*
SiO_2	63.38	63.41	63.30	62.87	62.91	63.40	62.97
TiO_2	–	–	–	–	–	–	–
Al_2O_3	20.03	19.99	20.11	20.10	19.94	20.32	20.16
Fe_2O_3							
FeO	n.d.	n.d.	n.d.	n.d.	n.d.	n.d.	n.d.
MnO							
MgO	–	–	–	–	–	–	0.02
CaO	0.82	1.04	0.84	0.90	0.78	0.89	0.66
Na_2O	2.14	2.03	2.12	1.95	1.66	2.24	1.42
K_2O	14.14	14.06	14.43	14.85	15.01	13.31	16.30
P_2O_5	0.04	–	0.03	0.02	0.01	0.05	–
H_2O	n.d.	n.d.	n.d.	n.d.	n.d.	n.d.	n.d.
CO_2							
TRACE ELEMENTS (ppm)							
S	28	61	40	67	55	51	198
Rb	370	510	386	332	292	614	836
Sr	651	704	876	299	588	482	385
Ba	535	478	662	588	1 221	230	365
Pb	139	54	83	100	52	135	80
K/Rb	317	229	310	371	427	180	162
K/Ba	219	244	181	209	102	481	371
Ca/Sr	9.00	10.60	6.90	21.50	9.50	13.20	12.30
Ba/Sr	0.82	0.68	0.78	1.97	2.08	0.48	0.95
Rb/Sr	0.57	0.72	0.44	1.11	0.50	1.27	2.17

1. Orthoclase; white 'granite' (KG.503.1).
2. Orthoclase; white 'granite' (KG.538.2).
3. Orthoclase; granite (KG.503.4).
4. Orthoclase; banded gneiss (KG.529.3).
5. Orthoclase; banded gneiss (KG.510.4).
6. Potash feldspar of variable obliquity; banded gneiss (KG.505.2).
7. Potash feldspar of variable obliquity; white 'granite' (KG.508.11).

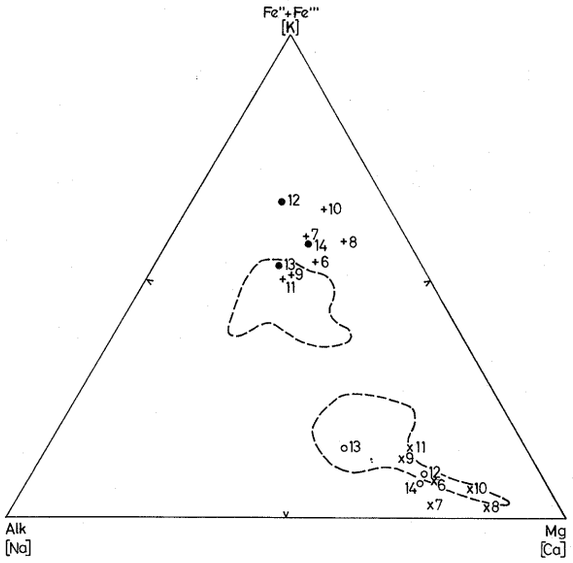

Fig. 42. Alk–(Fe″ + Fe‴)–Mg and Ca–Na–K triangular diagrams for older (+ and ×) and younger (● and ○) amphibolites, numbered as in Table VIII. Fields of the late basic and intermediate dykes (Fig. 66) are superimposed.

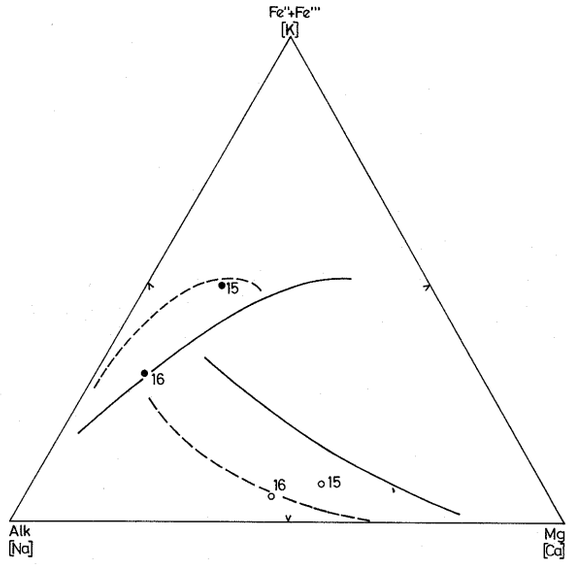

Fig. 43. Alk–(Fe″ + Fe‴)–Mg and Ca–Na–K triangular diagrams for quartz-plagioclase-amphibolites, numbered as in Table VIII. Variation trends of the Mesozoic volcanic rocks (Figs 52 and 53) are superimposed.

The local mobilization of the granites (p. 14) occurred after the emplacement of the amphibolites and hence after the formation of the banded gneisses. There is strong evidence that the plagioclase within these veins did not enter a liquid phase during emplacement, but the same cannot be said of the quartz. Injection of a crystal 'mush' in the presence of much water is considered the most likely explanation.

e. The term metamorphic differentiation was introduced by Stillwell (1918) to cover collectively the various processes by which contrasted mineral assemblages develop from an initially uniform parent rock during metamorphism. Segregation of biotite–hornblende and of epidote–labradorite enclosed in amphibolite, complimentary hornblende and feldspathic layers in amphibolite, and garnet porphyroblasts in otherwise fine-grained schists were cited as typical products of metamorphic differentiation. Several features in these rocks suggest the banding is the result of metamorphic differentiation.

i. The occurrence of both sharp and gradational contacts between leucosome and melanosome.

ii. 'Equally common (as a product of metamorphic differentiation) is the development of veins or laminae of simple mineral composition in initially homogeneous rocks' (Turner and Verhoogen, 1960, p. 583). In most of the banded gneisses the same mineral assemblage is present throughout the whole rock, but variations in the relative proportions of individual minerals in alternating layers result in strongly contrasted bulk chemical compositions when adjacent layers are compared. Thus in the quartz-mica-schists the quartz-rich bands contain small amounts of plagioclase and biotite, whilst smaller quartz grains are common in the mica-rich bands. Read (1933) suggested that such quartz-rich veins and stringers are products of metamorphic differentiation.

iii. 'The growth of porphyroblasts is also one of the most familiar results of metamorphic differentiation' (Turner and Verhoogen, 1960, p. 583). Potash feldspar is the only porphyroblast present in the banded gneisses and it is known to have grown after the formation of the banding, but the frequent garnet porphyroblasts leave no doubt that metamorphic differentiation was operative in the white granites. Although the white granites were most probably emplaced sometime before the tonalites, there is no reason to think the banding in the two rock types did not form simultaneously.

e. *Conclusions.* Of the possible alternatives considered, metamorphic differentiation seems to be the most likely mechanism for the formation of the banding in the white granites and banded gneisses. The physical process of differentiation was probably achieved by large-scale metamorphic diffusion. Metamorphic diffusion, the more general process of migration of rock components during metamorphism, whether or not the segregation of the migrating materials led to the development of definite metamorphism differentiates (Stillwell, 1918), has been recognized in many metamorphic terrains (e.g. Eskola, 1932; Turner, 1941; Gavelin, 1952; Roberts, 1953; Bowes and Park, 1966). Although anatexis and the presence of a silicate pore solution have been discounted, the dimensions of some of the differentiates suggest the diffusion might have been assisted by an aqueous intergranular pore fluid.

3. Amphibolites

The general field relations and textures preclude anything but an igneous origin for the younger amphibolites and several of the older suite but, where the latter occur (as remote lenses) within the banded gneisses and white granites and/or have completely recrystallized, the evidence is not clear cut. Ideally, the comparison of chemical trends is preferable to that of simple chemical abundances, since the latter are more susceptible to

such processes as metasomatism (Evans and Leake, 1960; Leake, 1964; van der Kamp, 1970), but the number of analyses available is insufficient to produce unequivocal results.

Considered as a group, the older amphibolites conform to several general chemical limitations, in particular, with regard to such elements as Ti, Y and Zr; the range of values of these elements (with the possible exception of specimen KG.541.1) is only marginally greater than that shown by such a group as the post-Andean basic dykes. Since there are, within this group of chemically similar metamorphic rocks, several which are undoubtedly metabasic dykes, it is not unreasonable to suppose that the older amphibolites are all (with the exception of specimen KG.541.1) of igneous origin. Certainly, Ti values for the older amphibolites are well within the field of igneous rocks (Goldschmidt, 1954).

On the basis of chemistry, the parentage of quartz-plagioclase-amphibolites was attributed to basic tuffs admixed with detrital quartz, a hypothesis which finds support in the following:

i. The absence of hornblende in the quartzo-feldspathic stripes (biotite being the only ferromagnesian mineral).
ii. The layer of hornblende crystals in specimen KG.525.10. In this instance the volcanic material is distinctly subordinate.

J. Metamorphic History

Three metamorphic events (Table II) of chronologically decreasing intensity have been widely recognized. The first predated the white granites and quartz-plagioclase-amphibolites but it had ceased before the intrusion of the older amphibolites. The second and third metamorphisms post-dated the emplacement of the older and younger amphibolites, respectively.

The mineral assemblages of the younger and older amphibolites (in particular the high An content of the plagioclase, the presence of cummingtonite, the rarity of epidote and the absence of garnet) and, to a lesser extent, the textures are typical products of the andalusite-sillimanite type of metamorphic facies series, and, as such, were formed under fairly low solid pressures (<5 kbar). This type of metamorphism is usually found in contact aureoles surrounding synkinematic intrusions but examples have been recorded in regional metamorphic terrains, e.g. the Ryoke metamorphic belt of Japan (Suwa, 1961) and some of the early Palaeozoic metamorphic belts of New South Wales. The type metamorphic terrain is in the central part of the Abukuma Plateau in Japan (Miyashiro, 1953, 1958; Shidô, 1958; Shidô and Miyashiro, 1959). The facies series of this type is composed of the greenschist and amphibolite facies (Miyashiro, 1961). It will be noted that neither andalusite nor sillimanite occur in any of the banded gneisses, and it must be assumed that their growth was inhibited by an excess of potassium.

1. Metamorphism of the white granites and quartz-plagioclase-amphibolites

Although no analyses of garnet from specimen KG.503.1 were undertaken, modal analysis of the rock suggests that most of the FeO is combined in the garnet (the development of biotite and chlorite are later events and need not be considered here). Since FeO + MgO + CaO + MnO is normally between 30 and 40% in most pyralspite garnet, it is evident the MnO content of this garnet must be less than 1%, which in turn indicates the metamorphic grade reached at least zone C or the upper amphibolite facies.

It is possible that the metamorphism proceeded beyond the amphibolite facies for, in the border field between the amphibolite and granulite facies, sphene undergoes several reversible reactions with common rock-forming minerals, with the liberation of rutile and/or ilmenite (Ramberg, 1952). There is no indication (Table X) of the quartz-plagioclase-amphibolites having been metamorphosed beyond zone C and it is probable that, as in the subsequent metamorphism, there was a westerly decrease in metamorphic grade.

Since there is no evidence to the contrary, the emplacement of the syn-orogenic tonalites occurred during this metamorphism, probably after the peak, as there are no indications of these rocks having been metamorphosed beyond zone C. It would seem that the formation of the banded gneisses by metamorphic differentiation occurred shortly afterwards.

Heier (1957) considered the behaviour of potash feldspar during metamorphism and concluded that if, as a result of syn-orogenic potash metasomatism, orthoclase is formed, the temperature must have been in excess of 500°C or above the amphibolite-granulite facies transition temperature. (Subsequent workers, e.g. Turner and Verhoogen (1960), have suggested the amphibolite-granulite facies transition temperature occurs at about 600–650°C and that 500°C is closer to the greenschist-amphibolite facies temperature.) In the Nakoso district of Japan (Shidô, 1958) the microcline–orthoclase transition takes place between the middle- and higher-grade parts of zone B.

Steiger and Hart (1967) and Wright (1967) examined potash feldspars within the aureole of a granitic stock and concluded that the microcline–orthoclase inversion took place at 375° ± 50°C. Since the volume change in the inversion is likely to be small, the temperature is unlikely to be affected by pressure, and hence a temperature obtained from purely thermal metamorphism is perfectly valid in regional metamorphism, particularly in a low-pressure facies series. However, it is

Table X. Summary of mineralogical associations in white 'granites' and quartz-plagioclase-amphibolites.

	Quartz-plagioclase-amphibolite		*White 'granite'*		
	KG.521.9	*KG.524.2*	*KG.503.1*	*KG.508.11*	*KG.538.2*
Epidote	tr.	–			
Calciferous amphibole	–	–			–
Chlorite	tr.	tr.	–	tr.	tr.
Calcite					
Clinopyroxene					–
Muscovite				tr.	
Biotite	–	–	–		tr.
Pyralspite			MnO = 2.7%		
Plagioclase	An_{27}	An_{28}	–	An_{28}	An_{31}
K-feldspar		tr.	O	O and M	O and M
Quartz	–	–	–	–	–

tr. Trace.
O Orthoclase; M Microcline.

possible that the lower temperature resulted from a higher water content. Hence it would seem that the potash feldspar was introduced into the banded gneisses at a temperature certainly in excess of 325°C and probably above 500°C but, as the potash feldspar was introduced after the peak, it follows that the first metamorphism reached at least the amphibolite facies.

Regarding the metamorphic history of the diorite-gneisses and the metagrabbros, two major alternatives must be considered:

i. That these were previously intruded plutonic rocks which were then regionally metamorphosed.
ii. That these are igneous rocks intruded during the metamorphism.

The first alternative is considered improbable, because the texture (particularly the partly recrystallized plagioclases), the lack of well-developed foliations and the relict igneous features such as zoning and primary twinning in plagioclase are incompatible with the rock having been involved in granulite-facies or even upper amphibolite-facies metamorphism. Thus, it is assumed that these rocks were intruded during the first metamorphism but after the main peak for, although the size of the intrusions and the coarse grain-size would offer resistance to the metamorphism for a time, complete recrystallization of basic dykes occurs before the migmatization of the country rocks (Sutton and Watson, 1951). Migmatization has not been recorded in this area but it is generally accepted (Mehnert, 1968) that such rocks form under high temperatures and moderate rock pressures, conditions more typical of the upper part of the amphibolite facies than the granulite facies. Also, it is evident from the mineralogy and chemistry that crystallization occurred after the potash metasomatism.

Harker (1950, p. 300) showed that, if shearing stress acts upon an igneous rock which has not fully crystallized, enforced flow will lead to parallelism of crystals of tabular or columnar habit. Such preferred orientations are occasionally developed in the metagabbros and are ubiquitous in the diorite-gneisses where the quartz was at least partly mobile while shearing stress was operative, since it provides abundant evidence of crystallization under strain. It is evident that the shearing did not persist for long after the crystallization of the diorite-gneisses, because crystal fracturing and granulation, although common, are never intense. It would seem therefore that the diorite-gneisses were intruded some time after the peak of the main metamorphism when high temperatures were dominant and that, as temperatures dropped, non-directional pressure was replaced by relatively weak shearing stress. Although the relative ages of the two rocks was never established, the absence of foliation in some of the metagabbros indicates they are the younger, and that they were intruded over a period of time which outlasted the first metamorphism.

2. Metamorphism of the older amphibolites

The occurrence of probable metagabbro xenoliths (p. 26) in some of the older amphibolites suggests they were emplaced after the cessation of the first metamorphism. Mineralogical and textural evidence regarding metamorphic grade is conflicting; the mineral assemblages (Fig. 33) are typical of the middle to upper amphibolite facies (zone C), whilst the presence of igneous textures and the absence of total recrystallization of plagioclase suggests (Sutton and Watson, 1951) that the metamorphism did not reach the lower part of the amphibolite facies, although dolerites still possessing their original compositions and textures have been found in some high-grade metamorphic terrains (Poldervaart, 1953, p. 262).

The preservation of relict textures is generally considered to be symptomatic of a failure to reach metamorphic equilibrium. Even in those rocks which have achieved total recrystallization, there is no evidence of the early stage conversion of basic plagioclase to albite and epidote. Fraser (1965) considered that, in the metamorphic rocks of Stonington and Trepassey islands, the above feature resulted from the injection of basic dykes into country rocks already undergoing metamorphism. The field relations of most of the older amphibolites are comparable with such an origin. If the basic dykes only participated in progressively decreasing metamorphism, complete recrystallization, albeit rare, would not occur. Thus intrusion probably occurred just before the peak of the metamorphism.

Apart from some local re-mobilization in the vicinity of the amphibolites, there is little evidence of the effect of this metamorphism on the banded gneisses. It is the difference in grade between the first and second metamorphisms that was not significant.

3. Metamorphism of the younger amphibolites

The orientation of the second set of basic dykes (younger amphibolites) appears to have been controlled by the principal joint directions in the banded gneisses, thereby establishing a time lapse between the second and third metamorphisms. In other words, the basic dykes were injected into 'cold' rocks and the metamorphism which affected them represents a separate event and not a waning phase of the second metamorphism. Further proof that the dykes underwent the full rigours of progressive metamorphism is evident in the frequency of total recrystallization (i.e. apart from the larger dykes which by virtue of their size have retained their igneous textre). The metamorphism of these dykes follows the path outlined by Sutton and Watson (1951) and the mineral assemblages (Fig. 35) are typical of the upper greenschist facies (zone A).

The effect of this metamorphism is also to be seen in the other metamorphic rocks; in the older amphibolites, the green hornblende has been partly replaced by actinolitic hornblende, whilst in the banded gneisses much of the orthoclase inverted to microcline. Potash metasomatism occurred again, but on a much reduced scale, and there are signs that this resulted rather from a re-distribution than from a further episode of potash introduction. Thus a few of the banded gneisses (e.g. KG.515.1) are noticeably deficient, whilst others (KG.526.3) have been relatively enriched. Potash was also absorbed into some of the diorite-gneisses and amphibolites, causing the growth of biotite on hornblende.

Having established (p. 35) the close connection between the two zones of abnormally low K/Rb ratios and the areas of maximum microclinization (and hence the areas most affected by the third metamorphism), it would seem that the third metamorphism was accompanied by a large-scale introduction of Rb. The zone of sheared banded gneisses corresponds to the westernmost of these belts and is thus assumed to be a product of this metamorphism.

IV. PRE-UPPER JURASSIC PLUTONIC ROCKS

Diorites and granodiorites which are demonstrably older than the Andean gabbros, and hence older than the Andean intermediate and acid rocks, occur within a 8 km wide north–south zone on the east coast of George VI Sound. The presence of similar fragments in the Upper Jurassic volcanic rocks further suggests emplacement occurred at the latest in Middle Jurassic times. Like their Andean counterparts, these rocks exhibit a basic to acid trend.

1. Field description

Granodiorites, which apparently pre-date the Andean gabbros, are present at the north tip of Moore Point (KG.570) and on the small east–west ridge 1 km to the north (KG.571 and 574). In both instances, the contact with the overlying basic rocks has a dip of 20–30° to the south-west at Moore Point (Fig. 44), and to the east at the other locality. On the western face of station KG.571, the granodiorite is cut by a vertical gabbro dyke which is visibly unconnected with the main mass, but it most probably represents a feeder. Flow banding paralleled by aplite veins was observed at both localities, and the frequent angular to sub-angular xenoliths (up to 10 cm across) of amphibolite and diorite are drawn out into thin discontinuous bands.

The close proximity of the sole occurrence of *lit-par-lit* injected granite and certain mineralogical affinities (e.g. the presence of microcline) between the two rock types would appear to be more than coincidental, and it is considered probable that these granites are late-stage apophyses of the granodiorites. Ranging in thickness from 1.25 to 60 cm and frequently pinched out, these acid sheets parallel the foliation of the diorite-gneisses (Fig. 25) but, where a transverse amphibolite pod is encountered, the intrusion is generally deflected along the contact; within the intrusion the basic rock is concordant with the foliation (Fig. 26). Lensoid xenoliths of diorite-gneiss are frequently encountered and the rocks possess a distinct foliation parallel to the margins with, more rarely, a *b* mineral lineation.

These rocks resemble the smaller of two granite dykes which intrude the quartz-plagioclase-amphibolites at station KG.521.

Fig. 44. Creswick Peaks (C) and Moore Point (M) viewed from the west, showing the gently inclined contact between older granodiorite (gr) and Andean gabbro.

The larger dyke comprises a coarse pink aggregate of quartz and potash feldspar with large plates of muscovite (enclosing biotite) whose common orientation parallels both the foliation and the margins of the dyke. At the contact, both the country rock and the intrusion are highly sheared.

The granodiorite, which forms most of Gurney Point, contains two bodies of diorite; the smaller has a sharp vertical contact with the granodiorite at the western end of the survey cairn ridge. The second body, 0.5 km north of the survey cairn, has a more gradational margin in which flow-banded granodiorite (with xenoliths of a slightly coarser hornblende-plagioclase aggregate) passes into a fine-grained dark rock with vaguely defined granodiorite bands. Since these fine-grained rocks occur patchily throughout the remainder of the outcrop, they cannot represent a chill feature. Rounded and frequently flattened inclusions of both diorite types, generally between 5 and 10 cm but occasionally up to 9 m across, are frequently encountered in the granodiorite. Of more restricted occurrence are inclusions of amphibolite, which are generally larger and more angular than the diorites and are readily distinguished by their distinctive foliation.

2. Petrography

Two rock types comprise these older granodiorites: a pink, slightly coarser, more acid rock which is dominant at Moore Point, and a greyish variety, not unlike the Andean rocks, that predominates at Gurney Point. Both rock types possess a coarse aggregate of quartz and plagioclase with subordinate potash feldspar and variable proportions of hornblende and biotite (the pinkish rock being in general more leucocratic).

In thin section, the subidiomorphic texture is dominated by lath-like or equidimensional euhedral plagioclase crystals (0.5–6 mm long; An_{20-30}) in the grey rock whereas they are highly sericitized with rims of clear albite in the pinkish rock. Alteration in the more basic plagioclase is far less pronounced, being mainly to epidote with only minor sericite, but bent twin lamellae and small irregular fractures filled with epidote are common. Much of the potash feldspar is microperthitic and recognizable microcline, but the additional presence of orthoclase is not definitely ruled out. The form of the potash feldspar varies again with rock type; in the pink rock the crystals are either interlocking or graphically intergrown with quartz, whereas in the grey variety the mineral is distinctly interstitial. Quartz occurs either as single anhedral crystals (strained and showing marginal recrystallization) up to 4 mm across or in aggregates of interlocking crystals. Green hornblende with α = straw, β = green, γ = sea-green and γ: $c = 22°$ forms ragged laths 0.3–2 mm long, and is occasionally poikilitically intergrown (KG.574.1) with plagioclase and, more rarely, quartz. Replacement by biotite is widespread, generally accompanied by sphene in the grey rock (e.g. KG.517.2) and by epidote and magnetite in the pink one (KG.570.1 and 574.1). In turn the biotite is universally altered to chlorite. Accessories include allanite, magnetite, zircon and sphene. Small discontinuous shear zones are common at Moore Point and they are filled either with epidote (KG.570.1) or recrystallized rock (KG.574.1). In Marmo's (1971) kinematic classification of granites, the combined presence of

microcline, sodic plagioclase and epidote is typical of late intrusions.

The *lit-par-lit* granites have strongly mylonitized relict igneous textures with blastophenocrysts of albite-oligoclase and microcline up to 2.5 mm in size. The plagioclase is equidimensional, rounded or lensoid with Carlsbad and Carlsbad-albite twins and faint zoning which may be outlined by fine brown alteration material. Zones of granulation are common; in these the grain-size is less than 0.1 mm and, next to the microcline, myrmekite is sparingly developed. The larger quartz crystals are strained and partly recrystallized with the development of ribbon structures. Rare minute flakes of pale green chlorite are frequently associated with magnetite and haematite.

3. *Geochemistry*

The two new analyses (Table XI) representing the pink (KG.574.1) and grey suites, display abnormally high CaO and low K_2O, Rb and Sr values for rocks in the 67–70 % SiO_2 range, features which are most readily explained by selective replacement of K_2O by CaO. In the case of specimen KG.574.1, which has the lower K_2O/SiO_2 ratio, the process could be connected with the emplacement of the nearby Andean gabbro, since the latter shows alkali enrichment in its margins. Otherwise these granodiorites compare favourably (Table XI), particularly in respect of Ba, Zr and Pb, with established pre-Upper Jurassic plutonic rocks from western Graham Land (West, 1974), and on a K–Ca–Na triangular diagram (Fig. 45) they plot on or close to the curve formed by these and other Jurassic rocks (from the east coast of Graham Land (Fleet, 1968; Marsh, 1968; Stubbs, 1968)). The same diagram serves to illustrate the remoteness of these rocks from the Andean trend and, coupled with the notable differences in Zr and Ba (cf. Table XI, analyses 1 and 2 with Table XX, analyses 25 and 24), supports the concept of two episodes of intrusion.

Table XI. Chemical analyses of pre-Upper Jurassic acid plutonic rocks from western Palmer Land and the Danco Coast, Graham Land.

	1	*2*	*3*	*4*
SiO_2	70.50	66.19	70.16	67.72
TiO_2	0.26	0.51	0.28	0.29
Al_2O_3	14.48	15.52	15.28	15.88
Fe_2O_3	1.63	2.39	1.64	2.04
FeO	1.07	2.10	0.85	1.06
MnO	0.06	0.11	0.06	0.06
MgO	0.57	1.27	0.57	0.80
CaO	2.78	3.86	1.83	2.68
Na_2O	4.10	4.19	4.60	4.00
K_2O	1.90	2.09	3.84	3.10
P_2O_5	0.04	0.12	0.08	0.09
H_2O	2.87	0.82	0.10	1.49
CO_2	0.05	0.09	0.01	0.13
Total	100.31	99.26	99.30	99.34
ELEMENT WEIGHT PERCENTAGES (ANHYDROUS)				
Ca^{2+}	2.04	2.80	1.32	1.96
Na^+	3.12	3.16	3.44	3.03
K^+	1.62	1.77	3.21	2.63
COORDINATES FOR TRIANGULAR DIAGRAMS				
Ca	30.10	36.30	16.50	25.70
Na	46.00	40.80	43.20	39.80
K	23.90	22.90	40.30	34.50
TRACE ELEMENTS (ppm)				
S				
Cr	9	7	8	13
Ni	2	3	–	–
Rb	48	77	172	133
Sr	143	209	294	293
Y	15	30	6	12
Zr	138	223	180	185
Ba	784	727	620	461
La	8	19	25	15
Ce	12	33	43	29
Pb	16	14	17	20
K/Rb	329	226	185	194
K/Ba	20	22	51	56
Ca/Sr	139	132	45	65
Ba/Sr	5.48	3.69	2.11	1.57
Rb/Sr	0.336	0.368	0.585	0.454

1. KG.574.1 Pink granodiorite, Moore Point.
2. KG.517.2 Grey granodiorite, Mount Crooker.
3. O.911.1 Adamellite, northern Neko Harbour (West, 1974).
4. O.576.2 Adamellite, western Charlotte Bay (West, 1974).

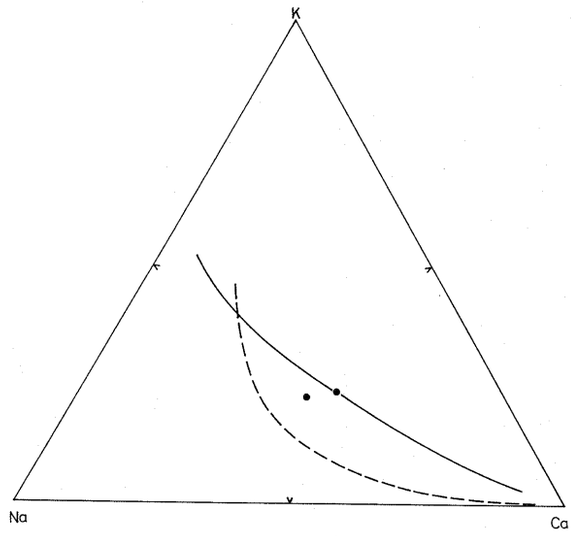

Fig. 45. Ca–Na–K triangular variation diagram for the pre-Upper Jurassic acid plutonic rocks. Variation trends for Graham Land Jurassic plutonic rocks (West, 1974) and Palmer Land Andean rocks (Fig. 62) are defined by continuous and broken lines, respectively.

4. *Discussion*

The contact between these acid rocks and the Moore Point gabbros fails to provide unequivocal evidence of their age relations. Skinner (1973) considered that the acid intrusions of the Moore Point area post-dated the emplacement of the gabbros, citing as evidence the presence of gabbroic xenoliths. However, all the coarser and non-foliated enclaves examined by the author were of diorite with nothing to suggest they had been derived from the overlying gabbro.

The rock which forms the neck of gabbro within the granodiorite is considerably more acid than usual (Table XXI, analysis 10) with interstitial quartz and orthoclase, and plagioclase zoned down to An_{32}; there are many features which suggest this has resulted from assimilation of acid material rather than from metasomatism, in particular:

i. The potash feldspar of the gabbro is orthoclase (the high-

temperature polymorph), whereas that of the granodiorite is microcline (evidently formed at a lower temperature).

ii. In most acid zones of the gabbros, the plagioclase is still more basic than that of the granodiorite.

iii. The texture is exclusively igneous with no evidence to suggest that quartz and orthoclase grew by replacement.

Thus it would seem that, certainly in the Moore Point area, these rocks pre-date the Andean gabbro and hence were probably the source of the microcline-bearing granodioritic fragments in the Upper Jurassic stratified rocks. A Middle Jurassic age is then inferred and, as these are late kinematic intrusions, it is reasonable to assume they were emplaced in the waning phase of the third metamorphism.

V. MESOZOIC STRATIFIED ROCKS

Field occurrence and character

Stratified volcanic rocks, including lavas and pyroclastic rocks, occur at Carse Point (Fig. 46), Gurney Point (Fig. 2) and in upper Millett Glacier (Fig. 3). Sedimentary rocks occur *in situ* below the volcanic rocks at Carse Point and as accidental inclusions in the pyroclastic members of the Millett Glacier succession. Because these outcrops are separated by distances up to 60 km, and since they were probably affected by late Tertiary block faulting and are without marker horizons of regional extent, a detailed correlation has not been attempted. Even the erection of detailed local successions at specific outcrops has been complicated by subsequent plutonic and hypabyssal intrusions.

Classifications and nomenclature

Because of the great diversity in rock types occurring at the above localities and the inherent difficulties in correlation, the successions of rocks exposed at each locality are regarded as separate units and are classified according to the location as:

A. Carse Point succession.
B. Millett Glacier succession.
C. Gurney Point succession.

Three major types of stratified rocks have been mapped: lavas, volcaniclastic and sedimentary rocks. The sedimentary rocks have been classified after Folk (1954), and for the volcaniclastic rocks the size divisions of Blyth (1940) are preferred to more recently proposed classifications (Fisher, 1961, 1966) with their rigid genetic connotations. A chemical classification of the lavas has been adopted using the Thornton and Tuttle (1960) differentiation index, which seems to give a broader mineralogical basis to the classification than the use of silica alone. The scheme, which broadly corresponds to that of Nicholls (1971), is:

	Differentiation index
Basalts	35
Basaltic andesites	35–50
Andesites	50–65
Dacites	65–81
Rhyodacites	81

The choice of 81 (instead of Nicholls' 80) for the rhyodacite/dacite boundary allows marginal rocks to be grouped with mineralogically similar specimens. A similar chemical classification has been applied to the tuffs with a further subdivision according to the type of included fragment:

Crystal tuffs—containing more than 50% crystal fragments.

Lithic tuffs—containing more than 50% rock fragments.

A. Carse Point Succession

1. Stratigraphy

The Carse Point succession consists of over 1 000 km of subhorizontal sedimentary and volcanic rocks which have been intruded by diorite and quartz-plagioclase-porphyry dykes. The lowest exposed rocks on the western face of Carse Point are massive blue-black mudstones with interbedded arkosic sandstones. The mudstones are 200 m thick and virtually homogeneous except for some thin arenaceous partings. The rocks are well-jointed, the more open joints commonly being coated with limonite that was probably derived from hydrothermal solutions associated with the intrusion of the adjacent diorite.

The lowest of the arenaceous beds is a grey-green conglomeratic sandstone containing large rounded pebbles and cobbles of sandstone and granodiorite, with slightly smaller mudstone clasts. Mudstone clasts also characterize some of the five succeeding beds of block-bedded greyish white sandstone. Several graded beds 20–25 cm thick occur at one level. The higher beds contain a greater proportion of volcanic fragments, and two andesite lava flows (1.5 m thick) occur within the mudstones at 40 and 80 m, respectively, above the base of the succession. The composition of the scree derived from the inaccessible bed immediately above the mudstones (Fig. 47) indicates a predominantly volcanic succession, though it is possible that the somewhat darker rock on the summit may represent a return to mudstone.

The strata on the west face have a persistent gentle (5–20°) dip to the south and it is possible that some of the rocks forming the south-west corner are representative of the inaccessible beds at the north-west corner. Certainly, the lowest bed is a dark mudstone (identical to that of station KG.584) and the overlying rocks are basalt and basaltic andesite lavas. At the south-west corner, however, the mudstone and volcanic rock are separated by approximately 30 m of coarse conglomerate. This succession can be traced along the north face of Carse Point to the western margin of the quartz-plagioclase-porphyry dyke. On the eastern side of this intrusion, a totally different succession, mainly tuffs and conglomerates with subordinate green and purple amygdaloidal andesite lavas, dips steeply to the south-west, but eastward the dip gradually decreases. As there is no definite break in the succession on the south face of Carse Point, the discrepancy in dip may represent a local downwarping of the strata possibly connected with the emplacement of the intrusions. These beds must therefore occur at a higher level in the succession than those on the western face.

These stratified rocks appear to extend over many square kilometres both to the north and west. Although neither Mount Dixey nor Mount Flower were visited.

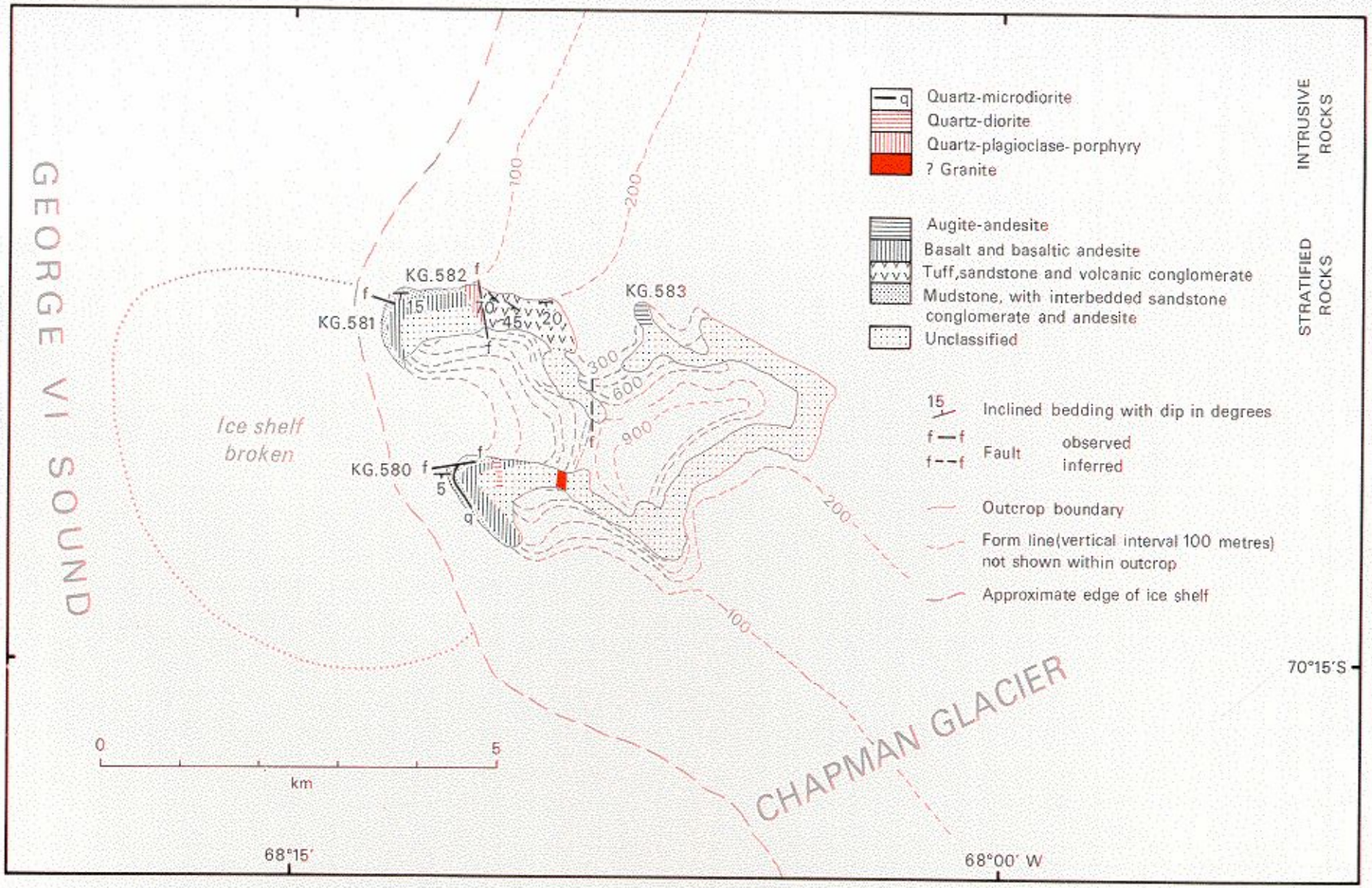

Fig. 46. Geological sketch map of the Carse Point area, showing geological stations.

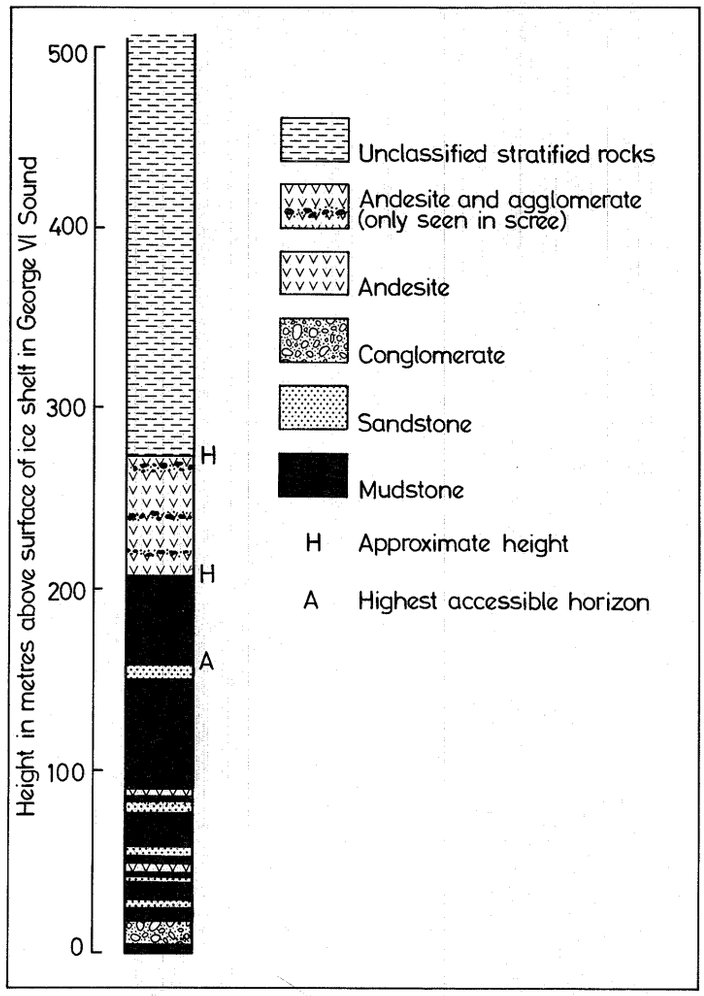

Fig. 47. Stratigraphical section of part of the succession at the north-west corner of Carse Point (KG.581).

2. Petrography

The sedimentary sequence forming the lower part of the Carse Point succession comprises mature mudstones with interbedded, immature arkosic sandstones and conglomerates. As insufficient material was available, no detailed statistical analyses were undertaken.

a. *Mudstones.* Apart from two intercalated conglomeratic pebbly beds, the mudstones are massive indurated rocks composed of sand- and silt-size grains of plagioclase and quartz with stringers of ore aligned parallel to faint microscopic bedding. The larger feldspar clasts are generally formed of aggregates of two or three grains. The clay fraction has been replaced by small mica plates (pleochroic from colourless to pale brown) which also occur within the feldspars. The light grey arenaceous partings seldom exceed 35 mm in thickness and grade from silt to medium sand. Although the large feldspar clasts resemble those in the argillaceous rock, the small lath-like clasts have no counterparts. Subhedral or granular, faintly pleochroic sphene is widespread, often in association with pale yellow chlorite enclosing zircon.

Ellipsoidal and sub-spherical structures 0.55 mm long enclosing large numbers of much smaller sub-rounded bodies 0.07–0.13 mm in diameter occur in specimen KG.581.1 (Fig. 48a). Some of the virtually unimodal spherules exhibit a crude concentric pattern, whereas others are framboidal and composed of numerous aggregated euhedral and anhedral pentagons (Fig. 48b). Several spherules are either partly or completely pyritized and the outer margin of the enclosing structure is also accentuated by the presence of pyrite. Most of the spherules are in contact with one another and some may overlap; none occurs in the matrix.

These spherules are similar to framboidal pyrite spherules and are probably early diagenetic and either organic or inorganic in origin (Love and Amstutz, 1966). Although the origin of these structures remains enigmatic, pseudomorphs after an organic spherule (such as immiscible globules, spherical coacervates or unicellular micro-organisms) or the infilling of gaseous vacuoles in sediments have recently been advocated as possible explanations (Rickard, 1969).

The lower of two pebbly mudstone units is 1.5 m thick, and contains rounded or ovoid pebbles of granite, granodiorite and trachytic andesite set in a silty matrix. In a malachite-stained zone, which extends 1 m below the contact with the coarse conglomerate, the mudstone contains rounded clasts of green sandstone (up to 5 cm in diameter) characterized by iron-stained margins, and white-weathered zones extending to a depth of 3 mm.

b. *Sandstones.* At least six beds of white or green sandstone (0.30–12 m thick) occur within the mudstones. Although they are predominantly of sand grade, two horizons include rare rounded to sub-rounded mudstone and sandstone clasts up to 60 cm in diameter. In relation to any of the widely accepted classifications of sandstones (e.g. Folk, 1954; Pettijohn, 1954), all sediments of sand grade in the Carse Point succession are arkoses. They are marine clastic sediments in which the content of non-sedimentary rock fragments is less than 30% (Table XII, analyses 1 and 2) and interstitial clay is generally absent.

Quartz. The quartz clasts were probably derived from an area of acid and intermediate plutonic rocks and acid volcanic rocks. A study of plutonic and metamorphosed plutonic rocks (which were probably similar to those of the source area) occurring to the south, suggests that the quartz crystals derived from these rocks cannot be distinguished from one another on criteria such as shape, strain, inclusions, etc., a conclusion reached by other workers in this field (e.g. Blatt and Christie, 1963; Horne, 1968). However, in the higher beds quartz derived from such plutonic and metamorphosed plutonic rocks can be distinguished by its undulose extinction and anhedral shape from euhedral and unstrained quartz derived from acid lavas (Fig. 48c).

Feldspar. Feldspar (mainly plagioclase) seldom forms more than 30% of the rock. Potash feldspar, mostly as micropegmatite (Fig. 48d), appears to form less than 0.1%, although more may occur in the finely divided groundmass. The composition of the detrital plagioclase in any specimen is related to the provenance of that particular horizon. Thus, in the lower horizons, where the sediment is rich in detritus from the more acid plutonic rocks, the plagioclase composition is in the range An_{28-32}, whereas in the sandstone, which is devoid of quartz but contains hornblende, the composition is An_{49}. The

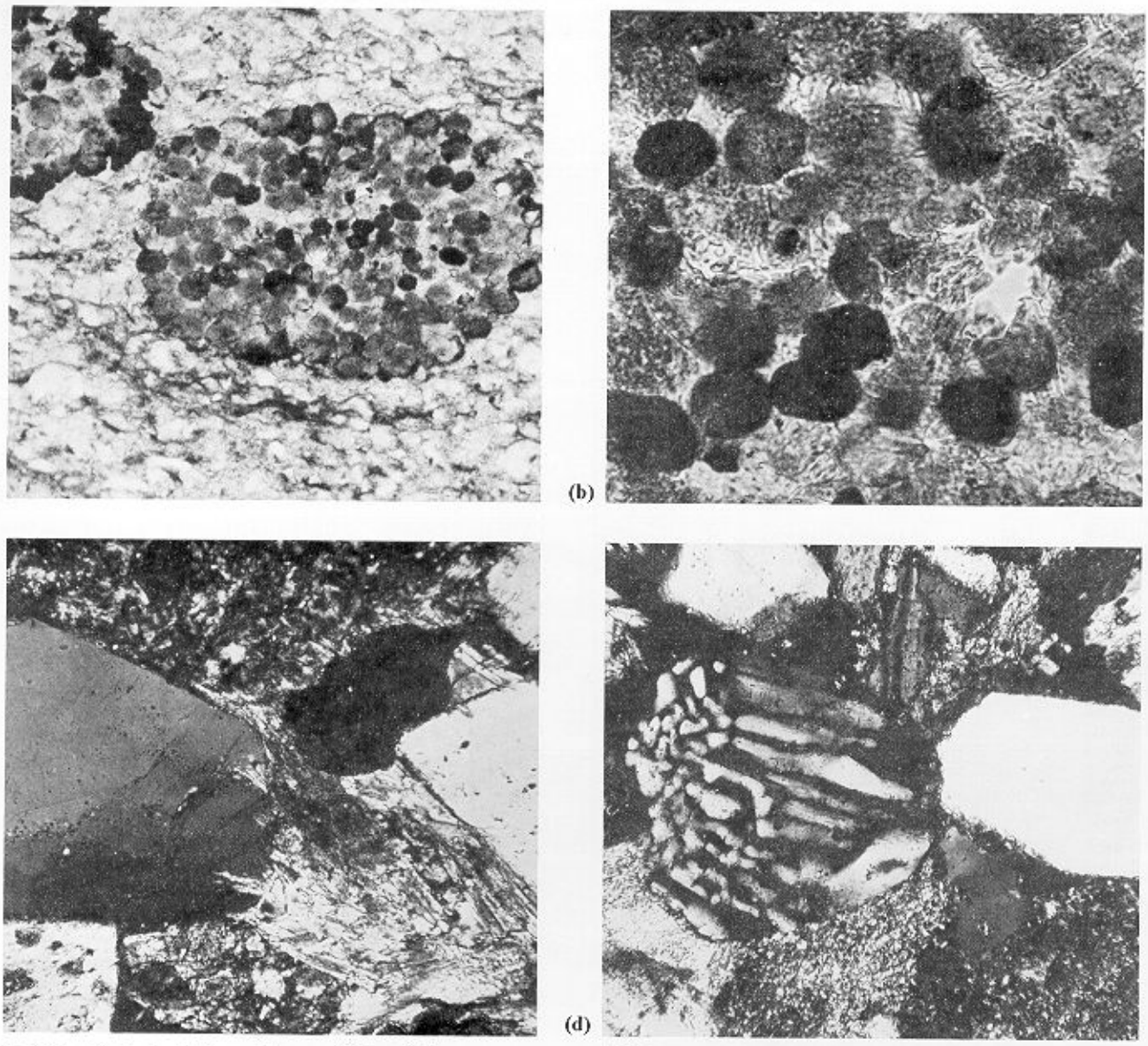

Fig. 48. a and b. (?) Framboidal pyrite in mudstone. a. Ellipsoidal structures composed of sub-rounded wholly or partly pyritized spherules (KG.581.1; ordinary light; × 220). b. Structures of the constituent spherules (KG.581.1; ordinary light; × 850). c. Strained and unstrained (volcanic) quartz, plagioclase and iron ore clasts with interstitial uralitic hornblende in arkosic sandstone (KG.581.2; X-nicols; × 15). d. Micropegmatite, quartz, plagioclase and mudstone clasts in arkosic sandstone (KG.581.2; X-nicols; × 15).

more acid plagioclase clasts are invariably euhedral, suggesting either rapid transportation or transport over a relatively short distance. In both cases loss of potash feldspar would be minimal, suggesting that the source rock was probably a quartz-diorite, although the Andean granodiorite (which may reflect the trend of the earlier intrusions) is noticeably deficient in potash feldspar. Rounding is frequently encountered on the more basic plagioclase clasts, but both compositional ranges show equal alteration to sericite and epidote.

Ferromagnesian minerals. These sediments are mostly deficient in ferromagnesian minerals. Biotite is absent and altered pale green hornblende is restricted to a bed which has a largely dioritic provenance. The heavy mineral fraction comprises iron ore, sphene, epidote and allanite. The cement in these sediments is either of authigenic chlorite, epidote or amphibole, or recrystallized fine-grained matrix.

Country-rock fragments. Three types of detrical rock fragments have been recognized in the coarser sandstones and gravels. Although cobble-size fragments are common in the lowest bed, coarse-grained granodiorite clasts are rare in the sand fraction and generally comprise only two or three bonded grains. Oligoclase (rarely zoned) predominates, with quartz (locally showing granophyric intergrowths), chlorite and (?) microcline. Although the potash feldspar content is much reduced, such rock fragments are more typical of the older granodiorite than either the metamorphic complex or the Andean granodiorite. The second and commonest are fragments of porphyritic andesite, or more rarely, feldspar-

Table XII. Modal analyses of Mesozoic sediments and tuffs.

		1	2	3	4
Quartz		29.84	8.80	1.42	1.03
Sanidine		–	–	0.36	–
Plagioclase		31.80	38.72	33.74	20.23
Hornblende		9.44	–	–	–
Chlorite		7.12	–	1.01	2.20
Magnetite		7.20	3.08	2.12	0.21
Calcite		–	0.24	0.55	2.54
Epidote		–	18.16	10.94	0.70
Lapilli	glassy	–	–	–	5.45
	crystalline	–	–	11.80	14.53
	sedimentary	–	–	1.96	7.35
Rock fragments	volcanic	12.08	1.64	–	–
	sedimentary	2.52	0.56	–	–
Groundmass		–	28.80	36.10	45.76
Plagioclase composition		An_{32-28}	An_{32}	–	An_{27}

1. KG.581.2 Arkosic sandstone, Carse Point succession.
2. KG.581.4 Arkosic sandstone, Carse Point succession.
3. KG.560.5 Andesitic crystal tuff, Millett Glacier succession.
4. KG.560.6 Dacitic lithic tuff, Millett Glacier succession.

porphyry and quartz-porphyry. A third type is represented by one fragment composed entirely of interlocking quartz grains with sutured margins (or occasionally with straight edges and 120° triple junctions), which was probably derived from a siliceous schist.

Indigenous rock fragments. Several of the sandstones, particularly the coarser beds, are partly composed of pellets of mudstone identical to those occurring in the same succession. They are regarded as earlier sediments of the same trough which have been re-worked by energetic fluvial currents. Rounded boulders of greenish sandstone (up to 60 cm in diameter) are rimmed by pale grey or iron-stained aureoles, similar to those occurring in the mudstone (p. 49).It is probable that these fragments were subaerially weathered before being transported to their present site.

c. *Conglomerates.* The sandstone-siltstone assemblage is overlain by approximately 30 m of coarse conglomerate, of which only the lower few metres are accessible. Angular or sub-angular fragments of greyish white sandstone, seldom more than 2.5 cm across, form most of the coarser fraction, although blocks of andesitic tuff (up to 9 m long) were recorded and mudstone pellets are common at the base of the bed. The fragments are enclosed in a grey sandstone matrix.

At least three conglomerates occur in the higher beds that crop out to the east of the quartz-plagioclase-porphyry. The lower two beds appear to be identical and contain fragments of bluish grey (?) andesite in a slaty matrix, whereas the third bed is composed of angular sandstone clasts, with smaller numbers of granodiorite and andesite clasts set in a sparse sandy matrix.

d. *Andesite crystal tuffs.* Evidence of contemporaneous volcanic activity is restricted to two andesite lava flows and one unit of crystal tuffs. The tuffs occur between the two lower conglomerates in the eastern succession and are bluish black rocks with thin partings of purple sandy mudstone. Euhedral plagioclase laths, ranging in length from 0.1 to 1.7 mm, have a composition of An_{50} with zoning only rarely seen. Albite and Carlsbad twins are frequently present and interpenetrant types are less common. Fresh crystals are rare, the main alteration products being calcite, sericite, epidote, chlorite and granular quartz. Anhedral and frequently subrounded grains of magnetite are rimmed by haematite, which also stains much of the surrounding rock. The groundmass is composed of plagioclase microlites and ilmenite, and it is cut by irregular amygdales of chlorite, quartz and occasionally calcite. The clastic fraction of the mudstone partings was derived from the tuff and includes sub-angular clasts of the mesostasis.

e. *Andesite lavas.* A thin flow (1.5 m) of greenish grey porphyritic andesite (KG.581.9; Table XIII, analysis 3) occurs within the mudstones 80 m above the base of the succession. In this section, the rock is composed of phenocrysts of plagioclase and hornblende in a felsic groundmass. The plagioclase phenocrysts, which occasionally consist of clusters of two to three sub-phenocrysts, are euhedral laths or equidimensional grains of andesine (An_{32}), 0.5–2.0 mm long, partly masked by finely divided iron ore. Single hornblende phenocrysts are exceedingly rare, the usual form consisting of glomero-porphyritic aggregates. The pleochroic scheme is α = pale yellow, β = pale green and γ = pale bluish green (γ: c = 20–25°), and partial alteration to calcite and rare clinozoisite is evident. Plagioclase (An_{30}) microlites (which are not veneered by ore like the larger grains), skeletal ilmenite and interstitial chlorite form the groundmass. The lava from the eastern succession (e.g. KG.583.1; Tabel XIII, analysis 4) is quite fresh, with plagioclase and pyroxene phenocrysts in a mesostasis of plagioclase together with interstitial iron ore and rare pyroxene. It is possible to distinguish two groups of phenocrysts both compositionally and dimensionally, here referred to as phenocrysts and microphenocrysts. Marginally corroded plagioclase phenocrysts (0.75–1.25 mm long) are invariably associated with pale yellow pyroxene phenocrysts (1–2 mm long) and exotic cruciform intergrowths between them are common. The plagioclase composition is in the range An_{60-71} but resorption by andesine (An_{47}) is common. The microphenocrysts (0.2 to 0.5 mm in length) are andesine of a similar composition. Universal-stage determinations on the pyroxene phenocrysts showed $2V_\alpha$ = 56–61°, γ: c = 24–25°, and c does not lie in the optic axial plane. These properties are not diagnostic of any single pyroxene but could represent a transitional phase, perhaps between pigeonite and hypersthene. Pyroxene microphenocrysts, seldom intergrown with plagioclase, are augite with $2V_\alpha$ = 43°, γ: c = 37–43°, optic axial plane (010). The pyroxene phenocrysts and microphenocrysts are twinned, both simply and polysynthetically with the composition plane parallel to (100), and altered to penninite and ilmenite rimmed by leucoxene. Deeply embayed magnetite anhedra are intergrown with the augite, frequently in myrmekite-like symplectites.

f. *Basaltic andesite lavas.* The flows overlying the sedimentary rocks are only accessible on the southern ridge (station KG.580), where specimens of basaltic andesite and basalt were collected. The basaltic andesite (e.g. KG.580.9) strongly resembles the andesite of the eastern succession, particularly in the plagioclase composition and the frequent cruciform-type intergrowths (plagioclase–plagioclase and plagioclase–pyroxene). However, in specimen KG.580.9, augite has been replaced by fibrous amphibole (γ:c = 20°) or ilmenite or

Table XIII. Modal analyses of Mesozoic lavas.

	1	*2*	*3*	*4*	*5*	*6*	*7*	*8*	*9*	*10*
Quartz	2.40	–	–	–	–	0.07	1.00	0.70	8.70	–
phenocrysts	28.41	24.60	17.48	22.38	14.17	29.60	28.20	30.70	6.03	33.48
Plagioclase groundmass	–	29.78	48.75	–	–	–	57.40	–	44.30	28.50
Augite	–	–	–	2.72	–	–	–	–	–	–
phenocrysts	3.06	13.10	4.89	–	–	–	–	–	–	–
Hornblende groundmass	–	27.15	18.76	–	–	–	–	–	–	24.60
Chlorite	2.19	0.74	7.49	1.32	0.56*	2.40*	5.40	2.00	16.48	–
Magnetite	2.79	4.63	1.23	0.82	1.88*	1.67*	7.70	1.70	4.86	9.86
Haematite	–	–	–	–	1.24	–	–	–	–	–
Calcite	–	–	1.40	6.46	1.52	0.07	–	–	1.20	–
Epidote	–	–	–	–	1.59*	7.26*	0.30	8.10	18.43	0.33
Sphene	–	–	–	–	–	–	–	–	–	3.23
Biotite	7.66	–	–	–	–	–	–	–	–	–
Groundmass	53.49	–	–	66.30	79.04	58.93	–	56.80	–	–
Plagioclase composition										
phenocrysts	An_{70}	An_{62-54}	An_{32}	An_{70-61}	An_{20-30}	An_{40-35}	An_{27}	An_{33}	An_{20-30}	An_{67}
groundmass	–	–	An_{28}	–	–	–	–	–	–	An_{42}

*Phenocrysts.

1. KG.580.9 Basaltic andesite, Carse Point succession.
2. KG.580.10 Basalt, Carse Point succession.
3. KG.581.9 Andesite, Carse Point succession.
4. KG.583.1 Augite-andesite, Carse Point succession.
5. KG.554.2 Rhyodacite, Millett Glacier succession.
6. KG.554.4 Dacite, Millett Glacier succession.
7. KG.556.2 Dacite, Millett Glacier succession.
8. KG.556.5 Andesite, Millett Glacier succession.
9. KG.560.2 Andesite, Millett Glacier succession.
10. KG.520.2 Basaltic andesite, Gurney Point succession.

penninite, and plagioclase is sieved with quartz, calcite and amphibole. The dominantly felsic groundmass contains irregular amygdales of dusty quartz and amorphous chlorite. It is probable that the degree of alteration is related to the higher gas content, in that the greater permeability of the rock assisted the circulation of deuteric solutions.

g. *Basalt*. The only basalt found in this area contains stumpy plagioclase phenocrysts slightly more sodic (An_{54-62}) than the basaltic andesite but the proportion of mafic phenocrysts is higher (Table XIII, analysis 2). Alteration of the pyroxene is similar to that in specimen KG.580.9 but, in addition, irregular cracks in the plagioclase are filled with amphibole. The groundmass is pilotaxitic, being composed of plagioclase, amphibole and iron ore.

4. Sedimentary environment

The sedimentary sequence in the Carse Point area is composed of two rock types which are the products of markedly different depositional environments. The mudstones were deposited slowly in still and probably deep waters, whereas the sandstones were transported rapidly from their source area and deposited under turbulent conditions. It is evident from the presence of graded bedding (Dott, 1963) that at least one sandstone bed was deposited by a turbidity current, but most of the beds lack the degree of sorting which characterizes such deposits. Some other form of deposition must therefore be considered. Kuenen and Menard (1952) have suggested that similar deposits (non-graded deep-sea sediments with no visible sorting) may arise from submarine slides without turbidity. The larger fragments in the overlying coarse conglomerate are probably the products of subaqueous rock falls (Dott, 1963), which suggests that the sedimentary basin was close to tectonically active land. Sudden disturbances of the sea floor would be commonplace in such an environment, and it is probable that many of the sandstones in the Carse Point succession were deposited from tectonically initiated submarine slides without turbidity.

It is tentatively suggested that the sedimentary rocks of the Carse Point succession were derived from a tectonically active upland to the east, on which active volcanoes were erupting predominantly andesitic lavas, and were subsequently deposited in an unstable shelf environment.

B. Millett Glacier Succession

1. Stratigraphy

Volcanic rocks, including lavas and pyroclastic rocks, occur along the line of jagged peaks on the southern side of upper Millett Glacier. The lack of any marker beds in the two contrasting assemblages, which flank the central stock of 'Andean' granite, has prevented the establishment of a detailed succession. Since these beds show little evidence of any post-depositional disturbance, it is probable that the direction of younging is coincident with the direction of dip, i.e. to the west.

The eastern part of the ridge, with an exposed succession of over 400 m, comprises at least four flows of bluish grey or green rhyodacite-andesite lava with interbedded agglomerates. Near the eastern end, a small vent (Fig. 49) which extruded the lowest flows contains a central plug of basaltic andesite surrounded by 6–9 m of vent agglomerate. On the northern side of the vent the flow adjacent to the agglomerate dips steeply into the vent, but within 30 m it dips gently in the opposite direction (Fig. 50). This flow is a blue-black, banded trachytic rhyodacite with pink feldspar phenocrysts and occasional volcaniclastic horizons.

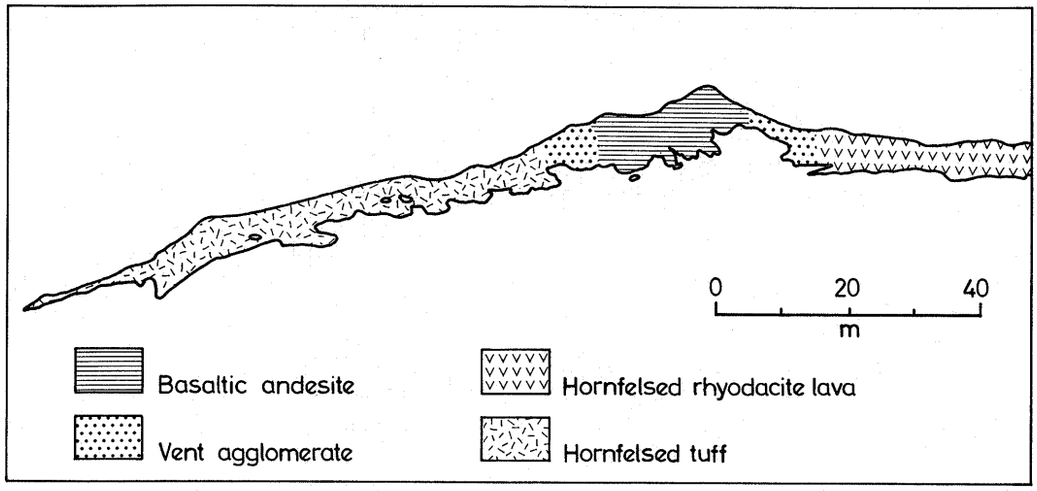

Fig. 49. Sketch from a photograph of the western side of the volcanic vent at station KG.553, Procyon Peaks.

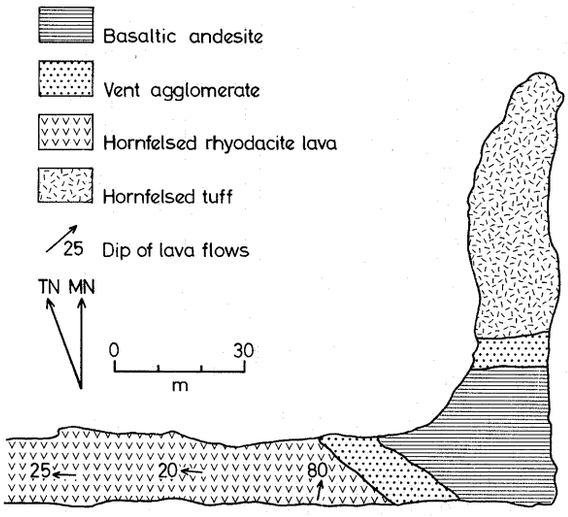

Fig. 50. Sketch map of the volcanic vent at station KG.553.

Despite the general homogeneity of this flow, thin iron-rich weathered zones and a single agglomeratic horizon suggest that it is composed of several smaller flows. Unlike the higher agglomerates (which are traceable along the length of the north face), the lowest unit, which ranges from 3 to 20 m in thickness, is only traceable for 200 m on its emergence from the snow line. Most of the succession above the second bed of agglomerate consists of a slightly darker porphyritic dacite with many accidental inclusions and two intercalated agglomerates.

West of the granite stock, the succession comprises over 250 m of dacitic and andesitic tuffs and one small andesite lava. On this part of the ridge the volcanic rocks, intruded by granite and granite-aplite dykes 30 cm to 12 m thick, contain many volcaniclastic xenoliths. A faintly bedded brown dacite tuff, containing lapilli up to 25 mm long and forming the lowest exposed bed, is separated from an overlying 6 m thick porphyritic andesite flow by the lowest of the granite dykes. The lava flow is overlain by 45 m of heavily epidotized, andesitic crystal tuffs in which the predominantly feldspathic fragments seldom exceed 3 mm. Dacitic tuffs, which form the remainder of the ridge, are faintly bedded pale green rocks in which the lapilli range up to 13 mm.

2. Petrography

a. *Rhyodacite lavas.* The flows below the second agglomerate, which weather out as jagged pinnacles because of complex columnar jointing, are blue-black aphanitic rocks with flow-aligned feldspar phenocrysts. They (e.g. KG.554.2; Table XIII, analysis 5) are composed of cloudy (?) oligoclase phenocrysts (occasionally glomeroporphyritic and frequently including epidote, chlorite and magnetite) and epidote–chlorite–ore pseudomorphs of hornblende set in a cryptofelsitic groundmass. Deeply embayed ilmenite phenocrysts are rimmed by leucoxene. Thin stringers filled with granular haematite are thought to represent short periods of quiescence between flows. On the edge of the vent, the flows lie within the metamorphic aureole of the 'Andean' granite pluton and, although the porphyritic texture has been preserved, the groundmass has been completely recrystallized. Partial recrystallization has occurred at the edges of the feldspar phenocrysts, and anhedral clusters of epidote, masked by finely divided ilmenite, have replaced hornblende. The matrix comprises a mosiac of (?) prehnitized granular plagioclase and subsidiary potash feldspar, with interstitial chlorite and iron ore. The many quartz-filled lenses and stringers cutting the groundmass may represent zones in which the more volatile constituents of the lava were concentrated as it cooled. Intergrowths of quartz and potash feldspar are indicative of a metasomatic origin for much of the quartz.

b. *Dacite lavas.* The main differences between the dacites and the rhyodacites are the higher proportion of phenocrysts and more basic plagioclase (An_{35-40}) in the former. The plagioclase phenocrysts, some with corroded margins, possess predominantly simple twins, many of the interpenetrant type.

The mafic phenocrysts are of chlorite, generally associated with epidote and ilmenomagnetite, and mantled by granular quartz. The groundmass comprises plagioclase microlites and ore in a cryptocrystalline base.

c. *Andesite lavas.* A solitary andesite flow, within the thick succession of pyroclastic rocks at the western end of the ridge, is a pale green lava with pink plagioclase phenocrysts up to 5 mm long, and epidotized vesicles. In thin section, this andesite (KG.560.2; Table XIII, analysis 9; Fig. 51a) is composed of euhedral, lath-like or equidimensional, cloudy oligoclase phenocrysts and ragged phenocrysts of penninite set in a felt of oligoclase microlites. There is an intersertal base of quartz, chlorite, iron ore and amorphous calcite. These secondary minerals are frequently included in the partly sericitized oligoclase phenocrysts. Epidote in vesicles varies from single anhedral crystals to interlocking aggregates with granular quartz.

d. *Agglomerates.* The lowest agglomerate bed consists mainly of angular or sub-rounded fragments of hemi-crystalline dacite with less common holocrystalline andesite and dacite, ranging from 11 cm to 2 m in diameter. The holocrystalline dacite is devoid of ferromagnesian minerals but it includes much iron ore (mainly ilmenite) both as stringers and anhedral skeletal crystals. Corroded oligoclase (An_{27}) phenocrysts, exhibit interpenetrant (often cruciform) twinning and marginal alteration. They occur in a groundmass of pilotaxitic plagioclase (masked by chlorite and sericite) and ilmenite, enclosing rounded amygdales of quartz, epidote and chlorite.

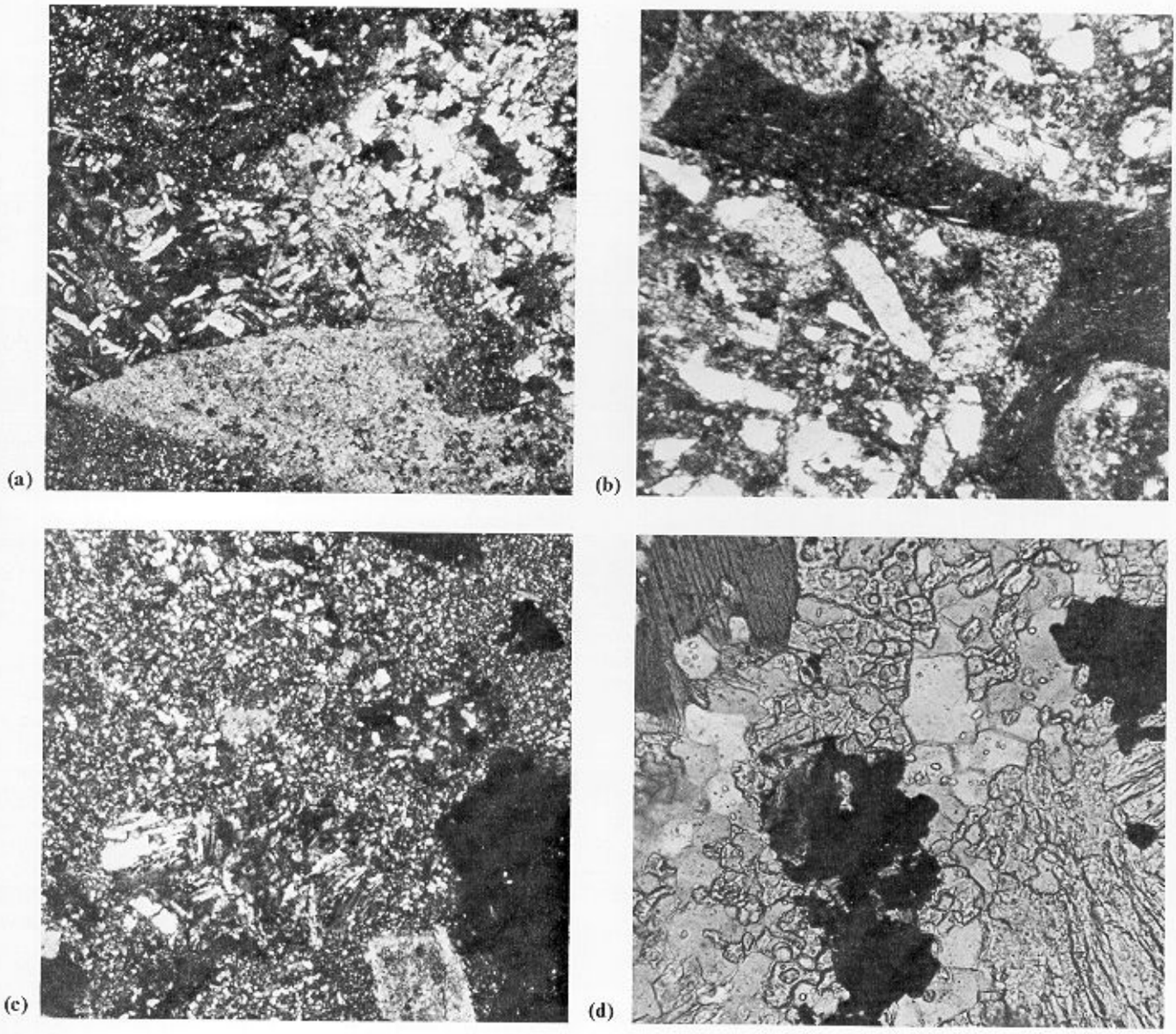

Fig. 51. a. Altered plagioclase phenocrysts and microlitic groundmass in porphyritic andesitic lava (KG.560.2; X-nicols; × 60). b. Hook-shaped lapilli of hemicrystalline (?) dacite in the tuffaceous matrix of agglomerate (KG.556.3; ordinary light; × 55). c. Hornfelsed dacitic tuff, with totally recrystallized groundmass, marginally reformed plagioclase and relatively unaltered trachytic lapilli (KG.553.2; X-nicols; × 60). d. Andalusite, biotite and magnetite with minor quartz in hornfelsed tuff (KG.553.6; ordinary light; × 150).

The matrix in the lowest part of the agglomerate is a black lithic tuff with well-developed joints which are frequently veneered with limonite. This tuff is composed of glassy and hemi-crystalline dacite, with minor holocrystalline dacite and andesite, and some sedimentary inclusions, in a gravelly matrix of oligoclase (An_{27}), ilmenite and chlorite, and with an intersertal base of feldspar, quartz, sericite and ore. Fragments of glassy and hemi-crystalline dacites range from perfect tear drops to angular or hooked lapilli (Fig. 51b), whereas the holocrystalline ones are predominantly sub-rounded. Spherulitic and perlitic structures occur in the green mafic glass which is partly devitrified and weakly isotropic. The holocrystalline dacites contain phenocrysts of oligoclase (An_{26}) and chlorite in a pilotaxitic felsic base. As secondary minerals (notably epidote) are uncommon in the tuffaceous matrix, it seems that the extensive deuteric alteration, which characterizes these andesites, may be due to hydrothermal solutions which percolated through the lavas as they cooled.

e. *Dacitic lithic tuffs*. Lithic tuffs, composed predominantly of dacitic lapilli, constitute over three-quarters of the pyroclastic rocks which crop out on the western side of the granite stock. The tuffs (e.g. KG.560.6; Table XII, analysis 4) underlying the solitary andesite lava flow are dark brown with both glassy and crystalline dacite lapilli, together with minor tuffaceous and sedimentary fragments in a felsic matrix. A peripheral concentration of iron ore characterizes the holocrystalline dacite lapilli, which contain phenocrysts of cloudy oligoclase (An_{27}) and chlorite set in a matrix of plagioclase microlites with interstitial chlorite. Amongst the other dacite lapilli are fragments resembling the lavas occurring on the eastern part of the ridge. The sedimentary fragments include quartzite and epidote-impregnated mudstone, neither of which were found *in situ*. The groundmass comprises chipped and fragmented plagioclase crystals, enclosed in a matrix of arcuate glass shards, partly replaced by quartz.

The ridge is capped by slightly finer, pale green dacitic tuffs, similar in composition to the brown tuffs but with a higher content of glassy fragments, many of which contain chipped and fractured plagioclase phenocrysts, and epidote-filled amygdales. Much of the glass has been replaced by chlorite and quartz, but fluxion structures, spherulites and perlites have been preserved. One pumiceous fragment was recorded, the remainder of the lithic content consisting of accessory holocrystalline dacite with some polysynthetic quartzite and (?) granodiorite.

f. *Andesitic crystal tuffs*. The pale green tuffs (e.g. KG.560.5) immediately above the andesitic lava contain a higher proportion of crystal than lithic fragments (Table XII, analysis 3). Much of the rock comprises chipped or embayed crystals of cloudy oligoclase which, with chlorite rimmed by ore, sphene, sanidine and ore, are set in an intersertal, epidote-impregnated unresolvable groundmass. A few grains of strained quartz are present and epidote and calcite fill vesicles and cracks. Sub-rounded fragments of the underlying porphyritic andesite form the bulk of the lithic fraction, together with quartzite, granite and micropegmatite. The absence of glassy lapilli and the moderate degree of sorting suggest that the rock has been re-worked.

g. *Vent agglomerates*. The agglomerate on the eastern flank of the basaltic andesite plugged vent is composed of sub-angular sedimentary fragments, up to 1 m in diameter, and less common cognate lapilli which seldom exceed 7.5 cm. The commonest of the included fragments are pale grey crystal tuffs, containing crystals of sanidine (partly replaced by quartz) with biotite, chlorite, sphene and iron ore, in a recrystallized matrix of interlocking quartz crystals. A few rounded lapilli of trachytic lava constitute the lithic fraction of these tuffs. Also common are pieces of a pale green fine-grained rock which comprises a polysynthetic aggregate of quartz and minor feldspar with interstitial biotite and epidote. Recrystallization in these fragments has obscured original textures and the origin of these and of the somewhat darker silt-grade fragments is unknown. Less common amongst the included fragments are porphyritic and andesite lapilli. The matrix of the agglomerate is a dark grey tuff composed of saussuritized plagioclase (An_{40}), iron ore and sphene in a base masked by finely divided biotite.

h. *Metamorphosed volcanic rocks*. Most of the volcanic rocks at station KG.553 (Procyon Peaks) appear to have been contact altered by a small body of Andean granite. Mineral assemblages in some of these rocks are those typical of the hornblende-hornfels facies of contact metamorphism. However, in most rocks the original texture has survived and recrystallization of the groundmass is the only real evidence of change. Thus, in specimen KG.553.8 (a rhyodacite from the north-west side of the vent) the (?) cryptocrystalline groundmass has been replaced by a mosaic of (?) prehnitized, granular plagioclase and subsidiary potash feldspar with interstitial chlorite and iron ore, but the plagioclase phenocrysts are intact apart from some minor marginal recrystallization. Hornblende phenocrysts have been universally replaced by anhedral clusters of epidote and ore, but such features also occur outside the contact aureole. Quartz-filled lenses and stringers cutting the groundmass are assumed to be relict amygdales.

The locality from which the above specimen was taken is at least 100 m from the nearest granite outcrop, but even in rocks from within 3 m of the granite's eastern margin (e.g. KG.553.1) the porphyritic texture is still discernible. The degree of recrystallization in the feldspar phenocrysts is, however, somewhat greater than in the previous specimen. These minerals also show extensive alteration, the commonest product being fine brown dust (? iron ore). Replacement by epidote, calcite and granular iron ore is occasionally evident. Pale green hornblende (γ: $c = 26°$), with attendant biotite and chlorite, occurs as inclusions in the feldspar phenocrysts and is also intergrown with granular quartz and oligoclase in the groundmass.

The fragmentary texture of the tuffs is still evident in rocks close to the granite though the margins of the lapilli are extremely diffuse (Fig. 51). The lithic fragments in the rocks east of the granite (e.g. KG.553.2) are all recognizably volcanic but some of the tuffs on the north side of the vent have fragments (Fig. 51) composed of biotite, andalusite, quartz, potash feldspar and magnetite, which may represent argillaceous sediments metamorphosed by the granite. In the adjacent vent agglomerate some recrystallization and a fine dissemination of biotite in the groundmass are the only outward signs of any change.

3. Summary

The volcanic rocks of the Millett Glacier succession are part of an original composite cone which was centred to the south of the present outcrop. It is probable that the original walls of the crater are preserved in the southern wall of the ridge and that the dips of the volcanic rocks have not been drastically altered by subsequent granite intrusions. The small vent exposed at the eastern end of the outcrop was probably a parasitic cone on the north-eastern flank of the main volcano.

It appears that the eruptions began with the outpouring of rhyodacite lava flows, with a certain amount of associated explosive activity which produced the interbedded agglomerates. It is evident from the lowest exposed unit that the apparently homogeneous rhyodacite and dacite flows are multiple and that the eruptions were frequently interrupted by short periods of quiescence, during which the surface of the lava was subjected to subaerial weathering. As time passed, the explosive activity increased at the expense of the outpourings of lava, so that a composite cone was built up. The explosive activity was punctuated by at least one period of quiescence, during which sedimentary processes were operative.

C. Gurney Point Succession

1. Stratigraphy

Volcanic rocks appear to form much of the north–south trending ridge 4.5 km east of the Gurney Point survey cairn, but geological observations were only possible at two localities. Dark, unbedded, porphyritic basaltic andesite lavas occur *in situ* midway along the ridge (KG.520) and as xenoliths in quartz-diorite on the lower slopes of the ridge (KG.519). The summit at station KG.520 is capped by approximately 170 m of bluish grey flinty tuffs which have been metamorphosed by a quartz-diorite intrusion. Although no contact between the two rock types was observed, thermal metamorphism of the tuffs suggests that they are the younger members of the formation.

2. Petrography

The basaltic andesite lavas are dark grey aphanitic rocks with white plagioclase phenocrysts up to 4 mm long. In thin section (Table XIII, analysis 10) the slightly sericitized labradorite (An_{67}) phenocrysts have rounded termini and contain epidote 'peppered' with iron one. Albite and Carlsbad twinning are invariably present and frequently accompanied by peripheral zoning. The mesostasis is formed of andesine (An_{42}) microlites with interstitial uralitic hornblende ($\gamma:c = 25°$) chlorite, iron ore and occasional sphene.

The metamorphism which accompanied the emplacement of the quartz-diorite affected the overlying tuffs, which are well-cleaved and much more indurated than any other tuffs in this area. The lithic fragments (trachytic and basaltic andesites) are flattened and aligned, and in the crystal fraction the larger plagioclase and uralitic hornblende crystals are deformed. The trachytic andesite fragments are composed of plagioclase microlites with interstitial ore and uralitic hornblende, whereas the basaltic andesite fragments resemble the underlying lavas. Corroded plagioclase crystals, up to 1 mm long, are fractured and may be replaced by aggregates of smaller crystals with sutured margins. One crystal appears to have been recrystallized in the nose of a small fold. Much of the groundmass is composed of uralitic hornblende which ranges from anhedral crystals (with an undulose extinction) to glomeroporphyritic aggregates enclosing small plagioclase crystals. Deformation of hornblende suggests that this mineral has resulted from the deuteric alteration of pyroxene and is not a product of the metamorphism.

D. Geochemistry

17 new analyses of volcanic rocks are presented (Table XIV). They include 11 lavas, four tuffs and two rocks of uncertain affinities from within the metamorphic aureole of a granitic stock. The limits which must be placed on the interpretation of data from a few randomly selected and often altered rocks are appreciated, but the reconnaissance nature of the survey and the aim of proportional representation (of analyses with respect to areal outcrop) are again emphasized. Also, it should be remembered that these are the first volcanic rocks from western Palmer Land to be analysed and their full potential may only be realized when further work has been undertaken.

The analyses have been corrected for the iron oxidation which may have occurred during the alteration process (Irvine and Baragar, 1971) and they have been recalculated on an H_2O- and CO_2-free basis.

1. Chemical characteristics

As a group, these volcanic rocks (Table XIV) are characterized by high Al_2O_3 (a well-established feature of orogenic igneous assemblages), Na_2O, Ba, Pb, Sr, variable but generally high Rb, and low K_2O, CaO and Cr. Zr values are low in the basalts and basaltic andesites but high in the more acid rocks. High La and Ce have been noted in some Graham Land rocks (West, 1974), and this may be a distinctive feature of the Upper Jurassic Volcanic Group. Despite their many common features, these rocks belong to two distinct chemical groups, defined mainly by variable alkali proportions and referred to here as the high- and low-potash series. The disparity between the two series of rocks is most obvious when they are plotted on a K–Ca–Na diagram (Fig. 52), but the differences in the other elements, and more significantly in the element ratios (Table XV), preclude an origin by soda or potash metasomatism. These differences cannot be explained by alteration, for altered and unaltered rocks are common to both rock series. On an A–F–M diagram (Fig. 53), the high-potash series, after slight initial iron enrichment, follows the typical calc-alkaline alkali-enrichment trend with a slight scatter of points in the intermediate region. The low-potash series shows a wider scatter but four of the plots (Nos. 2, 4, 8 and 11) define a curve, which, after initial strong iron enrichment, parallels the alkali-enrichment trend of the high-potash series but within the tholeiitic field.

2. Origin of the basalt and andesite

The single analysed basalt (KG.580.10) plots on the tholeiitic part of the A–F–M (Fig. 53) and $Na_2O + K_2O$ versus SiO_2 diagrams. Although island-arc tholeiites and high-alumina basalts generally have similar trace-element concentrations, it is possible to distinguish between the two groups (Table XVI) on the basis of Rb, Zr, La and Ce. Concentrations of these elements in the Palmer Land basalt resemble those of tholeiitic basalts, although it is acknowledged that the K/Rb ratio is more typical of the calc-alkaline suite. It is also apparent from

Table XIV. Chemical analyses of Mesozoic volcanic rocks.

	1	*2*	*3*	*4*	*5*	*6*	*7*	*8*	*9*	*10*	*11*	*12*	*13*	*14*	*15*	*16*	*17*
SiO_2	51.23	51.62	55.43	55.20	56.09	57.03	60.48	61.90	62.98	67.03	72.80	59.83	63.69	64.15	64.41	67.36	68.43
TiO_2	0.72	1.33	0.88	0.57	0.87	1.04	0.67	0.72	0.68	0.64	0.20	0.04	0.67	0.88	0.70	0.63	0.45
Al_2O_3	17.03	17.52	15.86	16.35	16.42	14.42	16.77	18.23	15.84	15.83	14.16	16.48	15.56	17.72	15.86	16.29	16.44
Fe_2O_3	2.38	4.35	3.49	3.83	4.18	3.77	3.49	3.71	3.26	1.98	2.79	3.16	2.68	2.82	2.52	1.83	1.52
FeO	6.01	3.68	5.35	5.78	2.75	2.52	2.30	2.02	1.42	0.81	0.38	1.87	1.70	4.52	1.63	1.11	0.70
MnO	0.12	0.14	0.16	0.15	0.19	0.14	0.11	0.07	0.10	0.13	0.03	0.11	0.12	0.10	0.11	0.02	0.35
MgO	7.58	4.66	5.58	4.73	4.49	4.73	2.48	0.69	1.80	0.59	0.24	2.70	1.77	0.83	1.47	0.99	0.60
CaO	10.23	9.79	5.61	5.23	3.52	5.13	6.17	1.87	3.63	1.64	1.19	4.86	2.80	1.25	2.88	2.71	1.62
Na_2O	2.16	4.29	3.40	5.68	5.96	3.49	3.57	5.99	4.89	5.24	5.34	4.08	4.31	3.09	4.39	5.58	5.54
K_2O	0.16	0.08	1.23	0.57	0.78	3.07	2.38	1.78	2.88	3.75	2.10	3.40	3.41	1.92	3.59	1.58	3.48
P_2O_5	0.08	0.16	0.09	0.18	0.18	0.22	0.16	0.21	0.18	0.10	0.02	0.14	0.13	0.04	0.13	0.11	0.09
H_2O	0.94	1.19	0.90	0.68	3.08	2.38	0.76	1.60	1.46	0.99	0.36	1.26	1.52	1.82	0.12	0.86	0.77
CO_2	0.86	0.63	1.11	1.02	0.81	1.34	0.85	0.66	0.68	0.86	0.43	0.94	0.64	0.46	1.30	0.67	0.57
Total	99.50	100.07	99.07	99.97	99.32	99.28	100.19	99.45	99.80	99.59	99.95	99.77	99.00	99.60	99.11	99.74	100.56
ANALYSES WITH AMENDED FeO VALUES (IRVINE AND BARAGAR, 1971) AND LESS TOTAL WATER AND CARBON DIOXIDE (RECALCULATED TO 100)																	
SiO_2	52.27	52.37	56.60	56.27	58.88	59.84	61.41	63.78	64.57	68.58	73.49	61.36	65.82	65.94	65.97	68.59	68.99
TiO_2	0.73	1.83	0.92	0.58	0.91	1.08	0.67	0.74	0.70	0.66	0.20	0.97	0.68	0.91	0.72	0.65	0.45
Al_2O_3	17.37	17.76	16.64	16.67	17.25	15.14	17.04	18.81	16.23	16.18	14.30	16.92	16.08	18.21	16.24	16.58	16.57
Fe_2O_3	2.60	2.88	2.93	2.10	2.48	2.56	2.20	2.28	2.23	2.03	1.71	2.56	2.24	2.44	2.25	1.86	1.54
FeO	6.30	5.15	6.54	7.51	4.59	3.80	3.54	3.46	2.45	0.83	1.37	2.53	2.24	5.05	1.96	1.14	0.70
MnO	0.12	0.14	0.17	0.15	0.20	0.14	0.11	0.07	0.10	0.13	0.03	0.11	0.12	0.11	0.11	0.02	0.35
MgO	7.74	4.72	5.86	4.82	4.72	4.96	2.54	0.70	1.84	0.61	0.25	2.77	1.82	0.85	1.51	1.01	0.60
CaO	10.43	9.93	5.89	5.33	3.71	5.38	6.27	1.93	3.74	1.69	1.20	4.98	2.89	1.29	2.95	2.75	1.63
Na_2O	2.20	4.98	3.56	5.79	6.25	3.67	3.64	6.18	5.01	5.36	5.40	4.18	4.45	3.18	4.49	5.68	5.58
K_2O	0.16	0.08	1.30	0.60	0.82	3.21	2.42	1.83	2.95	3.83	2.03	3.48	3.52	1.98	3.67	1.60	3.50
P_2O_5	0.08	0.16	0.09	0.18	0.19	0.22	0.16	0.22	0.18	0.10	0.02	0.14	0.14	0.04	0.13	0.12	0.09
ELEMENT WEIGHT PERCENTAGES LESS TOTAL WATER AND CARBON DIOXIDE																	
Si^{4+}	24.41	24.45	26.43	26.28	27.50	27.95	28.68	29.79	30.15	32.03	34.32	28.66	30.74	30.79	30.81	32.03	32.33
Ti^{4+}	0.44	1.10	0.55	0.35	0.55	0.65	0.40	0.44	0.42	0.40	0.12	0.58	0.41	0.55	0.43	0.39	0.27
Al^{3+}	9.19	9.40	8.80	8.82	9.13	8.01	9.01	9.95	8.59	8.56	7.56	8.95	8.51	9.63	8.59	8.77	8.77
Fe^{3+}	1.82	2.01	2.05	1.47	1.73	1.79	1.54	1.59	1.56	1.42	1.20	1.79	1.57	1.71	1.57	1.30	1.08
Fe^{2+}	4.90	4.00	5.08	5.84	3.57	2.95	2.75	2.69	1.90	0.64	1.06	1.97	1.74	3.92	1.52	0.89	0.54
Mn^{2+}	0.09	0.11	0.13	0.12	0.15	0.11	0.09	0.05	0.08	0.10	0.02	0.09	0.09	0.09	0.09	0.02	0.27
Mg^{2+}	4.67	2.85	3.53	2.91	2.85	2.99	1.53	0.42	1.11	0.37	0.15	1.67	1.10	0.51	0.91	0.61	0.36
Ca^{2+}	7.46	7.10	4.21	3.81	2.65	3.85	4.48	1.38	2.67	1.21	0.86	3.56	2.07	0.92	2.11	1.97	1.17
Na^{+}	1.63	3.70	2.64	4.30	4.64	2.72	2.70	4.59	3.72	3.98	4.01	3.10	3.30	2.36	3.33	4.21	4.14
K^{+}	0.13	0.07	1.08	0.50	0.68	2.66	2.01	1.52	2.45	3.18	1.68	2.89	2.92	1.64	3.05	1.33	2.91
P^{5+}	0.03	0.07	0.04	0.08	0.08	0.10	0.07	0.10	0.08	0.04	0.01	0.05	0.06	0.02	0.06	0.05	0.04
O^{2-}	45.23	45.14	45.46	45.52	46.47	46.22	46.74	47.48	47.27	48.07	49.01	46.68	47.49	47.86	47.53	48.43	48.23
C.I.P.W. NORMS																	
Q	5.94	0.26	10.17	2.14	6.76	11.66	16.54	17.86	15.51	20.42	32.28	11.76	19.26	34.72	20.57	23.82	20.08
C	–	–	1.57	–	1.62	–	–	5.13	–	2.26	1.95	–	1.35	9.56	2.68	2.22	1.97
Z	0.02	0.04	–	0.02	0.09	0.07	0.06	0.08	0.09	0.13	0.05	0.11	0.12	0.09	0.13	0.10	0.09
or	0.96	0.50	7.54	3.41	4.77	18.70	14.14	10.79	17.25	22.46	11.92	20.37	20.66	11.65	21.41	9.41	20.63
ab	18.47	42.03	29.76	48.34	52.32	30.39	30.35	51.74	41.98	44.90	45.35	34.95	37.35	26.69	37.49	47.70	46.93
an	36.70	25.77	20.91	17.52	11.94	15.08	22.79	3.96	12.97	2.51	3.42	16.84	9.65	3.31	5.74	8.82	4.30
di	7.05	14.45	–	0.90	–	1.07	1.50	–	0.18	–	–	0.91	–	–	–	–	–
hy	23.06	6.18	20.17	18.11	12.15	11.67	5.94	1.75	4.47	1.48	0.61	6.39	4.52	6.92	3.70	2.49	1.49
mt	3.53	6.38	5.19	5.59	6.28	5.63	5.08	4.71	2.98	1.11	0.70	3.62	3.98	4.18	3.60	1.84	2.07
il	1.37	2.55	1.72	1.09	1.71	2.03	1.28	1.40	1.31	1.22	0.39	1.82	1.29	1.70	1.34	1.20	0.85
hm	–	–	–	–	–	–	–	0.54	1.25	1.24	2.32	0.70	–	–	0.06	0.58	0.10
ap	0.19	0.38	0.22	0.42	0.45	0.53	0.38	0.51	0.43	0.24	0.04	0.33	0.32	0.10	0.30	0.27	0.20
pr	0.74	–	0.14	0.12	–	0.03	0.01	0.01	0.01	0.03	–	0.04	–	0.01	0.01	0.01	0.01
cc	1.98	1.45	2.61	2.33	1.91	3.14	1.94	1.53	1.57	1.98	0.98	2.17	1.49	1.07	2.98	1.54	1.30
COORDINATES OF TRIANGULAR DIAGRAMS																	
A	13.4	29.8	25.9	31.9	39.5	41.0	44.8	56.5	57.5	74.6	70.2	52.5	58.6	39.5	61.4	66.4	78.1
F	51.1	47.6	49.6	48.7	393.	36.2	40.7	39.6	32.2	21.5	27.9	32.9	31.1	55.5	29.8	26.3	17.9
M	35.5	22.6	24.5	19.4	21.2	22.8	14.5	3.9	10.3	3.9	1.9	14.6	10.3	5.0	8.8	7.3	4.0
K	1.4	0.7	13.6	5.8	8.6	28.8	21.9	20.3	27.7	38.0	25.6	30.3	35.2	33.3	35.9	17.7	35.4
Ca	80.9	65.3	53.1	44.3	33.2	41.7	48.7	18.4	30.2	14.4	13.2	37.2	25.0	18.7	24.9	26.2	14.2
Na	17.7	34.0	33.3	49.9	58.2	29.5	29.4	61.3	42.1	47.6	61.2	32.5	39.8	48.0	39.2	56.1	50.4

Table XIV. Chemical analyses of Mesozoic volcanic rocks (continued).

	1	*2*	*3*	*4*	*5*	*6*	*7*	*8*	*9*	*10*	*11*	*12*	*13*	*14*	*15*	*16*	*17*
TRACE ELEMENTS (ppm)																	
S	3886	24	736	621	21	132	29	39	29	180	16	197	14	59	25	34	43
Cr	162	40	68	25	14	38	16	30	16	6	–	20	16	13	16	–	2
Ni	71	14	39	14	12	29	7	11	8	4	–	11	9	4	9	–	1
Rb	3	–	42	21	31	102	87	111	85	143	61	142	123	98	145	64	105
Sr	466	374	440	420	712	553	713	517	507	315	252	559	437	271	406	332	307
Y	11	28	25	10	34	23	27	20	27	40	21	20	30	31	28	35	28
Zr	76	174	158	121	455	328	293	398	462	627	233	527	587	450	635	484	438
Ba	119	120	323	260	609	1256	836	785	1364	1639	1197	1532	1558	758	1507	797	1594
La	–	2	9	22	49	26	25	36	36	44	–	28	35	49	42	–	39
Ce	11	16	21	42	94	67	6	57	69	96	–	56	74	95	94	–	68
Pb	38	41	19	6	41	179	27	45	39	30	69	34	35	90	36	26	21
K/Rb	446	∞	244	227	208	249	227	133	281	218	274	199	230	163	205	204	275
Ba/Rb	39.7	∞	7.7	12.4	19.7	12.3	9.6	7.0	16.1	11.5	19.6	10.8	12.7	7.7	10.4	12.5	15.2
Ba/Sr	0.26	0.32	0.73	0.62	0.86	2.30	1.17	1.52	2.70	5.20	4.80	2.70	3.60	2.80	3.70	2.40	5.20
Rb/Sr	0.01	–	0.10	0.05	0.04	0.18	0.12	0.22	0.17	0.45	0.24	0.28	0.28	0.36	0.36	0.19	0.34
K/Ba	14.0	5.8	31.1	18.3	10.6	20.3	23.7	18.8	17.5	19.0	14.0	18.4	18.4	21.1	19.8	16.4	18.1
D.I.	25.47	42.79	47.47	53.83	63.85	60.75	61.03	80.39	74.74	87.78	89.57	67.08	77.27	73.06	79.47	80.93	87.64

1. KG.580.10 Basalt, Carse Point succession.
2. KG.520.2 Basaltic andesite, Gurney Point succession.
3. KG.580.9 Basaltic andesite, Carse Point succession.
4. KG.581.9 Andesite, Carse Point succession.
5. KG.556.5 Andesite, Millett Glacier succession.
6. KG.560.2 Andesite, Millett Glacier succession.
7. KG.583.1 Augite-andesite, Carse Point succession.
8. KG.556.2 Dacite, Millett Glacier succession.
9. KG.554.4 Dacite, Millett Glacier succession.
10. KG.554.2 Rhyodacite, Millett Glacier succession.
11. KG.553.8 Hornfelsed rhyodacite, Millett Glacier succession.
12. KG.560.5 Andesite crystal tuff, Millett Glacier succession.
13. KG.560.3 Dacitic lithic tuff, Millett Glacier succession.
14. KG.556.3 Agglomerate matrix, Millett Glacier succession.
15. KG.560.6 Dacitic lithic tuff, Millett Glacier succession.
16. KG.553.2 Hornfels, Millett Glacier succession.
17. KG.553.1 Hornfels, Millett Glacier succession.

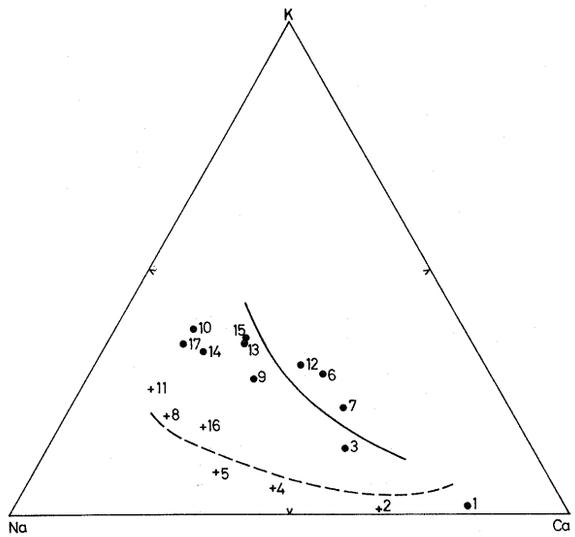

Fig. 52. Ca–Na–K triangular variation diagram for the Mesozoic volcanic rocks, numbered as in Table XVI (+, low-potassium series; ●, high-potassium series). The solid line is the trend determined by Adie (1955) for some of the Graham Land Upper Jurassic volcanic rocks, and the broken line is the variation trend for the Deception Island volcanic rocks (Hawkes, 1961).

Table XV. Principal chemical and petrological differences between the high- and low-potassium series in the Mesozoic volcanic rocks.

Low potassium	*High potassium*
Lower K_2O, Ba, Rb. Marginally lower CaO and MgO. Sr variable but generally lower. Na_2O and Fe_2O_3 + FeO higher. Lower Rb/Sr, Ba/Sr and (mostly) K/Ba	
Plot of Ba against D.I. almost linear	Sudden increase of Ba at D.I. = 60 with wide scatter of points at higher D.I.
Higher An content, both normative and in phenocrysts	
Mostly devoid of mafic phenocrysts but where present are hornblende and chlorite	Pyroxene phenocrysts in one rock; otherwise replaced by fibrous amphibole

Table XVI that similar conclusions may be drawn concerning the average Danco Coast basalt. Comparisons between the two main groups of the calc-alkaline andesites are hindered by a dearth of data from the continental margins, as is evident in the similarity between Jakes and White's (1972) averaged island-arc andesite and Taylor's (1969) average 'andesite'. However, Forbes and others (1969) have demonstrated higher FeO values in island-arc andesites from Alaska, whilst Yoder (1969) has noted differences in the Al_2O_3: (FeO + Fe_2O_3) ratios, Jakes and White (1972) expressed doubts over these conclusions, claiming that in major-element chemistry the continental margin rocks have equivalents in the high-potash calc-alkaline rocks of island arcs, but they acknowledged the relative abundance of Zr and potassium-type trace elements (Ba, Sr and Rb) in continental rocks as noted by Siegers and others (1969). Thus, it is apparent from Table XVI that the andesite and basaltic andesite of the low-potash series have Ba, Rb, Cr and Ni contents typical of the island-arc calc-alkaline series (and, incidentally, marginally higher FeO values), whereas concentrations of these elements in the high-potash series are

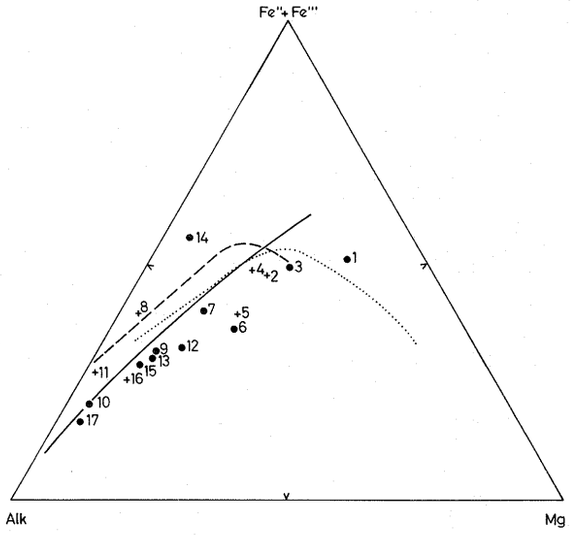

Fig. 53. Alk–(Fe″ + Fe‴)–Mg triangular variation diagram for the Mesozoic volcanic rocks, as numbered in Table XIV (+, low-potassium series; ●, high-potassium series). The solid line is the trend determined by Adie (1955) for some of the Graham Land Upper Jurassic volcanic rocks, and the broken line is the variation trend of the Deception Island volcanic rocks (Hawkes, 1961). The dotted line separates the tholeiitic (above) and calc-alkaline (below) fields.

more typical of continental margin rocks. Like the tholeiitic basalt, the island-arc andesites have unusually low K/Rb ratios, a common enough occurrence in the Danco Coast rocks (West, 1974) to suggest it is a characteristic feature of the group.

The Upper Jurassic Volcanic Group (Adie, 1964a) of the Antarctic Peninsula has, in the past, been assigned to the continental branch of the calc-alkaline suite (Baker, 1972) solely on the grounds of large volumes of rhyolites, and it is therefore significant that, in the two areas (i.e. Palmer Land and the Danco Coast) where trace-element determinations have been carried out, the basic rocks are more typical of island-arc tholeiites. Although West (1974) did not distinguish between the two branches in the andesites, the specimen (O.990.2) she used to illustrate the calc-alkaline affinities has trace-element values closely resembling the average low-potash andesite of western Palmer Land.

The two rock series do not conform to any pattern of geographical distribution but, though the age relationships (Figs 52 and 53) are not absolutely certain, it is probable in most cases that the low-potash series is the older. Thus, in western Palmer Land, during the Mesozoic there was a transition from island-arc to continental margin environment without any apparent movement of volcanic centres.

Accepting the basic concept of plate tectonics and, in consequence, assuming the presence of an easterly dipping

Table XVI. Average trace-element concentrations for basalts and andesites from the Antarctic Peninsula compared with published world averages.

A. Basalts

	Oceanic	*Tholeiites Continental*	*Island arc*		*Calc-alkaline Island arc*		*Antarctic Peninsula Danco Coast*	*Palmer Land*
	e	f	f	a	b	a	g	
Cr	297	–	–	50	18	40	115	162
Ni	97	124	79	30	7	25	32	71
Rb	< 10	36	5	5	15	10	5	3
Sr	130	428	397	200	384	330	500	466
Y	43	–	–	–	–	20	12	11
Zr	95	224	45	70	87	100	64	76
Ba	14	352	148	75	126	115	160	119
La	< 80	–	–	1.1	–	9.6	3	–
Ce	–	–	–	2.6	–	19	9	11
Pb	–	–	–	–	–	–	8	19
K/Rb	1 300	185	–	1 000	450	340	456	446

B. Andesites

	Tholeiites Island arc	*Island arc*		*Calc-alkaline Continental*	*Average andesite*	*Danco Coast*	*Antarctic Peninsula Palmer Land*	
	a	a	b	c	d	g	Low potassium	High potassium
Cr	15	15	7	50	56	18	26	40
Ni	20	18	2	90	18	5	13	25
Rb	60	30	–	77	31	34	32	77
Sr	220	385	286	800	385	460	502	569
Y	–	21	–	7.6	21	18	24	25
Zr	70	110	95	210	110	180	250	260
Ba	100	270	295	680	270	479	330	805
La	2.4	11.9	–	–	11.9	22	24	20
Ce	–	24	–	–	24	42	51	31
Pb	–	–	–	–	6.7	12	29	75
K/Rb	–	–	–	–	–	–	–	–

a. Jakes and White (1972).
b. Baker (1968).
c. Siegers and others (1969).
d. Taylor (1969).
e. Engel and others (1965).
f. Condie and others (1969).
g. West (1974).

subduction zone beneath western Palmer Land, a suitable model can be constructed to explain the genesis of these two rock series. The model broadly parallels that used by Hietanen (1973), for the origin of andesitic and granitic magmas in the Sierra Nevada, where water from the descending oceanic plate ascends to the peridotitic mantle of the upper plate and lowers the melting point of peridotite. The first product of such melting will be an andesite (Yoder, 1969) low in potassium. The subsequent change to a potash-enriched magma may 'have resulted from the exhaustion of available water and from a higher temperature at deeper levels (still above the Benioff zone) where magma was now generated from the mantle by partial melting in anhydrous conditions, in a manner suggested by Yoder and Tilley's experimental work (1962)' (Hietanen, 1973, p. 2115). The product on this occasion is a tholeiitic basalt (Yoder, 1969). Hietanen ascribed the deeper level to crustal thickening (by accumulation of new material and by deformation in a period from Devonian to Permian', whereas in Palmer Land the episode is intra-Upper Jurassic and crustal thickening would have been relatively minimal. A steeply dipping or even vertical subduction zone seemed to be a reasonable alternative or even more acceptable, the detached slab concept (Barazangi and others, 1973; Oliver and others, 1973) offering possibilities of relatively rapid descent.

With increasing acidity, both rock series show (Fig. 54) higher absolute values of K, Ba and Rb, higher Rb/Sr and Ba/Sr and lower K/Rb ratios—features generally regarded (e.g. Taylor, 1969) as products of fractional crystallization. The frequent absence of early formed magnesia-rich mafic phenocrysts suggests fractionation was stronger in the low-potash series, possibly as a result of the higher water content. However, it is normal in fractional crystallization or differentiation for the Ba/Rb ratio and the Ba content to fall in the final product, whilst in the present Antarctic example the trends appear to be reversed. A sudden upsurge in the Ba content occurs at D.I. = 60 and sympathetic movements are detectable in Rb, Sr and K, whilst corresponding decreases in Mg, Ni and Cr are also apparent at this point. Such trends can be readily explained by the inclusion of large amounts of siliceous crust.

3. *Origin of the more acid lavas*

Four mechanisms are considered to explain the origin of the more acid lavas:

i. Complete or partial melting of the country rocks.
ii. Extensive contamination of a basaltic magma with siliceous crust.
iii. Fractional crystallization of a basaltic magma.
iv. A combination of any of the above three explanations.

It is assumed that the country rocks in Late Jurassic times were formed by members of the metamorphic complex and more rarely by the older granodiorite. Thus, in Table XVII the average composition of the analysed dacite and rhyodacite, and their associated tuffs, is compared with a pre-volcanic granodiorite and the average of two homogeneous tonalites from the metamorphic complex. Although these lavas are relatively enriched in Na, Sr, Zr, Ba, La, Ce and Pb, and are deficient in Ca, there is an unusually high degree of correlation with the average tonalite. However, partial melting of such a rock would in theory produce a rock with a considerably higher potash content than any of those analysed. Discussing the origin of volcanic rocks from the Danco Coast, where no metamorphic rocks are exposed, West (1974) compared the average of eight acid lavas with the compositions of pre-Jurassic granodiorites and Carboniferous siltstones, and concluded that partial or complete melting of the sediments could have produced the acid lavas. However, lavas in the 55–66% SiO_2 range were not recorded on the Danco Coast and, when the available analyses are plotted on A–F–M, Mg–Fe–Al and A–Ca–F triangular diagrams, they exhibit distinct bimodal distributions. No such pattern is evident in the Palmer Land rocks (the only break in the series occurring in the andesite field), and partial or complete melting of the country rocks is not considered a major process in the formation of the acid volcanic rocks. The principal argument against fractional crystallization of basalt or basaltic andesite as the sole process in the formation of the western Palmer Land dacites and rhyodacites is the predominance of acid rocks. Fractional crystallization was, however, demonstrated in the more basic andesites with contamination becoming more evident in the more silicic members. With continued contamination, the magma would become more acid and gradually approach the composition of the (? tonalitic) country rock. Continued fractionation could then produce the rhyodacites. Thus, it would seem that the most likely process involved in the formation of the acid volcanic rocks was prolonged fractionation of a highly contaminated basalt or basaltic andesite magma.

Table XVII. Major oxide and trace-element concentrations of the computed average acid volcanic rock, the mean of two metamorphic complex tonalites and a pre-Upper Jurassic granodiorite.

	1	*2*	*3*	*4*
SiO_2	66.18	65.86	65.50	66.19
TiO_2	0.56	0.62	0.66	0.51
Al_2O_3	16.02	16.21	15.46	15.52
Fe_2O_3	2.94	2.57	2.46	2.39
FeO	1.15	1.59	2.40	2.10
MnO	0.08	0.11	0.11	0.11
MgO	0.83	1.00	1.09	1.27
CaO	2.08	2.18	3.53	3.86
Na_2O	5.36	4.93	3.39	4.19
K_2O	2.61	2.71	2.94	2.09
P_2O_5	0.13	0.11	0.18	0.12
H_2O	1.10	1.06	0.84	0.82
CO_2	0.66	0.70	0.97	0.09
Total	99.70	99.65	99.53	99.26
S	66	49	68	–
Cr	17	14	10	7
Ni	8	7	5	3
Rb	100	104	109	77
Sr	398	372	239	209
Y	27	29	29	30
Zr	430	479	264	223
Ba	1246	1244	1049	772
La	39	40	26	19
Ce	65	75	47	33
Pb	46	43	28	14

1. Average of two dacites and two rhyodacites (Table XIV, analyses 8–11).
2. Average of column 1, three dacitic tuffs and two rhyodacitic tuffs (Table XIV, analyses 13–17).
3. Average of two undifferentiated gneissose tonalites; Metamorphic Complex (Table VII, analyses 4 and 6).
4. Pre-Upper Jurassic granodiorite, Mount Crooker (Table XI, analysis 2).

VI. ANDEAN INTRUSIVE SUITE

Some time after the cessation of the Mesozoic volcanicity and before the Tertiary dyke phase, much of western Palmer Land underwent the emplacement of extensive basic and acid plutons which currently occupy a greater surface area than either the preceding or succeeding rocks. In many respects (e.g. relationships with adjacent rocks; gabbro to granite trend) they resemble intrusive rocks occurring throughout Graham Land to which the collective name Andean Intrusive Suite has frequently been applied. Adie (1955) considered these rocks represented a single Upper Cretaceous–Lower Tertiary intrusive episode, but Rex (1972) has subsequently demonstrated by radiometric dating the presence of at least four post-Upper Jurassic intrusive episodes:

i. Jurassic–Cretaceous boundary (140–130 Ma).
ii. Mid-Cretaceous (120–80 Ma).
iii. Late Cretaceous basic rocks (75–70 Ma).
iv. Early Tertiary acid rocks (60–45 Ma).

No dates are yet available for these Palmer Land rocks but there is no evidence to suggest more than one period of intrusion occurred. The term 'Andean' is retained for convenience for rocks which are demonstrably younger than the Mesozoic volcanic rocks and the whole intrusive episode is referred to the Andean orogeny.

A. Peridotites and Gabbros

1. *Field description*

After granodiorites, gabbros are the most widespread of the plutonic rocks occurring in the Pegasus Mountains, upper Millett Glacier and on the coast between Wade Point and Burns Bluff. The sudsidiary ridge on the north side of station KG.518 (south-west Pegasus Mountains) is composed almost entirely of a deeply weathered coarse-grained dark green rock with porphyritic pyroxene and subordinate plagioclase. Unusual features of this rock are large patches of coarsely crystalline pyrite, generally associated with the development of hornblende. No contact with the adjacent metamorphosed tonalite is visible, and throughout this area the postulated Andean age is based on the intrusive relationship with the pre-Upper Jurassic granodiorite at Moore Point and the lack of identical fragments in the Mesozoic pyroclastic and sedimentary rocks. Veins of microgranite 5–8 cm thick cut the gabbros at station KG.518, and at eastern Procyon Peaks a large vertically sided gabbroic intrusion (approximately 500 m wide), which occupies much of the south-western shoulder of stations KG.555 and 557, is flanked by pink granite from which 15–23 cm thick microgranite veins penetrate into the basic rock often along fissures parallel to the joint planes. The contact with the granite is sharp but the occurrence of gabbroic xenoliths is restricted. Both rock types contain rounded inclusions of amphibolite which strongly resemble that occurring in the metamorphic complex to the south-east. A second dyke-like body of gabbro occurs within the granodiorite immediately below the summit of the nunatak, where both acid and basic rocks are extensively veined by microgranite. No granodiorite veins were observed in the gabbro but numerous rounded or sub-rounded gabbroic xenoliths in the granodiorite adjacent to the contact indicate that the basic rock is older. However, at Canis Heights gabbro is invaded by both granite and granodiorite. The basic rock is finer-grained and more melanocratic than at station KG.555 and the contact with the granodiorite is gradational. A thin veneer of calcite commonly coats joint planes. Blocks of gabbro and peridotite, which are common in the lateral moraine beneath the cliffs at station KG.563, are presumed to have originated from the crags at the head of the glacier. Apart from a 5 m wide microgranodiorite dyke, the entire western face of Wade Point is composed of a medium- to coarse-grained aggregate of blackish green pyroxene and pale green feldspar with rare veins of gabbro-pegmatite. A slightly more leucocratic variety was found in the moraine below the survey cairn ridge but not *in situ*. Gabbros are thought to comprise most of the Moore Point ridge and at the northern tip they are in contact with pre-Upper Jurassic granodiorite (p. 45). A considerable variety of rock types is present within this outcrop, including olivine- and hypersthene-gabbros, and approximately 800 m south of Moore Point proper a 60 m wide body of peridotite cuts the basic rocks. Numerous subsidiary dykes, ranging from 30 cm to 1 m, branch into the country rock which is considerably more leucocratic and finer-grained than the typical gabbro of the area. Crude pinch-and-swell structures in the smaller dykes suggest that they were emplaced while the gabbro was still warm. Extensive mineralization accompanied the intrusion and the more open joints in the country rock are frequently veneered with calcite and limonite.

2. *Petrography*

As a result of crystal accumulation and possible contamination, the gabbros possess a characteristic heterogeneity and diversity of mafic minerals which is seldom seen in the other Andean rocks.

a. *Peridotites.* Despite the obviously intrusive relationship at station KG.572, the ultrabasic member of this suite is regarded as having formed by crystal accumulation from a primary gabbroic magma. In the hand specimen, it is coarse-grained, fresh in appearance and composed of highly reflecting pyroxene either with (KG.572.2) or without (KG.563.2) irregular white feldspar 'spots' up to 4 mm across. In this section, olivine with an approximate compositional range of $Fo_{85}Fa_{15}$–$Fo_{65}Fa_{35}$ is the primary mafic mineral forming 1–3 mm wide subhedral or rounded crystals. Unusually well-developed cleavage planes are common and they are generally infilled with iron ore, whereas within individual crystals tiny rod-like inclusions of ore have a common two-directional orientation. Alteration to green antigorite and magnetite appears to commence along irregular cracks (which frequently pass into clinopyroxene) and complete destruction of the olivine is not uncommon. Although some of the larger grains of olivine are ophitically intergrown with clinopyroxene, most are poikilitically enclosed in large plates (up to 4 mm across) of colourless augite with $2V = 58°$ and $\gamma:c = 42°$. Both augite and colourless hypersthene ($2V = 92°$) are extensively pseudomorphed by hornblende (α = colourless, β = pale pink, γ = pale brown and $\gamma:c = 20°$) which has been partly replaced by pale green amphibole ($\gamma:c = 15°$) and orange-brown biotite. Extremely rare plagioclase, locally showing polysynthetic twinning, is mostly

masked by alteration products (mainly sericite). Anhedral green or light brown spinel, usually accompanied by chromite, is commonly included in the clinopyroxene and plagioclase, whereas islands of colourless euhedral crystals are interstitial to olivine. In all of its forms, this mineral is associated with brownish turbid areas which under high power appear to be composed of a fibrous mineral with an extremely low birefringence. Subhedral magnetite forms the remainder of the rock. Specimen KG.563.2, a peridotite collected from the moraine, possesses a similar mineralogy with the addition of pale pink to colourless phlogopite.

b. *Olivine-gabbros*. The only occurrence of olivine-gabbro is on the west face of Moore Point immediately above the gabbro–granodiorite contact. No layering was visible on the outcrop but the rock itself is heterogeneous, the melanocratic patches having an almost ultrabasic mineralogy. Later veins of gabbro-pegmatite are common. In thin section, the melanocratic fraction (e.g. KG.570.3) lacks the usual gabbroic texture, being dominated by anhedral 2–4 mm long crystals of optically negative olivine which are rarely altered to pale yellow antigorite. The imperfect cleavage is similar to that recorded in the olivine of the peridotite. Between crossed nicols, several crystals show faint banding which, where the two occur together, is parallel to the cleavage. These bands vary greatly in thickness and are frequently wedged out. Pale pink, slightly pleochroic hypersthene, with $2V_\alpha = 80°$ and $\gamma:c$ commonly between 10° and 20°, invariably forms a reaction rim with the olivine. In contrast, augite with $2V_\gamma = 54°$ and $\gamma:c = 43°$ forms 1–2 mm wide anhedral plates and frequently includes olivine and rounded plagioclase. Rare hornblende with α = yellow, β = green, γ = greenish brown and $\gamma:c = 19°$ has developed from both pyroxenes but it is itself partly replaced by biotite.

Lath-like plagioclase (An_{92-84}) is intergrown with and frequently included in the clinopyroxene, but where it is adjacent to olivine a reaction rim of orthopyroxene forms, or there is a lobate myrmekite-like intergrowth of plagioclase and orthopyroxene growing into the plagioclase (Fig. 55a). Albite, Carlsbad and pericline twins are common and their lamellae are commonly bent. The composition planes of the Carlsbad twins are generally curved and very irregular, suggesting an origin similar to that of Vance's (1961, p. 1107) synneusis twins.

Within the olivine regularly orientated dendritic magnetite (Fig. 55b), often following the cleavage, appears to have formed before the clinopyroxene. Irregular trails of granular ilmenomagnetite in the olivine and orthopyroxene may have formed synchronously with the myrmekite-like ilmeno-magnetite and orthopyroxene intergrowths that are invariably present at the olivine–orthopyroxene interfaces.

Hamilton (1957) considered that the banding in olivine was the result of some form of deformation and there is ample evidence here (e.g. the unusual optical orientation of the orthopyroxene and the bending of the plagioclase twin lamellae) to support this theory. To affect the plagioclase, such deformation must have occurred late in the crystallization history, or may even have taken place after crystallization. Bent plagioclase twin lamellae are common in the quartz-diorites but they are absent from the granodiorites despite textural evidence in the latter of externally generated pressures during emplacement. Hence it would seem that these deformational features in the gabbros have probably resulted from internal stresses during late crystallization.

c. *Gabbros*. The gabbro surrounding the peridotite at station KG.572, which differs from the more widespread hypersthene-gabbro both in grain-size and colour index (p. 62), consists of an ophitic intergrowth of plagioclase and clinopyroxene. In 0.5–1.5 mm long laths, plagioclase (An_{80-92}) is generally idiomorphic towards clinopyroxene and possesses albite, pericline and Carlsbad twinning. The abrupt termination of pyroxene inclusions against Carlsbad twin planes strongly suggests the presence of synneusis twins. Alteration is mainly to prehnite and, more rarely, sericite while slight marginal recrystallization is apparent. The pyroxene ($\gamma:c = 40°$) is subhedral, generally 0.5 mm in size with a maximum of 4 mm and a low 2V (less than 40°) suggestive of a sub-calcic augite. The crystals frequently have a sieved appearance, resulting from the patchy replacement by pale green hornblende which in turn is rarely replaced by chlorite. An unusual aspect of this rock (KG.572.1) is the absence of iron ore (except for tiny pyrite crystals rimmed by limonite). Small shears cutting the rock are filled with granular plagioclase and prehnite. Specimen KG.569.4, taken from the moraine below Wade Point, shows a rather coarser ophitic intergrowth with plagioclase (An_{74}) crystals up to 4 mm. Well-defined primary albite, pericline and Carlsbad twins are cut by vague secondary twins with characteristic wedge-shaped terminations. Zoning is extremely rare but patchy extinction is common. Replacement of sub-calcic augite by hornblende with α = yellow, β = brownish green, γ = green and $\gamma:c = 26°$ has advanced somewhat further than at station KG.572 (Table XVIII, analysis 7) as has the development of penninite, principally at the expense of hornblende but also within the plagioclase. In sharp contrast to specimen KG.572.1, magnetite forms crystals up to 2.5 mm across and is poikilitically intergrown with plagioclase. In addition, rounded crystals, seldom more than 0.25 mm in diameter, occur within the mafic minerals. Interstitial quartz, having apparently grown at the expense of plagioclase, is another feature of this rock.

d. *Hypersthene-gabbros*. The hypersthene-bearing variety is the commonest of the gabbros occurring at all localities except station KG.555. Most of these rocks have an ophitic texture but there is ample evidence that, with prolonged crystallization probably accompanied by some movement, this inverts to the xenomorphic granular texture characterizing specimen KG.569.3 (Fig. 55c). This is particularly evident in the case of plagioclase—forming, for the most part, euhedral to subhedral laths (1–2.5 mm long) with irregular and often rounded crystal boundaries, but frequently replaced by granular (0.25–0.5 mm) aggregates with 120° triple junctions and straight crystal edges. The plagioclase composition is generally about An_{74} but it ranges from An_{92} (KG.571.4) to An_{60} (KG.569.3) though zoning and patchy extinction are restricted to the latter rock. The freshness of the plagiocalse is most unusual with only rare sericite and clinozoisite (KG.518.4). Primary Carlsbad, albite and pericline twins are common in the lath-like plagioclases but less so in the granular aggregates. Both the albite and pericline twin lamellae are bent and frequently attenuated by vague ghost-like secondary twinning. Unlike the orthopyroxene of the olivine-gabbro, hypersthene with $2V_\alpha = 67–72°$ (60° in

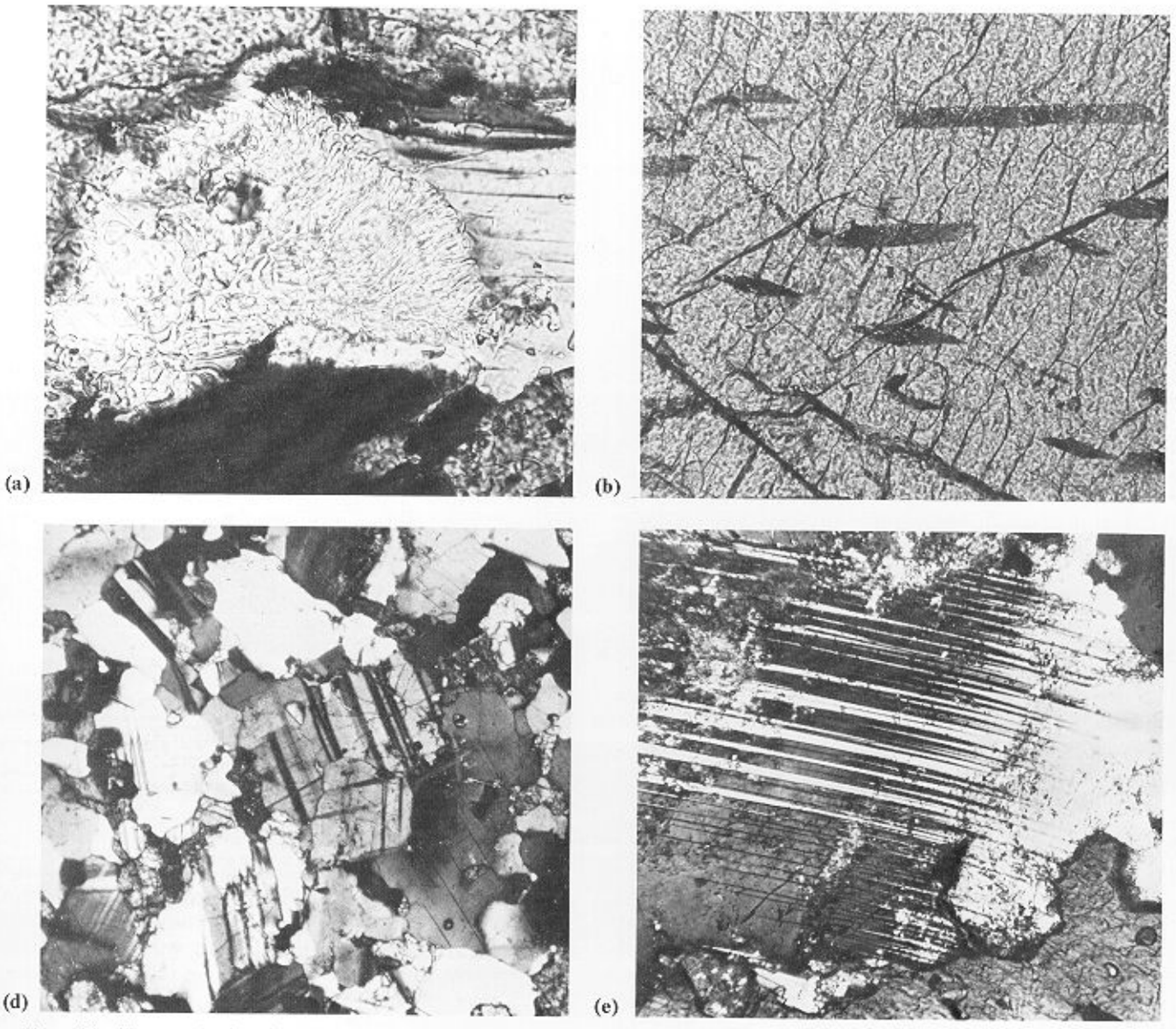

Fig. 55. a. Myrmekite-like symplectite of plagioclase and orthopyroxene at plagioclase–olivine interface in olivine-gabbro (KG.570.3; X-nicols; × 390). b. Large olivine plate in olivine-gabbro, showing dendritic plates of magnetite regularly orientated in two directions and trails of granular ilmenomagnetite (KG.570.3; ordinary light; × 146). c. Granular texture in hypersthene-gabbro (KG.569.3; X-nicols; × 58). d. Secondary glide twinning in plagioclase subophitically intergrown with hornblende in quartz-diorite (KG.575.2; X-nicols; × 149).

specimen KG.569.3), although subordinate to the clinopyroxene, forms larger crystals which are occasionally replaced by aggregates of smaller crystals in optical continuity. The extinction angle, $\gamma:c$, may be up to 18° and the mineral is pleochroic from pale pink to colourless. Sub-calcic augite with $2V_\alpha = 25–32°$, $\gamma:c = 35–42°$ and the optic axial plane parallel to (010) generally occurs in anhedral plates 2–3 mm across or more rarely (KG.569.3) in aggregates of 0.5–1 mm crystals. Since both pyroxenes are ophitically intergrown with plagioclase, it is assumed they crystallized simultaneously, but the mantling of orthopyroxene by clinopyroxene in specimen KG.571.4 points to a late-stage period of one-pyroxene crystallization. Hornblende with α = yellow, β = yellow-brown, γ = brown and $\gamma:c = 26°$ formed by reaction between clinopyroxene and magma, commencing around the margins, along cracks and patchily within the augite (KG.518.4). A green hornblende with α = pale yellow, β = light green, γ = sea-green and $\gamma:c = 20°$, usually in optical continuity, mantles the brown hornblende and replaces clinopyroxene often in association with brown biotite. Much of the hypersthene has been replaced by glomeroporphyritic aggregates of green hornblende ($\gamma:c = 25–30°$). This has subsequently been partly replaced by a much paler green variety with similar optical orientation, which occurs as fibrous or decussate aggregates reminiscent of the more usual green hornblende. Biotite, penninite and more rarely epidote are secondary after

Table XVIII. Modal analyses of Andean gabbros and quartz-diorites.

	1	2	3	4	5	6	7	8	9	10
Quartz	–	–	–	–	–	0.03	0.80	23.48	13.37	14.72
Plagioclase‡	60.70	65.37	65.60	54.00	65.03	52.80	78.00	57.94†	60.30	63.04
Hypersthene	–	6.86	14.00	4.20	5.84	–	–	–	–	–
Augite	30.50	4.62	16.20	12.70	7.20	0.18	2.80	2.76	–	–
Hornblende	6.00	9.72	0.40	4.70	10.04	23.61	14.10	4.26	21.20	9.40
Uralitic hornblende	–	7.72	–	12.90	6.12	8.79	–	–	–	–
Biotite	–	0.57	–	–	0.84	4.06	–	7.95	0.77	9.24
Chlorite	2.10	–	–	–	0.48	0.03	2.40	1.16	0.66	–
Magnetite	–	5.07	3.50	10.30	4.44	9.76*	1.90	2.32	3.50	1.76
Sphene	–	–	–	–	–	0.12	–	0.07	–	1.60
Apatite	–	–	0.10	–	0.01	0.62	–	0.03	0.20	0.24
Epidote	–	0.07	–	1.20	–	–	–	0.03	–	–
Antigorite	–	–	0.20	–	–	–	–	–	–	–
Prehnite	0.50	–	–	–	–	–	–	–	–	–
Pyrite	0.20	–	–	–	–	–	–	–	–	–
Plagioclase composition	An_{79}	An_{80}	An_{60}	An_{74}	An_{74}	An_{71}	An_{74}	An_{60-32}	An_{50}	An_{46}

* Ilmenite.
† Including 3.60% orthoclase.
‡ Including sericite.

1. KG.572.1 Leucocratic gabbro, Moore Point.
2. KG.571.4 Hypersthene-gabbro, Moore Point.
3. KG.569.3 Hypersthene-gabbro, Wade Point.
4. KG.518.4 Hypersthene-gabbro, Gurney Point.
5. KG.561.2 Hypersthene-gabbro, Canis Heights.
6. KG.555.7 Hornblende-gabbro, Procyon Peaks.
7. KG.569.4 Hornblende-gabbro, Wade Point.
8. KG.574.2 Acidified gabbro, Moore Point.
9. KG.575.2 Quartz-diorite, Burns Bluff.
10. KG.522.2 Quartz-diorite, Gurney Point.

hornblende. Much of the clinopyroxene contains exsolved iron ore, mostly along cleavages, but most of the ore is primary magnetite generally associated with the mafic minerals and frequently with kelyphitic rims of colourless hornblende. Titaniferous magnetite is present in several of the rocks; in specimen KG.518.4 it forms large plates mantled by leucoxene and poikilitically enclosing green spinel.

e. *Hornblende-gabbros*. Table XVIII illustrates the wide modal variations in the proportion of amphibole in these gabbros, but in all cases, whether it be brown or green hornblende, crystallization is at the expense of pyroxene. However, in specimen KG.555.7, some of the smaller hornblende crystals are almost interstitial to the plagioclase and probably crystallized from the magma. As columnar crystals 1.5–2 mm across with α = yellow, $\beta = \gamma$ = pale brown or greenish brown and $\gamma : c = 30°$, the hornblende is slightly different from that of the previously described gabbros. A second pale green to colourless amphibole occurs in the cores of some of the brown hornblende crystals, indicating growth on pyroxene. The accessory minerals, apatite, sphene and ilmenite (with only a trace of magnetite), also distinguish this rock from the other gabbros. Near Burns Bluff, where mafic minerals are uncharacteristically dominant (KG.575.4), pyroxene has been entirely pseudomorphed by hornblende (α = pale yellow, β = green, γ = sea-green and $\gamma : c = 22°$) containing a wide variety of 'foreign material' such as:

i. Rare magnetite and pyrite, anhedral 0.5 mm, often mantled by sphene.
ii. Rod-like magnetite and limonite, commonly orientated and most probably resulting from exsolution.
iii. Rutile, also orientated.
iv. Sphene.

This rock also illustrates the effect of stress during crystallization; the original ophitic intergrowth of plagioclase (An_{72-82}) and pyroxene, with an average grain-size of 1–1.5 m, has largely been overprinted by a granular aggregate with an average grain-size of 0.25 mm.

f. *Acidified gabbros*. The only minor gabbroic intrusion is a dyke of a rock type not recorded elsewhere in this area. Probably as a result of contamination by the granitic country rock, it is more acid than any of the previously described gabbros and possesses the following distinctive features:

i. Porphyritic texture.
ii. Plagioclase zoned from labradorite to andesine.
iii. Interstitial quartz and potash feldspar.

A specimen from the northern side of the dyke has plagioclase phenocrysts up to 5 mm in size, and more rarely of hornblende, set in a light grey aggregate cut by thin epidotic veinlets. In thin section, euhedral plagioclase phenocrysts with heavily sericitized cores and clear rims are continuously zoned from An_{60} to An_{32}. The albite twin lamellae are frequently bent and displaced by small cracks, while recrystallization to granular aggregates and replacement by quartz are notable marginal features. The bulk of the rock, however, comprises an interlocking aggregate of a similar plagioclase (average grain-size of 1.5 mm) enclosing subordinate sub-calcic augite, most of which has been pseudomorphed by hornblende with α = yellow, β = green, γ = sea-green and $\gamma : c = 23°$. Reaction between the magma and the mafic minerals led to the formation of biotite and subsequently chlorite. Titaniferous magnetite is present as inclusions in all of the primary minerals, particularly the mafic ones, and in biotite it is mantled by sphene. Zircon is confined to inclusions in biotite whereas pistacite occurs

exclusively in cracks. Pools of quartz and anhedral orthoclase occur interstitially and in places the quartz appears to have grown at the expense of plagioclase.

B. Quartz-Diorites

1. Field description

Quartz-diorites are the least widespread of all the plutonic intrusions between Carse Point and Gurney Point, and south of Ryder Glacier there is no record of any dioritic rocks (Ayling, 1966). Such an apparent paucity of intermediate rocks is unusual in the northern part of the Antarctic Peninsula (Adie, 1955), although the quartz-diorites of Adelaide Island are simply local variations in the quartz-gabbro (Dewar, 1965). The largest outcrop of quartz-diorite occupies the lower slopes of the ridge 6 km north of Mount Crooker, where the rock has intruded and metamorphosed the Mesozoic lavas and tuffs. Most of the included material is of a volcanic origin but smaller rounded or sub-angular xenoliths of amphibolite are common.

Near Burns Bluff (KG.575), the quartz-diorite was only observed on the higher slopes but many veins, some of pegmatitic proportions, intrude the gabbros and diorite-gneisses below. The distribution of ferromagnesian minerals within these veins is random and aggregates up to 5 cm in diameter are not uncommon. Xenoliths are rare in the main body of the intrusion and the faint flow banding is concordant with the foliation of the metamorphic rocks. The country rock is frequently stained with epidote and malachite.

A slightly more leucocratic diorite occurs within the granodiorite at the eastern end of station KG.552. Its contact with the granodiorite is sharp and, like the numerous lensoid amphibolite xenoliths, is parallel to the sub-vertical flow banding. The strike of the flow banding, however, differs by 35° from that of the granodiorite (Fig. 56). At the contact there is no chilling in either rock and the joint system of the granodiorite passes through the diorite. The sedimentary and volcanic sequence forming the southern wall of the large west-facing cirque at Carse Point is intruded by a highly altered medium-grained white rock with a tonalite mineralogy. This intrusion comprises a single 50 m wide dyke with chilled margins, but on the western face a 6 m thick sill of similar appearance intrudes the mudstones.

2. Petrography

Apart from specimens KG.552.1 and 580.11, the quartz-diorites are coarse-grained dark grey aggregates of plagioclase and amphibole resembling the hornblende-gabbros. Near Burns Bluff the rock has a distinct gabbroic (ophitic) texture (e.g. KG.575.2), in which the pyroxene is pseudomorphed by hornblende with α = yellow, β = yellowish green, γ = green or pale blue-green and $\gamma:c = 21°$. Vermicular or acicular inclusions of exsolved ilmenomagnetite are aligned parallel to the (110) and (011) planes in the hornblende. The plagioclase (An_{50}) is remarkably fresh despite common strain-induced secondary glide twinning (Fig. 55d) and slight marginal recrystallization. Interstitial quartz forms amoeboid aggregates with sutured margins.

The rocks from the Gurney Point area (e.g. KG.519.2 and 522.2) have a hypidiomorphic texture (with cataclastic overtones), in which rarely twinned subhedral 1–2 mm long laths of andesine are separated by granular quartz and flakes of brown biotite. Ragged anhedral crystals of hornblende with α = yellow, β = green, γ = pale blue-green and $\gamma:c = 25°$ are subordinate and even interstitial to the plagioclase. Euhedral sphene and apatite, together with anhedral magnetite, are the principal accessories. In addition to the sub-mylonitic texture, shear zones up to 2 mm wide, containing flattened and stained quartz and plagioclase crystals, cut the diorite and the xenoliths. The Carse Point dyke represents a much higher level of intrusion than the others and the rock examined (KG.580.11) exhibits many unusual features which are thought to have been produced by rapid transport from depth and subsequent chilling. In particular, the original mafic mineral has been replaced by 3–4 mm diameter clusters of fibrous biotite, penninite and colourless chlorite enclosing rods and stringers of iron ore, while unstrained quartz forms granular aggregates with 120° triple junctions. Euhedral plagioclase laths are continuously zoned from An_{64} to An_{32} and slightly sericitized. Calcite and epidote form the remainder of the rock.

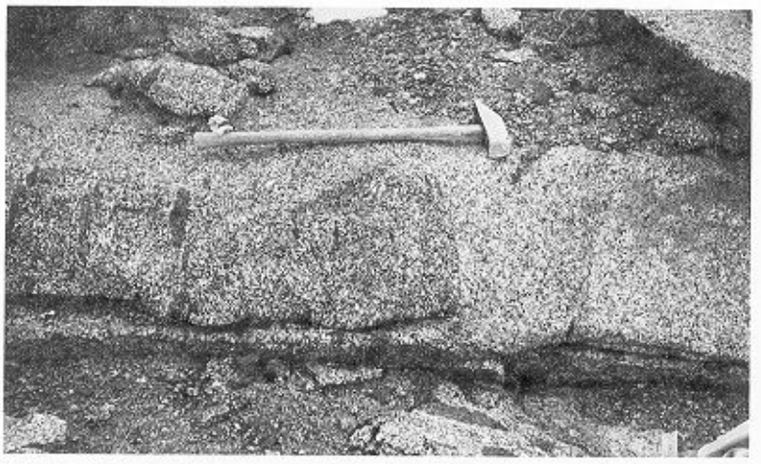

Fig. 56. Contact between quartz-diorite (left) and granodiorite at station KG.552, eastern Perseus Crags. The vertical flow-banding and amphibolite schlieren parallel the contact and make an angle of 30° with similar structures in the granodiorite. The hammer shaft is 55 cm long.

3. Xenoliths

In comparison with the *in situ* volcanic rocks at station KG.520, the xenoliths in the diorite do not appear to have undergone much alteration. However, the amphibolites in specimen KG.519.2 have been almost completely digested, although their porphyritic texture is still preserved. All of the groundmass plagioclase and most of the porphyroblasts (An_{42}) have been replaced by a more sodic andesine (An_{32}) and granular quartz, whereas the larger hornblende crystals have been replaced by decussate aggregates.

C. Granodiorites

1. Field description

From long 66°45′W as far as the eastern limit of exposure on the plateau edge, the geology is dominated by a medium- to coarse-grained light grey intrusive rock which, despite its widespread occurrence, shows little variation in composition. Intrusions of a similar rock were also recorded within the

Pegasus Mountains. Amongst the group of nunataks in upper Bertram Glacier (Fig. 3), no contacts with the older rocks, with the exception of quartz-diorite at station KG.552 and quartz-plagioclase-porphyry at station KG.551, were observed. However, the almost universal presence of flow structures (both linear and planar) seems to suggest that these rocks were originally close to the roof of the batholith. (Ayling (1966) noted a capping of 'Upper Jurassic' volcanic rocks on granodiorites with similarly aligned structures east of Taurus Nunataks.) Although horizontal and sub-horizontal flow structures occur locally, most are steeply inclined, suggesting that each group of nunataks represents a separate cupola of the same batholith. It is evident from the fine section through the granodiorite in the Pegasus Mountains that considerable relief can develop in the roof zones of these intrusions. At station KG.541 (Capella Rocks), where the western boundary of the main plateau batholith is within 5 km of the metamorphic rocks, xenoliths and screens of foliated and unfoliated amphibolite are abundant (Fig. 57), though the frequency and size of the included bodies decrease rapidly eastward. This suggests that most of these were incorporated during the emplacement of the granodiorite, but some of them may be more intimately connected with the genesis of the magma (p. 77–78). The inclusions are frequently aligned, flattened or drawn out into schlieren parallel to the flow structures. In upper Millett Glacier, granodiorite is common but is not the dominant rock type. At station KG.561 (Canis Heights), the contact with gabbros shows a gradual increase in the colour index and xenolith content as the basic rock is approached, but no flow structures are present. However, the main body of the granodiorite is more leucocratic than usual.

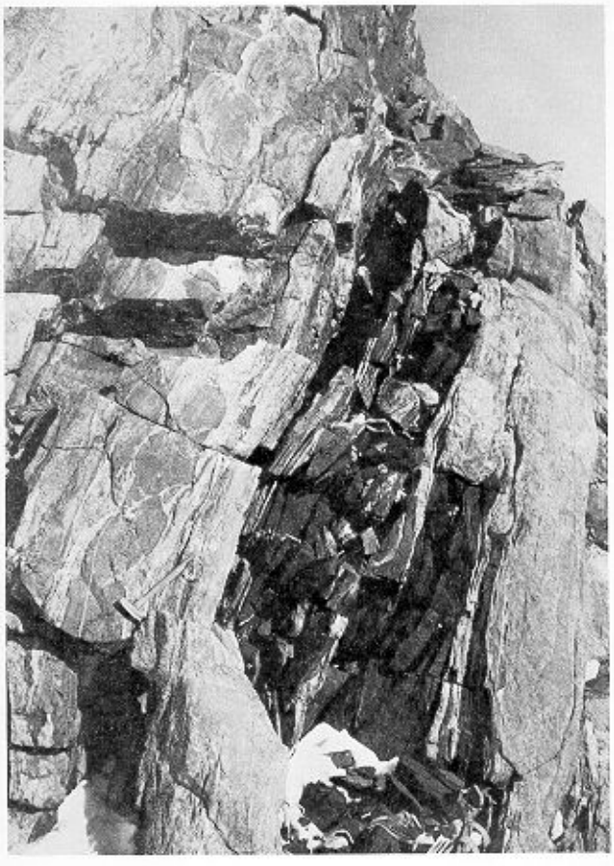

Fig. 57. Flow-banded granodiorites containing amphibolite screens and xenoliths, and cut by microgranite veins (KG.541). The hammer shaft is 30 cm long.

Fig. 58. Flow-banded granodiorites cut by granite-pegmatite (KG.557). Narrow veins of granite-aplite parallel the banding and the schlieren have been drawn out to form attenuated bands. The clinometer edge is 10 cm long.

At station KG.557, eastern Procyon Peaks, the contact between granodiorite and enclosed gabbro is always sharp. Although inclusions of gabbro are present in the granodiorite, the majority of the rounded xenoliths are amphibolites, which also occur in the gabbro. Flow banding and schlieren at station KG.577 (Fig. 58) suggest that the western limit of the intrusion was fairly close to the present western face of the nunatak.

2. Petrography

The granodiorites are light grey coarse- to medium-grained aggregates of plagioclase, quartz, hornblende and biotite, which, despite local variations in the mineral proportions (Table XIX), show a marked consistency in appearance. Their texture is predominantly hypidiomorphic or more rarely porphyritic. Euhedral plagioclase forms broad laths or equidimensional plates averaging 1–2 mm in length (or 7.5–9 mm in the case of the phenocrysts) and, more rarely, granular crystals 0.3–0.5 mm in diameter. The composition is mainly in the range An_{42-48}; zoning, usually continuous down to An_{23}, is common in the Gurney Point intrusions (e.g. KG.526.5 and 528.1) but it is exceedingly rare in the plateau rocks with flow structures and, where present, it is oscillatory. However, in one of the rocks (KG.542.4) two generations of plagioclase are present, the larger of composition An_{49} and the smaller An_{39-43}. Twinning is extremely common and the following laws were identified: pericline, Carlsbad-albite and albite-AlaB. Synneusis twins are also exceedingly common (Fig. 59a). Subordinate potash feldspar, mainly untwinned microperthite, occurs either interstitially or in 2–3 mm wide irregular plates commonly enclosing plagioclase and quartz. A secondary origin for the potash feldspar is indicated by the following features:

i. Serrated intergranular boundaries.
ii. Development of myrmekite within plagioclase adjacent to orthoclase.

Table XIX. Modal analyses of Andean granodiorites, adamellites and granites.

	1	*2*	*3*	*4*	*5*	*6*	*7*	*8*	*9*	*10*	*11*	*12*	*13*	*14*	*15*
Quartz	12.30	21.60	26.48	21.88	20.00	25.60	5.57	20.90	30.60	33.73	27.60	29.27	15.02	30.40	24.80
Orthoclase	9.00	13.60	14.64	7.64	6.58	3.60	28.05*	12.50	19.30	22.18	25.20	29.14	35.83	42.53	43.00
Plagioclase†	57.30	56.40	49.18	55.91	55.35	51.70	49.62	46.00	46.30	37.01	42.30	35.34	44.55	21.64	27.00
Hornblende	17.70	3.70	3.70	8.99	3.27	4.80	10.03	8.30	–	–	tr.	–	0.20	0.35	1.70
Biotite	–	2.40	3.22	3.38	12.01	11.40	0.99	7.30	1.30	3.32	2.80	2.66	3.10	2.26	2.20
Chlorite	0.70	0.80	1.63	0.46	1.75	0.60	0.80	1.70	1.80	1.96	0.50	1.92	0.05	2.22	–
Magnetite	2.80	1.00	1.03	0.35	0.72	1.10	4.38	2.40	0.70	0.68	1.10	0.87	1.15	0.35	0.90
Sphene	–	0.40	0.12	0.05	0.08	0.20	0.32	0.40	–	0.08	0.40	0.13	–	0.15	0.40
Apatite	0.20	–	–	0.15	0.08	0.30	0.24	0.10	–	0.08	0.10	tr.	0.10	0.10	tr.
Zircon	–	–	–	–	–	–	–	0.10	–	–	–	0.07	–	tr.	tr.
Epidote	–	0.10	tr.	1.19	0.16	0.70	–	0.20	–	0.96	–	0.53	tr.	tr.	–
Allanite	–	–	–	–	–	–	–	–	–	–	–	0.07	–	–	tr.
Pyrite	–	–	–	–	–	–	–	–	–	–	–	–	–	tr.	–
Calcite	–	–	–	–	–	–	–	0.10	–	–	–	–	–	–	–
Fluorite	–	–	–	–	–	–	–	–	–	–	–	–	–	tr.	–
Plagioclase composition	An_{40}	An_{48-38}	An_{48}	An_{46}	An_{48}	An_{48-42}	An_{58-45}	An_{38-35}	An_{35-24}	An_{34}	An_{38-30}	An_{35-24}	An_{54-26}	–	An_{38-29}

tr. Trace.
* Micropegmatite.
† Including sericite.

1. KG.501.2 Granodiorite, Aldebaran Rock.
2. KG.526.4 Granodiorite, Pegasus Mountains.
3. KG.526.5 Granodiorite, Pegasus Mountains.
4. KG.541.3 Granodiorite, Capella Rocks.
5. KG.542.4 Granodiorite, Capella Rocks.
6. KG.544.1 Granodiorite, Perseus Crags.
7. KG.557.1 Granodiorite, Procyon Peaks.
8. KG.552.3 Granodiorite, Perseus Crags.
9. KG.561.3 Granodiorite, Canis Heights.
10. KG.542.5 Adamellite, Capella Rocks.
11. KG.561.1 Adamellite, Canis Heights.
12. KG.501A.1 Adamellite, Aldebaran Rock.
13. KG.558.1 Adamellite, Procyon Peaks.
14. KG.502.3 Granite, Aldebaran Rock.
15. KG.555.1 Granite, Procyon Peaks.

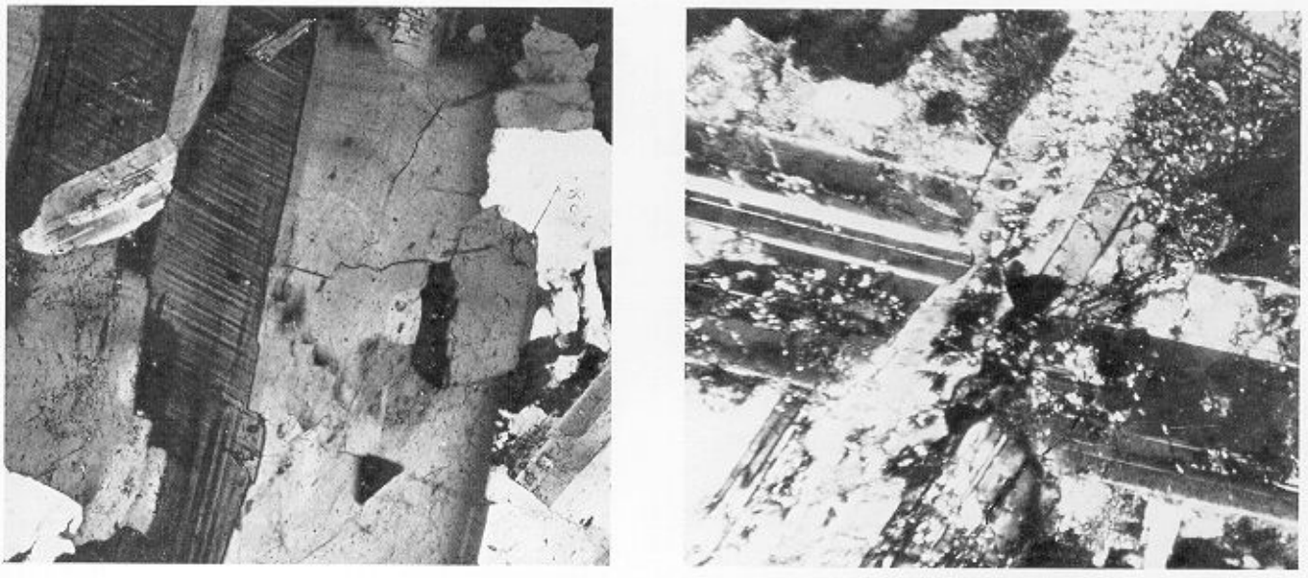

Fig. 59. a. Plagioclase zoning and twinning in granodiorites: synneusis twin (KG.526.4; X-nicols; × 59). b. Granodiorite showing cruciform intergrowth of plagioclase (KG.557.1; X-nicols; × 51).

iii. Virtual absence of sericite in plagioclase except around myrmekite.

Quartz, mostly strained, forms 1.5–2 mm anhedral crystals which may occur either singly or form mosaics with curved intergranular boundaries. For the most part, crystallization occurred after plagioclase and before orthoclase, but graphic intergrowths with both minerals are occasionally present.

The modal mafic mineral content of the Gurney Point and upper Millett Glacier rocks (Table XIX; analyses 2, 3 and 9) is somewhat lower than that of the main plateau outcrops (Table XIX; analyses 4–7). The modal mafic mineral content of specimen KG.552.3 is distorted by the presence of unusually large hornblende crystals and is not considered to be truly representative, because the rock in outcrop is considerably more leucocratic than the typical plateau type, lacking flow structures. With the exception of the upper Millett Glacier rocks, green hornblende is the primary mafic mineral and forms ragged 1–2 mm long laths with α = yellow, β = green, γ = bluish green and $\gamma : c$ = 22–27°, having crystallized almost

simultaneously with plagioclase. Biotite occurs as glomeroporphyritic aggregates after hornblende, although there is ample evidence that some also crystallized directly from the magma. Pale green chlorite seems to be an alteration product growing on the hornblende and biotite. Sphene, the commonest of the accessory minerals after magnetite, ranges in form from euhedral wedges to granular aggregates and, from its intimate association with the mafic minerals, it is regarded as a product of the degradation of hornblende. Apatite and reddish brown allanite are rare, whereas tiny zircon crystals with characteristic pleochroic haloes occur either within the biotite or the replacing chlorite. Large subhedral epidote crystals (mainly pistacite), forming in and around plagioclase, hornblende and biotite, demonstrate the widespread occurrence of late-stage hydrothermal solutions. At Procyon Peaks (stations KG.557 and 558) a pale pink porphyritic rock completely unlike any rock described previously is thought to have resulted from the assimilation of gabbroic material. Two specimens, KG.557.1 from within 100 m of the gabbro and KG.558.1 1.5 km away, illustrate the effects of contamination. The former is dominated by euhedral tabular labradorite (An_{58}) phenocrysts up to 4.5 mm long which occasionally occur as cruciform-like intergrowths (Fig. 59b) set in an intergrowth of andesine (An_{45}), 1–2 mm long, and brown hornblende, 0.5 mm in size, almost identical with that in the adjacent hornblende-gabbro (p. 65). By comparison, specimen KG.558.1 is finer-grained with equidimensional plagioclase phenocrysts 1–2 mm across (maximum 3 mm) set in a groundmass averaging 0.25 mm in grain-size. Zoning is particularly common in the phenocrysts, mainly normal discontinuous, giving rise to three distinct divisions—core (An_{54}), inner zone (undefined) with rare oscillatory zoning, and continuously zoned rim (averaging An_{25}) which occasionally resorbs the inner zone and the core. The composition of the groundmass plagioclase is the same as that of the rim in the phenocrysts. Twinning in the phenocrysts is mainly polysynthetic, the lamellae frequently terminating before reaching the outer zone, whereas in the groundmass simple twins predominate. Although brown hornblende occurs both as phenocrysts and in the groundmass, it is considerably scarcer than in specimen KG.557.1, where it has been partly replaced by a pale green actinolitic hornblende, and subsequently pseudomorphed by biotite and chlorite. Two generations of quartz are present: an earlier development consisting of slightly strained anhedra, apparently unconnected with the later interstitial graphic intergrowth with orthoclase.

On the north side of the glacier the rock (KG.561.1) is more acidic than usual; on the basis of the plagioclase: potash feldspar ratio it is strictly an adamellite. Besides the higher percentage of perthitic orthoclase, this rock differs from the other granodiorites in the following respects:

i. The plagioclase is sodic andesine with a compositional range of An_{30-38}.
ii. Hornblende is virtually absent, biotite being the main mafic mineral.

3. Discussion

Middlemost (1969) delineated mesozonal granites as those possessing the following characteristics:

i. Complex contacts that are partly discordant and partly concordant.
ii. Planar foliation which is most strongly developed away from the core.
iii. Not directly related to volcanic rocks.
iv. Contain pegmatites and aplites.
v. May have well-developed contact aureoles.

The first three of these are established features of the Palmer Land granodiorites. Microgranites and pegmatites commonly cut the granodiorites and, although some of them can be traced directly to the granite, the general absence of late-stage veins within the more acid plutons suggests that most are connected with the granodiorite. In this respect, it is significant that the most extensive network of veins occurs at station KG.557 cutting the only granodiorite with a granophyric texture. (Such textures are generally regarded as the product of rapid crystallization in a volatile-rich environment (Mehnert, 1968; Barker, 1970). Although the texture of the diorite-gneiss adjacent to the granodiorite at station KG.526 has a thermal overprint (p. 24; Fig. 27a), the contact effect on the volcanic rocks east of Taurus Nunataks (Ayling, 1966) is negligible, particularly when compared with the extensive aureole surrounding the much smaller granite body intruding the Millett Glacier succession. The presence of flow structures suggests that the granodiorite could have been emplaced in a semi-crystalline state and, hence, at a sufficiently low temperature to preclude the development of an aureole.

D. Granites

1. Field description

Compared with the granodiorite, large intrusions of granite are rare and the outcrop at Aldebaran Rock (KG.502) is the only occurrence in Bertram Glacier. The contact with the granodiorite is sharp and small veins of granite-aplite penetrate the country rock to a depth of 30 m. Immediately west of the contact, a smaller granite body (not visibly connected to the main mass) overlying the granodiorite is fed by a 1 m wide dyke.

The smaller ridge 0.6 km to the east (KG.501) is composed of a similar well-jointed pink rock with considerable amounts of included material especially towards the eastern end. These rounded to sub-angular xenoliths have diameters ranging from 2.5 cm to 6 m. They consist exclusively of white feldspar and thin amphibole laths in a medium-grained aggregate which becomes porphyritic with increased assimilation of feldspar.

Within the confines of these two nunataks, the granite is cut by eight basic dykes all of which parallel the prominent north–south vertical joints. Close to their contacts the country rock is generally shattered with deposits of calcite, epidote and limonite on the joints.

The remaining granite intrusions are confined to Procyon Peaks. At station KG.553 gently dipping lavas are cut by a granite body 50 m wide. The exact nature of the contact is obscured by snow but it is assumed to be vertical, and the metamorphic aureole extends for at least 100 m into the volcanic rocks.

At the south-western corner of station KG.555, where pink granite intrudes hornblende-gabbros, the contact relations are similar to those with the granodiorite at Aldebaran Rock and, although xenoliths of the basic rock (similar to those of station KG.501) are present, most of the included material comprises amphibolite.

The only other major acid intrusion occupies the narrow ridge (KG.559) linking the two volcanic outcrops, 3.5 km west of station KG.553, and the small nunatak just to the north. Like its counterpart on station KG.553, this rock is somewhat darker than usual with close jointing, which greatly reduces its resistance to weathering.

2. Petrography

The acid member of the suite is a coarse-grained pink rock formed of pink potash feldspar and brownish quartz with minor plagioclase that nevertheless imparts a porphyritic texture to the rock. Small amounts of hornblende and biotite are also present. In thin section the hypidiomorphic texture is dominated by anhedral plates of perthitic orthoclase with an incipient brown coloration that probably results from minute inclusions rather than from alteration. Graphic intergrowths with quartz are common. Quartz also occurs with the alkali feldspar, mostly as 0.1–1.0 mm anhedral crystals, but in one specimen (KG.502.3) the crystals are euhedral. Both fluid and crystal inclusions are present and strain shadows are ubiquitous. In most cases, hornblende is the primary mafic mineral both as subhedral crystals or aggregates of more rounded crystals (KG.555.1). The usual variety is greenish brown with α = pale straw to colourless, β = brownish green or light green, γ = greenish brown and $\gamma : c = 25°$, and in the case of specimen KG.502.3 it is practically identical with that in the adjacent granodiorite. An early primary origin for the hornblende is in accord with the assimilation process described below, and this offers a possible explanation why biotite is the only mafic mineral in the specimen from station KG.501A (Aldebaran Rock), where there are no xenoliths. However, biotite is dominant in all the present granites, forming mostly glomeroporphyritic aggregates after hornblende and (apart from specimen KG.555.1) showing partial replacement by chlorite and epidote. In specimen KG.555.1, biotite often forms a myrmekite-like intergrowth with magnetite which is the commonest of the accessory minerals and generally forms anhedral crystals, frequently mantled by granular sphene. Sphene also forms idiomorphic edges. Zircon, apatite and allanite (pleochroic from pale brown to colourless) with the addition in specimen KG.502.3 of pyrite and pale violet fluorite form the remainder of the rock.

3. Xenoliths

Xenoliths, showing a varying degree of assimilation, occur at station KG.555, where the majority are of hornblende-gabbro, and at station KG.501 where granodiorite predominates. The process of digestion appears to commence with recrystallization of plagioclase; in specimen KG.501.2 a few of the original laths (1.5 mm long and of an unknown composition) remain, the rest having been replaced by a framework of randomly orientated andesine (An_{40}) laths 0.25–0.5 mm long. An untwinned and slightly more acid plagioclase which rims the andesine probably resulted from the replacement of plagioclase by perthitic orthoclase. Where plagioclase and potash feldspar are adjacent myrmekite has developed although, like the orthoclase, it may simply represent the invasion of granitic material. The destruction of primary greenish brown hornblende is not generally as advanced as that of plagioclase. All stages of replacement by plagioclase, ranging from skeletal euhedral to tiny crystals totally enclosed in the feldspar, are present and replacement by decussate actinolite frequently occurs. Quartz is mostly interstitial but it includes small plagioclase crystals.

4. Discussion

The intrusive nature of the granites is undeniable, and that a temperature gradient developed across the contact is apparent from the metamorphic aureole in the volcanic country rocks. This suggests that the Palmer Land granites most probably represent high-level intrusions. In his discussion of the granite spectrum, Middlemost (1969) considered the following to be typical of epizonal (0–6 km) granites:

i. Discordant and sharp contacts, and sometimes chilled.
ii. Relatively small in size.
iii. Lack of lineation and foliation.
iv. Association with volcanic rocks—sometimes associated with ring dykes and cauldron subsidence.
v. Glassy, porphyritic and lamprophyric dykes are common.
vi. Microlitic structures and granophyric textures are also common.

With the exception of iv and vi, the Palmer Land granites either wholly or partly satisfy the above conditions. At Procyon Peaks, the granites, although they are considerably younger, do occur in association with volcanic rocks. The relatively small outcrop dimensions and the predominantly vertical contacts indicate some form of tectonic control.The general absence of granophyric textures implies that these rocks either crystallized rapidly or the magma was relatively poor in volatiles. The frequency of porphyritic textures and the absence of extensive alkali and silica metasomatism points to the latter condition. However, it would seem that as crystallization progressed the magma became sufficiently saturated to permit a limited phase of microgranite veining.

E. Geochemistry

The 27 new analyses given in Table XX are regarded as a faithful representation of the broad spectrum of rock types which form the post-volcanic intrusive suite. With overall moderate total alkalis (Fig. 60), high alumina in the basic members and little iron enrichment in the intermediate rocks, this suite can be classified as calc-alkaline and hence resembles the main post-volcanic 'Andean' intrusive suite of Graham Land (Adie, 1955; West, 1974). However, when plotted on A–F–M and Ca–Na–K triangular diagrams (Figs 61 and 62), the Palmer Land rocks are displaced relative to Adie's (1955) curves towards the A–K and K–Na bases, respectively. That such differences might have resulted from different analytical techniques is considered unlikely, since a similar feature is evident when all known analyses (the majority of which were carried out by classical chemical methods) of apparently contemporaneous Graham Land plutonic rocks are plotted on an A–F–M diagram (West, 1974; fig. 17). Since comparisons of absolute element concentrations obtained by differing analytical methods are undesirable, the Palmer Land rocks will, for the most part, be compared only with Graham Land rocks analysed by X-ray fluorescence (i.e. the Danco Coast rocks), but it should be added that these are typical of the post-volcanic plutonic rocks which occur extensively in the northern

Table XX. Chemical analyses of Andean plutonic rocks.

	Peridotites				*Gabbros*						*Quartz-diorites*	
	1	*2*	*3*	*4*	*5*	*6*	*7*	*8*	*9*	*10*	*11*	*12*
SiO_2	44.38	41.10	47.48	45.22	47.06	47.61	49.26	48.73	44.14	62.70	53.99	56.38
TiO_2	0.14	0.20	0.21	0.46	0.38	0.42	1.12	1.59	0.84	0.66	1.43	1.47
Al_2O_3	3.71	3.03	21.17	13.09	26.48	23.91	20.07	14.30	17.96	16.43	16.63	16.73
Fe_2O_3	3.35	5.38	0.19	2.65	1.35	2.72	2.18	5.57	4.07	2.75	3.58	3.65
FeO	5.66	6.93	2.58	10.89	3.04	2.92	7.74	5.41	5.66	2.55	5.14	3.33
MnO	0.16	0.21	0.07	0.20	0.08	0.09	0.16	0.23	0.10	0.11	0.17	0.17
MgO	31.35	33.20	8.39	14.69	4.27	5.05	4.19	7.54	8.66	2.04	3.62	2.75
CaO	7.51	5.31	17.18	10.90	14.19	13.74	11.30	9.97	15.43	5.29	8.81	6.11
Na_2O	0.81	0.29	1.26	0.77	1.92	1.82	3.27	3.39	0.89	4.36	3.51	5.10
K_2O	0.30	0.06	0.15	0.06	0.13	0.32	0.10	0.82	0.11	1.40	0.42	1.20
P_2O_5	0.04	0.02	0.01	0.02	0.01	0.02	0.13	0.61	0.01	0.12	0.36	0.36
H_2O^+	1.02	1.79	1.02	0.77	0.76	1.27	0.49	1.47	1.65	1.50	1.09	1.49
H_2O^-												
CO_2	1.95	1.92	0.83	0.98	0.75	0.71	0.44	0.75	0.74	0.59	0.65	1.73
Total	100.38	99.42	100.54	100.70	100.42	100.60	100.45	100.38	100.26	100.50	99.40	100.47
ANALYSES LESS TOTAL WATER (RECALCULATED TO 100)												
SiO_2	44.67	42.10	47.72	45.25	47.23	47.93	49.29	49.27	44.76	63.68	54.91	56.95
TiO_2	0.14	0.20	0.21	0.46	0.38	0.42	1.12	1.60	0.85	0.67	1.45	1.48
Al_2O_3	3.73	3.08	21.27	13.10	26.57	24.07	20.08	14.46	18.21	16.68	16.92	16.90
Fe_2O_3	3.37	5.51	0.19	2.65	1.35	2.74	2.18	5.63	4.13	2.79	3.64	3.69
FeO	5.70	7.10	2.59	10.90	3.05	2.94	7.74	5.47	5.74	2.59	5.23	3.36
MnO	0.16	0.22	0.07	0.20	0.08	0.09	0.16	0.23	0.10	0.11	0.17	0.17
MgO	31.55	34.00	8.43	14.70	4.28	5.09	4.19	7.62	8.78	2.07	3.68	2.78
CaO	7.56	5.44	17.26	10.91	14.24	13.83	11.30	10.08	15.65	5.37	8.96	6.17
Na_2O	0.82	0.30	1.27	0.77	1.93	1.83	3.27	3.43	0.90	4.43	3.57	5.15
K_2O	0.30	0.06	0.15	0.06	0.13	0.32	0.10	0.83	0.11	1.42	0.42	1.22
P_2O_5	0.04	0.02	0.01	0.02	0.01	0.02	0.13	0.62	0.01	0.12	0.37	0.36
CO_2	1.96	1.97	0.83	0.98	0.75	0.72	0.44	0.76	0.75	0.06	0.66	1.75
ELEMENT WEIGHT PERCENTAGES (ANHYDROUS)												
Si^{4+}	20.86	19.66	22.29	21.13	22.06	22.38	23.02	23.01	20.90	29.77	25.67	26.62
Ti^{4+}	0.08	0.12	0.13	0.28	0.23	0.25	0.67	0.96	0.51	0.40	0.87	0.89
Al^{3+}	1.97	1.63	11.25	6.93	14.06	12.73	10.62	7.65	9.63	8.83	8.95	8.94
Fe^{3+}	2.36	3.85	0.13	1.85	0.94	1.92	1.52	3.94	2.89	1.95	2.55	2.58
Fe^{2+}	4.43	5.52	2.01	8.47	2.37	2.28	6.01	4.25	4.46	2.01	4.07	2.61
Mn^{2+}	0.12	0.17	0.05	0.15	0.06	0.07	0.12	0.18	0.08	0.08	0.13	0.13
Mg^{2+}	19.02	20.50	5.08	8.86	2.58	3.07	2.53	4.59	5.29	1.25	2.22	1.68
Ca^{2+}	5.41	3.89	12.34	7.80	10.18	9.89	8.08	7.21	11.19	3.84	6.40	4.41
Na^+	0.61	0.22	0.94	0.57	1.43	1.36	2.43	2.55	0.67	3.29	2.65	3.82
K^+	0.24	0.05	0.12	0.05	0.11	0.27	0.08	0.69	0.09	1.18	0.35	1.01
P^{5+}	0.02	0.01	–	0.01	–	0.01	0.06	0.27	–	0.05	0.16	0.16
C^{4+}	0.54	0.54	0.23	0.27	0.20	0.20	0.12	0.20	0.20	0.02	0.18	0.48
O^{2-}	44.34	43.84	45.43	43.63	45.78	45.57	44.74	44.50	44.09	47.32	45.78	46.64
C.I.P.W. NORMS												
Q	–	–	–	–	–	1.26	–	–	–	18.49	10.59	10.70
C	–	–	–	–	–	–	–	–	–	–	–	0.72
Z	–	–	–	–	–	–	–	0.02	–	0.04	0.02	0.04
or	1.75	0.38	1.11	0.56	0.56	1.67	0.56	4.91	0.65	8.39	2.49	7.14
ab	6.85	2.49	10.73	6.29	16.24	15.72	27.75	28.99	7.61	37.44	30.16	43.28
an	5.61	6.86	51.98	31.97	63.38	56.43	39.75	21.68	45.31	21.43	28.88	17.34
di	15.03	5.91	22.03	12.53	1.94	6.05	9.94	15.55	21.38	3.42	7.34	–
hy	16.59	25.30	2.83	23.62	12.20	12.28	11.28	13.58	9.52	5.04	10.05	7.79
ol	43.79	45.77	8.66	17.54	1.08	–	3.52	0.87	5.25	–	–	–
mt	4.86	7.96	0.23	3.94	1.86	3.94	3.25	8.12	6.03	4.04	5.28	5.32
cm	0.73	0.46	0.08	0.07	–	0.03	–	–	–	–	–	–
il	0.27	0.38	0.40	0.76	0.76	0.76	2.13	3.04	1.67	1.27	2.75	2.80
hm	–	–	–	–	–	–	–	–	–	–	–	–
ap	0.10	0.04	0.02	0.05	0.02	0.05	0.31	1.48	0.02	0.28	0.88	0.85
pr	0.01	0.01	0.03	0.06	0.10	0.11	0.01	0.01	0.54	0.01	0.06	0.07
cc	4.43	4.45	1.90	2.20	1.70	1.63	1.00	1.73	1.73	0.14	1.50	3.95
COORDINATES FOR TRIANGULAR DIAGRAMS												
A	3.19	0.89	13.0	3.1	20.7	18.3	19.9	20.1	5.7	46.1	25.3	41.3
F	25.47	31.09	25.8	52.1	44.6	47.3	60.0	51.2	54.8	12.9	55.9	44.4
M	71.34	68.02	61.2	44.8	34.7	34.5	20.1	28.7	39.5	41.0	18.8	14.3
K	3.83	1.20	0.9	0.6	0.9	2.3	0.8	6.6	0.8	14.2	3.7	10.9
Ca	86.42	93.51	91.9	92.6	86.9	85.9	76.3	69.0	93.6	46.2	68.1	47.8
Na	9.75	5.29	7.2	6.8	12.2	11.8	22.9	24.4	5.6	39.6	28.2	41.3

Table XX. Chemical analyses of Andean plutonic rocks (continued).

	Granodiorites									Adamellites			Granites	
	13	*14*	*15*	*16*	*17*	*18*	*19*	*20*	*21*	*22*	*23*	*24*	*25*	*26*
SiO_2	58.36	58.84	59.16	59.42	59.94	61.49	64.55	65.33	70.71	67.30	68.63	65.19	70.61	70.78
TiO_2	0.52	0.77	0.70	0.53	0.47	0.53	0.46	0.39	0.22	0.36	0.19	0.61	0.30	0.33
Al_2O_3	17.80	18.31	17.54	17.80	17.59	17.41	16.87	16.49	16.16	16.69	17.21	17.00	15.61	15.43
Fe_2O_3	2.95	3.20	2.96	3.15	2.79	2.62	2.29	2.06	0.98	1.57	1.21	2.40	1.37	1.20
FeO	2.72	1.85	3.10	2.65	2.69	1.79	1.32	1.50	0.59	0.99	0.80	1.04	0.73	0.74
MnO	0.11	0.09	0.12	0.10	0.10	0.09	0.06	0.07	0.03	0.04	0.06	0.06	0.05	0.04
MgO	2.54	2.18	2.34	2.59	2.43	2.07	1.76	1.78	0.47	1.00	0.53	1.31	0.64	0.62
CaO	6.73	6.49	6.70	6.75	6.36	5.84	4.23	3.97	2.37	2.89	3.29	2.90	1.93	1.68
Na_2O	3.41	4.26	4.07	3.32	3.16	4.02	3.83	3.74	4.25	4.00	3.53	4.54	3.78	3.91
K_2O	1.77	2.16	1.83	1.80	2.07	1.93	2.87	2.99	3.17	3.61	3.43	3.27	4.23	4.39
P_2O_5	0.20	0.27	0.21	0.19	0.10	0.20	0.13	0.14	0.05	0.09	0.07	0.14	0.07	0.06
H_2O^+														
H_2O^-	1.37	1.00	0.58	1.05	1.04	1.10	1.05	1.03	1.04	1.26	0.59	0.79	0.36	0.61
CO_2	0.98	0.76	0.80	0.83	0.92	0.73	0.76	0.77	0.63	0.80	0.46	0.82	0.66	0.50
Total	99.46	100.18	100.11	100.18	99.66	99.82	100.18	100.26	100.66	100.60	100.00	100.07	100.34	100.29
ANALYSES LESS TOTAL WATER (RECALCULATED TO 100)														
SiO_2	59.49	59.32	59.46	59.94	60.79	62.31	65.12	65.82	70.97	67.75	69.05	65.67	70.64	71.01
TiO_2	0.53	0.78	0.70	0.53	0.48	0.54	0.47	0.39	0.22	0.37	0.19	0.61	0.30	0.33
Al_2O_3	18.15	18.46	17.62	17.96	17.83	17.64	17.02	16.61	16.22	16.80	17.31	17.12	15.61	15.48
Fe_2O_3	3.00	3.23	2.97	3.18	2.83	2.65	2.31	2.08	0.99	1.58	1.22	2.42	1.37	1.20
FeO	2.77	1.87	3.11	2.67	2.73	1.81	1.33	1.52	0.59	0.99	0.80	1.04	0.73	0.74
MnO	0.11	0.09	0.12	0.10	0.10	0.09	0.06	0.07	0.03	0.04	0.06	0.06	0.05	0.04
MgO	2.59	2.20	2.35	2.61	2.46	2.09	1.77	1.79	0.47	1.01	0.53	1.32	0.64	0.62
CaO	6.86	6.54	6.73	6.81	6.45	5.92	4.27	4.00	2.38	2.91	3.31	2.92	1.93	1.69
Na_2O	3.48	4.30	4.09	3.35	3.20	4.07	3.86	3.77	4.26	4.02	3.55	4.57	3.78	3.92
K_2O	1.81	2.17	1.84	1.82	2.10	1.96	2.90	3.02	3.18	3.63	3.45	3.30	4.23	4.41
P_2O_5	0.20	0.28	0.21	0.19	0.10	0.20	0.14	0.14	0.05	0.09	0.07	0.14	0.07	0.06
CO_2	1.00	0.76	0.80	0.84	0.93	0.71	0.76	0.78	0.63	0.80	0.46	0.82	0.66	0.50
ELEMENT WEIGHT PERCENTAGES (ANHYDROUS)														
Si^{4+}	27.81	27.73	27.77	27.99	28.39	29.13	30.44	30.77	33.18	31.67	32.25	30.70	33.02	33.20
Ti^{4+}	0.32	0.47	0.42	0.32	0.29	0.32	0.28	0.24	0.13	0.22	0.11	0.37	0.18	0.20
Al^{3+}	9.60	9.77	9.32	9.50	9.43	9.33	9.00	8.79	8.58	8.89	9.16	9.06	8.26	8.19
Fe^{3+}	2.10	2.26	2.08	2.22	1.98	1.82	1.61	1.45	0.99	1.10	0.85	1.96	0.96	0.84
Fe^{2+}	2.15	1.45	2.42	2.07	2.12	1.41	1.04	1.18	0.46	0.77	0.62	0.81	0.57	0.57
Mn^{2+}	0.09	0.07	0.09	0.08	0.08	0.07	0.04	0.05	0.02	0.03	0.05	0.05	0.04	0.03
Mg^{2+}	1.56	1.33	1.42	1.57	1.48	1.26	1.07	1.08	0.29	0.61	0.32	0.80	0.38	0.37
Ca^{2+}	4.90	4.68	4.81	4.87	4.61	4.23	3.05	2.86	1.71	2.08	2.37	2.08	1.38	1.21
Na^{+}	2.58	3.19	3.03	2.49	2.37	3.02	2.87	2.80	3.16	2.98	2.63	3.39	2.80	2.91
K^{+}	1.50	1.81	1.53	1.51	1.74	1.63	2.41	2.50	2.64	3.01	2.86	2.74	3.51	3.66
P^{5+}	0.09	0.12	0.09	0.08	0.04	0.09	0.06	0.06	0.02	0.04	0.03	0.06	0.03	0.02
C^{4+}	0.27	0.21	0.22	0.23	0.25	0.19	0.21	0.21	0.17	0.22	0.13	0.22	0.18	0.14
O^{2-}	47.01	46.93	46.80	47.07	47.22	47.45	47.92	47.99	48.95	48.36	48.62	48.02	48.68	48.65
C.I.P.W. NORMS														
Q	16.02	11.73	12.74	17.10	18.46	17.45	21.98	23.19	29.99	24.87	28.77	20.78	29.28	28.22
C	0.66	–	–	0.31	0.92	0.04	1.67	1.85	2.96	2.84	2.86	2.92	2.95	2.45
Z	0.04	–	0.04	0.03	0.03	0.04	0.04	0.04	0.03	0.05	0.03	0.07	0.06	0.06
or	10.67	12.84	10.88	10.56	12.22	11.57	17.10	17.84	18.76	21.46	19.91	19.51	25.02	26.09
ab	29.38	36.31	34.57	28.29	27.23	34.41	32.65	31.84	36.03	33.98	29.84	38.61	31.94	33.16
an	26.73	24.64	24.19	27.78	25.56	23.91	15.95	14.41	7.67	9.28	13.62	8.47	5.06	4.90
di	–	1.23	2.59	–	–	–	–	–	–	–	–	–	–	–
hy	8.38	4.90	6.82	7.93	8.15	5.62	4.40	4.02	1.18	2.51	1.56	3.29	1.58	1.54
ol	–	–	–	–	–	–	–	–	–	–	–	–	–	–
mt	4.35	4.05	4.41	4.64	4.18	3.84	3.12	3.01	1.32	2.26	1.86	1.76	1.65	1.56
cm	–	–	–	–	–	–	–	–	–	–	–	–	–	–
il	1.01	1.48	1.37	1.01	0.91	1.02	0.89	0.75	0.42	0.69	0.30	1.16	0.57	0.62
hm	–	0.43	–	–	–	–	0.15	–	0.07	0.02	–	1.20	0.23	0.12
ap	0.48	0.65	0.50	0.45	0.24	0.47	0.32	0.34	0.12	0.21	0.17	0.34	0.15	0.13
pr	–	0.01	0.07	–	–	0.01	–	0.06	0.02	–	–	0.01	0.01	0.01
cc	2.28	1.74	1.82	1.90	2.10	1.62	1.74	1.77	1.43	1.82	1.00	1.87	1.50	1.15
COORDINATES FOR TRIANGULAR DIAGRAMS														
A	41.2	49.8	43.5	40.5	42.4	50.7	58.7	58.8	80.1	70.7	75.3	65.0	76.8	78.6
F	43.0	37.0	42.9	43.5	42.2	35.6	29.4	29.2	15.9	22.2	20.3	26.6	18.6	16.9
M	15.8	13.2	13.6	16.0	15.4	13.7	11.9	12.0	4.0	7.2	4.4	8.4	4.6	4.5
K	16.7	18.7	16.3	17.0	19.9	18.3	28.9	30.7	35.2	37.3	36.4	33.3	45.6	47.1
Ca	54.6	48.4	51.3	55.0	52.8	47.6	36.7	35.0	22.7	25.8	30.1	25.4	17.9	15.5
Na	28.7	32.9	32.4	28.0	27.3	34.1	34.4	34.3	42.1	36.9	33.5	41.3	36.4	37.4

Table XX. Chemical analyses of Andean plutonic rocks (continued).

	Peridotites		*Gabbros*								*Quartz-diorites*	
	1	*2*	*3*	*4*	*5*	*6*	*7*	*8*	*9*	*10*	*11*	*12*
TRACE ELEMENTS (ppm)												
S	30	–	150	274	479	514	32	57	2514	45	335	348
Cr	3241	1990	344	306	58	145	61	40	42	19	19	8
Ni	1083	951	81	173	17	36	21	2	31	8	9	6
Rb	9	–	5	1	2	9	1	34	3	58	10	44
Sr	160	58	346	189	432	406	119	696	285	215	322	421
Y	5	6	5	4	10	11	6	19	5	29	21	32
Zr	43	19	25	12	27	49	31	115	22	188	79	221
Ba	134	44	66	79	85	113	84	343	235	481	228	349
La	1	–	–	–	–	–	–	11	–	12	6	17
Ce	–	–	14	9	5	4	5	29	–	33	23	44
Pb	3	3	2	5	3	–	–	2	–	13	1	8
K/Rb	273	–	246	465	544	296	789	199	315	200	345	227
Ca/Y	10738	6327	24562	19489	10142	8932	13461	3751	22068	1305	2998	1366
Mg/Ni	175	211	624	512	1513	845	1204	22718	1685	1534	n.d.	n.d.
$\frac{MgO}{Fe_2O_3 + FeO}$	3.48	2.70	3.03	1.08	0.97	0.90	0.42	0.68	0.89	0.38	n.d.	n.d.
D.I.	8.60	2.87	11.84	6.85	16.80	18.65	28.31	33.90	8.26	64.32	43.24	61.12

1. KG.563.2 Peridotite, Canis Heights.
2. KG.572.2 Peridotite, Moore Point.
3. KG.572.1 Leucocratic gabbro, Moore Point.
4. KG.470.3 Melanocratic gabbro, Moore Point.
5. KG.571.4 Hypersthene-gabbro, Moore Point.
6. KG.569.4 Hornblende-gabbro, Wade Point.
7. KG.569.3 Hypersthene-gabbro, Wade Point.
8. KG.555.7 Hornblende-gabbro, Procyon Peaks.
9. KG.518.4 Hypersthene-gabbro, Pegasus Mountains.
10. KG.574.2 Acidified gabbro, Moore Point.
11. KG.575.2 Quartz-diorite, Burns Bluff.
12. KG.522.2 Quartz-diorite, Gurney Point.

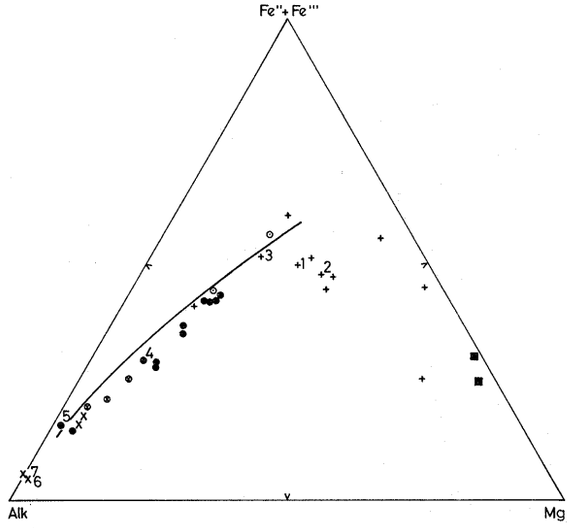

Fig. 61. Alk–(Fe″ + Fe‴″)–Mg triangular variation diagram for plutonic rocks of the Andean Intrusive Suite and associated minor intrusions, numbered as in Table XXIII (■, peridotite; +, gabbro; ⊙, quartz-diorite; ●, granodiorite; ⊗, adamellite; ×, granite). The variation trend for some of the Graham Land Andean plutonic rocks (Adie, 1964*b*) is superimposed.

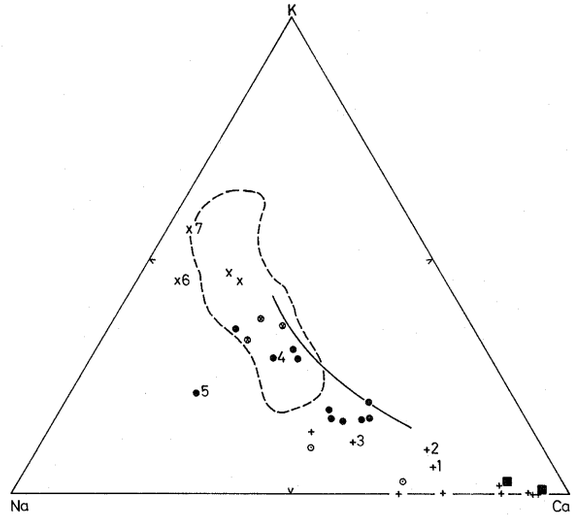

Fig. 62. Ca–Na–K triangular variation diagram for plutonic rocks of the Andean Intrusive Suite and associated minor intrusions, numbered as in Table XXIII (■, peridotite; +, gabbro; ⊙, quartz-diorite; ●, granodiorite; ⊗, adamellite; ×, granite). The solid line is the trend determined by Adie (1964*b*) for some of the Graham Land Andean plutonic rocks and the broken line encloses the field occupied by magmatic granitic rocks (after Raju and Rao, 1972).

part of the Antarctic Peninsula. Comparing individual element concentrations with Gribble's (1969) distribution curves for the normal calc-alkaline sequence, the Palmer Land rocks have high Al_2O_3, CaO and Na_2O, and low $\Sigma Fe[O]$, MgO, K_2O, Rb, Cr and Ni.

1. Peridotites and gabbros

The two analysed peridotites, the first to be described from the Antarctic Peninsula, are fairly typical early cumulates with high MgO, Cr and Ni, and low Al_2O_3, Na_2O and K_2O. However, the unusually leucocratic gabbro (p. 62), which is intruded by peridotite, has exceptionally low iron (mainly as a result of the depressed ferric content) though the MgO/(Fe_2O_3 + FeO) ratio is similar to that of the ultrabasic rocks.

Table XX. Chemical analyses of Andean plutonic rocks (continued).

	Granodiorites								Adamellites				Granites	
	13	*14*	*15*	*16*	*17*	*18*	*19*	*20*	*21*	*22*	*23*	*24*	*25*	*26*
TRACE ELEMENTS (ppm)														
S	18	39	233	12	17	31	13	320	75	19	357	53	37	30
Cr	11	16	11	12	14	17	–	15	12	15	7	10	6	11
Ni	6	8	5	6	7	7	9	7	4	6	–	4	1	1
Rb	54	66	63	54	64	63	90	114	85	107	92	115	173	182
Sr	603	671	487	607	497	701	628	562	554	538	528	432	264	243
Y	13	17	17	13	12	10	8	10	6	14	6	20	19	21
Zr	173	–	207	162	143	196	188	184	164	264	132	362	288	303
Ba	974	939	649	974	1094	811	1445	1308	170	1690	2112	168	142	140
La	17	29	15	24	–	16	25	21	24	35	3	35	37	35
Ce	14	50	40	45	13	32	45	38	38	55	19	59	68	63
Pb	16	23	–	16	16	14	28	16	36	31	42	19	18	30
K/Rb	273	271	241	277	268	255	265	218	309	280	310	236	203	200
Ca/Y	3701	2730	2819	3711	3788	4176	3784	2839	2828	1476	3923	1035	726	573
Mg/Ni	n.d.	n.d.	n.d.	n.d.	n.d.	n.d.	n.d.	n.d.	n.d.	n.d.	n.d.	n.d.	n.d.	n.d.
$\frac{MgO}{Fe_2O_3 + FeO}$	n.d.	n.d.	n.d.	n.d.	n.d.	n.d.	n.d.	n.d.	n.d.	n.d.	n.d.	n.d.	n.d.	n.d.
D.I.	56.07	60.88	58.19	55.95	57.91	63.43	71.73	72.87	84.78	80.31	78.52	78.90	86.24	87.47

13. KG.543.1 Granodiorite, Capella Rocks.
14. KG.557.1 Granodiorite, Procyon Peaks.
15. KG.501.2 Granodiorite, Adebaran Rock.
16. KG.544.1 Granodiorite, Perseus Crags.
17. KG.541.3 Granodiorite, Capella Rocks.
18. KG.538.1 Granodiorite, Pegasus Mountains.
19. KG.552.3 Granodiorite, Perseus Crags.
20. KG.526.4 Granodiorite, Pegasus Mountains.
21. KG.561.3 Granodiorite, Canis Heights.
22. KG.561.1 Adamellite, Canis Heights.
23. KG.542.5 Adamellite, Capella Rocks.
24. KG.558.1 Adamellite, Procyon Peaks.
25. KG.501A.1 Granite, Aldebaran Rock.
26. KG.555.1 Granite, Procyon Peaks.

Although not evident from the hand specimen, the rock has chemical similarities (low iron in particular) with a plagioclase-augite-hypersthene cumulate from the Stillwater complex (Hess, 1960). Such a rock may have formed by flotation subsequent to the early removal of olivine and later magnetite, for although they have not been recorded so far in Palmer Land, iron-enriched gabbros are occasionally present in Graham Land. Two further gabbros which plot close to the F–M base of the A–F–M triangular diagram are interpreted as cumulates (specimens KG.570.3 and KG.518.4). Despite the close proximity of these two rocks on the A–F–M diagram, they have markedly different Cr, Ni and Cu concentrations, and the Mg/Ni ratio of specimen KG.518.4 is greater than that of specimen KG.570 by a factor of 40. Prinz (1967) concluded that Cr is initially incorporated into chrome spinels, whereas Ni is more abundant in olivine relative to orthopyroxene; hence these two elements are likely to diminish in later formed rocks. This being the case, then the high Mg/Fe ratio and low magnetite content of specimen KG.518.4 are further indicators of a possible removal of ferric iron. Perhaps one of the more unusual mineralogical aspects of these gabbros is the presence of clinopyroxene with a low $2V_\alpha$, generally referred to as low-calcium augite, which has been observed in all but the olivine-bearing and dominantly hornblende-bearing varieties. The normative diopside contents of these rocks do not correlate with modal clinopyroxene values, but compared with data from the Danco Coast they are not unusually low. However, these rocks have noticeably high alumina values and somewhat higher normative An/Ab ratios than the optically determined values. The An discrepancy results mainly from the failure of the CIPW norms to acknowledge the presence of hornblende, but it is equally possible that some of the alumina could have been incorporated into the pyroxene lattice, giving rise (Poldervaart and Hess, 1951) to an anomalously low optic axial angle. Specimen KG.555.7 (Table XX, analysis 8) has higher K, Rb, Y, Zr and Ba, and slightly higher MnO and Na_2O, the result presumably of late-stage emanations from the adjacent granite. The extremely low K/Rb ratio reflects the preferential incorporation of rubidium into biotite. The trace-element concentrations in the average non-cumulative Palmer Land gabbros are frequently at variance with those of Prinz's (1967) average basalt, in particular the relatively low Ni, Rb, Y, Sr and P_2O_5 contents. Cr, Ni, Y and Ba correspond well with rocks from the Danco Coast (West, 1974) and from other parts of Graham Land (Adie, 1955). Zr is marginally lower than in the Graham Land rocks which are themselves sufficiently depleted to suggest this as a characteristic feature of the suite (Prinz, 1967; Gribble, 1969). Whereas the Graham Land gabbros have above-average strontium concentrations, the Palmer Land rocks are deficient, presumably reflecting the more calcic plagioclase of the latter. The presence of cumulative rocks indicates that some form of crystal fractionation occurred during the formation of these gabbros. The few non-cumulative gabbros exhibit chemical trends which are consistent with continued fractional crystallization; notably, when plotted against the Thornton and Tuttle (1960) differentiation index (Fig. 60), there is a positive correlation for $\Sigma Fe[O]$, TiO_2, MnO, Na_2O and P_2O_5, and a sympathetic decrease in MgO and CaO. Also, as expected, Cr and Ni decrease steeply while the Mg/Ni ratio (Fig. 63) increases. An attempt to establish statistically a primary magma composition is ruled out because of the limited number of analyses, particularly of rocks with low $MgO/(Fe_2O_3 + FeO)$. However, it is of interest to note that the more basic of the non-cumulative rocks (e.g. KG.569.4) have

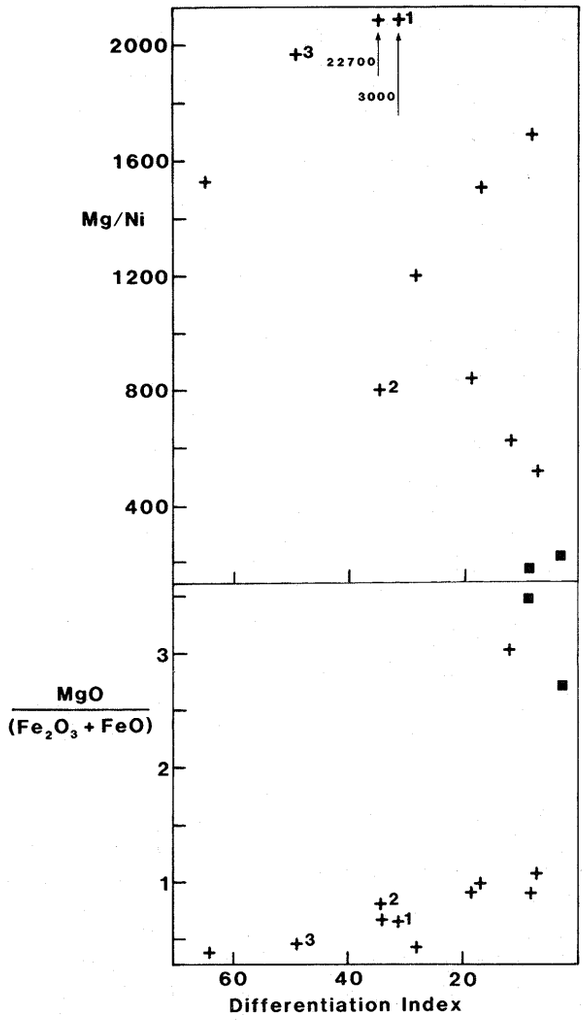

Fig. 63. Plots of Mg/Ni and $MgO/Fe_2O_3 + FeO$ against the Thornton and Tuttle differentiation index for Andean peridotites (■), gabbros (+) and early basic dykes (+, numbered as in Table XXIII).

Cr, Ni, Rb, Sr and Ba concentrations similar to those in Jakes and White's (1972) average basalt, and the $MgO/(Fe_2O_3 + FeO)$ ratios are almost identical with the primary tholeiitic basalt of the volcanic series.

2. Quartz-diorites

Despite their mineralogical dissimilarities, the two quartz-diorites possess similar concentrations of TiO_2, Al_2O_3, MgO and P_2O_5. When plotted against the Thornton and Tuttle (1960) differentiation index, TiO_2, Na_2O, K_2O, Rb, Ba, Pb, Y and the Ca/Y ratio lie on the possible extension of the gabbro curves, suggesting that the quartz-diorites may have been derived by continued fractionation of a gabbro magma. Such a process would readily explain their relatively high concentrations of Y and Zr. In passing, it is interesting to note the similarity between specimen KG.575.2 and Adie's (1955) primary gabbroic magma.

3. Granodiorites and granites

The Palmer Land granodiorites have high Al_2O_3, CaO, Na_2O, Sr, Zr and Ba, and low TiO_2, ΣFe[O], MgO, K_2O, Cr and Ni. Compared with Graham Land rocks, the average Palmer Land granodiorite possesses lower Cr, Ni, Y and Zr, and higher Ba, Rb and Sr, though the major and minor element concentrations are broadly similar. Despite the variations in estimates for the average calc-alkaline granite (e.g. Nockolds, 1954; Turekian and Wedepohl, 1961; Gribble, 1969), the granites of western Palmer Land can be said to have high Al_2O_3, Na_2O, Zr and Pb, and low K_2O. The average Palmer Land granite has strong chemical affinities with the granites of Trinity Peninsula (Adie, 1955, table VIIIb) and the granophyres of the Danco Coast (West, 1974), so it is suggested that these are characteristic features of the post-volcanic intrusive suite. The Palmer Land rocks have, in addition, high Cao and MgO, and low ΣFe[O], which reflect the presence of hornblende. However, the latter was ascribed (p. 70) to assimilation of granodioritic xenoliths, which leads to the interesting possibility that the chemical anomalies of the 'Andean' granites may indicate widespread contamination. Close scrutiny of the various plots against the Thornton and Tuttle differentiation index reveals the apparently homogeneous granodiorite–granite group is in fact composed of two smaller groups and, since the difference is most apparent in the plots involving yttrium, the terms high- and low-yttrium series have been adopted.

a. *Low-yttrium series.* This series, which includes all the granodiorites and two of the adamellites, shows the following differences relative to the high-yttrium series: higher Sr and Pb, lower $Na_2O + K_2O$, P_2O_5 and Zr, slightly higher SiO_2, and lower ΣFe[O] and MgO. Plotted against the differentiation index, the analyses frequently show a wide scatter (e.g. Na_2O, K_2O and Rb) and the curvilinear trends usually associated with fractional crystallization (Nockolds and Allen, 1953) are frequently absent. Also, the late decrease in zirconium and the corresponding increase in K/Rb ratios are not in keeping with any differentiation processes.

b. *High-yttrium series.* The high-yttrium series (embracing two granites, one adamellite and the gabbro–older granodiorite hybrid) commonly plots on well-defined curves (Fig. 60) which, if projected at the basic end, are coincident with the smooth gabbro–diorite curves. This is particularly evident on the Ca–Na–K triangular diagram and on the Ca/Y ratio against differentiation index plot. It is aso noticeable that, when plotted on the Ca–Na–K diagram, the granites fall within the field of magmatic rocks. The hybrid rock shows departures from the curves for some elements (e.g. Si, La, Ce, Mg, Na, P and Sr) and element ratios (K/Rb), but the differences can be related to variations in the compositions of the parent rocks.

F. Origin and Emplacement of the Intrusive Suite

The occurrence of volcaniclastic rocks within the Lower Cretaceous sedimentary assemblages of Alexander Island (Horne and Thomson, 1972) suggests that the consumption of oceanic crust beneath western Palmer Land had continued into the Cretaceous. It is now generally accepted that basaltic magmas are produced by the partial melting of the mantle, and Ringwood (1974) has demonstrated that such processes may be initiated by the subduction of oceanic crust to depths of 100–150 km. Under continued high P_{H_2O}, partial melting of quartz-

eclogite produces a rhyodacite magma which reacts with the overlying mantle pyrolite to form pyroxenite. Partial melting of pyroxenite diapirs, rising from the Benioff Zone, then produces calc-alkaline basaltic magmas. Such an origin is considered possible for the Palmer Land gabbros. To explain the evolution of the more acid rocks of the calc-alkaline series, Ringwood (1974) invoked fractionation of this basic magma by the removal of eclogite (80–150 km) or amphiboles (30–100 km). It has been demonstrated (p. 76) that fractional crystallization of gabbroic magma could have produced the high-yttrium gabbro–granite series, and a mechanism involving the removal of amphibole is preferred to the eclogite model for the following reasons:

i. The occasional presence of hornblendic clots.
ii. The development of a 'J' trend on the Ca/Y plot (Fig. 64); Lambert and Holland (1974) considered that such a trend could have developed by amphibole-controlled fractionation.

These authors also noted that such trends frequently develop above a subduction zone. One argument favouring eclogite fractionation is the continued increase of the K/Na ratio with

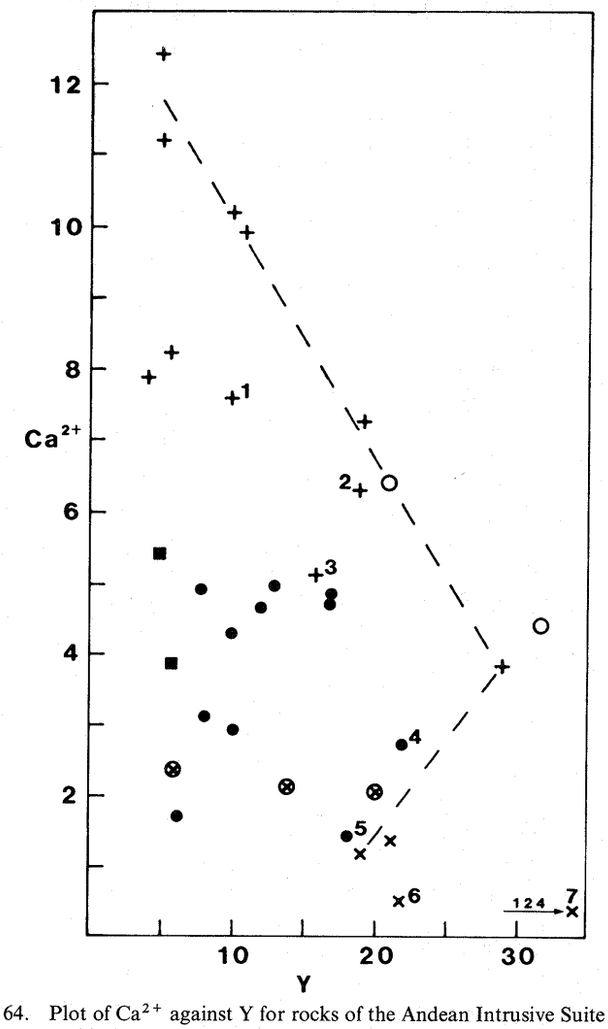

Fig. 64. Plot of Ca^{2+} against Y for rocks of the Andean Intrusive Suite (■, peridotite; +, gabbro; ○, quartz-diorite; ●, granodiorite; ⊗, adamellite; ×, granite) and associated minor intrusions numbered as in Table XXIII.

increasing silicon. However, it is envisaged that in the latter stages (approximating to the diorite-evolving epoch) incorporation of sialic crust supersedes amphibole crystallization as the main agent of differentiation. This hypothesis finds support in the presence on the curve of the gabbro-older granodiorite hybrid and explains the overall paucity of diorites. Kleeman (1965) has suggested that granitic magmas derived from contaminated basic magmas may be deficient in water and are therefore capable of rising to relatively high crustal levels, which is in agreement with the field and textural observations.

Granodiorite magmas may be formed by: fractional crystallization of basaltic magma; contamination of basaltic magma with sialic crust; melting or partial melting of crustal rocks. Even if the chemistry had not been contradictory, the shear volume of granodiorite relative to gabbro would cast grave doubts on the fractional crystallization hypothesis. The overall homogeneity, both chemical and mineralogical, of the granodiorites combined with chemical distinctions with respect to proven contaminated rocks (the high-yttrium series) suggests that melting or partial melting of crustal rocks was more likely to have been responsible for the genesis of the low-yttrium series.

It is a reasonable assumption that, in the late Mesozoic, the upper part of the crust underlying Palmer Land was composed of metamorphic rocks similar to those at present exposed. The acid intrusive and metamorphic rocks do in fact display similarly anomalous concentrations of certain trace elements (Ba, Zr, Pb, La, Ce, Cr, Ni and Y) and it is possible to detect variations in the K/Rb ratios of the granodiorites which conform to the zonal distribution in the metamorphic complex (p. 35). However, the deficiency of SiO_2 and K_2O in the average Andean granodiorite relative to the banded gneisses rules out partial or even complete melting of upper crust, and derivation from a lower level must be considered instead. Of all the suggestions for the composition of the lower crust, the granulitic model would appear to be the most acceptable, since this is the dominant rock type in the deeply eroded shield areas such as north-west Scotland (Drury, 1973), Norway (Heier and Thoresen, 1971) and Canada (Ermanovics and Davison, 1976). In Norway, non-granulitic gneisses, believed to be representative of the upper crust (Green and others, 1972), differ chemically from adjacent granulites in precisely the same way as do the Palmer Land metamorphic and Andean rocks. It has been shown that the high potassium content of many of the banded gneisses is the result of potash metasomatism, and the most likely mechanism for this process would be upward migration from the lower crust, which would in turn explain the relatively low potassium content of the granodiorites. The granodiorites contain numerous plagioclase-amphibolite xenoliths whose relict igneous texture and lack of refractory alumino-silicates mitigate strongly against them being the unmelted residue after partial melting of the lower crust. They have strong mineralogical and textural affinities with the older amphibolite dykes and are most likely to be remnants of feeders to those emplaced in the metamorphic complex rocks. The chemical similarities between the xenoliths and dykes have been described (p. 38) and attention is drawn particularly to the close correspondence of the Zr and Y concentrations, and the low Cr and Ni with respect to those of the average basalt. The main chemical differences (high K_2O and low TiO_2) appear to

have resulted from the growth of potash feldspar and magnetite, and as such they are secondary features presumably associated with melting of the granodiorite. The amount of water available will strongly influence the temperature and pressure at which crustal melting will commence. The presence of hydrates (e.g. biotite and hornblende) in all the examined granodiorites confirms that water was present in the melt though the predominance of hornblende amongst the hydrates indicates that the amount was small.

It is possible that this water could have been introduced from the mantle. Certainly, where there is evidence of a high water content in sub-crustally derived rocks, the adjacent granodiorites show many signs of being volatile-rich. This is exemplified by the close association at stations KG.555 and 557 of hornblende-gabbro, micropegmatitic granodiorite and the most extensive microgranite net veining so far recorded in western Palmer Land. In general, however, the more acid rocks of the high-yttrium series seem deficient in water relative to the low-yttrium series acid rocks and, since they were probably derived from sub-crustal material, it would seem that the mantle was not characterized by an excess of water.

Since derivation from overlying wet rocks is considered improbable, it must be assumed that most of the water originated in the granulitic crust. If, as has been suggested, the white 'granites' are typical of the lower crust, then small amounts of water in the form of hydrates were present. Fyfe (1973) considered that most crustal units (either partial or total) are formed by water which is released as hydrates but which cannot escape from the rocks.

It is apparent from experimental work on the melting behaviour of average crust, in which hydrates are present, and the compositional trends of the resultant melts (Fyfe, 1973) that, if the granodiorites formed by crustal melting, they did so at temperatures between 800 and 900°C and at pressures in the order of 8–9 kbar (corresponding to a depth of 30–35 km). The heat required for the generation of syntectic magmas may be obtained in a number of ways (Middlemost, 1971), including:

i. Frictional heating such as is produced by shearing during orogenesis or by one crustal plate being thrust under another.
ii. The upwelling and emplacement of high-temperature magma into the crust.
iii. The lowering of crustal material into a higher temperature environment.

It is clear from the above discussion that the heat for the granodiorite magma could have been produced by the processes summarized in i and ii. Continuous sedimentation in Alexander Island during the Late Jurassic and Early Cretaceous could have resulted in the situation outlined in iii. It is suggested that a melt so generated could have migrated laterally into an area of lower pressure, viz. western Palmer Land.

Discussing possible methods of batholith emplacement, Lacy (1960) has suggested that 'if partial fusion occurs over an extensive tract, and through a considerable thickness of rock, a condition of gravitational instability will arise. The sial above such a region will, by virtue of its elevated temperature, be capable of a plastic response to small stresses. Triggered by minor tectonic forces or by variations in density in a particular area, an upward bulge forms and a granitic mush of melt and crystals commences to rise as a diapir'. Although the Palmer Land rocks are considered to have been produced by syntexis and not anatexis, the above process could equally well provide the mechanism for the movement of the granodiorite from the lower crust to the upper crust. Now the effect of increased pressure will result in an increase in the amount of water that is soluble in the magma, which in turn results in a lowering of the liquidus temperature. Thus, when the magma rises through the crust into a lower-pressure environment, water separates from the melt and part of the melt is forced to crystallize (Middlemost, 1971). This process is likely to continue until so much of the magma has crystallized that it is no longer able to be emplaced into higher crustal levels. The gradual upward movement of a semi-consolidated magma would readily explain the retention of xenoliths and the development of flow structures. The extensive microgranite and pegmatite phase is also symptomatic of the release of volatiles, though the occasional presence of garnet suggests water was not a major constituent.

The granites and at least one of the quartz-diorites form relatively small plutons which are thought to represent intrusion along zones of weakness. Since a rapid ascent of magma is implied, it is possible that rapid chilling inhibited the escape of volatiles and this prevented the formation of microgranite and pegmatite. However, microgranites have developed locally (e.g. KG.502) and only rarely is there evidence of excessive deuteric alteration. Hence, it would seem that the granite magma was deficient in volatiles.

VII. HYPABYSSAL ROCKS

Dyke rocks are widespread throughout western Palmer Land and, although they are dominated by a late basic to intermediate suite, more silic examples are also present. Several suites may be related to the Andean plutonic intrusions, a few may be closely bracketed by rocks of known age but, for the majority, the assumed age is deduced from the age of the host rock and comparisons with apparently contemporaneous intrusions to the north.

This is exemplified by the late basic and intermediate dykes which post-date the Andean plutonic rocks and are analogous to the ubiquitous Tertiary dykes of Graham Land. Hence in Table XXI, the dykes are listed in assumed chronological order and their relationships with other rock groups are also given. The single radiometric age (92 ± 5 Ma (Rex, 1972)) is for a rock type known only from one outcrop.

1. Quartz-plagioclase-porphyries

Two quartz-plagioclase-porphyry intrusions were recorded in the area mapped. The smaller of these crops out within the confines of the easternmost granodiorite cupola at the eastern end of Perseus Crags (KG.551). The intrusion has a minimum width of 27 m although the contact with the granodiorite is

Table XXI. Stratigraphy of the hypabyssal rocks of western Palmer Land.

Age	*Rock type*	*Intrusive relationship*
Tertiary	Late basic and intermediate suite	Post-date all other rocks (≡ Tertiary dykes of Graham Land)
Tertiary to late Cretaceous	Acid porphyry dykes	Post-Andean granite; pre-late dyke suite
Cretaceous	Microgranite	More than one suite; one definitely post-granite. Remainder post-granodiorite
	Microgranodiorite	Post-Metamorphic Complex. Probably ≡ granodiorite
Middle Cretaceous 95 ± 5 Ma (Rex, 1972)	Early basic dykes	Intrude Mesozoic volcanic rocks and older granodiorites. Probably ≡ gabbros
Lower Cretaceous to Upper Jurassic	Quartz-plagioclase-porphyries	Intrude Upper Jurassic sedimentary and volcanic rocks

obscured by snow. The larger intrusion forms a stock cutting the sedimentary rocks on the northern flank of Carse Point (KG.582). This intrusion narrows from 250 m width at the foot of the cliffs to 100 m near the summit of the ridge where part of the roof is preserved. The western margin of the intrusion cuts undisturbed sub-horizontal strata and small apophyses penetrate the country rocks. By contrast, on the eastern side the country rocks have been down-warped (possibly to accommodate the intrusion) and their dip increases sharply from 45° to 70° as the contact is approached.

Extensive hydrothermal alteration and the presence of euhedral quartz phenocrysts up to 2.5 mm wide distinguish the quartz-plagioclase-porphyries from all other intrusions. The quartz, typically in small clusters of two to three crystals, is deeply embayed and contains globular calcite-epidote aggregates. Plagioclase (An_{25}), in euhedral laths or equant crystals ranging from 1 to 2.5 mm in length, shows a marked preference for simple twinning (with frequent curved composition planes) and is extensively replaced by calcite and sericite together with occasional granular epidote. Subhedral hornblende has been universally replaced by epidote (with associated allanite), chlorite and ilmenite (KG.551.2). Invariably, pale yellow pistacite showing a wide variety of habit (e.g. granular, columnar and radial fibrous aggregates) forms the core of the pseudomorphs, being surrounded by fibrous green chlorite and granular or rod-like ilmenite. However, in specimen KG.582.2 the chlorite–calcite pseudomorphs contain minute laths or needles or exsolved (?) epidote whose orientation is apparently controlled by the directions in the amphibole lattice. The arrangement of the needles (Fig. 65) appears to be analogous to the Widmanstätten figure, which is developed in 'aged' metal solutions (Geisler, 1953; McLean, 1957; Doan, 1958).

Although there is insufficient evidence in this area to date these rocks accurately, they are similar to quartz-porphyry lavas of supposed Late Jurassic age in the Batterbee Mountains (Ayling, 1966) and to quartz-porphyry dykes of a similar age which cut metamorphic rocks on the east coast of George VI Sound (Procter, 1959), 70 km north of Carse Point. The limited occurrence of these rocks and their extensive hydrothermal alteration also suggest they were emplaced before the genesis of the Andean Intrusive Suite.

2. Early basic dykes

The principal occurrence of the early basic dykes is within the older granodiorites of the Moore Point area, but it is possible that several inaccessible dykes cutting similar acid rocks at Gurney Point may be of comparable age. Although the larger dykes are chilled against granodiorite, the frequent necking of the smaller intrusions suggests that emplacement occurred while the country rock was still warm; since the granodiorite was most probably re-heated during the intrusion of the Andean gabbro, both pre- and post-Upper Jurassic ages are possible. Of the dykes cutting the rocks of the Millet Glacier succession, one (KG.554.3) is known to be of a mid-Cretaceous age (Rex, 1972) and another (KG.560.1—texturally and mineralogically similar to the first) has strong chemical affinities with the Moore Point dykes. Hence the early basic dykes were probably emplaced in the mid-Cretaceous. Ranging in thickness from 30 cm to 6 m, these dykes always have sharp contacts with the host rocks and, at Moore Point, they are frequently cut by microgranite veins.

The early basic dykes include a fine-grained, faintly porphyritic, dark grey aphanitic rock (e.g. KG.571.1) which is considerably fresher than the constituents of the later suite. Euhedral phenocrysts of plagioclase (An_{68-74}) occur mostly in glomeroporphyritic aggregates up to 2 mm in diameter. Sericite is abundant but alteration to epidote and calcite (with chlorite

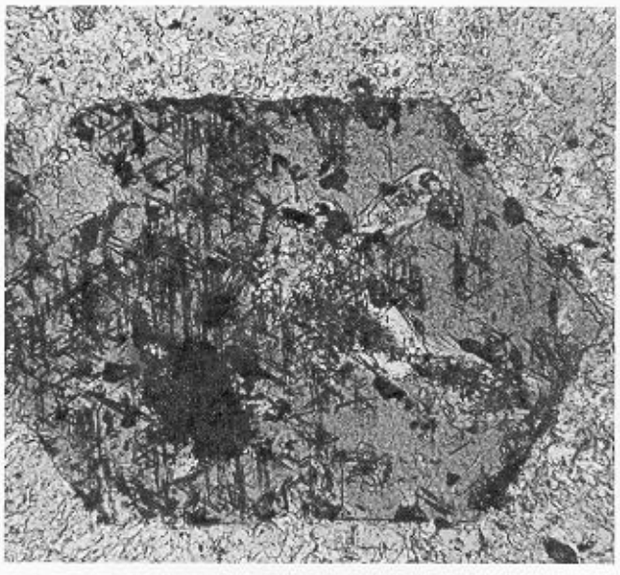

Fig. 65. Chlorite pseudomorph after (?) hornblende with ilmenite, and acicular epidote with a Widmanstätten-like pattern in acid porphyry dyke (KG.506.3; ordinary light; × 130).

developing along the cleavage traces) is limited. Single phenocrysts of pale yellow augite ($\gamma : c = 48°$ and $2V_\gamma = 40°$), between 0.25 and 0.75 mm in length, are slightly more abundant than those of plagioclase but again aggregates are commoner. Alteration of the pyroxene varies (Table XXII) from minor marginal penninite (KG.570.5) to complete replacement by uralitic hornblende (KG.571.1) with α = pale straw, β = green, γ = pale blue-green and $\gamma : c = 25°$, but brown magmatic hornblende is only sparingly present. Deeply embayed or skeletal ilmenite (with marginal magnetite) and, less commonly, anhedral iron pyrites are intergrown with the ferromagnesian minerals. The groundmass is a felted intergrowth of labradorite and biotite (KG.571.1) or hornblende (α = yellow, β = yellow-brown, γ = brown and $\gamma : c = 23°$) with granular magnetite which commonly occurs within the amphibole. Prehnite fills cracks and has partly replaced plagioclase. The 0.5 mm wide zone (KG.570.5) containing pilotaxitic plagioclase (of indeterminate composition), finely divided magnetite and rare brown hornblende probably represents a channel along which magma continued to flow after the remainder of the rock had solidified. A more equigranular intergrowth of pale yellow augite and bytownite (An_{72}) is common to both of the Procyon Peaks dykes, but 3 mm wide calcite-chrysotile-antigorite pseudomorphs (after (?) olivine) and occasional antigorite microphenocrysts are unique to specimen KG.554.3. The additional presence of amygdaloidal chlorite and colloform silica in specimen KG.560.1 suggests that the more uniform texture may have resulted from crystallization at higher crustal levels. The early basic dykes (Table XXIII) can be distinguished from the later ones by their low K_2O, Y, Zr, La, Ce and Ba contents. Conversely, with their high Al_2O_3 (particularly in specimen

Table XXII. Modal analyses of hypabyssal rocks from western Palmer Land.

	1	*2*	*3*	*4*	*5*	*6*	*7*	*8*	*9*	*10*	*11*	*12*	*13*	*14*	*15*	*16*
Phenocrysts																
Quartz	–	–	–	0.47	–	–	–	0.30	0.10	–	–	2.50	–	–	–	–
Plagioclase	33.22	7.30	–	28.70	4.10	–†	–	18.00	7.30	0.30	22.70	37.10	19.76	38.20	34.70	–
Clinopyroxene	–	1.10	–	–	–	23.90	–	–	–	–	2.48	4.50	–	–	–	–
Hornblende	–	–	–	–	–	–	–	37.60	–	5.00	–	–	4.10	–	–	–
Uralitic hornblende	3.22	–	–	–	–	–	–	–	10.50	10.10	–	tr.	3.73	7.70‖	5.10	–
Chlorite	tr.	–	–	5.24	0.30	5.60	–	0.50	–	–	4.44	14.40	–	–	0.90	–
Calcite	–	–	–	3.10	0.30	3.60	–	3.00	–	–	2.40	–	–	–	–	–
Epidote	–	–	–	–	–	5.70	–	1.30	4.60	–	–	7.10	–	–	0.70	–
Sphene	–	–	–	–	–	–	–	–	–	–	–	–	–	1.60	0.30	–
Iron ore	0.14	0.20	–	0.57	0.40	0.70	–	1.40	–	–	0.32§	3.10	11.62	1.50	0.90	–
TOTAL	36.58	8.60	–	38.08	5.10	39.50	–	62.10	22.50	15.40	32.34	68.70	39.21	49.00	42.60	–
Groundmass																
Quartz	–	–	17.70	tr.	–	–	0.60	–	1.65	–	1.00	—	—	–	0.80	1.36
Orthoclase	–	–	11.15*	–	–	–	–	–	–	–	–	–	–	–	–	0.08
Plagioclase	25.81	34.91	56.45	61.92	73.26	–	55.40	37.90	53.56	36.70	33.48	24.60	43.86	28.70	38.60	58.10
Clinopyroxene	–	–	–	–	–	–	17.60	–	–	–	18.06	–	–	–	–	8.92
Hornblende	0.30	45.52	6.35	–	–	–	–	–	–	34.80	–	–	tr.	–	–	10.51
Uralitic hornblende	29.63	–	–	–	–	–	–	–	10.17	8.60	–	2.60	5.00	8.15	1.00	–
Biotite	0.43	–	0.30	–	–	–	–	–	–	–	–	–	10.39	5.10	–	–
Chlorite	0.14	1.65	2.90	–	14.71	–	14.20	tr.	3.00	–	5.24	tr.	–	1.90	6.30	12.55
Calcite	–	–	–	tr.	–	–	1.30	–	0.10	–	1.76	0.10	–	–	–	5.44
Epidote	tr.	0.27	2.75	–	3.89	–	–	–	3.59	–	–	tr.	0.12	1.30	8.20	1.28
Sphene	–	–	1.10	–	–	–	0.50	–	–	–	–	–	1.42	–	0.30	–
Iron ore	5.65	9.05	0.55	tr.	3.04	–	10.40	tr.	5.43	4.50	8.12	4.00	tr.	5.85	2.20	1.72
Pyrite	tr.	–	0.55	–	–	–	–	–	–	–	–	–	–	–	–	–
Apatite	–	–	0.20	–	–	–	–	–	–	–	–	–	–	–	–	0.04
Prehnite	1.46	–	–	–	–	–	–	–	–	–	–	–	–	–	–	–
TOTAL	63.42	91.40	100.00	61.92	94.90	60.50‡	100.00	37.90	77.50	84.60	67.66	31.30	60.79	51.00	57.40	100.00
Plagioclase composition																
phenocrysts	An_{80}	An_{74-68}	–	An_{42}	(?)An_{13}	–	–	An_{52}	An_{56}	–	An_{64-60}	An_{70}	An_{72}	An_{60-56}	An_{75-60}	–
groundmass	An_{56}	–	An_{25}	–	–	–	–	–	–	–	–	–	An_{52}	–	–	An_{73-65}

* Microcline.
† Pseudomorphed by chlorite, calcite and epidote.
‡ Epidote, chlorite, calcite, ore and altered glass.
§ Includes 0.02% pyrite.
‖ Tremolite-actinolite.

1. KG.571.1 Early basic dyke, Moore Point.
2. KG.570.5 Early basic dyke, Moore Point.
3. KG.525.6 Microgranodiorite, Pegasus Mountains.
4. KG.506.3 Porphyry dyke, Pegasus Mountains.
5. KG.546.1 Porphyry dyke, Perseus Crags.
6. KG.553.5 Late basic dyke, Procyon Peaks.
7. KG.537.1 Late basic dyke, Auriga Nunataks.
8. KG.552.2 Late basic dyke, Perseus Crags.
9. KG.547.1 Late basic dyke, Perseus Crags.
10. KG.529.5 Late basic dyke, Pegasus Mountains.
11. KG.541.5 Late intermediate dyke, Capella Rocks.
12. KG.548.5 Late intermediate dyke, Perseus Crags.
13. KG.557.3 Late intermediate dyke, Procyon Peaks.
14. KG.550.2 Late intermediate dyke, Perseus Crags.
15. KG.547.2 Late intermediate dyke, Perseus Crags.
16. KG.515.7 Hornblende-microgabbro, Mount Alpheratz.

KG.571.1) and CaO, and low alkalis, Y, Zr, La and Ce, they strongly resemble the Andean gabbros. Specimen KG.570.5 plots close to two of the hypersthene-gabbros on an A–F–M diagram (Fig. 69), while the other two are not far removed from the quartz-diorites. Plotted on a Ca–Na–K diagram (Fig. 66), these three rocks have a poorly defined curvilinear trend which skirts the soda-rich side of the late basic dyke field but it is deficient in soda relative to the Andean trend. Since these dykes are enriched in K_2O, Ba and Rb relative to the gabbros, have lower K/Rb and Ba/K ratios (Table XXIV), and plot close to the fractiometric curve on the plot of Ca/Y against the Thornton and Tuttle differentiation index, they could readily have evolved by fractional crystallization from the primary Andean basic magma. The higher K_2O content of the dykes possibly reflects a higher degree of crustal contamination. If the Millett Glacier dykes are contemporaneous, the Andean basic rocks of western Palmer Land belong to Rex's (1972) third or mid-Cretaceous intrusive episode.

3. Microgranodiorites

Small microgranodiorite intrusions, which are visibly unconnected with any of the large plutons, cut the Wade Point gabbro and the metamorphic rocks on the ridge immediately south of Mount Markab. At the northernmost locality, the 3–4.5 m wide sub-vertical dyke has sharp contacts with the host rock from which small tongues penetrate the gabbro to a depth of 2.5 cm. This intrusion is a medium-grained aplitic granodiorite in which anhedral quartz, plagioclase and orthoclase form a mosaic of interlocking crystals (with an average grain-size of 0.2 mm), but phenocrysts of both quartz and plagioclase may be up to 2 mm in size. The larger quartz crystals are strained, the plagioclase is noticeably sericitized and the orthoclase is cloudy. Pale green penninite in ragged plates (enclosing granular quartz) is intergrown with muscovite and magnetite (with associated ilmenite).

The second example is of similar dimensions but it is composed of a more melanocratic rock (e.g. KG.525.6) with a hypidiomorphic texture. Sieved hornblende, in which the pleochroism (α = yellow, β = pale green, γ = sea-green) may be masked by brown (? iron) staining, forms subhedral laths up to 3 mm in length and is partly replaced by biotite, particularly along the perimeters. The hornblende has also been hydrothermally altered to chlorite, epidote and ilmenite. Plagioclase (An_{25}) occurs as equant crystals (or occasionally as euhedral laths), in which oscillatory zoning is emphasized by concentric shells of sericite, and on which clear albite forms narrow rims. Quartz is predominantly interstitial but it also occurs myrmekitically within the plagioclase where the latter is in contact with characteristically twinned and slightly strained microcline. Sphene is the main accessory mineral, occurring in euhedral wedges or as tiny granules in the hornblende (or its replacements), while allanite (pleochroic from yellow to red-brown), magnetite and iron pyrites comprise the remainder. Despite their many apparent differences, these two rocks (KG.569.1 and 525.6; Table XXV, analyses 5 and 4) show some remarkably similar trace-element values, in particular in Y, Zr, Ba and Ce. Both have considerably higher K/Rb and lower Rb/Sr ratios than the later acid porphyry dykes. On an A–F–M diagram, specimen KG.525.6 lies in the granodioritic field of the Andean rocks but specimen KG.569.1 has affinities with the granites. In some respects (e.g. high SiO_2 and low K_2O), specimen KG.569.1 resembles the Moore Point older granodiorite but the Rb/Sr and Ca/Sr ratios are more typical of the Andean rocks (cf. Table XXIV, analyses 6 and 7). When plotted on a Ca–Na–K diagram (Fig. 62), the Wade Point rock, because of its low K_2O, lies outside the field of normal magmatic granites; since extensive replacement of potash feldspar was not apparent in thin sections, it follows that such a rock most probably originated by melting of pre-existing potassium-poor siliceous rocks, e.g. the quartz-mica-schists. Furthermore, the close similarity of trace-element concentrations in these two dykes suggests similar parental rocks.

4. Microgranites

Microgranite dykes and veins, ranging in thickness from 1.5 cm to 20 m are common and cut most earlier rock types. Locally they appear to have followed pre-existing joints but, for the most part, they describe extremely sinuous courses with apophyses extending into the surrounding rock from the longer bodies. In the granodiorites, they may be aligned parallel to the flow structures and in places themselves have faint planar structures. Contacts with the country rock are always sharp and chilled margins are invariably absent. Included fragments are rare, but at Canis Heights (KG.561) and on the coast dioritic xenoliths are present and blocks of coarse tuff up to 15 cm abound in the highest of the three dykes at western Procyon Peaks (KG.560). The constituent rock is either pink or greyish white and generally medium-grained. At station KG.561, the dyke rock is coarse (KG.561.3) and strongly resembles one of the major intrusions (KG.501A.1). Of rather more limited occurrence are pegmatitic aggregates (with crystals up to 2 cm) of quartz and pink feldspar, either with or without biotite and varying in width from 5 to 60 cm. Although several of the granite bodies have associated microgranite veins and dykes, the volume is small (KG.555). However, at station KG.557, less than 2 km away from KG.553 where veins are non-existent, microgranite veins cutting granodiorite form the most extensive net-vein complex observed in western Palmer Land. The development of such complexes requires an abundance of volatiles and, whereas the granites were considered to have been relatively 'dry', this particular granodiorite (e.g. KG.557.1) shows abundant evidence (e.g. granophyric textures) of a high gas content. Evidence of a third episode of intrusion is provided by a single more basic dyke which at station KG.502 has chilled against granite.

In thin section the microgranite has a weak saccharoidal to hypidiomorphic texture comprising quartz, oligoclase and microcline. The plagioclase (An_{28}) is subhedral but marginal replacement by quartz and potash feldspar frequently destroys any vestige of crystal outline. Primary quartz forms large strained anhedra and graphic intergrowths with microperthitic microcline, while myrmekitic quartz has developed within the oligoclase. Biotite, in minute ragged laths, is extremely limited. Some veins (e.g. KG.541.8) possess a porphyritic texture with (frequently fractured and sericitized) plagioclase phenocrysts (An_{25}) up to 2 mm in size. This particular rock is characterized by euhedral pink garnet which seldom exceeds 0.2 mm in diameter and is partly replaced by a pale chlorite. A similar chlorite of primary origin is often accompanied by muscovite.

Two microgranites (Table XXIII, analyses 6 and 7) were analysed, one (KG.517.4) from a vein cutting older granodiorites and the other representing those veins paralleling

Table XXIII. Chemical analyses of some hypabyssal rocks from western Palmer Land.

	Early basic dykes			*Micrograno-diorite dykes*		*Microgranite dykes*		*Acid porphyry dykes*				*Late basic and intermediate dykes*		
	1	*2*	*3*	*4*	*5*	*6*	*7*	*8*	*9*	*10*	*11*	*12*	*13*	*14*
SiO_2	48.43	49.64	53.06	63.68	74.92	73.46	74.52	61.16	65.98	67.52	71.98	45.71	47.96	48.74
TiO_2	0.95	0.83	1.37	0.54	0.18	0.06	0.05	0.47	0.80	0.24	0.26	1.00	1.08	1.09
Al_2O_3	20.11	16.31	15.70	16.75	14.17	15.70	14.52	17.26	14.97	17.25	14.98	11.36	13.98	16.70
Fe_2O_3	4.34	4.79	4.92	2.15	0.84	0.27	0.41	2.86	2.54	1.26	0.85	4.80	4.14	4.94
FeO	3.97	4.12	4.99	1.72	0.59	0.29	0.25	1.75	1.64	0.77	0.43	4.24	6.48	5.02
MnO	0.11	0.12	0.13	0.08	0.04	0.13	0.02	0.08	0.09	0.05	0.03	0.04	0.20	0.16
MgO	5.49	7.31	4.55	1.50	0.15	0.04	–	1.77	1.04	0.64	0.49	11.99	8.92	7.07
CaO	10.40	8.56	6.97	3.77	1.95	0.75	0.45	4.43	2.21	1.98	1.79	9.54	8.52	7.57
Na_2O	3.02	2.49	4.12	4.37	4.71	4.90	4.03	4.20	4.71	4.19	4.04	0.74	2.10	2.85
K_2O	0.79	1.07	1.29	2.95	1.68	4.22	5.02	2.79	4.05	3.40	4.76	4.40	2.65	1.49
P_2O_5	0.10	0.13	0.15	0.22	0.03	0.01	–	0.18	0.09	0.10	0.04	0.58	0.17	0.15
H_2O^+														
H_2O^-	1.11	2.54	1.64	1.42	0.98	0.44	0.70	1.04	1.00	1.67	0.42	3.44	1.96	2.72
CO_2	0.78	1.78	0.75	0.61	0.41	0.38	0.37	1.35	0.78	1.23	0.58	2.00	1.36	1.36
Total	99.60	99.69	99.64	99.76	100.65	100.65	100.34	99.34	99.90	100.30	100.65	99.94	99.52	99.86
ANALYSES LESS TOTAL WATER (RECALCULATED TO 100)														
SiO_2	49.18	51.10	54.15	64.76	75.17	73.32	74.79	62.22	66.72	68.46	71.69	47.39	49.16	50.17
TiO_2	0.96	0.85	1.40	0.55	0.18	0.06	0.05	0.48	0.81	0.24	0.26	1.04	1.11	1.13
Al_2O_3	20.42	16.79	16.02	17.03	14.22	15.66	14.57	17.56	15.14	17.49	15.01	11.77	14.32	17.19
Fe_2O_3	4.41	4.93	5.02	2.19	0.84	0.27	0.41	2.91	2.57	1.28	0.86	4.97	4.25	5.09
FeO	4.03	4.24	5.09	1.75	0.59	0.29	0.25	1.78	1.66	0.78	0.43	4.40	6.64	5.17
MnO	0.11	0.13	0.13	0.08	0.04	0.13	0.02	0.08	0.09	0.05	0.03	0.14	0.21	0.16
MgO	5.57	7.52	4.64	1.52	0.15	0.04	–	1.80	1.05	0.64	0.49	12.42	9.14	7.28
CaO	10.56	8.81	7.11	3.83	1.96	0.74	0.45	4.51	2.23	2.01	1.79	9.88	8.73	7.79
Na_2O	3.07	2.57	4.21	4.44	4.73	4.89	4.05	4.27	4.76	4.25	4.05	0.77	2.15	2.94
K_2O	0.80	1.10	1.31	3.00	1.68	4.21	5.04	2.84	4.09	3.45	4.77	4.56	2.72	1.53
P_2O_5	0.10	0.13	0.15	0.23	0.03	0.01	–	0.18	0.09	0.10	0.04	0.60	0.18	0.15
CO_2	0.79	1.83	0.77	0.62	0.41	0.38	0.37	1.37	0.79	1.25	0.58	2.06	1.39	1.40
ELEMENT WEIGHT PERCENTAGES (ANHYDROUS)														
Si^{4+}	22.97	23.88	25.30	30.27	35.14	34.27	34.97	29.06	31.19	31.97	33.51	22.15	22.98	23.45
Ti^{4+}	0.58	0.51	0.84	0.33	0.11	0.03	0.03	0.29	0.48	0.15	0.16	0.62	0.66	0.68
Al^{3+}	10.80	8.89	8.48	9.01	7.52	8.29	7.71	9.29	8.01	9.25	7.94	6.23	7.58	9.10
Fe^{3+}	3.08	3.45	3.51	1.53	0.59	0.19	0.29	2.03	1.80	0.89	0.60	3.48	2.97	3.56
Fe^{2+}	3.13	3.30	3.95	1.36	0.46	0.22	0.19	1.38	1.29	0.60	0.34	3.42	5.16	4.02
Mn^{2+}	0.09	0.10	0.10	0.06	0.03	0.10	0.01	0.06	0.07	0.04	0.02	0.11	0.16	0.12
Mg^{2+}	3.36	4.54	2.80	0.92	0.09	0.03	–	1.08	0.63	0.39	0.30	7.49	5.52	4.39
Ca^{2+}	7.54	6.30	5.08	2.74	1.40	0.53	0.32	3.21	1.60	1.43	1.28	7.06	6.24	5.57
Na^{+}	2.27	1.90	3.12	3.29	3.51	3.63	3.00	3.16	3.53	3.14	3.01	0.57	1.60	2.18
K^{+}	0.67	0.91	1.09	2.49	1.40	3.50	4.18	2.35	3.40	2.85	3.96	3.79	2.25	1.27
P^{5+}	0.04	0.06	0.07	0.10	0.01	0.01	–	0.08	0.04	0.18	0.02	0.26	0.08	0.07
C^{4+}	0.22	0.50	0.21	0.17	0.11	0.10	0.10	0.37	0.22	0.34	0.16	0.56	0.38	0.38
O^{2-}	45.25	45.66	45.45	47.73	49.63	49.10	49.20	47.64	47.74	48.77	48.70	44.26	44.42	45.21
C.I.P.W. NORMS														
Q	0.28	6.07	5.40	18.79	37.88	27.90	31.92	18.24	19.14	28.68	26.86	–	–	2.06
C	–	–	–	1.34	2.05	2.59	2.47	2.65	0.72	6.12	1.26	–	–	–
Z	–	0.02	0.02	0.04	0.04	–	0.03	–	0.17	–	–	0.06	0.03	0.04
or	4.75	6.48	7.75	17.76	9.94	24.96	29.83	16.68	24.19	20.57	28.16	26.93	16.07	9.03
ab	25.88	21.69	35.56	37.53	39.99	41.36	34.23	36.16	40.22	36.16	34.27	6.48	18.20	24.83
an	39.53	31.03	20.93	13.96	7.00	1.24	–	13.07	5.84	1.39	5.23	15.14	21.35	29.15
di	5.86	0.39	7.00	–	–	–	–	–	–	–	–	13.60	9.75	0.01
hy	13.26	21.05	11.24	4.38	0.51	0.55	0.07	4.50	2.61	1.70	1.22	11.58	16.17	21.81
ol	–	–	–	–	–	–	–	–	–	–	–	10.85	6.51	–
mt	6.38	7.14	7.26	3.17	1.22	0.40	0.60	3.48	3.28	1.62	0.72	7.19	6.15	7.37
cm	–	0.02	–	–	–	–	–	–	–	–	–	0.07	0.04	–
il	1.82	1.62	2.65	1.04	0.34	0.11	0.09	0.91	1.53	0.46	0.50	1.97	2.10	2.10
hm	–	–	–	–	–	–	–	0.32	0.30	0.06	0.36	–	–	–
ap	0.24	0.32	0.35	0.54	0.07	0.03	–	0.34	0.21	0.24	0.09	1.41	0.42	0.37
pr	0.20	0.01	0.10	0.05	0.03	0.01	0.01	0.48	–	0.14	–	0.03	0.04	0.01
cc	1.80	4.16	1.74	1.41	0.94	0.86	0.83	3.10	1.79	2.80	1.32	4.68	3.17	3.18
COORDINATES FOR TRIANGULAR DIAGRAMS														
A	23.5	20.0	29.1	60.3	81.2	94.1	93.7	55.1	65.1	76.1	85.0	23.2	22.0	22.4
F	49.6	47.8	51.5	30.1	17.3	5.5	6.3	34.1	29.0	19.0	11.4	36.8	46.5	49.1
M	26.9	32.2	19.4	9.6	1.5	0.4	–	10.8	5.9	4.9	3.6	40.0	31.5	28.5
Ca	72.0	69.1	54.7	32.1	22.2	6.9	4.3	36.9	18.7	19.3	15.5	61.9	61.9	61.7
Na	21.6	20.9	33.6	38.7	55.6	47.4	40.0	36.2	41.5	42.3	36.5	5.0	15.8	24.2
K	6.4	10.0	11.7	29.2	22.2	45.7	55.7	26.9	39.8	38.4	48.0	33.1	22.3	14.1

Table XXIII. Chemical analyses of some hypabyssal rocks from western Palmer Land (continued).

	Late basic and intermediate dykes												
	15	*16*	*17*	*18*	*19*	*20*	*21*	*22*	*23*	*24*	*25*	*26*	*27*
SiO_2	50.18	51.48	52.00	53.55	54.06	54.19	54.38	55.11	55.40	56.97	57.03	56.20	56.35
TiO_2	1.04	0.89	1.08	0.91	1.03	1.05	1.03	0.90	1.11	0.77	0.80	0.76	0.77
Al_2O_3	15.68	17.82	13.11	15.85	15.25	15.25	15.61	16.43	16.45	16.88	16.77	16.64	15.25
Fe_2O_3	4.76	4.68	3.67	4.51	4.31	5.17	4.53	4.07	4.44	3.98	3.96	4.13	4.24
FeO	3.85	3.68	4.70	3.33	4.35	3.80	3.79	3.17	2.96	2.80	2.52	2.75	2.69
MnO	0.12	0.10	0.12	0.13	0.16	0.15	0.13	0.11	0.13	0.10	0.05	0.12	0.11
MgO	6.92	5.25	8.94	7.29	4.33	4.40	4.67	5.03	4.55	4.40	4.36	4.34	5.05
CaO	7.59	7.39	7.63	6.96	5.96	6.03	6.79	6.74	6.78	6.65	6.03	6.91	5.71
Na_2O	3.89	4.08	3.63	3.22	3.03	2.86	3.59	3.27	4.44	3.82	4.28	3.50	3.76
K_2O	1.90	1.59	1.88	1.91	2.56	2.34	1.55	2.47	1.79	1.97	2.01	2.15	2.53
P_2O_5	0.19	0.24	0.25	0.13	0.20	0.19	0.18	0.23	0.30	0.21	0.20	0.18	0.13
H_2O^+ H_2O^-	1.99	1.92	1.52	1.50	3.66	3.25	2.16	1.71	1.17	1.20	1.70	1.47	2.37
CO_2	1.73	0.44	1.05	1.12	1.77	1.84	1.28	0.63	0.78	0.57	0.65	1.31	1.31
Total	99.84	99.56	99.58	100.41	100.67	100.52	99.69	99.87	100.30	100.32	100.36	100.46	100.27
ANALYSES LESS TOTAL WATER (RECALCULATED TO 100)													
SiO_2	51.28	52.73	53.04	54.14	55.74	55.70	55.77	56.14	55.92	57.47	57.81	56.77	57.55
TiO_2	1.06	0.91	1.10	0.92	1.07	1.08	1.05	0.92	1.12	0.78	0.81	0.77	0.79
Al_2O_3	16.02	18.25	13.37	16.02	15.72	15.68	16.01	16.74	16.60	17.03	17.00	16.80	15.58
Fe_2O_3	4.87	4.79	3.74	4.56	4.44	5.32	4.64	4.14	4.48	4.02	4.01	4.17	4.32
FeO	3.94	3.77	4.79	3.37	4.48	3.90	3.89	3.23	2.98	2.82	2.56	2.77	2.75
MnO	0.12	0.10	0.12	0.13	0.16	0.15	0.13	0.11	0.13	0.10	0.05	0.12	0.11
MgO	7.07	5.37	9.12	7.37	4.46	4.53	4.79	5.12	4.60	4.44	4.42	4.41	5.15
CaO	7.76	7.57	7.78	7.04	6.14	6.20	6.96	6.87	6.84	6.71	6.11	6.98	5.86
Na_2O	3.98	4.18	3.70	3.26	3.12	2.94	3.68	3.33	4.48	3.85	4.34	3.54	3.84
K_2O	1.94	1.63	1.92	1.93	2.64	2.41	1.59	2.51	1.81	1.99	2.03	2.17	2.58
P_2O_5	0.19	0.25	0.25	0.13	0.21	0.20	0.18	0.24	0.26	0.21	0.20	0.18	0.13
CO_2	1.77	0.45	1.07	1.13	1.82	1.89	1.31	0.64	0.78	0.58	0.66	1.32	1.34
ELEMENT WEIGHT PERCENTAGES (ANHYDROUS)													
Si^{4+}	23.97	24.64	25.65	25.31	26.05	26.04	26.06	26.25	26.14	26.87	27.02	26.53	26.89
Ti^{4+}	0.64	0.55	0.63	0.55	0.64	0.65	0.63	0.55	0.67	0.47	0.49	0.46	0.47
Al^{3+}	8.48	9.66	6.80	8.48	8.32	8.30	8.47	8.86	8.79	9.01	8.99	8.89	8.24
Fe^{3+}	3.40	3.35	2.51	3.19	3.11	3.72	3.25	2.90	3.13	2.81	2.80	2.92	3.02
Fe^{2+}	3.06	2.93	3.58	2.62	3.48	3.03	3.02	2.51	2.32	2.19	1.99	2.16	2.13
Mn^{2+}	0.10	0.08	0.09	0.10	0.12	0.12	0.10	0.09	0.10	0.08	0.04	0.09	0.09
Mg^{2+}	4.27	3.24	5.28	4.44	2.69	2.73	2.89	3.09	2.77	2.68	2.67	2.66	3.11
Ca^{2+}	5.55	5.41	5.35	5.03	4.39	4.43	4.98	4.91	4.89	4.80	4.37	4.99	4.19
Na^{+}	2.95	3.10	2.64	2.42	2.32	2.18	2.73	2.47	3.32	2.86	3.22	2.62	2.85
K^{+}	1.61	1.35	1.53	1.60	2.19	2.00	1.32	2.09	1.50	1.65	1.69	1.80	2.14
P^{5+}	0.08	0.11	0.11	0.06	0.09	0.09	0.08	0.10	0.11	0.09	0.09	0.08	0.06
C^{4+}	0.48	0.12	0.28	0.31	0.50	0.52	0.36	0.18	0.21	0.16	0.18	0.36	0.36
O^{2-}	45.41	45.46	45.55	45.89	46.10	46.19	46.11	46.00	46.05	46.33	46.45	46.44	46.45
C.I.P.W. NORMS													
Q	–	0.55	2.95	5.36	11.55	14.27	9.96	7.69	6.08	9.23	8.14	10.44	9.27
C	–	–	–	–	1.11	1.68	–	–	–	–	–	–	–
Z	0.04	0.04	0.03	0.05	0.06	0.06	0.06	0.07	0.05	0.06	0.06	0.06	0.14
or	11.45	9.63	10.93	11.41	15.65	14.25	9.36	14.83	10.56	11.72	12.01	12.78	15.24
ab	33.61	35.29	30.03	27.54	26.40	24.88	31.11	28.13	37.73	32.55	36.65	29.87	32.43
an	20.09	26.21	13.60	23.35	17.96	17.82	22.42	23.28	20.02	23.28	20.86	23.54	17.59
di	5.13	5.66	12.41	2.96	–	–	2.34	4.37	5.40	4.26	3.40	1.55	2.00
hy	14.40	12.30	19.85	18.05	14.17	12.53	12.56	11.86	9.20	9.79	9.52	10.79	12.14
ol	1.73	–	–	–	–	–	–	–	–	–	–	–	–
mt	7.04	6.94	5.20	6.61	6.43	7.70	6.72	6.00	6.50	5.81	5.80	6.04	6.26
cm	–	–	0.07	0.02	–	–	–	–	–	–	–	–	–
il	2.01	1.73	2.00	1.75	2.02	2.05	2.00	1.74	1.98	1.47	1.55	1.46	1.50
hm	–	–	–	–	–	–	–	–	–	–	–	–	–
ap	0.46	0.59	0.58	0.31	0.49	0.46	0.43	0.56	0.68	0.50	0.48	0.42	0.31
pr	0.01	0.04	0.01	0.01	0.02	0.01	0.06	0.02	–	0.02	0.02	0.04	0.10
cc	4.10	1.02	2.34	2.57	4.14	4.30	2.98	1.46	1.80	1.31	1.50	3.00	3.04
COORDINATES FOR TRIANGULAR DIAGRAMS													
A	29.8	31.8	26.8	28.2	32.7	30.6	30.6	34.9	37.0	37.0	39.7	36.4	37.7
F	42.3	45.0	39.2	40.7	47.8	49.4	47.5	41.4	41.8	41.0	38.7	41.7	38.9
M	27.9	23.2	34.0	31.1	19.5	20.0	21.9	23.7	21.2	22.0	21.6	21.9	23.4
Ca	54.9	54.8	56.2	55.6	49.3	51.4	55.1	51.9	50.4	51.6	47.1	53.0	45.6
Na	29.2	31.4	27.7	26.7	26.0	25.4	30.3	26.1	34.2	30.7	34.7	27.9	31.0
K	15.9	13.8	16.1	17.7	24.7	23.2	14.6	22.0	15.4	17.7	18.2	19.1	23.4

Table XXIII. Chemical analyses of some hypabyssal rocks from western Palmer Land (continued).

	Early basic dykes			*Micrograno-diorite dykes*		*Microgranite dykes*		*Acid porphyry dykes*				*Late basic and intermediate dykes*		
	1	*2*	*3*	*4*	*5*	*6*	*7*	*8*	*9*	*10*	*11*	*12*	*13*	*14*
TRACE ELEMENTS (ppm)														
S	1047	50	552	239	152	25	33	2255	11	523	21	171	185	68
Cr	17	79	18	23	10	10	9	10	5	8	9	310	172	41
Ni	11	55	14	10	–	2	1	5	4	5	1	113	42	13
Rb	31	22	49	113	31	223	197	172	186	240	272	104	124	49
Sr	714	630	605	654	203	93	14	692	400	534	266	933	370	813
Y	10	19	16	22	18	22	124	44	50	47	45	31	22	22
Zr	68	116	117	208	199	64	155	322	820	301	380	267	163	178
Ba	235	418	393	924	929	50	16	1534	1038	1607	1464	714	450	641
La	–	8	4	18	28	7	11	27	35	45	34	30	3	6
Ce	2	13	18	45	46	18	40	67	93	85	76	70	25	32
Pb	8	22	7	37	24	60	35	37	33	28	42	30	21	1
K/Rb	212	402	218	217	449	157	212	137	181	119	146	351	177	252
K/Na	0.30	0.48	0.35	0.76	0.40	0.96	1.39	0.74	0.96	0.91	1.32	6.65	1.41	0.58
Ca/Y	7438	3222	3115	1224	776	242	26	730	316	304	284	2200	2769	2461
D.I.	30.91	34.24	48.71	74.08	87.81	94.22	95.98	71.08	83.55	85.41	89.29	33.41	34.27	35.92

1. KG.571.1 Early basic dyke, Moore Point.
2. KG.560.1 Early basic dyke, Procyon Peaks.
3. KG.570.5 Early basic dyke, Moore Point.
4. KG.525.6 Microgranodiorite, Pegasus Mountains.
5. KG.569.1 Microgranodiorite, Wade Point.
6. KG.541.8 Microgranite, Capella Rocks.
7. KG.516.4 Microgranite, Mount Crooker.
8. KG.506.5 Acid porphyry dyke, Pegasus Mountains.
9. KG.546.1 Acid porphyry dyke, Perseus Crags.
10. KG.508.8 Acid porphyry dyke, Pegasus Mountains.
11. KG.555.3 Acid porphyry dyke, Procyon Peaks.
12. KG.553.5 Late altered basic dyke, Procyon Peaks.
13. KG.527.2 Late altered basic dyke, Pegasus Mountains.

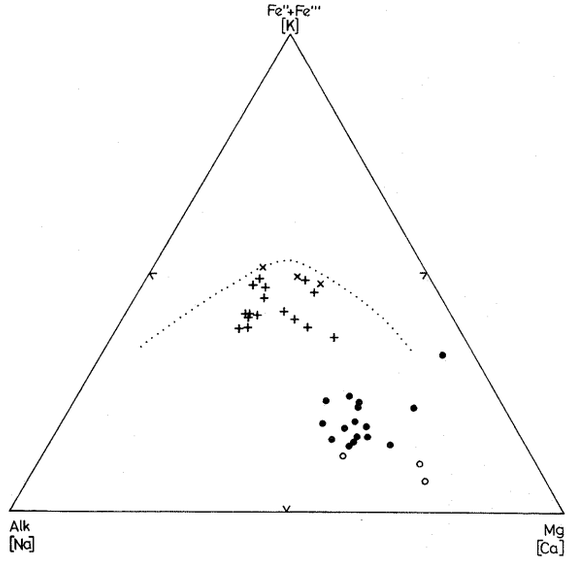

Fig. 66. Alk–(Fe″ + Fe‴)–Mg and Ca–Na–K triangular variation diagrams for early basic (× and ⊙) and late basic to intermediate dykes (+ and ●). The dotted line separates the tholeiitic (above) and calc-alkaline (below) fields in the Alk–(Fe″ + Fe‴)–Mg diagram.

the flow structures in the Andean granodiorites. Despite the fact that most of the microgranites were assumed to be associated with the granodiorites, these two appear to form the granitic end members of the high-yttrium series and in consequence they are more akin to the granites than the granodiorites. They have the typically high Al_2O_3 content of this suite but otherwise they have element concentrations (high K_2O, Rb, Y and Pb; low TiO_2, FeO + Fe_2O_3, MgO, MnO, CaO and Cr) characteristic of residual magmas. The marginally higher MnO, MgO and FeO in specimen KG.541.8 can be accounted for by the presence of garnet as the principal ferromagnesian mineral, whereas the low concentrations of La and Ce reflect the lack of CaO and O_2O_5. The Zr contents are unusually low and it can only be assumed that crystallization reached its zenith in the granites.

5. Acid porphyry dykes

A suite of acid porphyry dykes of limited extent was emplaced after the major intrusive phase but before the more widespread basic dykes. Unlike the late basic dykes, they are restricted to two distinct centres: in the eastern part of the Pegasus Mountains (KG.506 and 508) and at Procyon Peaks (KG.555 and 557). Of the four acid dykes which cut the banded gneisses on the summit of station KG.506, two are parallel to the foliation of the country rock. Ranging in thickness from 1.8 to 6 m, they have sharp contacts with the host rock and they enclose rounded gneissose xenoliths with diameters in excess of 4 cm. The relative ages of the basic and acid dykes were established at station KG.508 where narrow basic dykes have been intruded along the margins of a 5 m wide plagioclase-porphyry dyke. Small basic tongues intrude the country rock and the basic rock has a microscopically small chilled margin. These acid dykes invariably possess idiomorphic plagioclase and ferromagnesian phenocrysts set in a pale purple aphanitic groundmass.

The Andean intrusions forming the spur at the south-western corner of station KG.555 are cut by two porphyry dykes. At the tip of the spur a 2 m wide, faintly banded purplish biotite-plagioclase-porphyry dyke intrudes granite with numerous small veins branching into the country rock. Specimen KG.555.3 contains pink plagioclase and brown biotite

Table XXIII. Chemical analyses of some hypabyssal rocks from western Palmer Land (continued).

	Late basic and intermediate dykes												
	15	*16*	*17*	*18*	*19*	*20*	*21*	*22*	*23*	*24*	*25*	*26*	*27*
TRACE ELEMENTS (ppm)													
S	56	207	39	34	80	25	294	109	23	102	129	205	504
Cr	36	12	324	80	13	13	61	20	25	10	17	16	33
Ni	33	7	151	57	7	7	27	19	15	16	15	9	15
Rb	56	57	176	98	175	170	47	79	64	69	94	84	128
Sr	1 400	867	781	677	615	539	719	847	875	1 004	926	897	610
Y	17	17	18	25	26	25	30	25	22	21	23	17	17
Zr	181	173	178	256	272	273	286	335	265	286	314	281	244
Ba	751	478	325	343	1 025	703	572	737	702	734	727	892	882
La	18	18	17	14	20	21	25	26	25	14	20	28	17
Ce	34	36	51	33	50	48	47	77	56	36	50	58	49
Pb	15	11	17	9	14	41	21	15	16	20	17	30	23
K/R	282	232	89	161	122	114	273	259	232	237	198	212	167
K/Na	0.55	0.44	0.58	0.66	0.94	0.92	0.48	0.85	0.45	0.58	0.52	0.69	0.75
Ca/Y	3 194	3 107	3 032	1 990	1 637	1 725	1 619	1 928	2 203	2 266	1 875	2 907	2 465
D.I.	45.06	45.47	43.91	44.31	53.60	53.40	50.43	50.65	54.37	53.50	56.80	53.09	56.94

14. KG.537.1 Late altered basic dyke, Auriga Nunataks.
15. KG.552.2 Late altered basic dyke, Perseus Crags.
16. KG.547.1 Late altered basic dyke, Perseus Crags.
17. KG.529.5 Late altered basic dyke, Pegasus Mountains.
18. KG.557.4 Late altered basic dyke, Procyon Peaks.
19. KG.506.9 Late altered intermediate dyke, Pegasus Mountains.
20. KG.506.8 Late altered intermediate dyke, Pegasus Mountains.
21. KG.541.5 Late intermediate dyke, Capella Rocks.
22. KG.548.4 Late intermediate dyke, Perseus Crags.
23. KG.557.3 Late intermediate dyke, Procyon Peaks.
24. KG.550.2 Late intermediate dyke, Perseus Crags.
25. KG.547.2 Late altered intermediate dyke, Perseus Crags.
26. KG.515.3 Hornblende-microgabbro, Mount Alpheratz.
27. KG.533.1 Altered hornblende-microgabbro, Mount Mackab.

Table XXIV. Selected element ratios for some of the hypabyssal and plutonic rocks.

	1	*2*	*3*	*4*	*5*	*6*	*7*	*8*	*9*	*10*	*11*	*12*
Ba/K	0.042–0.248	0.036	0.047	0.037	–	–	–	–	–	–	–	–
K/Rb	789–199	212	402	218	217	449	266	277	137	181	119	146
Rb/Sr	–	–	–	–	0.173	0.153	0.132	0.352	0.249	0.465	0.449	1.023
Ca/Sr	–	–	–	–	104.18	97.16	82.37	135.50	46.39	39.45	26.78	48.12

1. Range of values in seven Andean gabbros (Table XX, analyses 3–9).
2. KG.571.1 Early basic dyke.
3. KG.560.1 Early basic dyke.
4. KG.570.5 Early basic dyke.
5. KG.525.6 Microgranodiorite.
6. KG.569.1 Microgranodiorite.
7. Average of nine Andean granodiorites (Table XX, analyses 13–21).
8. Mean of two pre-Upper Jurassic granodiorites (Table XI, analyses 1 and 2).
9. KG.506.5 Acid porphyry dyke.
10. KG.546.1 Acid porphyry dyke.
11. KG.508.8 Acid porphyry dyke.
12. KG.555.3 Acid porphyry dyke.

phenocrysts with large angular granite xenoliths and the dyke bears a stronger resemblance to the dykes in the Pegasus Mountains. The second dyke, 20 m farther east, is intruded parallel to a major joint direction in the granite and is devoid of associated smaller veins. This dyke closely resembles those intruding granodiorite on the north side of the nunatak (KG.557; Fig. 67). These dykes have a bright greenish hue, imparted by secondary epidote, although they are greenish grey where fresh. The larger of these dykes may be more than 15 m wide and, since their dips seldom exceed 45°, it is probable that their intrusion was joint-controlled by their host. Despite these differences, all the acid porphyry dykes are considered to be of similar age.

A characteristic feature of these rocks (e.g. KG.506.3) is the complete pseudomorphing of the (?) hornblende phenocrysts by pale green fibrous chlorite and anhedral calcite with minor amounts of dusty epidote and ilmenite. Many of the pseudomorphs contain acicular crystals of a colourless or pale yellow mineral, which are arranged in a Widmanstätten-like

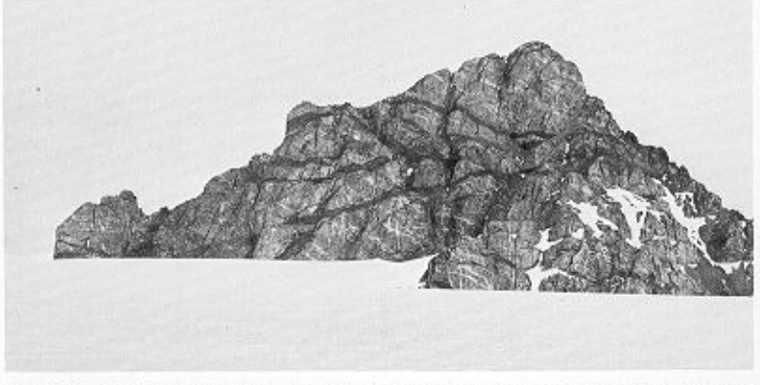

Fig. 67. Microgranite net-vein complex in granodiorite on the north face of station KG.557. Subsequent acid porphyry dykes are cut by smaller members of the late basic–intermediate suite. The summit of the nunatak is approximately 200 m above the surface of the ice.

pattern. They have parallel extinction and a birefringence similar to that of the epidote. Rare brown biotite is present within the hydrothermal minerals, evidently as the product of deuteric alteration of the hornblende. Although albite twins were observed in a few of the crystals, the twinning in the extensively sericitized plagioclase phenocrysts (1–3.5 mm long) is mainly simple and of the interpenetrant type. The composition of the phenocrysts is generally between An_{40} and An_{46} but labradorite (An_{54}) cores are present in specimen KG.506.5, and in KG.546.1 a very sodic oligoclase (? An_{13}) is dominant. Magnetite forms smaller subhedral and embayed phenocrysts containing small amounts of (?) ilmenite. The mesostasis is composed of tiny oligoclase laths with interstitial quartz, epidote, calcite and magnetite. Although the late basic dykes chill against the acid porphyries, there is little evidence of any metamorphism in the older rock. However, the high degree of alteration in these rocks, particularly in specimen KG.508.8, may be related to this later event.

No pseudomorphs occur in specimen KG.555.3, the ferromagnesian constituent being brown biotite containing granular sphene and ore. The groundmass comprises lath-like plagioclase, frequently growing into spherulites of pale brown devitrified felsitic glass, granular quartz, orthoclase, sphene and magnetite.

One of the analysed acid porphyry dykes (KG.508.8; Table XXIII, analysis 10) has a somewhat higher K/Na ratio than the others and when plotted on a Ca–Na–K diagram (Fig. 62) it falls outside the field of magmatic rocks. However, abundant plagioclase phenocrysts testify to the magmatic origin of this rock, and the raising of the K/Na ratio most probably occurred concomitantly with the extensive alteration noted in the thin section. Hence, the unusual aspects of this rock are secondary features attributable to metasomatic action, which was presumably connected with the emplacement of the adjacent late basic dykes. It may be that these changes represent an associated event and therefore are not connected with the genesis or emplacement of the acid dykes. In general, the acid porphyry dykes perpetuate several of the well-established chemical features of the Palmer Land igneous rocks (e.g. high Al_2O_3, Zr, Ba and Rb, and low $\Sigma Fe[O]$), from which it may be deduced that the processes responsible (i.e. crustal melting or contamination of basic magmas) for the generation of the earlier rocks also produced these dykes. Compared with the average Palmer Land granodiorite, these rocks are slightly more acidic with conspicuously lower CaO and higher K_2O, Rb, Zr, La and Ce, but the average of the four analysed dykes is almost identical with the average banded gneiss (Table XXV). However, the intrusive relationship of the dykes with respect to the metamorphic complex denies any involvement with the present exposed crustal level, and partial melting of a lower level must be considered instead. The rare plagioclase phenocrysts, which are more basic than those of either the banded gneisses or the granodiorites, are indicative of some form of contamination, possibly by fragments of relict amphibolite pods or, more likely by basic magmas. Although partial melting might have been initiated by lowering of the crust into higher temperature levels, the heat might also have been obtained from basic magmas such as those responsible for the (Tertiary) late dykes.

Table XXV. Chemical comparison of the average acid porphyry dyke and the average banded gneiss.

	1	*2*
SiO_2	66.66	68.14
TiO_2	0.44	0.49
Al_2O_3	16.12	15.60
Fe_2O_3	1.88	1.59
FeO	1.15	1.62
MnO	0.06	0.06
MgO	0.99	1.04
CaO	2.60	2.32
Na_2O	4.29	3.44
K_2O	3.75	3.70
P_2O_5	0.10	0.13
TRACE ELEMENTS (ppm)		
Cr	8	20
Ni	4	9
Rb	218	193
Sr	473	290
Y	47	43
Zr	334	281
Ba	1410	1022
La	35	32
Ce	80	62
Pb	35	40
K/Rb	146	169

1. Average of four acid porphyry dykes (Table XXIV, analyses 8–11).
2. Average of 16 banded gneisses (Table V, analyses 4–19).

6. Late basic and intermediate dykes

Igneous activity in western Palmer Land ceased (probably in the Tertiary) with the intrusion of an extensive suite of dykes, which have a strong lithological uniformity, apart from varying degrees of alteration. However, chemical analyses of several specimens revealed a range in the Thornton and Tuttle differentiation index (Table XXIII) from 33 to 57 (corresponding to a silica range of 45.71–57.93 %) and, recalling the classification adopted for the volcanic rocks (p. 47), the suite includes both basic and intermediate rocks. The distribution of these dykes is random; there are no definite intrusion centres, although locally several dykes occur in close proximity. The orientation of these dykes is seldom influenced by pre-existing structures (Figs 67, 68 and 69). However, in the Andean granite they frequently parallel vertical joints and at station KG.521.5 the microgabbros are concordant with the schistosity. Ranging from 15 cm to 15 m in width, these dykes have sharp contacts with the host rocks but macroscopic chilling is generally absent. Mineralization often followed the emplacement of these dykes and the joints of both the intrusion and the country rock are frequently veneered by calcite, epidote and rarely limonite. Pyritiferous clusters and large malachite stains were also recorded. Most of the dykes are formed of fine-grained blue-grey holocrystalline rocks in which weathering out of the plagioclase and less commonly the pyroxene phenocrysts results in a distinctive honeycomb texture. The plagioclase phenocrysts are predominantly euhedral, occurring as equant crystals (e.g. KG.557.3 and 557.4) or more commonly as laths averaging 1.5 mm in length and reaching a maximum of 3 mm. Their composition is mostly in the range An_{66-54} and, although some oscillatorily zoned crystals have cores of An_{72}, they are generally more acidic than those of the early basic dykes. Where microphenocrysts are present, they are of sodic labradorite or calcic andesine. Granular or

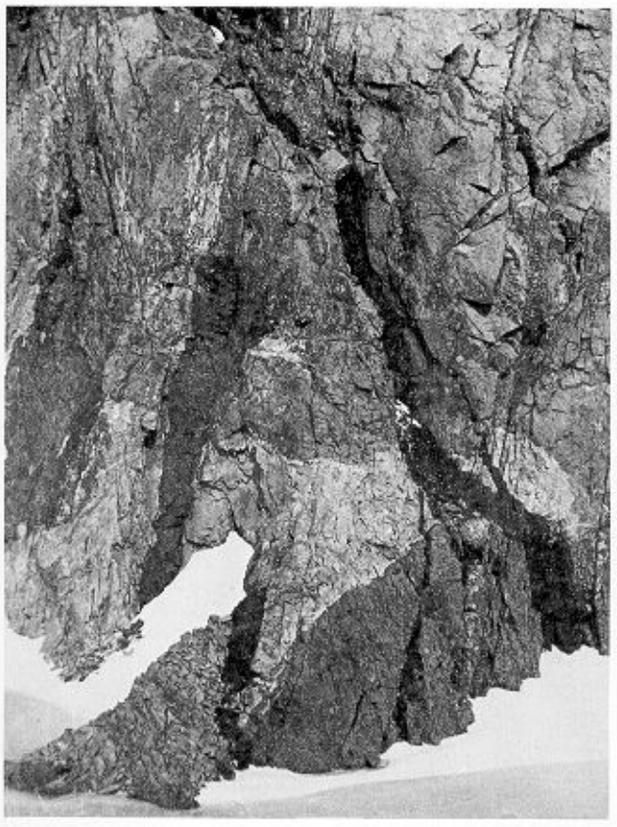

Fig. 68. Irregular late basic dykes (10–70 cm thick) cutting granodiorite and microgranite at station KG.548, Perseus Crags.

Fig. 69. One of the few late basic dykes whose orientation is controlled by major joint directions in Andean granodiorite (KG.552). The hammer shaft is 55 cm long.

euhedral epidote often replaces the plagioclase and sericite is frequently developed to the point of total replacement. The clinopyroxene, which forms slightly smaller (average 1 mm) euhedral phenocrysts, is predominantly a pale yellow or green to colourless augite with $\gamma : c = 43°$ and $2V_\gamma = 58°$, but in specimen KG.548.4 a pale pinkish variety with $2V_\gamma = 40°$ occurs. In most of the dykes examined, partial or complete replacement by one or more of the following aggregates has occurred:

calcite + chlorite + iron core,

calcite + chlorite + actinolite,

epidote + actinolite.

Whereas the other alteration products give rise to anhedral or occasionally (in the case of epidote) euhedral forms, the actinolite occurs in fibrous aggregates which have generally grown inwards from the margins. Locally (e.g. KG.547.1) the microphenocrysts are of a finer-grained granular (?) actinolite which also mantles the larger aggregates and is conspicuous in the groundmass in a finely divided form. Intergrowths of anhedral sphene and actinolite suggest that the two minerals crystallized together. As the augite does not appear to be particularly rich in titanium, the sphene must have originated from the late magmatic solutions. Pilotaxitic plagioclase (labradorite/andesine in the basic rocks and andesine/oligoclase in the intermediate ones) forms most of the groundmass with interstitial magnetite (and more rarely ilmenite), quartz, calcite and epidote. In addition to pyroxene, epidote and amorphous calcite, the groundmass of specimen KG.553.3 includes devitrified felsitic glass which shows partial spherulites and feathery structures, and contains acicular calcite (?) pseudomorphs. Devitrified glass also occurs within the chlorite-epidote-calcite pseudomorphs after (?) plagioclase and it presumably reflects the high-level nature of the intrusion. Where it is present, in the groundmass, acicular amphibole (e.g. KG.547.1 and 547.2) and pyroxene (KG.541.5) are intergrown with the plagioclase, whereas chlorite is characteristically interstitial. Of rather more limited extent are texturally similar dykes carrying magmatic hornblende rather than augite. This mineral is particularly well developed in specimen KG.529.5; its pleochroic scheme is α = straw, $\beta = \gamma$ = orange-brown and $\gamma : c = 21°$. In specimen KG.522.2 a slightly paler variety forms both phenocrysts up to 12 mm and glomeroporphyritic aggregates. Twinning is commonly developed and alteration to chlorite proceeds along narrow cracks. In both of these rocks, plagioclase phenocrysts are subordinate in size and numbers, and they are rather more acidic (An_{52}) than the usual variety. With α = pale yellow, β = brownish green, γ = pale green and $\gamma : c = 30°$, the hornblende in specimen KG.57.3 is slightly paler in colour than the hornblende in the host granodiorite but it is darker than those of the other intrusions (e.g. in specimen KG.547.2). Thus it probably represents a transition between common and uralitic hornblende.

At station KG.553.1 the banded gneisses are cut by a 3 m wide north-west trending dyke of hornblende-microgabbro, and 7.5 km to the south-east two sills intrude the quartz-mica-schists on the lower slopes of station KG.515. The lower intrusion is 4.5 m thick and comprises a homogeneous light green aggregate of plagioclase, hornblende and pyroxene with conspicuous iron staining. The higher sill, which crops out 18 m above, is a composite intrusion. Most of it is formed by a microgabbro that is slightly darker than the rock of the lower sill, but its lower 0.3 m are of a coarser-grained hornblende-microgabbro with needle-like hornblende phenocrysts up to 12 cm long. The contact between the two rock types is sharp with no apparent chilling, although numerous hornblende-microgabbro xenoliths indicate that the finer-grained rock was intruded at a slightly later time. Both of these rocks have sharp contacts with the country rock and xenoliths of quartz-mica-schist are freely distributed throughout. The dominant rock forming the sills (e.g. KG.515.7a) is a relatively fresh subophitic intergrowth of euhedral lath-like plagioclase and subhedral brown hornblende with stumpy prisms (frequently glomeroporphyritic) of pale yellow augite ($\gamma:c = 40°$ and $2V_\gamma = 60°$) and interstitial anhedral quartz. Plagioclase (An_{73-65}) crystallized simultaneously with hornblende (α = yellow, β = light brown, γ = brown and $\gamma:c = 25°$) which frequently nucleated on augite, the first mineral to form. Hornblende is commonly twinned, less frequently zoned and, unlike augite (which is frequently pseudomorphed by irregular intergrowths of calcite, chlorite and epidote), is only rarely altered to fibrous pale green penninite. At the northern outcrop (KG.533.1), plagioclase has been extensively replaced by sericite and epidote, and alteration of the augite has progressed almost to its total destruction though the hornblende remains relatively untouched. The essential mineralogy of the coarser hornblende-microgabbro xenoliths (e.g. KG.515.6) is similar, although most of the clinopyroxene has been replaced by brown hornblende or hydrothermally altered to penninite, epidote and haematite. Extensively sericitized zoned plagioclase is subophitically intergrown with hornblende and

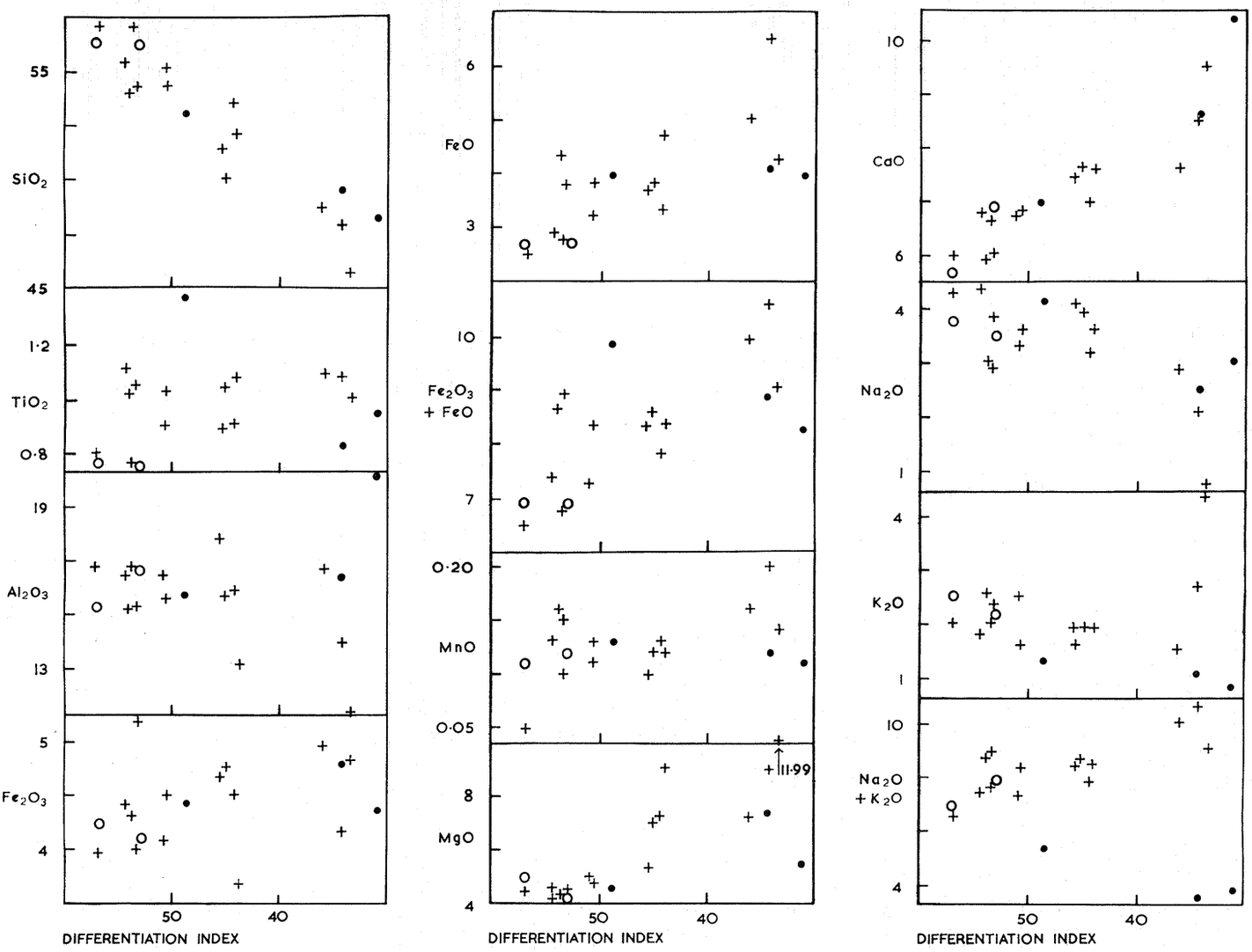

Fig. 70. Plots of major oxides (weight percentages), trace elements (ppm) and element ratios against the Thornton and Tuttle differentiation index for the late basic to intermediate dykes (+) and microgabbros (○). Plots of the early basic dykes (●) are superimposed for comparison.

frequently mantled by cloudy orthoclase which, together with the rare interstitial quartz, was probably derived from assimilated siliceous schists. The hornblende with α = yellow, $\beta = \gamma$ = orange-brown or yellow-brown and $\gamma:c = 27–30°$ shows a greater development of ophitic texture than in the augite-bearing microgabbro and skeletal grains are not uncommon. Zoning, displaced twin lamellae and irregular banding (similar to that of the banded olivines (p. 63)) are attributed to post-crystallization deformation, probably caused by stretching of the xenolith. The accessory minerals comprise subhedral skeletal ilmenite mantled by magnetite, sphene, rare anhedral iron pyrites and amygdaloidal calcite. The close association between the hornblende-microgabbros and the late intermediate dykes is particularly apparent (Table XXIII) in the TiO_2, MnO, MgO, Y and Zr contents. Indeed, the only significant differences between the two rocks are the higher concentrations of K_2O and related elements (Rb, Ba and Pb) in the microgabbros, and even these may be accounted for in terms of assimilated country rocks. Both specimens have higher CO_2 contents than the intermediate dykes and, whereas the marginally higher CaO content of specimen KG.515.3 suggests calcite, the chemistry of specimen KG.533.1 indicates a more dolomitic carbonate. On an A–F–M triangular diagram (Fig. 66), the 16 analysed rocks plot in the calc-alkaline field where they show a wide scatter and are displaced relative to the Andean basic rocks towards the alkali apex. These characteristics are also apparent on the Ca–Na–K diagram (Fig. 66) with the result that the field of the dykes is analogous to that of the Andean granodiorite. When the oxides and trace elements are plotted against the Thornton and Tuttle differentiation index (Fig. 70), curvilinear trends are only poorly defined but, as the scatter of points is not abnormally large when compared with those of the Mesozoic volcanic and Andean plutonic rocks (cf. Figs 54, 60 and 70), this probably reflects the absence of acid rocks.

Compared with the Mesozoic basic and intermediate volcanic rocks and the Andean gabbro–quartz-diorite assemblage, these late dykes have lower Al_2O_3, CaO and K/Rb

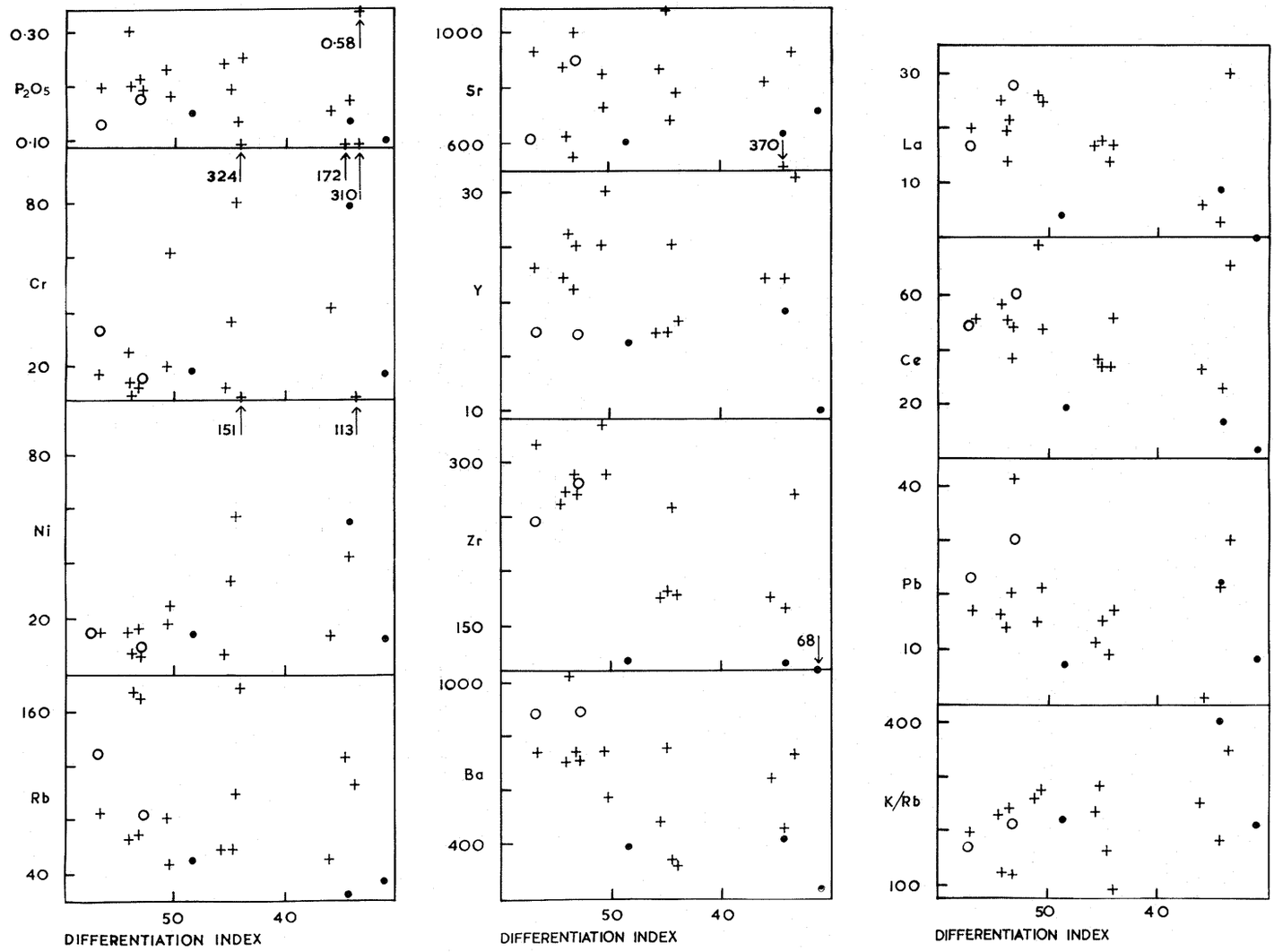

Fig. 70 continued

ratios, marginally higher MgO and higher K_2O (particularly relative to Na_2O), Rb, Ba and K/Na ratios. The most significant difference (both qualitatively and genetically) is the enrichment in K_2O which may be the result of:

i. Deuteric alteration.
ii. Assimilation of crustal material.
iii. An original feature of the magma.

An insight into the possible chemical changes during deuteric alteration is afforded by comparing the respective chemistries of the two hornblende-microgabbros (Table XXIII, analyses 26 and 27). The net effect would appear to be a decrease in Al_2O_3, CaO, P_2O_5 and Sr with a sympathetic increase in MgO, alkalis (particularly K_2O) and Rb. However, the increase in K_2O seems insignificant when compared with the difference between the dykes and earlier rocks. The absence of any significant rise in total alkalis with increasing SiO_2 (Fig. 71) is the expected trend of a contaminated magma, but specimen KG.553.5, which shows that greatest departure from the high-alumina field, has (p. 87) a devitrified glassy matrix perhaps resulting from rapid transport from depth. Such an intrusion would be less able to absorb country rock and in consequence is more likely to reflect the original composition of the magma. The absolute values of Rb, Ba, Sr and K/Rb ratios are closer to the shoshonitic association than to the calc-alkaline rocks (Jakes and White, 1972), though these rocks lack the typically high K/Na ratio (generally about unity) of true shoshonites. However, the overall increase in K_2O may indicate (Dickinson, 1968) that these dykes formed farther from the trench than the preceding rocks, and their shoshonitic affinities suggest they represent a later phase in the island-arc evolution (Jakes and White, 1972).

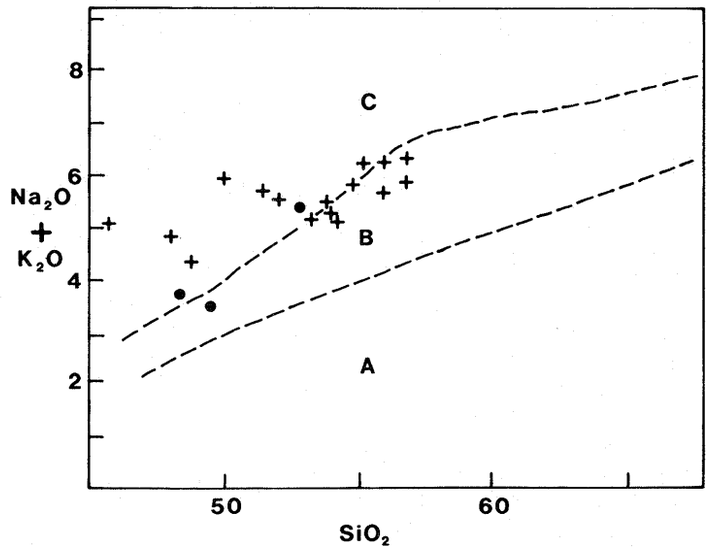

Fig. 71. Plot of $Na_2O + K_2O$ against SiO_2 (all weight percentages) for the late basic to intermediate dykes (+). Plots of the early basic dykes (●) are superimposed for comparison. Broken lines are boundaries between tholeiitic (A), high-alumina basalt (B) and alkali (C) fields (after Kuno, 1965).

VIII. STRUCTURES

As part of this reconnaissance survey, the orientations of structural features were noted wherever possible, but the number of observations is only sufficient to give a broad indication of the general structural trend of the area. The magnetic variation in this area is about 23°E; all field data were recorded and the orientation diagrams (Figs 72–75) have been plotted with respect to magnetic north.

1. Folds

Except for minor foliation flexures and numerous ptygmatic acid veins, folds are conspicuously absent from rocks of the metamorphic complex, particularly those of the banded gneiss group. This may be a feature of low-pressure metamorphism but the occurrence, albeit rare, of vague isoclines in quartz-plagioclase-amphibolites (? metavolcanic rocks) and, in Graham Land, of well-developed tight folds in apparently penecontemporaneous metasediments points to the lithology being the controlling factor.

2. Planar and linear structures

The remarkable constancy in orientation of the metamorphic foliation (and co-parallel banding) described on p. 7 is apparent in Fig. 72. Major variations in strike are restricted to the easternmost nunataks and, since these lie on or close to the roof of the granodiorite batholith, they are, in company with the relatively shallow dips, most probably the result of tilting during the intrusive episode. The low dips of the westernmost rocks may have resulted from similar movements or from down-warping along the adjacent north–south fault, while the moderately inclined schistosity of the central zone is a modification due to the third metamorphism.

The foliation and lineation of the main Andean granodiorite batholith are products of flow, presumably resulting from the injection of semi-crystalline magma. The lineations in the central parts of cupolas indicate a dominantly north-north-west–south-south-east horizontal movement, implying that the predominantly vertical foliation of the marginal zones developed by compression of the magma against a wall of metamorphic country rock. Since the Andean and metamorphic structures are essentially parallel, it follows that the envelope was delineated by pre-existing structures. The exact nature of the batholith's western margin is obscured but its presumed orientation is coincident with several major faults, and it is possible that these pre-existing structures took the form of faults which developed parallel to joint directions in the metamorphic complex. It has been demonstrated (Cobbing and Pitcher, 1972; Pitcher, 1972) that the emplacement of the Peruvian batholith was essentially fault-controlled.

3. Joints

Although some of the joints parallel the foliation in the metamorphic complex, those at right-angles predominate

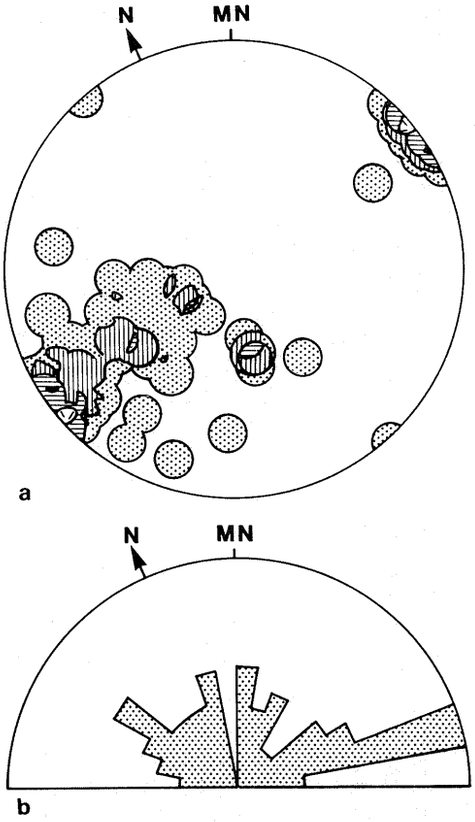

Fig. 72. Orientation diagrams for structures in the banded gneisses: a. Lower-hemisphere equal-area projection of poles to foliations; 52 points; contours at 2, 6, 10 and 16% per 1% area. b. Strike–frequency diagram for 183 joints.

(Fig. 72b). These cross joints developed before the third metamorphism (being host to the vertical younger amphibolites), presumably as a product of tension. Where flow structures are present in the Andean granodiorite, it is possible to distinguish cross, longitudinal and diagonal joints (Fig. 74a and c). Price (1966) noted that aplites or 'dyke' materials develop preferentially in cross joints, whereas in the granodiorites the microgranite dykes and veins are quasi-parallel to longitudinal joints. The orientation and sinuosity of the microgranites in fact suggest they were emplaced before the granodiorite had completely solidified and hence supports their suggested affinity (p. 84) with the granodiorites. On several of the nunataks on the south side of Bertram Glacier, the granodiorite is cut by horizontal or sub-horizontal joints which often give rise to mesa summits. Since these joints are restricted to the lineated rocks, it was assumed they were the 'flat-lying' members of the joint pattern, but near the summits they are closely spaced and resemble sheet joints (Price, 1966). As such, they may have formed in a number of ways including (Hills, 1963) expansion of the feldspar and ferromagnesian minerals on weathering, removal of the load of superincumbent rock by erosion, and seasonal variations in temperature affecting the rock near the surface. The mesas are frequently surmounted by small 'tor'-like structures up to 1.5 m high which are almost certainly post-glacial.

Since the granodiorites were emplaced mainly in the mesozone, only the roof is in contact with the volcanic rocks (Ayling, 1966) and the latter exert no influence on the orientation of the batholith. However, the granites are epizonal rocks and the close correspondence in the orientation of structures in the two groups is shown in Figs 74 and 75. In many instances the dominant vertical joints in the granite are very closely spaced, possibly reflecting late shearing. At station KG.501, gentle folding reduces the dip from 80° to 60°.

4. Faults

Small faults occur in the volcanic and sedimentary rocks; they are predominantly east–west and less commonly north–south trending with downthrows generally less than 10 m. The positive identification of displacements in the igneous and metamorphic rocks was more difficult but the wide range of crustal levels across the ice-filled valleys and the marked depression of the topography around Bertram Glacier (compared with the dissected plateau to the north and the Batterbee Mountains to the south) suggest extensive block faulting.

The abrupt topographical break, the rectilinearity of the coasts and the contrasting rock assemblages of Palmer Land

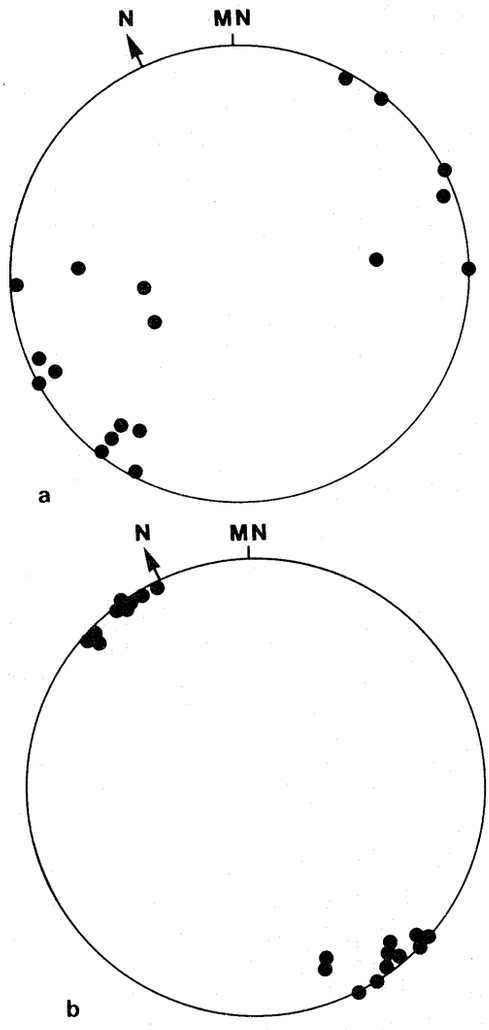

Fig. 73. a and b. Lower-hemisphere equal-area projections of (a) 15 poles to foliation and (b) 11 lineations in Andean granodiorites.

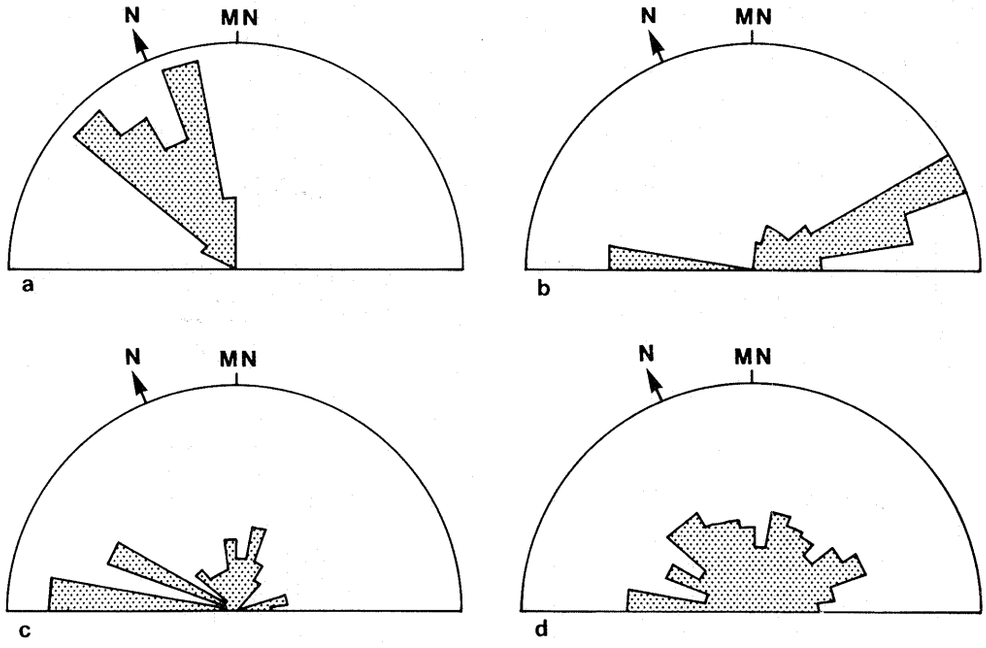

Fig. 74. Strike–frequency diagrams for joints in Andean granodiorites: a. Longitudinal (24); b. Cross (36); c. Diagonal (50); d. All (316). The number of readings is shown in brackets.

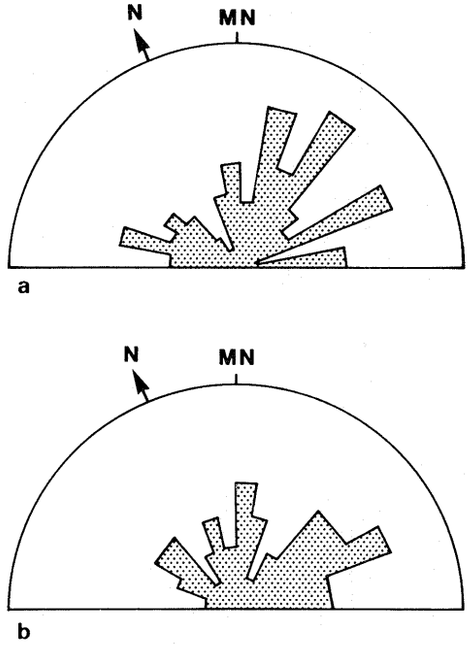

Fig. 75. Strike–frequency diagrams for joints in: a. Mesozoic volcanic rocks (89 readings); b. Andean granites (47 readings).

and Alexander Island leave little doubt that George VI Sound is a major tectonic feature. However, its structural origin is speculative, and from the considerable discussion which follows its discovery by the British Graham Land Expedition (Stephenson and Fleming, 1940) two contrasting hypotheses have emerged:

i. It is a rift valley bounded by faults generated by the uplift of a cymatogenic arch (King, 1964).

ii. Its inception was an integral part of the Alexander Island orogenesis and is not related to the uplift of Palmer Land. 'The uplift of a thick sequence of superimposed thrust sheets due to over-riding their marginal geanticline would result in the development of an eastward-facing mountain front or escarpment ... [which] ... would overlook the trough of George VI Sound, whose elevation would be reduced both by the under-thrusting movement and by isostatic depression by loading of the superimposed thrust sheet.' (Horne, 1967*a*, p. 21).

Horne's suppositions, which are based on field observations in south-eastern Alexander Island, require a northerly increase in compression, but this has not been substantiated by subsequent work in other parts of the island (Grikurov, 1972; Bell, 1974*b*). Regarding the age of the orogenesis in Alexander Island, Horne's only conclusion was that it was post-Aptian, but the main phase of deformation is not known to have preceded the emplacement of the camptonite dykes (Horne and Thomson, 1967) in the Miocene (15 $\pm$ 1 Ma ago; Rex, 1972). This implies that uplift occurred while the sediments were relatively unconsolidated, and Bell (1974*a*) has pointed out that in such a medium the evolution by thrusting of a major scarp and its subsequent survival is highly unlikely. Bell (1974*a*) has also noted the extension of the scarp beyond the northern limit of the Alexander Island sedimentary rocks and, more recently, gravity measurements have indicated a northerly extension of the George VI Sound trough of at least 190 km (personal communication from R. G. B. Renner).

Horne (1967*a*, p. 20) maintained that the west coast of Palmer Land is less elevated and more deeply dissected than might be expected for a fault scarp of supposed Tertiary age. However, the height of the coastal cliffs is partly masked by the greater thickness of ice on that side of George VI Sound, and the deep dissection probably developed as a result of block faulting in the following manner. The absence of thrusts and

reverse faults indicates that uplift occurred under conditions of regional tension and, hence, was probably controlled for the most part by isostatic adjustment. Thus the amount of vertical displacement would be far more varied on the Antarctic Peninsula than in the south-eastern part of Alexander Island.

One of Horne's principal arguments against the faulting hypothesis was the almost total absence of parallel faults in south-eastern Alexander Island. In Palmer Land, however, lithological breaks behind Wade (Fig. 4) and Gurney points (Fig. 2) imply the existence of a parallel fault which may extend northward along the western face of Creswick Peaks and this can certainly be traced southward into the Batterbee Mountains (Ayling, 1966). Otherwise, cataclasis is restricted to small crush zones, one of which had well-developed pseudo-ripple marks.

Under conditions of regional tension, movement would occur preferentially along pre-existing faults and boundaries without extensive crushing. Direct evidence of pre-existing structures around George VI Sound is lacking but it is noteworthy that the coastal scarps are parallel to the regional structural trend and that, in Upper Jurassic times, the outer (western) edge of the volcanic arc probably lay close to the Alexander Island coast.

IX. RECENT DEPOSITS

Despite the widespread evidence of current glacial retreat in Antarctica, only seven moraines were observed and two of these were lateral deposits on cirque glaciers. The largest, a 5 km lateral moraine on the north side of upper Millett Glacier, ranges from 60 to 6 m in width and is composed of frost-shattered boulders with occasional blocks up to 2 m in diameter. Scree cones, on which the maximum recorded angle of slope was 30°, rise above the general level of the deposit and resemble Priestley's (1923) hummocky moraines. It is noticeable that where this moraine emerges from the zone of perpetual shadow beneath the plateau edge it suffers a marked reduction in size, and the scree cones abruptly disappear, suggesting that there is an inverse relationship between the size of the moraines and the degree of insolation. Similar cones occur on the moraines in the amphitheatre 2 km to the north but, as these moraines receive considerable sunshine, their formation is probably a result of the blanket effect (Priestley, 1923). However, the size of these cones is related to the degree of insolation, since those nearest the cliffs on the northern side are the largest.

The two deposits on the south-western side of Perseus Crags were lateral moraines to an earlier larger glacier which flowed between the two adjacent rock outcrops. The smaller moraine is perfectly straight but the larger one is arcuate and probably represents the coalescence of the lateral moraine with a terminal deposit.

The paucity of supraglacial deposits can be attributed to a number of factors but it is primarily the result of the extremely high ratio of snow to exposed rock. Except for those deposits associated with cirque glaciers, the moraines occur exclusively below south-facing cliffs, and their intimate association with blue icefields suggests their appearance is due to local ablation by strong winds. The absence of such deposits on north-facing slopes, where the erosion potential is vastly greater, is due to:

i. The frequent occurrence of windscoops which prevent material reaching the surface of the glacier.
ii. The greater accumulation to cover debris.
iii. The rapid sinking of supraglacial material as demonstrated by occasional cryoconite holes.

The only englacial deposits observed on the north sides of glaciers were occasional rock fragments below patches of clear ice at the bottoms of windscoops.

X. CONCLUSIONS

A. Regional Correlations and Geological History

The Antarctic Peninsula represents a segment of the circum-Pacific orogenic belt. Its geology is dominated by post-Middle Jurassic magmatism and uplift, but not to the total exclusion of earlier events (Table XXVI).

Except for the white 'granites', the metamorphic complex of western Palmer Land has strong affinities with the Basement Complex of Neny Fjord, Marguerite Bay, in particular, the dominance of *ortho*gneisses over *para*schists (Fraser, 1965) and the number and intensity of the metamorphic events (Hoskins, 1963). A specimen from Marguerite Bay gave a Triassic Rb–Sr whole-rock age (200 ± 10 Ma; Halpern, 1972) and this is interpreted here as the age of the first or second metamorphism, since the third, certainly in western Palmer Land, occurred during Middle Jurassic (152 ± 7 Ma; Rex, 1972) times.

On the Bowman and Wilkins coasts (150 km south-east of Neny Fjord), Fraser and Grimley (1972) found wedges of possibly contemporaneous rocks (? *ortho*gneisses, amphibolites and mica-schists) but they were unable to elucidate their relationship with the surrounding assemblage of meta-sediments, metavolcanic rocks and synkinematic intrusions. The absence of chemical analyses of rocks from the east coast precludes any definite correlation with the west coast synkinematic intrusions but, if they are penecontemporaneous, by analogy with western Palmer Land, the east coast wedges are not only products of the same metamorphism but upthrust blocks of a higher-grade assemblage. Fraser and Grimley (1972) employed similar reasoning to explain the higher degree of metamorphism and migmatization of the sediments relative to apparently penecontemporaneous rocks in Graham Land. Since these sediments belong to the (?) Carboniferous Trinity

Table XXVI. Stratigraphy of western Palmer Land, and comparison with the Alexander Island and Graham Land successions.

			Western Palmer Land		*Alexander Island*	
			Stratigraphy	*Stratigraphical and tectonic events*	*Adie (1964a), Bell (1974a), Elliott (1974)*	*Graham Land Adie (1964a)*
Cenozoic	Quaternary		Moraines	Glaciation and deposition	Moraines (glaciation)	Sea-level changes (Recent) Glaciation (Pleistocene) Pecten Conglomerate (Pliocene)
					Palagonite-tuffs and olivine-basalts Block faulting and southerly tilting Erosional planation	
						(Osterrieth Range volcanic rocks and associated dykes) (M. Miocene)
	Tertiary			Erosion, planation, block faulting and uplift	Camptonite dykes (M. Miocene)	James Ross Island Volcanic Group
						Seymour Island (L. Miocene)
			Basic and intermediate dykes ((?) Eocene–Oligocene)	Intrusion	Dolerite dykes	
		(?)	Acid porphyry dykes	Intrusion		Andean Intrusive Suite (late Cretaceous to early Tertiary)
		Upper			Hornblende-porphyry-tuffs and agglomerates	Snow Hill Island Cape Longing Series (U. Cretaceous)
	Cretaceous (?)	Middle	Gabbro–granite (Andean Intrusive Suite) and early basic dykes	Intrusion		O'Higgins Formation
		Lower	Basalt rhyodacite volcanic group	Extrusion. Minor erosion and sedimentation	Fossil Bluff Series	
Mesozoic		Upper	Mudstones, conglomerates, sandstones and basalts)	Sedimentary deposition and minor extrusion	Ablation Point Beds and Belemnite Point Beds	Andesite-rhyolite volcanic group (U. Jurassic)
	Jurassic (?)	Middle	Granodiorite and diorite	Intrusion	Granite, granodiorite and micro-granodiorite (age uncertain)	Mount Flora plant beds
				Metamorphism		Church Point plant beds (M. Jurassic)
			Sheared banded gneisses			
		(?) Lower	Younger amphibolites	Intrusion	Diorite (age uncertain)	Basal-conglomerate
				Metamorphism		
	(?) Triassic		Older amphibolites	Intrusion		
				Metamorphism		
			Metagabbros Diorite-gneisses Banded gneisses	Synkinematic intrusions		
	(?) Carboniferous		Quartz-plagioclase-amphibolites	(?) Extrusion	Sedimentary and volcanic rocks	Trinity Peninsula Series
Palaeozoic	(?) Palaeozoic		White 'granites'	(?) Intrusion	Volcanic rocks ((?) Early Palaeozoic)	Intrusive Suite Volcanic rocks ((?) Early Palaeozoic)
						Basement Complex ((?) Precambrian)

Peninsula Series (Adie, 1957; Grikurov and Dibner, 1968), it follows that the metamorphism is post-Palaeozoic, thus substantiating the radiometric evidence.

It would appear then that the western Palmer Land metamorphic complex was created during the early Mesozoic Gondwanian (Du Toit, 1937) or Ellsworth (Craddock, 1972) orogeny and, since most of the constituent units are synkinematic intrusions, it follows that this was also a period of extensive calc-alkaline magma generation. No data on the grade of the first metamorphism in Neny Fjord are available but it must be assumed to have exceeded the almandine-amphibolite grade of the second, while the occurrence of cummingtonite in some of the east coast rocks (Fraser and Grimley, 1972) suggests that high temperature–low pressure conditions, similar to those of western Palmer Land, prevailed.

Both the quartz-plagioclase-amphibolites and the white 'granites' are considered to have been in existence prior to the first metamorphism. It has been suggested (p. 43) that the former are metavolcanic rocks and as such may be analogous to rocks lying above the (?) Carboniferous Trinity Peninsula

Series on the east coast. Although they are absent from the western part of the Antarctic Peninsula, presumed Carboniferous sedimentary rocks have been recorded in central Alexander Island (Grikurov and Dibner, 1968; Bell, 1973*b*, 1974*a*, *b*), where they do in fact contain a high proportion of volanic debris.

The relationship of the white 'granites' to the quartz-plagioclase-amphibolites is not known but they definitely pre-date all other rocks of the metamorphic complex and are probably the oldest in this area. Of limited occurrence in Palmer Land, they are totally unrecorded in Graham Land and, since the magnitude of uplift of the northern half of the peninsula is somewhat less than in Palmer Land, it is possible that they represent a deeper crustal level. They are most probably Palaeozoic or even Precambrian, though no age greater than 502 Ma (Craddock, 1970*a*) has not so far been recorded in western Antarctica. Whatever their age, they point to the existence of pre-Mesozoic continental crust beneath the Antarctic Peninsula, and the presence of deep-water sediments amongst the (?) Carboniferous of Alexander Island confirms that the western continental slope lay in the general area of central Alexander Island.

The older (or pre-Upper Jurassic) granodiorites and associated diorites were not considered to be a part of the metamorphic complex, because they lack evidence of deformation and such structures as they do possess are attributable to flow. It has been noted (p. 45), however, that the granodiorites have features typical of late-kinematic granites. They must pre-date the third metamorphism and, since they also pre-date the deformation of the older amphibolites, it is concluded that they were emplaced late in the second metamorphism. A Lower to Middle Jurassic age is therefore inferred.

Bell (1974*a*) has described similar plutonic rocks from Alexander Island which he tentatively assigned to the Lower and Middle Jurassic, though their relationship with the surrounding rocks is far from certain. In Graham Land, some of the pre-Upper Jurassic plutonic rocks were assigned an early Palaeozoic age (Adie, 1954; Goldring, 1962) mainly on the basis of their relationship to the (supposed Precambrian) Basement Complex. However, no age greater than 200 Ma has been obtained from these metamorphic rocks and West (1974) has shown that, on the Danco Coast, the early plutonic rocks pre-date the (?) Carboniferous Trinity Peninsula Series. Thus it is possible that these intrusions are contemporaneous with the (?) Middle Jurassic rocks of western Palmer Land.

The sedimentary hiatus which persisted (apparently continuously) from the end of the Carboniferous to the beginning of the Upper Jurassic points to an emergent but planed peninsula. Uplift evidently commenced towards the end of the Middle Jurassic, presumably at the close of the Gondwanian orogeny and, in view of the apparent instability of the Carse Point basin and the early (relative to Alexander Island) cessation of sedimentation therein, it extended well into the Upper Jurassic.

The rocks of the east coast of Alexander Island immediately west of Carse Point have not yet been described but viewed from some distance they appear to be stratified. They may therefore represent a northerly extension of the Upper Jurassic–Lower Cretaceous sedimentary assemblage of south-eastern Alexander Island (Taylor, 1966; Horne, 1967*b*). Since these rocks young to the south (Horne, 1967*a*) and Oxfordian–Middle Kimmeridgian belemnites (Willey, 1973) occur at Belemnite Point (50 km south of Carse Point), it is possible that, in the latitude of Carse Point, Upper Jurassic stratified rocks are present on both sides of George VI Sound.

The first detailed synthesis of the sedimentological and tectonic history of south-eastern Alexander Island (Horne, 1969) envisaged the basin as a 'back trough related to an early Mesozoic orogenic phase', a concept which in the light of more recent work (Bell, 1974*a*, *b*) demands some modification. The understanding of the tectonic setting cannot be criticized, particularly as the rocks show no evidence of geosynclinal type deformation. However, the existence of a mainly volcanic geanticline on the western margin has been discounted by Bell (1974*a*), and Horne's shelf and shelf-edge facies have been re-interpreted as the western continental shelf and continental edge, respectively, of Antarctica. Thus, there would have been a westerly thinning of continental crust, and it may be that the relative movements between the Antarctic Peninsula and Alexander Island were primarily the result of gravity differences.

There were no indications at Carse Point of palaeocurrent direction but Taylor (1966), Horne (1969) and Elliott (1974), on the basis of both lithology and facies change, were able to establish a predominantly westerly transport direction. Moreover, these workers have shown that, south of Belemnite Point, the shoreline lay close to the present east coast of Alexander Island throughout the history of the basin. Thus, if the Carse Point depositional basin represents an easterly extension of Horne's (1969) shelf facies, there must have been a fairly dramatic change in the orientation of the coastline. This may be interpreted as evidence of a channel through the peninsula. It is possible that the purple and green volcanic sandstones, which Skinner (1973) recorded 45 km north-east of Carse Point, were deposited close to the shoreline of this channel.

In marked contrast to Alexander Island, where subsidence continued into the Aptian, the Carse Point rocks are conformably overlain by apparently subaerially erupted volcanic rocks. However, the high proportion of volcanic debris in some of the Alexander Island units, in particular the Upper Jurassic Belemnite Point beds, indicates their close proximity to the western edge of the volcanic arc. Thus, the area now comprising George VI Sound probably contained several large volcanoes between which westerly flowing rivers continued to feed the Alexander Island basin. It is therefore possible that the present somewhat scattered distribution of volcanic rocks in western Palmer Land is an original and not an erosional or tectonic feature. Since the Upper Jurassic in Graham Land is represented almost exclusively by volcanic rocks and the Jurassic Latady Formation of the Lassiter Coast (Williams and others, 1972) is overlain by lavas and tuffs, it is evident that the arc incorporated the whole of the Antarctic Peninsula and that its eastern boundary lay close to the present east coast.

Determination of an upper age limit for the volcanic rocks was not possible in this area but it is evident from Alexander Island that activity continued spasmodically into the Cretaceous and hence could have overlapped the probable time span of the batholiths. Although the Andean batholiths form the root zones of volcanoes in parts of Chile and Peru

(Hamilton, 1969; Cobbing and Pitcher, 1972), there is no apparent connection between them in western Palmer Land. Indeed, notwithstanding the obvious chemical differences between the two groups, some of the plutonic rocks are seen to intrude and metamorphose the volcanic rocks.

The post-Upper Jurassic plutonic rocks have been compared with the Andean intrusions of Graham Land which invariably display a basic to acid trend (Adie, 1955) and demonstrate a similar preponderance of granodioritic rocks. The apparent absence of ultrabasic rocks outside this area is presumed to be an erosional feature.

The Andean evolutionary trend was originally considered by Adie (1955) to reflect fractional crystallization of a basic magma, and it has been shown that such a process could have produced the quartz-diorites and granites. The absence of layering in the gabbros of this area and the subsequent intrusion of the ultrabasic rocks militate against *in situ* differentiation and, coupled with the obviously late-stage deformational features (p. 63), suggest that emplacement occurred some time after the magma had begun to crystallize.

The granodiorites do not plot on the fractionation curves and there are many features, including their immense volume relative to gabbro and certain chemical affinities with the banded gneisses, which point to them being re-melted *ortho*gneisses. Like the gabbros, emplacement occurred when the magma was quite viscous but, in view of the common orientation of their structures, this occurred under slight directional stress. In common with most of the major batholiths throughout the length of the Antarctic Peninsula, the granodiorites are aligned parallel to its main structural trend which, in this area, means parallelism with the metamorphic foliation and the trend of major faults. Such an association of compression, faulting and intrusion is an environment comparable to that of the Peruvian batholith, which Cobbing and Pitcher (1972) believed was emplaced in an envelope bounded by wrench faults. Their concept of doming and upward displacement of the roof is the type of situation which would be expected to develop in a relatively viscous magma (such as the granodiorite) which would also be incapable of incorporating much roof material.

The granodiorite magma was apparently quite rich in volatiles, which gave rise to an extensive network of microgranite and pegmatite veins. In marked contrast, the granites were quite dry and only rarely developed apophyses. They are essentially high-level intrusions and their orientation was determined by faults and joints in the volcanic rocks. Thus, it can be concluded that in the late Mesozoic regional compression was succeeded by an episode of regional tension which outlasted the post-Andean dyke phase.

Within this episode of minor intrusions, acid porphyries were locally prominent but by far the majority are constituents of a later basic to intermediate suite which represents the final magmatic event in this area. Since these rocks pre-date planation and uplift, they are almost definitely Tertiary in age and are probably contemporaneous with the widespread post-Andean basic dykes of Graham Land. Similar dykes are less common in Alexander Island (Bell, 1973*b*, 1974*b*) and their relationship to the Miocene (15 ± 1 Ma) camptonite dykes (Horne and Thomson, 1967; Rex, 1972) is unknown. Since the camptonites are relatively undeformed and are only found on the eastern coastal scarp, their emplacement would appear to be connected with the formation of George VI Sound and hence (p. 92) with the major uplift. Thus, it would seem that the Tertiary basic dykes of Alexander Island and western Palmer Land are older than the Miocene camptonites. It is possible that they formed during the Eocene–Oligocene magmatic episode which is represented by volcanic rocks on Tower and Two Hummock islands off the west coast of Graham Land (Rex, 1972).

Although late Tertiary to Recent volcanic rocks occur in a few specific areas, for most of the Antarctic Peninsula the post-Oligocene history can be summarized under three headings which, in chronological order, are planation, uplift and glaciation. From the above discussion, it would seem that the main uplift occurred more than 15 Ma ago. The higher proportion of older rocks and the corresponding lack of supercrustal rocks (relative to Graham Land) supports Fraser and Grimley's (1972) suggestion that uplift was a more pronounced feature in Palmer Land.

B. Geological History and Plate Tectonics

Several unusual features, including the great differences in intensity between the Gondwanian and Andean orogenies and the gradual increase in the potash content of the magmas are best understood by a re-appraisal of the geological history with respect to the plate-tectonic hypothesis and to the geological histories of adjacent areas (such as South America and continental Antarctica).

It is now generally accepted that the break-up of the Gondwana supercontinent commenced in the Mesozoic with initial rifting between Antarctica and the Africa–America block. Opinion on the exact date of this event is, however, divided (e.g. cf. Dietz and Holden (1970) with Elliot (1972)) mainly because different workers have employed differing techniques. Smith and Hallam (1970) suggested this event took place in Upper Jurassic–Lower Cretaceous times based on the age of the Serra Geral volcanic rocks. Concurrent with this break-up, oceanic crust was being produced along the East Pacific Rise and consumed below the western continental margin of Antarctica. The setting of western Antarctica in fact was analogous to that of the west coast of South America: the type area of Dewey and Bird's (1970) Pacific, or Andean, plate junction.

The recent discovery of Cretaceous magnetic anomalies in the Bellingshausen Sea (Hayes, 1971), together with records of a Triassic Benioff Zone-related magmatism and metamorphism in parts of western Antarctica indicate that subduction commenced early in the Mesozoic. Because the peninsula has, probably since the (?) late Palaeozoic, occupied a position close to the continental margin of western Antarctica, its Mesozoic geology would be expected to provide some indication of the position of the Benioff Zone. Thus, the combination within the metamorphic complex of considerable volumes of calc-alkaline intrusions (the banded gneisses), and conditions of high temperatures and low pressures, points to Palmer Land being above and presumably east of the subduction zone. The trench would then have lain below Alexander Island and it is remotely possible that the highly sheared (?) Carboniferous sediments, with their deep-water affinities and basic volcanic fragments, accumulated in such an environment and were subsequently

deformed in the high pressure–low temperature 'paired' metamorphic belt (Miyashiro, 1973). Metamorphism in such an environment normally reaches the blue-schist facies and, since these rocks reflect a somewhat lower grade (zeolite facies), they are considered more likely to be deep-sea sediments scraped off the down-going plate and deposited on the overlying continental edge. However, as such, they would still confirm the close proximity of the trench.

A re-interpretation of Blundell's (1962) palaeomagnetic data by Dalziel and others (1973) suggested the present shape of the Antarctic Peninsula has persisted since before the beginning of the Cretaceous and therefore must be Gondwanian or even older. The distinctive curvature of the Antarctic Peninsula resembles that of the Mesozoic fold belt through the Ellsworth and Pensacola Mountains (Craddock, 1970*b*) and, since the mountain arcs differ in trend by approximately 30°, it is possible that the Antarctic Peninsula has rotated in an anti-clockwise direction relative to continental Antarctica. A seismic traverse across the largely snow-covered base of the Antarctic Peninsula (Bentley, 1973) revealed a tectonic break which was assumed to be a fault, but it could equally well be a hinge zone.

Since the overall geology of the Upper Jurassic and Cretaceous is now more fully understood, it is possible to consider the various areas and assemblages in terms of Dickinson's (1971) reconstructions of past arc–trench systems. To date there is no evidence of typical trench assemblages in western Alexander Island but it should be remembered that the arc in question is largely snow-covered and, as yet, not completely surveyed.

If the western margin of the volcanic arc was concordant with the present east coast of Alexander Island, the eastern part of this island would have formed the arc trench gap. The Mesozoic sediments of south-eastern Alexander Island, inasmuch as they are undisturbed and undeformed, and accumulated on unstable shelves and transverse slopes, are typical of such an environment (Dickinson, 1971).

In contrast to the sections illustrated by Dickinson, the ratio of the arc width to that of the arc–trench gap is greater than unity. The actual width of the arc–trench gap is, of course, directly related to the slope of the down-going plate, and hence the comparatively narrow feature in this area is further evidence of a steeply dipping subduction zone.

In many respects, the structures of the back arc are more important, because the style and intensity of the deformation appears to be dependent on whether a marginal basin or continent is adjacent. The essentially low-key deformation of Mesozoic sediments on the east coast of Graham Land (Elliot, 1966) has led Dalziel (1974) to consider the existence of a marginal basin in the Weddell Sea, though with the present state of knowledge of that section of Antarctica this is highly speculative. On the other hand, at the southern end of the Antarctic Peninsula (Williams and others, 1972) the deformation is of sufficient intensity to warrant the closer proximity of continental Antarctica. The most plausible explanation of this apparent contradiction requires that when the marginal basin opened in the Weddell Sea, the rate of spreading was much greater in the north, which in turn could have resulted in an anti-clockwise rotation of the Antarctic Peninsula about its base.

Since the spreading is assumed to have taken place between the beginning of the Upper Jurassic and the end of the Cretaceous (Elliot, 1972), it must have occurred coincidentally with the initial southerly drift of Antarctica. Rifting between South America and the Antarctic Peninsula is a pre-requisite to movement in such a direction, and its absence may have been the result of either transform faulting between eastern and western Antarctica (Elliot, 1972) or clockwise rotation of continental Antarctica as suggested above.

The earlier views that the Antarctic Pensinsula is a southerly continuation of the South American Andes was based primarily on petrological and chemical comparisons with apparently contemporaneous magmatic rocks in Chile (e.g. Barrow, 1831; Adie, 1954). It was also clear that, both north and south of Drake Passage, the major uplift (and some of the intrusive episodes) occurred during the late Mesozoic–early Cenozoic. More recent work (e.g. Katz, 1972; Dalziel, 1974) has revealed significant differences in the direction, intensity and style of the South American deformation compared with the Antarctic Peninsula which indicate that the two areas probably evolved separately. Furthermore, because the deformation in Patagonia could be related to the closure of a marginal basin, Dalziel (1974) concluded that no such event had occurred south of Drake Passage, which adds some support to the concept that the Weddell Sea formed as a post-Middle Jurassic marginal basin. In passing, it is interesting to speculate on the difference in intensity between the two orogenies in Palmer Land, particularly whether the intense deformational Gondwanian episode was coupled with the closure of a pre-Mesozoic marginal basin.

In parts of Peru and Chile, magmatism appears to have migrated with time away from the trench (James, 1971; Levi, 1973), a feature which could have resulted from attrition of the western continental edge, presumably by the down-going plate. No sense of movement was detectable in western Palmer Land but the scarcity (Williams and others, 1972) or total absence (Fraser and Grimley, 1972) of Tertiary dykes in parts of the east coast may be interpreted as evidence of a westerly (or trenchward) migration. However, the gradual increase in the K_2O/Na_2O ratios of successive magmas reflects increasing distances from the trench, and it would seem that as western Antarctica grew by accretion throughout the Mesozoic and early Cenozoic the subduction zone underwent progressive westerly displacement. In this respect, the contrasting behaviours of South America and the Antarctic Peninsula probably reflect differing rates of plate convergence, for the former has been moving (apparently continuously) since the Mesozoic, whereas Antarctica has been stationary since the late Cretaceous (Francheteau and Sclater, 1969).

Finally, there are many aspects of the geology of the Antarctic Peninsula which invite comparisons with Japan, in particular, the generation of an island arc on continental crust and the possible presence of an extensive marginal basin. Japan is known to comprise a number of interpenetrant arc–trench systems (Dickinson, 1971) and, hence, if the above comparison between these two regions is valid, the preceding account of the geological history is probably a gross oversimplification. However, the recent discovery (Davey, 1972) of a small trench on the oceanic side of the South Shetland Islands and the somewhat sporadic distribution of the late Tertiary–Recent volcanic centres (Baker, 1972; Bell, 1973*a*) may indicate a number of arc–trench systems in the Antarctic Peninsula. It is possible that, amongst the older rocks of the peninsula, the frequent juxtaposition of differing assemblages is the result of different arc–trench systems rather than of block-faulting.

XI. ACKNOWLEDGEMENTS

I wish to thank Professors F. W. Shotton and A. Williams for making available the facilities of the Department of Geological Sciences, University of Birmingham, and Dr R. J. Adie for his supervision of this work. The helpful advice and assistance of colleagues in the Department of Geological Sciences and at Stonington Island is gratefully acknowledged. I am indebted to D. Horley for his plane-table surveys and the use of several photographic negatives. Finally, I wish to thank my wife for checking the manuscript and for her constant support and encouragement.

XII. REFERENCES

ADIE, R. J. 1954. The petrology of Graham Land: I. The Basement Complex; early Palaeozoic plutonic and volcanic rocks. *Falkland Islands Dependencies Survey Scientific Reports*, No. 11, 22 pp.

ADIE, R. J. 1955. The petrology of Graham Land: II. The Andean Granite–Gabbro Intrusive Suite. *Falkland Islands Dependencies Survey Scientific Reports*, No. 12, 39 pp.

ADIE, R. J. 1957. The petrology of Graham Land: III. Metamorphic rocks of the Trinity Pensinsula Series. *Falkland Islands Dependencies Survey Scientific Reports*. No. 20, 26 pp.

ADIE, R. J. 1964*a*. Stratigraphic correlation in west Antarctica. (*In* ADIE, R. J., *ed. Antarctic geology*. Amsterdam, North-Holland Publishing Company, 307–13.)

ADIE, R. J. 1964*b*. The geochemistry of Graham Land. (*In* ADIE, R. J., *ed. Antarctic geology*. Amsterdam, North-Holland Publishing Company, 541–7.)

AHRENS, L. H., PINSON, W. H. *and* KEARNS, M. M. 1952. Association of rubidium and potassium and their abundance in common igneous rocks and meteorites. *Geochim. cosmochim. Acta*, **2,** No. 4, 229–42.

ASKLUND, B. 1925. Petrological studies in the neighbourhood of Stavsjö at Kolmården. Granites and associated basic rocks of Stavsjö area. *Sver. geol. Unders.*, Ser. C, No. 325, 1–122. [Årsbok 17 (1923) No. 6.]

AYLING, M. E. 1966. *The geology of the 'St. Valentine's' area, and related observations in the Batterbee Mountains, Palmer Land.* M.Sc. thesis, University of Birmingham, 119 pp. [Unpublished.]

BAKER, P. E. 1968. Comparative volcanology and petrology of the Atlantic island-arcs. *Bull. volcan.*, Sér. 2, **32,** No. 1, 189–206.

BAKER, P. E. 1972. Recent volcanism and magmatic variation in the Scotia arc. (*In* ADIE, R. J., *ed. Antarctic geology and geophysics*. Oslo, Universitetsforlaget, 57–60.)

BARAZANGI, M., ISACKS, B., OLIVER, J., DUBOIS, J. *and* PASCAL, G. 1973. Evidence for detached slabs. *Nature, Lond.*, **242,** No. 2, 98–101.

BARKER, D. S. 1970. Compositions of granophyre, myrmekite, and graphic granite. *Geol. Soc. Am. Bull.*, **81,** No. 11, 3339–50.

BARROW, J. 1831. Introductory note. (*In* KENDALL, E. N. Account of the island of Deception, one of the New Shetland Isles. *J. R. geogrl Soc.*, **1,** 62–6.)

BARTH, T. F. W. 1969. *Feldspars*, New York, London, Sydney, Toronto, Wiley-Interscience (John Wiley and Sons Inc.).

BECKE, F. 1908. Über Myrmekit. *Mineralog. petrogr. Mitt., N.S.*, **27,** 377–90.

BELL, C. M. 1973*a*. The geology of Beethoven Peninsula, south-western Alexander Island. *British Antarctic Survey Bulletin*, No. 32, 75–83.

BELL, C. M. 1973*b*. The geology of southern Alexander Island. *British Antarctic Survey Bulletin*, Nos. 33 and 34, 1–16.

BELL, C. M. 1974*a*. *The geology of parts of Alexander Island.* Ph.D. thesis, University of Birmingham, 125 pp. [Unpublished.]

BELL, C. M. 1974*b*. Geological observations in northern Alexander Island. *British Antarctic Survey Bulletin*, No. 39, 35–44.

BENTLEY, C. R. 1973. Crustal structure of Antarctica. *Tectonophysics*, **20,** Nos. 1–4, 229–40.

BINNS, R. A. 1965. Hornblendes from some basic hornfelses in the New England region, New South Wales. *Mineralog. Mag.*, **34,** No. 268, 52–65.

BLATT, H. *and* CHRISTIE, J. M. 1963. Undulatory extinction in quartz of igneous and metamorphic rocks and its significance in provenance studies of sedimentary rocks. *J. sedim. Petrol.*, **33,** No. 3, 559–79.

BLUNDELL, D. J. 1962. Palaeomagnetic investigations in the Falkland Islands Dependencies. *British Antarctic Survey Scientific Reports*, No. 39, 24 pp.

BLYTH, F. G. H. 1940. The nomenclature of pyroclastic deposits. *Bull. volcan.*, Sér. 2, **6,** 145–56.

BOWES, D. R. *and* PARK, R. G. 1966. Metamorphic segregation banding in the Loch Kerry basite sheet from the Lewisian of Gairloch, Ross-shire, Scotland. *J. Petrology*, **7,** Pt. 2, 306–30.

CARMAN, J. H. *and* TUTTLE, O. F. 1963. Experimental study bearing on the origin of myrmekite. *Spec. Pap. geol. Soc. Am.*, No. 76, 29.

CARR, M. H. *and* TUREKIAN, K. K. 1962. Chromium in granitic rocks. *Geochim. cosmochim. Acta*, **20,** No. 3, 411–15.

CARSTENS, H. 1967. Exsolution in ternary feldspars. II. Intergranular precipitation in alkali feldspar containing calcium in solid solution. *Contr. Miner. Petrol. (Beitr. Miner. Petrogr.)*, **14,** No. 4, 316–20.

COBBING, E. J. *and* PITCHER, W. S. 1972. The coastal batholith of central Peru. *J. geol. Soc. Lond.*, **128,** Pt. 5, 421–51.

CONDIE, K. C., BARSKY, C. K. *and* MUELLER, P. A. 1969. Geochemistry of Precambrian diabase dikes from Wyoming. *Geochim. cosmochim. Acta*, **33,** No. 11, 1371–88.

CRADDOCK, C. 1970*a*. Radiometric age map of Antarctica. (*In* BUSHNELL, V. C. *and* CRADDOCK, C., *eds.* Geologic maps of Antarctica. *Antarct. Map Folio Ser.*, Folio 12, Pl. XIX.)

CRADDOCK, C. 1970*b*. Tectonic map of Antarctica. (*In* BUSHNELL, V. C. *and* CRADDOCK, C., *eds.* Geologic maps of Antarctica. *Antarct. Map Folio Ser.*, Folio 12, Pl. XXI.)

CRADDOCK, C. 1972. Antarctic tectonics. (*In* ADIE, R. J., *ed. Antarctic geology and geophysics*. Oslo, Universitetsforlaget, 449–55.)

DALZIEL, I. W. D. 1974. Evolution of the margins of the Scotia Sea. (*In* BURK, C. A. *and* DRAKE, C. L., *eds. Geology of continental margins*. Berlin, Springer-Verlag, 567–79.)

DALZIEL, I. W. D., KLIGFIELD, R., LOWRIE, W. *and* OPDYKE, N. D. 1973. Paleomagnetic data from the southernmost Andes and Antarctandes. (*In* TARLING, D. H. *and* RUNCORN, S. K., *eds. Implications of continental drift to the earth sciences*. New York, Academic Press, 87–101).

DAVEY, F. J. 1972. Marine gravity measurements in Bransfield Strait and adjacent areas. (*In* ADIE, R. J., *ed. Antarctic geology and geophysics*. Oslo, Universitetsforlaget, 39–45.)

DEER, W. A. 1938. The composition and paragenesis of the hornblendes of the Glen Tilt complex, Perthshire. *Mineralog. Mag.*, **25,** No. 161, 56–74.

DEER, W. A., HOWIE, R. A. *and* ZUSSMAN, J. 1963. *Rock-forming minerals. Vol. 2. Chain silicates*. London, Longmans, Green and Co. Ltd.

DEWAR, G. J. 1965. *The geology of Adelaide Island, British Antarctic Territory.* Ph.D. thesis, University of Birmingham, 189 pp. [Unpublished.]

DEWEY, J. F. *and* BIRD, J. M. 1970. Mountain belts and the new global tectonics. *J. geophys. Res.*, **75,** No. 14, 2625–47.

DICKINSON, W. R. 1968. Circum-Pacific andesite types. *J. geophys. Res.*, **73,** No. 6, 2261–9.

DICKINSON, W. R. 1971. Reconstruction of past arc-trench systems from petrotectonic assemblages in the island arcs of the western Pacific. (*In Pacific Science Congress. The Western Pacific*. Perth, University of Western Australia, 569–601.)

DIETZ, R. S. *and* HOLDEN, J. C. 1970. Reconstruction of Pangaea: breakup and dispersion of continents, Permian to present. *J. geophys. Res.*, **75,** No. 26, 4939–56.

DOAN, G. E. 1958. *The principles of physical metallurgy*. New York, McGraw-Hill Book Company Inc.

DOTT, R. H. 1963. Dynamics of subaqueous gravity depositional processes. *Bull. Am. Ass. Petrol. Geol.*, **47,** No. 1, 104–28.

DRURY, S. A. 1973. The geochemistry of Precambrian granulite facies rocks from the Lewisian complex of Tiree, Inner Hebrides, Scotland. *Chem. Geol.*, **11,** 167–88.

DU TOIT, A. L. 1937. *Our wandering continents*. Edinburgh, Oliver and Boyd.

ELLIOT, D. H. 1966. Geology of the Nordenskjöld Coast and comparison with north-west Trinity Peninsula, Graham Land. *British Antarctic Survey Bulletin*, No. 10, 1–43.

ELLIOT, D. H. 1972. Aspects of Antarctic geology and drift reconstructions. (*In* ADIE, R. J., *ed. Antarctic geology and geophysics*. Oslo,

Universitetsforlaget, 849–58.)

ELLIOTT, M. H. 1974. Stratigraphy and sedimentary petrology of the Ablation Point area, Alexander Island. *British Antarctic Survey Bulletin*, No. 39, 87–113.

ENGEL, A. E., ENGEL, C. G. *and* HAVENS, R. G. 1965. Chemical characteristics of oceanic basalts and the upper mantle. *Geol. Soc. Am. Bull.*, **76,** No. 7, 719–33.

ERMANOVICS, I. F. *and* DAVISON, W. L. 1976. The Pikwitonei Granulites in relation to the north-western Superior Province of the Canadian Shield. (*In* WINDLEY, B. F., *ed. The early history of the Earth*. London, New York, Sydney, Toronto, John Wiley and Sons, 331–47.)

ESKOLA, P. 1932. On the principles of metamorphic differentiation. *Bull. Commn géol. Finl.*, **16**, No. 97, 68–77.

ESKOLA, P. 1950. Paragenesis of cummingtonite and hornblende from Muuruvesi, Finland. *Am. Miner.*, **35,** Nos. 9 and 10, 728–34.

EVANS, B. W. *and* LEAKE, B. E. 1960. The composition and origin of the striped amphibolites of Connemara, Ireland. *J. Petrology*, **1,** Pt. 3, 337–63.

FISHER, R. V. 1961. Proposed classification of volcaniclastic sediments and rocks. *Bull geol. Soc. Am.*, **72,** No. 9, 1409–14.

FISHER, R. V. 1966. Rocks composed of volcanic fragments and their classification. *Earth-Sci. Rev.*, **1,** No. 4, 287–98.

FLEET, M. 1968. The geology of the Oscar II Coast, Graham Land. *British Antarctic Survey Scientific Reports*, No. 59, 46 pp.

FOLK, R. L. 1954. The distinction between grain size and mineral composition in sedimentary-rock nomenclature. *J. Geol.*, **62,** No. 4, 344–59.

FORBES, R. F., RAY, D. K., KATSURA, T., MATSUMOTO, H., HARAMURA, H. *and* FURST, M. J. 1969. The comparative chemical composition of continental vs island arc andesites in Alaska. (*In* MCBIRNEY, A. P., *ed.* Proceedings of the andesite conference. *Bull. Ore. St. Dep. Geol. Miner. Ind.*, No. 65, 21–42.) [International Upper Mantle Project, Scientific Report 16.]

FRANCHETEAU, J. *and* SCLATER, J. G. 1969. Paleomagnetism of the southern continents and plate tectonics. *Earth & planet. Sci. Lett.*, **6,** No. 2, 93–106.

FRASER, A. G. 1965. The petrology of Stonington and Trepassey Islands, Marguerite Bay. *British Antarctic Survey Scientific Reports*, No. 52, 51 pp.

FRASER, A. G. *and* GRIMLEY, P. H. 1972. The geology of parts of the Bowman and Wilkins Coasts, Antarctic Peninsula. *British Antarctic Survey Scientific Reports*, No. 67, 59 pp.

FYFE, W. S. 1973. The granulite facies, partial melting and the Archaean crust. *Phil. Trans. R. Soc. Lond. A.*, **273,** 457–61.

GAVELIN, S. 1952. Lime metasomatism and metamorphic differentiation in the Adak area. *Års. Sver. geol. Unders*, **45**, No. 2, 1–62.

GEISLER, A. H. 1953. *Phase transformation in solids*. New York, John Wiley and Sons.

GOLDRING, D. C. 1962. The geology of the Loubet Coast, Graham Land. *British Antarctic Survey Scientific Reports*, No. 36, 50 pp.

GOLDSCHMIDT, V. M. 1954. *Geochemistry*. Oxford, Oxford University Press.

GREEN, D. H., BRUNFELT, A. O. *and* HEIER, K. S. 1972. Rare earth element distribution and K/Rb ratios in granulites, mangerites and anorthosites, Lofoten-Vesteraalen, Norway. *Geochim. cosmochim. Acta*, **36,** 241–57.

GRIBBLE, C. D. 1969. Distribution of elements in igneous rocks of the normal calc-alkaline sequence. *Scott. J. Geol.*, **5,** No. 4, 322–7.

GRIKUROV, G. E. 1972. Tectonics of the Antarctandes. (*In* ADIE, R. J., *ed. Antarctic geology and geophysics*. Oslo, Universitetsforlaget, 163–7.)

GRIKUROV, G. E. *and* DIBNER, A. F. 1968. Novye dannye o Serii Triniti (C_{1-3}) v zapadnoy Antarktide [New data on the Trinity Series (C_{1-3}) in west Antarctica]. *Dokl. Akad. Nauk SSSR*, Geology, **179,** No. 2, 410–12. [English translation: More information on the Trinity Series (C_{1-3}) of western Antarctica. *Dokl.* (*Proc.*) *Acad. Sci. U.S.S.R.*, Geological Sciences sect., **179,** 39–41.]

HALPERN, M. 1972. Rb–Sr total-rock and mineral ages from the Marguerite Bay area, Kohler Range and Fosdick Mountains. (*In* ADIE, R. J., *ed. Antarctic geology and geophysics*. Oslo, Universitetsforlaget, 197–204.)

HAMILTON, J. 1957. Banded olivines in some Scottish Carboniferous olivine-basalts. *Geol. Mag.*, **94,** No. 2, 135–9.

HAMILTON, W. 1969. The volcanic central Andes—a modern model for the Cretaceous batholiths and tectonics of western North America. (*In* MCBIRNEY, A. R., *ed.* Proceedings of the andesite conference. *Bull. Ore. St. Dep. Geol. miner. Ind.*, No. 65, 165–84.) [International Upper Mantle Project, Scientific Report 16.]

HARKER, A. 1909. *The natural history of igneous rocks*. New York, Macmillan.

HARKER, A. 1950. *Metamorphism: a study of the transformations of rock-masses*. 3rd edition. London, Methuen and Co. Ltd.

HAWKES, D. D. 1961. The geology of the South Shetland Islands: II. The geology and petrology of Deception Island. *Falklands Islands Dependencies Survey Scientific Reports*, No. 27, 43 pp.

HAYES, D. E. 1971. *Eltanin* cruise 43. *Antarct. Jnl U.S.*, **6,** No. 1, 15–16.

HEIER, K. S. 1957. Phase relations of potash feldspar in metamorphism. *J. Geol.*, **65,** No. 5, 468–79.

HEIER, K. S. 1961. The amphibolite-granulite facies transition reflected in the mineralogy of potassium feldspars. *Curs. Confs Inst. Lucas Mallada Invest. geol.*, Fasc. 8, 131–7.

HEIER, K. S. *and* THORESEN, K. 1971. Geochemistry of high-grade metamorphic rocks, Lofoten-Vesteralen, north Norway. *Geochim. cosmochim. Acta*, **35,** 89–99.

HEIER, K. S. *and* TAYLOR, S. R. 1959. Distribution of Ca, Sr and Ba in southern Norwegian Precambrian alkali feldspars. *Geochim. cosmochim. Acta*, **17,** Nos. 3 and 4, 286–304.

HESS, H. H. 1960. Stillwater igneous complex, Montana. A quantitative mineralogical study. *Mem. geol. Soc. Am.*, No. 80, 230 pp.

HIETANEN, A. 1973. Origin of andesitic and granitic magmas in the northern Sierra Nevada, California. *Geol. Soc. Am. Bull.*, **84,** No. 6, 2111–18.

HILLS, E. S. 1963. *Elements of structural geology*. London, Methuen and Co. Ltd.

HORNE, R. R. 1967*a*. Structural geology of part of south-eastern Alexander Island. *British Antarctic Survey Bulletin*, No. 11, 1–22.

HORNE, R. R. 1967*b*. *The geology of part of south-eastern Alexander Island*. Ph.D. thesis, University of Birmingham, 164 pp. [Unpublished.]

HORNE, R. R. 1968. Petrology and provenance of the Cretaceous sediments of south-eastern Alexander Island. *British Antarctic Survey Bulletin*, No. 17, 73–82.

HORNE, R. R. 1969. Sedimentology and palaeogeography of the Lower Cretaceous depositional trough of south-eastern Alexander Island. *British Antarctic Survey Bulletin*, No. 22, 61–76.

HORNE, R. R. *and* THOMSON, M. R. A. 1967. Post-Aptian camptonite dykes in south-east Alexander Island. *British Antarctic Survey Bulletin*, No. 14, 15–24.

HORNE, R. R. *and* THOMSON, M. R. A. 1972. Airborne and detrital volcanic material in the Lower Cretaceous sediments of south-eastern Alexander Island. *British Antarctic Survey Bulletin*, No. 29, 103–11.

HOSKINS, A. K. 1963. The Basement Complex of Neny Fjord, Graham Land. *British Antarctic Survey Scientific Reports*, No. 43, 49 pp.

HUBBARD, F. H. 1966. Myrmekite in charnockite from south-west Nigeria. *Am. Miner.*, **51**, Nos. 5 and 6, 762–73.

HUBBARD, F. H. 1967. Exsolution myrmekite: a proposed solid-state transformation model. *Geol. För. Stockh. Förh.*, **89,** 410–22.

HUGHES, C. J. 1970. The significance of biotite selvedges in migmatites. *Geol. Mag.*, **107**, No. 1, 21–4.

IRVINE, T. N. *and* BARAGAR, W. R. A. 1971. A guide to the chemical classification of the common volcanic rocks. *Can. J. Earth Sci.*, **8,** No. 5, 523–48.

JAKES, P. *and* WHITE, A. J. R. 1972. Major and trace element abundances in volcanic rocks of orogenic areas. *Geol. Soc. Am. Bull.*, **83,** No. 1, 29–39.

JAMES, D. E. 1971. A plate tectonics model for the evolution of the central Andes. *Geol. Soc. Am. Bull.*, **82,** No. 12, 3325–46.

KATZ, H. R. 1972. Plate tectonics and orogenic belts in the south-eastern Pacific. *Nature, Lond.*, **237,** No. 5354, 331–2.

KING, L. 1964. Pre-glacial geomorphology of Alexander Island. (*In* ADIE, R. J., *ed. Antarctic geology*. Amsterdam, North-Holland Publishing Company, 53–64.)

KLEEMAN, A. W. 1965. The origin of granitic magmas. *J. geol. Soc. Aust.*, **12,** Pt. 1, 35–52.

KNOWLES, P. H. 1945. Geology of southern Palmer Peninsula, Antarctica. *Proc. Am. phil. Soc.*, **89,** No. 1, 132–45.

KUENEN, P. H. *and* MENARD, H. W. 1952. Turbidity currents, graded and non-graded deposits. *J. sedim. Petrol.*, **22,** No. 2, 83–96.

KUNO, H. 1965. Fractionation trends of basalt magmas in lava flows. *J. Petrology*, **6,** Pt. 2, 302–21.

LACY, E. D. 1960. Melts of granitic composition, their structure, properties and behaviour. *21st Int. geol. Congr., Norden, 1960*, Pt. 14, 7–15.

LAMBERT, R. ST. J. *and* HOLLAND, J. G. 1974. Yttrium geochemistry applied to petrogenesis utilizing calcium-yttrium relationships in minerals and rocks. *Geochim. cosmochim. Acta*, **38,** No. 9, 1393–1414.

LEAKE, B. E. 1964. The chemical distinction between ortho- and para-amphibolites. *J. Petrology*, **5,** Pt. 2, 238–54.

LEAKE, B. E., HENDRY, G. L., KEMP, A., PLANT, A. G., HARVEY, P. K., WILSON, J. R., COATS, J. S., AUCOTT, J. W., LÜNEL, T. *and* HOWARTH, R. J. 1969. The chemical analysis of rock powders by automatic X-ray fluorescence. *Chem. Geol.*, **5,** No. 1, 7–86.

LEVI, B. 1973. Eastward shift of Mesozoic and early Tertiary volcanic centers in the Coast Range of central Chile. *Geol. Soc. Am. Bull.*, **84,** No. 12, 3901–10.

LOVE, L. G. *and* AMSTUTZ, G. C. 1966. Review of microscopic pyrite. *Fortschr. Miner.*, **43,** Ht. 2, 273–310.

LUTH, W. C., JAHNS, R. H. *and* TUTTLE, O. F. 1964. The granite system at pressures of 4 to 10 kilobars. *J. geophys. Res.*, **69,** No. 4, 759–73.

MCLEAN, D. 1957. *Grain bounaries in metals*. London, Oxford University Press.

MARMO, V. 1971. *Developments in petrology. Vol. 2. Granite petrology and the granite problem*. Amsterdam, London, New York, Elsevier Publishing Company.

MARSH, A. F. 1968. *Geology of parts of the Oscar II and Foyn Coasts, Graham Land*. Ph.D. thesis, University of Birmingham, 291 pp. [Unpublished.]

MEHNERT, K. R. 1968. *Developments in petrology. Vol. 1. Migmatites and the origin of granitic rocks*. New York, Elsevier Publishing Company.

MIDDLEMOST, E. A. K. 1969. The granite spectrum. *Lithos*, **2,** No. 3, 217–22.

MIDDLEMOST, E. A. K. 1971. Classification and origin of the igneous rocks. *Lithos*, **4,** No. 2, 105–30.

MIYASHIRO, A. 1953. Calcium-poor garnet in relation to metamorphism. *Geochim. cosmochim. Acta*, **4,** No. 3, 179–208.

MIYASHIRO, A. 1958. Regional metamorophism of the Gosaisyo–Takanuki district in the central Abukuma plateau. *J. Fac. Sci. Tokyo Univ.*, Sect. 2, **11,** Pt. 2, 219–72.

MIYASHIRO, A. 1961. Evolution of metamorphic belts. *J. Petrology*, **2,** Pt. 3, 277–311.

MIYASHIRO, A. 1973. Paired and unpaired metamorphic belts. *Tectonophysics*, **17,** No. 3, 241–54.

NICHOLLS, I. A. 1971. Petrology of Santorini volcano, Cyclades, Greece. *J. Petrology*, **12,** Pt. 1, 67–119.

NOCKOLDS, S. R. 1954. Average chemical compositions of some igneous rocks. *Bull. geol. Soc. Am.*, **65,** No. 10, 1007–32.

NOCKOLDS, S. R. *and* ALLEN, R. 1953. The geochemistry of some igneous rock series. *Geochim. cosmochim. Acta*, **4,** No. 3, 105–42.

OLIVER, J., ISACKS, B., BARAZANGI, M. *and* MITRONOVAS, W. 1973. Dynamics of the down-going lithosphere. *Tectonophysics*, **9,** No. 2, 133–47.

PARSONS, I. *and* BOYD, R. 1971. Distribution of potassium feldspar polymorphs in intrusive sequences. *Mineralog. Mag.*, **38,** No. 295, 295–311.

PETTIJOHN, F. J. 1954. Classification of sandstones. *J. Geol.*, **62,** No. 4, 360–65.

PHILLIPS, E. R. *and* RANSOM, D. M. 1968. The proportionality of quartz in myrmekite. *Am. Miner.*, **53,** Nos. 7 and 8, 1411–13.

PITCHER, W. S. 1972. The Coastal Batholith of Peru: some structural aspects. *24th Int. geol. Congr., Canada, 1972*, Sect. 2, 156–63.

POLDERVAART, A. 1953. Metamorphism of basaltic rocks: a review. *Bull. geol. Soc. Am.*, **64,** No. 3, 259–74.

POLDERVAART, A. *and* HESS, H. H. 1951. Pyroxenes in the crystallization of basaltic magma. *J. Geol.*, **59,** No. 5, 472–89.

PRICE, N. J. 1966. *Fault and joint development in brittle and semi-brittle rock*. Oxford, etc., Pergamon Press.

PRIESTLEY, R. E. 1923. *Physiography (Robertson Bay and Terra Nova Bay regions)*. London, Harrison and Sons, Ltd. [British (Terra Nova) Antarctic Expedition, 1910–1913.]

PRINZ, M. 1967. Geochemistry of basaltic rocks: trace elements. (*In* HESS, H. H. *and* POLDERVAART, A., *ed. Basalts: the Poldervaart treatise on rocks of basaltic composition. Vol. 1*. New York, London, Sydney, John Wiley and Sons: Interscience Publishers, 271–323.

PROCTER, N. A. A. 1959. The geology of northern Marguerite Bay and the Mount Edgell area. *Falkland Islands Dependencies Survey Preliminary Geological Report*, No. 4, 18 pp. [Unpublished.]

RAJU, R. D. *and* RAO, J. S. R. K. 1972. Chemical distinction between replacement and magmatic rocks. *Contr. Miner. Petrol. (Beitr. Miner. Petrogr.)*, **35,** No. 2, 169–72.

RAMBERG, H. 1952. *The origin of metamorphic and metasomatic rocks: a treatise on recrystallization and replacement in the Earth's crust*. Chicago, The University of Chicago Press.

READ, H. H. 1933. On quartz-kyanite rocks in Unst, Shetland Islands. *Mineralog. Mag.*, **23,** No. 140, 317–28.

REX, D. C. 1972. K–Ar age determinations on volcanic and associated rocks from the Antarctic Peninsula and Dronning Maud Land. (*In* ADIE, R. J., *ed. Antarctic geology and geophysics*. Oslo, Universitetsforlaget, 133–6.)

RICKARD, D. T. 1969. The microbiological formation of iron sulphides. *Stockh. Contr. Geol.*, **20,** 49–66.

RINGWOOD, A. E. 1974. The petrological evolution of island arc systems. *J. geol. Soc. Lond.*, **130,** Pt. 3, 183–204.

ROBERTS, W. A. 1953. Metamorphic differentiates in the Blackbird mining district, Idaho. *Econ. Geol.*, **48,** No. 6, 446–56.

SCHWANKTE, A. 1909. Die Beimischung von Ca im Kalifeldspar und die Myrmekitbildung. *Zentbl. Miner. Geol. Paläont.*, 1909, 311–16.

SEITSAARI, J. 1952. On association of cummingtonite and hornblende. *Suomal. Tiedeakat. Toim.*, Ser. A.III, No. 30, 20 pp.

SEN, S. K. 1959. Potassium content of natural plagioclase and the origin of antiperthites. *J. Geol.*, **67,** No. 5, 479–95.

SHELLEY, D. 1964. On myrmekite. *Am. Miner.*, **49,** Nos. 1 and 2, 41–52.

SHELLEY, D. 1966. The significance of granophyric and myrmekitic textures in the Lundy Granites. *Mineralog. Mag.*, **35,** No. 273, 678–92.

SHELLEY, D. 1967. Myrmekite and myrmekite-like intergrowths. *Mineralog. Mag.*, **36,** No. 280, 491–503.

SHELLEY, D. 1969. The proportion of quartz in myrmekite: a discussion. *Am. Miner.*, **54,** Nos. 5 and 6, 982–3.

SHELLEY, D. 1970. The origin of myrmekitic intergrowths and a comparison with rod-eutectics in metals. *Mineralog. Mag.*, **37,** 290, 674–81.

SHIDÔ, F. 1958. Plutonic and metamorphic rocks of the Nakoso and Iritōno districts in the central Abukuma plateau. *J. Fac. Sci. Tokyo Univ.*, Sect. 2, **11,** Pt. 2, 131–217.

SHIDÔ, F. *and* MIYASHIRO, A. 1959. Hornblendes of basic metamorphic rocks. *J. Fac. Sci. Tokyo Univ.*, Sect. 2, **12,** Pt. 1, 85–102.

SIEGERS, A., PICHLER, H. *and* ZEIL, W. 1969. Trace element abundances in the 'andesite' formation of northern Chile. *Geochim. cosmochim. Acta*, **33,** No. 7, 882–7.

SKINNER, A. C. 1973. Geology of north-western Palmer Land between Eureka and Meiklejohn Glaciers. *British Antarctic Survey Bulletin*, No. 35, 1–22.

SMITH, A. G. *and* HALLAM, A. 1970. The fit of the southern continents. *Nature, Lond.*, **225,** No. 5228, 139–44.

SMITH, C. G. 1977. *The geology of parts of the west coast of Palmer Land, Antarctica*. Ph.D. thesis, University of Birmingham, 193 pp. [Unpublished.]

SMITH, J. V. 1962. Genetic aspects of feldspar twinning. *Norsk geol. Tidsskr.*, **42,** Hb. 2, 244–63.

SPRY, A. 1969. *Metamorphic textures*. Oxford, London, Edinburgh, etc., Pergamon Press.

STEIGER, R. H. *and* HART, J. R. 1967. The microcline-orthoclase transition in the contact aureole of the Eldorado Stock, Colorado. *Am. Miner.*, **52,** Nos. 1 and 2, 87–116.

STEPHENSON, A. 1940. Graham Land and the problem of Stefansson Strait. *Geogrl J.*, **96,** No. 3, 167–74.

STEPHENSON, A. *and* FLEMING, W. L. S. 1940. King George the Sixth Sound. *Geogrl J.*, **96,** No. 3, 153–64.

STEWART, F. H. 1947. The gabbroic complex of Belhelvie in Aberdeenshire. *Q. Jl geol. Soc. Lond.*, **102** (for 1946), Pt. 4, No. 408, 465–96.

STILLWELL, F. L. 1918. The metamorphic rocks of Adelie Land. *Scient. Rep. Australas. Antarct. Exped.*, Ser. A, **3,** Geology, Pt. 1, 1–230.

STUBBS, G. M. 1968. *Geology of parts of the Foyn and Bowman Coasts, Graham Land*. Ph.D. thesis, University of Birmingham, 244 pp. [Unpublished.]

STURT, B. A. 1970. Exsolution during metamorphism with particular reference to feldspar solid solutions. *Mineralog. Mag.*, **37,** No. 291, 815–32.

SUTTON, J. *and* WATSON, J. 1951. Varying trends in the metamorphism of dolerites. *Geol. Mag.*, **88,** No. 1, 25–35.

SUWA, K. 1961. Petrological and geological studies on the Ryoke metamorphic belt. *J. Earth Sci.*, **9,** 224–303.

TAYLOR, B. J. 1966. *The stratigraphy and palaeontology of the Aptian of the central east coast of Alexander Island*. Ph.D. thesis, University of Birmingham, 245 pp. [Unpublished.]

TAYLOR, S. R. 1969. Trace element chemistry of andesites and associated calc-alkaline rocks. (*In* MCBIRNEY, A. R., *ed.* Proceedings of the andesite conference. *Bull. Ore. St. Dep. Geol. miner. Ind.*, No. 65, 43–63.) [International Upper Mantle Project, Scientific Report 16.]

THORNTON, C. P. *and* TUTTLE, O. F. 1960. Chemistry of igneous rocks: I. Differentiation index. *Am. J. Sci.*, **258,** No. 9, 664–84.

TUREKIAN, K. K. *and* WEDEPOHL, K. H. 1961. Distribution of the elements in some major units of the Earth's crust. *Geol. Soc. Am. Bull.*, **72,** No. 2, 175–91.

TURNER, F. J. 1941. The development of pseudo-stratification by metamorphic differentiation in the schists of Otago, New Zealand. *Am. J. Sci.*, **239,** No. 1, 1–16.

TURNER, F. J. *and* VERHOOGEN, J. 1960. *Igneous and metamorphic petrology*. 2nd edition. New York, Toronto and London, McGraw-Hill Book Company, Inc.

TUTTLE, O. F. *and* BOWEN, N. L. 1958. Origin of granite in the light of experimental studies in the system $NaAlSi_3O_8$–$KAlSi_3O_8$–SiO_2–H_2O. *Mem. geol. Soc. Am.*, No. 74, 153 pp.

VANCE, J. A. 1961. Polysynthetic twinning in plagioclase. *Am. Miner.*, **46,** Nos. 9 and 10, 1097–119.

VAN DER KAMP, P. L. 1970. The green beds of the Scottish Dalradian series. Geochemistry, origin and metamorphism of mafic sediments. *J. Geol.*, **78,** No. 3, 281–303.

VOLL, G. 1960. New work on petrofabrics. *Lpool Manchr geol. J.*, **2,** No. 3, 503–67.

WASHINGTON, H. S. 1917. Chemical analyses of igneous rocks published from 1884 to 1913 inclusive. *Prof. Pap. U.S. geol. Surv.*, No. 99, 1201 pp.

WATTERS, W. A. 1959. An association of hornblende and cummingtonite from Ringaringa, Stewart Island, New Zealand. *N.Z. Jl Geol. Geophys.*, **2,** No. 1, 248–56.

WEST, S. M. 1974. The geology of the Danco Coast, Graham Land. *British Antarctic Survey Scientific Reports*, No. 84, 58 pp.

WHITE, A. J. R. 1966. Genesis of migmatites from the Palmer region of South Australia. *Chem. Geol.*, **1,** No. 3, 165–200.

WIDENFALK, I. 1969. Electron micro-probe analyses of myrmekitic plagioclase and coexisting feldspar. *Lithos*, **2,** No. 3, 295–309.

WILLEY, L. E. 1973. Belemnites from south-eastern Alexander Island: II. The occurrence of the family Belemnopseidae in the Upper Jurassic and Lower Cretaceous. *British Antarctic Survey Bulletin*, No. 36, 33–59.

WILLIAMS, P. L., SCHMIDT, D. L., PLUMMER, C. C. *and* BROWN, L. E. 1972. Geology of the Lassiter Coast area, Antarctic Peninsula: preliminary report. (*In Adie, R. J., ed. Antarctic geology and geophysics*. Oslo, Universitetsforlaget, 143–8.)

WRIGHT, T. L. 1967. The microcline-orthoclase transformation in the contact aureole of the Eldorado Stock, Colorado. *Am. Miner.*, **52,** Nos. 1 and 2, 117–36.

YODER, H. S. 1969. Calcalkalic andesites: experimental data bearing on the origin of their assumed characteristics. (*In McBirney, A. R., ed.* Proceedings of the andesite conference. *Bull. Ore. St. Dep. Geol. miner. Ind.*, No. 65, 77–89.) [International Upper Mantle Project, Scientific Report 16.]

YODER, H. S. *and* TILLEY, C. E. 1962. Origin of basalt magmas: an experimental study of natural and synthetic rock systems. *J. Petrology*, **3,** Pt. 3, 342–532.